APDA-143

SUMMARY
OF THE
APDA FUEL DEVELOPMENT PROGRAMS

W. G. Blessing, J. S. Busch, J. G. Duffy, R. J. Hennig,
W. H. Jens, F. W. Knight, E. C. Kovacic, D. O. Leeser,
G. L. O'Neill, A. A. Shoudy, and R. G. Rateick

April 1961

PREFACE

During the past several years, Atomic Power Development Associates, Inc., (APDA) have been engaged in four separate fuel development programs:

1. Core A

The U-10 w/o Mo fuel and the U-3 w/o Mo blanket for the Enrico Fermi reactor. The development program was sponsored by APDA for Power Reactor Development Company (PRDC). Although a great deal of the work was done by APDA, some of the development work was subcontracted to other organizations.

2. Core B

The UO_2-SS cermet and the UO_2 axial blanket for the Enrico Fermi reactor. The fabrication, development, and irradiation program was done at Oak Ridge National Laboratory (ORNL) under the AEC-PRDC contract. The design and out-of-pile testing was sponsored and carried out by APDA.

3. Advanced Fast Reactor Fuel Development

This work was supported both by the AEC and by APDA.

4. Paste Fuel

This work was sponsored entirely by APDA. The work was performed by APDA and other subcontractors.

The following report, which has been prepared for presentation to the AEC Sodium Fuel Element Design Group, summarizes the status of these fuel development programs through the calendar year 1960. The work done at ORNL on Core B and on advanced fast reactor fuels was written as a separate summary and is not included in this report.

TABLE OF CONTENTS

TABLE OF CONTENTS (Continued)

TABLE OF CONTENTS (Continued)

LIST OF ILLUSTRATIONS

LIST OF ILLUSTRATIONS (Continued)

LIST OF ILLUSTRATIONS (Continued)

LIST OF TABLES

I. INTRODUCTION AND STATUS OF CORE A

A. EARLY FAST BREEDER REACTOR REQUIREMENTS

The initial requirements for the fast breeder reactor were established by the Dow-Detroit Edison Study Group in the early 1950's. These requirements were

1. High Breeding Ratio

The long-range economic potential of the fast breeder reactor depends on the superior ability of the reactor to breed excess fissionable material.

2. High Specific Power and High Power Density

The economics of the fast breeder, with its compact core, requires very high specific power and high power density to reduce inventory charges to an acceptable level.

3. Remote Fabrication of Fuel

With recycled plutonium, the fissionable material used will be alpha and gamma active and will require semi-remote and shielded fabrication. Therefore, rapid reprocessing of the fuel with small fission product decontamination such as pyrometallurgical techniques was attractive since rapid reprocessing also reduces the out-of-pile inventory of fissionable material.

B. INITIAL DEVELOPMENT

To achieve a high fissionable and fertile atom density for a high breeding gain and a reproducible axial expansion for safety, metal alloys were considered initially. The direct casting of the fuel alloy into a radiator appeared to be the most suitable fabrication technique for remote fabrication coupled with pyrometallurgical reprocessing.

The eutectic U-5 w/o Cr, which has a melting point of only 1640 F and a thermal conductivity superior to uranium, was the first alloy investigated. Uranium was selected as the fissionable material because of the unavailability of, and the difficulties in, working with plutonium; however, an unsatisfactory bond was obtained when the U-5 w/o Cr alloy was cast against iron or zirconium radiator tubes.

The use of a U-2 w/o Zr alloy was then investigated. Since this alloy has a higher melting point than the U-5 w/o Cr alloy, it was considerably more difficult to maintain the required dimensional tolerances of the radiator structure and, even with the zirconium alloy, a satisfactory metallurgical bond was not obtained by casting.

The next effort was oriented to various types of sodium-bonded fuel

elements in which the fuel alloy was cast separately and then placed in a clad structure. The following designs were studied:

1. Fuel wafers containing regularly spaced holes were stacked over round or hexagonal coolant tubes to form a radiator-type subassembly.

2. Because an axial temperature expansion was not guaranteed in the fuel wafer arrangement described above, corrugated plates running the full length of the core were considered next; the plates were stacked between the coolant tubes that formed the radiator structure.

3. An alternative to the use of corrugated plates, was the use of flat plates placed between rectangular coolant channels to form a radiator subassembly.

4. The most straightforward design considered was one consisting of rods of fuel in round tubes similar to the present EBR-II fuel element. Although successful castings were made of the above-mentioned fuel configurations using U-2 w/o Zr and 5 w/o Cr alloys, it was concluded that thermal bonding using liquid sodium had the following drawbacks:

1. An acceptable thermal sodium bond with small clearances could not be obtained consistently and, as a result, a good nondestructive test for 100 per cent inspection was required. For all geometries except the round tube, the testing appeared to be formidable.

2. Very little was known about the behavior of fission product gases which could be released by rupture, diffusion, or recoil from the fuel alloys. These gases could destroy the thermal bond and cause a hot spot.

3. The consequences of a fuel hot spot in contact with an iron alloy tube could result in melting through the cladding because of formation of the low temperature eutectic of iron and uranium or plutonium.

The initial irradiation tests were made using U-5 w/o Cr. These tests showed that the material had very poor irradiation stability--worse than unalloyed uranium.

C. THE DECISION TO BUILD PHASE

In 1955, a firm decision was made to participate in the USAEC Power Demonstration Program. Since the reactor was to be located near Detroit, the safety aspects of the design became of overriding importance. For this reason, the specific power as reflected by heat flux was reduced from 2×10^6 to 1×10^6 Btu/hr-ft^2, and greater emphasis was placed on radiation stability. As a result of work by the Westinghouse Electric Corporation in connection with the PWR, a clad element with a ductile metallurgical diffusion bond made by coextrusion was selected as the reference design. The initial burnup goal was about 3 a/o burnup at a fabrication cost of about $15.00 per pin. Remote fabrication and reprocessing were abandoned since time did not permit further development by the project.

Safety considerations related to meltdown indicated an alloy having a high melting point to be the most suitable. ANL data at that time indicated

that U-2 w/o Zr with a chill cast heat treatment could possibly meet the burnup requirements. This alloy appeared also to have good mechanical properties that would insure acceptable thermal expansion characteristics. Therefore, the U-2 w/o Zr alloy was selected as the reference alloy.

The reference design was a fuel pin, 0.158 inch in diameter and 30-1/2 inches long, with a zirconium cladding 0.007 inch thick. The cladding was to be metallurgically bonded to the U-2 w/o Zr by hot coextrusion of both materials. Integrally extruded end closures were to be obtained by the same extrusion process. The final sizing was to be by swaging, and the pins were to be spaced one from another by means of a spirally wound spacer wire attached to the cladding by spot welding.

Pins of the reference design were subsequently developed and irradiated. The irradiation results were discouraging, and as a consequence other alloys were investigated.

D. EVALUATION OF U-10 W/O MO

Of the alloys reviewed, the only alloys that showed radiation stabilities comparable or superior to the "chilled cast" U-2 w/o Zr were the "gamma" stabilized alloys of uranium-molybdenum having from 9 to 13 w/o Mo. These alloys were also being studied by Westinghouse for possible use in the PWR.

The processing of irradiated U-10 w/o Mo was simple since it was easily dissolved in nitric acid. A slight increase in critical mass was expected, and a decrease in breeding ratio could be tolerated. These penalties were more than offset by the anticipated gains resulting from greater burnup. Although it was considered that some radiation stability could be gained by specifying the 13 w/o Mo alloy, the fabrication difficulties made the gain to be of questionable value. In December, 1955, the decision was made to use U-10 w/o Mo as the reference alloy.

This change of fuel alloy also prompted other studies which showed that the cladding could be reduced from 0.007 inch to 0.004 inch. The use of U-10 w/o Mo did not permit the use of integral end closures. Further, from a fabrication cost viewpoint, coextrusions containing many lengths of fuel pin were considered desirable. As a result, a mechanically locked end cap was developed to protect the bare alloy at the ends of the fuel pins. The thinner cladding prevented spot welding of the spiral spacing wire that could occur because of diffusion during spot welding. Integral extrusions with spacers were attempted, but the process was too expensive. Finally it was decided to use a separate wire structure to space the pins in the subassembly.

E. DETAILED DESIGN AND TESTING

1. Fabrication Costs

Bids were obtained early in 1958, and a contract was awarded in June 1958. Instead of meeting the goal of $15.00 per pin, the cost was about $50.00 per pin. A cost breakdown of a Core A subassembly and blanket subassembly and the resulting fuel cycle costs is given in the section on Core A Economics.

2. Irradiation Results

Under contract to APDA Battelle Memorial Institute (BMI), carried out an evaluation of the effect of radiation on U-10 w/o Mo. Initially, U-10 w/o Mo was irradiated in the MTR. Very high fission rates were used to accelerate the tests.

The results of the tests indicated that an average burnup of 1 a/o should be obtainable under the design temperature conditions for the Fermi reactor. Further, an average burnup of almost 2 a/o could be achieved if either the power or sodium temperatures were reduced so that the fuel would operate at a temperature 200 F lower than the design temperature.

Later a prototype irradiation test was made of full-length fuel pins in CP-5. The fission rates were less than Fermi full-power conditions and considerably less than the MTR tests because of the low neutron flux in CP-5. The results indicated excessive swelling in the transformation temperature region of from 850 F to 950 F. As a result, the predicted average burnup was reduced to 0.5 a/o. The resulting fuel cycle cost nearly doubled as a result of this change in burnup.

3. Structural Stability

During the development and testing of prototype subassemblies, which employed the fuel pin support scheme shown in Figure 1, a number of problems were encountered.

a. The chevron wires broke at the welds to the side plate. The fatigue failures were due to flow-induced vibrations; however, these failures were eliminated by reversing the direction of the chevron wires.

b. The flow distribution within the subassembly was not uniform. The flow velocity was greatest at the center of the subassembly when the chevron wires pointed upstream and was greatest at the wall of the subassembly when the chevron wires pointed downstream. In either case, the flow variation was as great as 2 to 1 from center to the wall and was unacceptable from a design standpoint.

c. Examination of the fuel subassembly after it had operated under full flow conditions at 900 F for 700 hours disclosed that the fuel pins had undergone serious distortion. Pairs of fuel elements touched, and the bundle of fuel elements within the wire structure was no longer tight within the square outer tube. During operation, this distortion would result in fuel pin bowing, which could produce the positive power coefficient that must be avoided in fast reactors.

Because of the vibration, flow distribution, and distortion problems, the support structure was completely redesigned. The present design, which employs a firm symmetrical support of the pin as opposed to a point contact unsymmetrical support employed initially, has been proven to be superior and acceptable. The present support structure has a greater thermal hydraulic resistance, which has resulted in a small reduction in flow rate and a reduction in power to maintain the same primary coolant temperature rise.

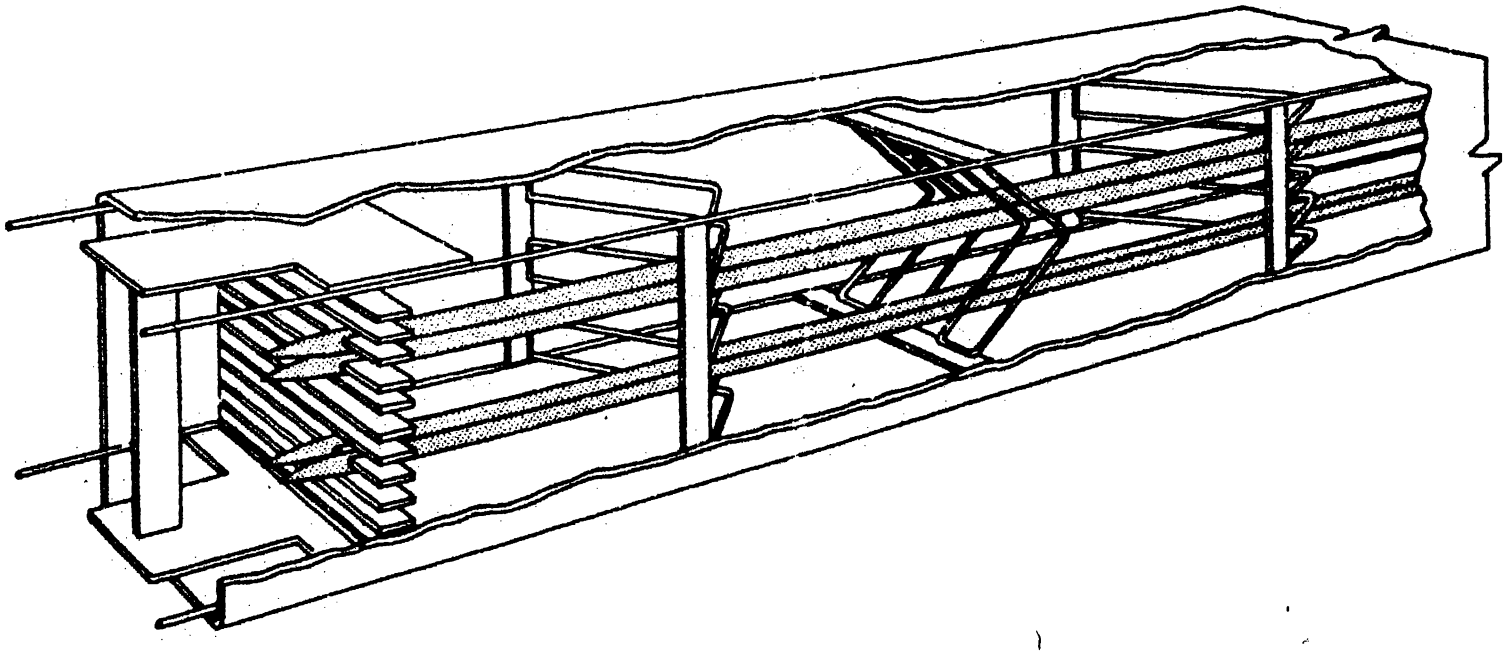

BIRDCAGE FUEL ELEMENT SUPPORT

FIGURE 1

F. STATUS OF FUEL FABRICATION

Contracts were awarded in 1958 to two different fabricators for a full core loading of 100 core subassemblies and one-half blanket loading of 300 blanket subassemblies. This arrangement was made to insure delivery of at least one complete core, since possibly a fabricator might not be able to make the fuel elements specified or could not meet the schedule for fabricating the core subassemblies. One of the fabricators was Nuclear Metals, Inc. (NMI), working with D. E. Makepeace (DEM); the other was Sylvania Corning Nuclear Corporation (Sylcor). After considerable difficulties, Sylcor in 1960 informed PRDC that they would not be able to supply the core subassemblies ordered. As a result, an additional 100 core subassemblies were ordered from DEM. Sylcor continued, however, to supply blanket subassemblies. As of April 1, 1961, Sylcor had delivered 280 blanket subassemblies and DEM had delivered 100. A total of 10 core subassemblies have been completed; however, the equivalent of 130 subassemblies of fuel pins have been fabricated and are presently awaiting assembly. The production of core subassemblies has been delayed because of the design changes to the pin support structure previously discussed.

II. CORE A AND BLANKET OPERATING CONDITIONS

A. GENERAL CONSIDERATIONS

Core A and its associated radial blanket are designed for a total heat output of 200 Mw. Approximately 90 per cent of the power is produced in the core; the remainder is produced in the axial and radial blankets. The division of power between the core and blanket will vary somewhat, depending on the extent of plutonium buildup in the blanket. As plutonium builds up in the blanket, the blanket fission rate increases relative to the core. For example, in a completely clean reactor approximately 89 per cent of the heat is produced in the core, one per cent in the axial blanket, and 10 per cent in the radial blanket. When the reactor life has reached 75 Mw-years, with an average burnup in the core of 0.25 a/o, residual plutonium concentration in the radial blanket changes the division of power so that the core now produces 87 per cent of the total, and the axial and radial blankets produce 1 per cent and 12 per cent, respectively.

The design average temperature rise over the reactor is 250 F, which requires a total sodium flow rate of 8.85×10^6 lb/hr. Under these conditions, the numerical coolant temperature rise in the hottest central core subassembly, is 395 F, while at the outer edge the rise is 158 F. It should be recalled here that core subassemblies are not orificed, and therefore the radial temperature distribution of the core follows the radial neutron flux distribution.

To limit the central metal temperature of the inner radial blanket subassemblies to 950 F, the average coolant temperature rise over these subassemblies has been limited to 169 F.

The operating characteristics of the core and blanket are given in Table I.

The power distribution in the hottest core pin is shown in Figure 2.

B. HOT CHANNEL FACTORS

In the calculation of maximum temperatures, the deviations from nominal values of physical constants, the use of empirical correlations, and uncertainties in the physics calculations were taken into account by the introduction of hot channel factors. The factors for the core are summarized in Table II. The hot channel factors are used to convert each nominal ΔT to maximum expected ΔT. They are determined for the effect of each uncertainty on each ΔT involved and are based on specified tolerance limits, maximum experimental errors, or on engineering judgment.

Statistical variance analysis was applied for the determination of the maximum expected temperature increase above the nominal uranium hot spot temperature.

REACTOR POWER = 200 MW
REACTOR COOLANT TEMPERATURE RISE = 250 F
CORE SUBASSEMBLIES = 105
EQUILIBRIUM CORE BURNUP = 0.25 %
BURNUP IN HOTTEST SUBASSEMBLY = 0 %

NO HOT-CHANNEL FACTORS USED FOR THESE CURVES

REACTOR LIFE = 75 MW-YR
CORE COOLANT FLOW RATE = 7.08 X 10^6 LB/HR
CORE POWER = 174 MW
(171 MW GENERATED IN FUEL ALLOY)

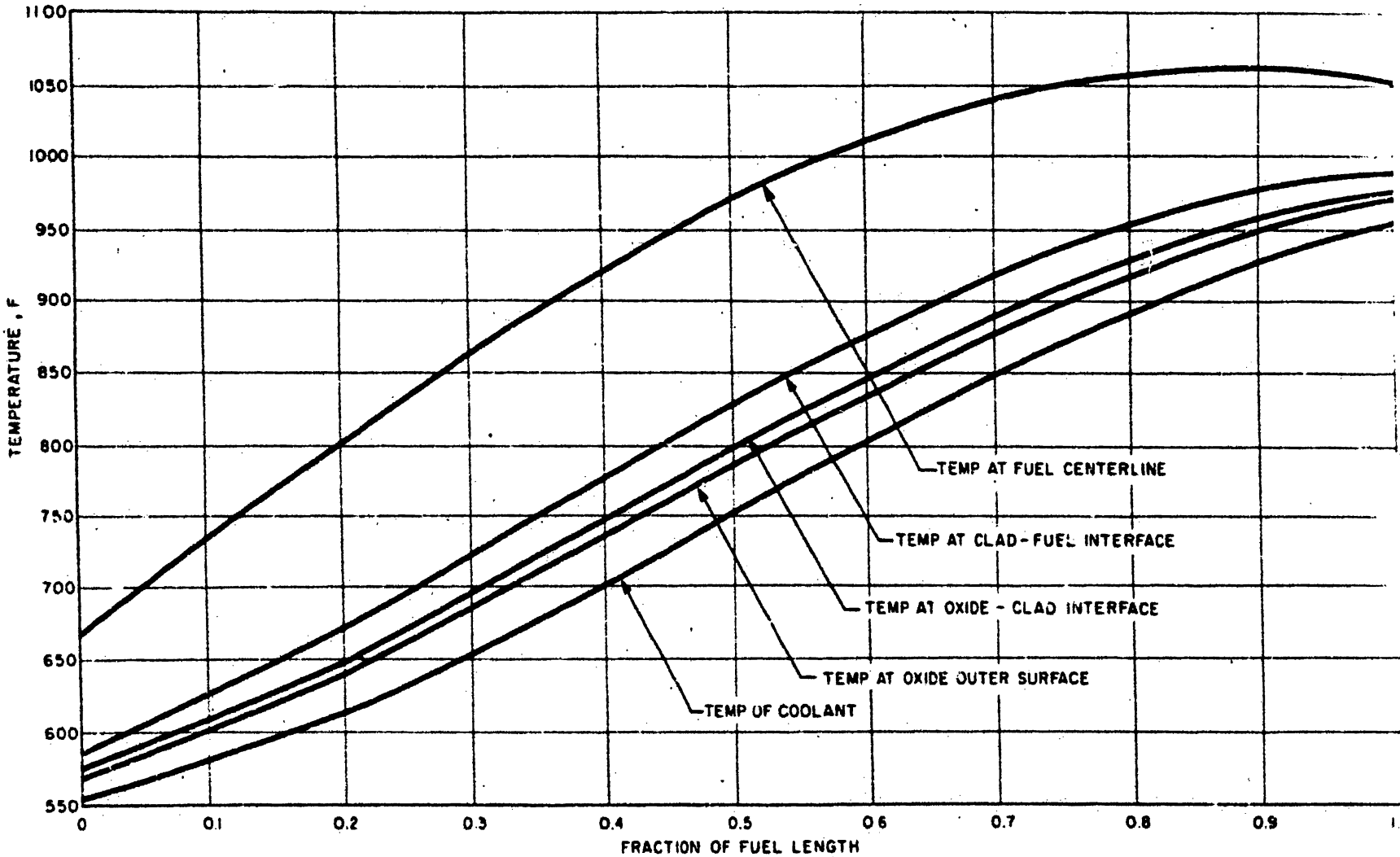

TEMPERATURES IN HOTTEST CORE PIN

FIGURE 2

TABLE I - OPERATING CHARACTERISTICS OF CORE AND BLANKET

General Characteristics	Core Section	Axial Blanket Section	Inner and Outer Radial Blanket Section
Maximum/average power density	1.69	4.1	21.7
Coolant inlet temperature, F	552	550 (lower)	550
Average coolant temperature rise, F	272	4	175
Average Coolant outlet temperature, F	824	826	725
Removal burnup, max a/o	0.40	-	0.25
Power, Mw (at 0.25 a/o average core burnup)	174	2.4	23.6
Coolant flow rate, lb/hr	7.08×10^6	7.08×10^6	1.50×10^6
Maximum heat flux, Btu/hr-sq ft	640,000	72,200	217,000
Coolant velocity, ft/sec	15.6	14.0	
Δp through subassembly, psi	40.0		
Maximum nominal coolant temperature, F	954	961	878
Maximum nominal outer clad temperature, F	991	962	878
Maximum nominal uranium temperature, F	1061	993	931
Maximum coolant temperature, F	1022	1029	971
Maximum outer clad temperature, F	1062	1030	971
Maximum uranium temperature, F	1135	1061	1040

TABLE II - HOT CHANNEL FACTORS FOR URANIUM HOT SPOT IN HOTTEST FUEL PIN

Uncertainty	Factor for Coolant Temp Rise ΔT_c = 374.8F		Factor for Temp Drop Thru Film ΔT_f = 23.8F		Factor for Temp Drop Thru Oxide Layer ΔT_o = 7.5F		Factor for Temp Drop Thru Clad ΔT_{Zr} = 19.0F		Factor for Temp Drop Thru Fuel ΔT_U = 75.8F		SUMMARY	
	F	3σ	F	3σ	F	3σ	F	3σ	F	3σ	Σ(3σ)	$[\Sigma(3\sigma)]^2$
Maldistribution of coolant												
a) To subassemblies	1.02	7.5									7.5	56
b) Within subassemblies	1.10	37.5									37.5	1406
Deviation from nominal dimensions and Maldistribution of U-235	1.095	35.6	1.015	0.4	1.015	0.1	1.015	0.3	1.015	1.1	37.5	1406
			.982	-0.4	.982	-0.1	1.184	3.5	.987	-1.0	2.0	4
					2.000	7.5					7.5	56
Maldistribution of Power	1.08	30.0	1.08	1.9	1.08	0.6	1.08	1.5	1.08	6.1	40.1	1608
Power measurement and control	1.05	18.7	1.05	1.2	1.05	0.4	1.05	1.0	1.05	3.8	25.1	630
Film heat transfer coefficient			1.30	7.1							7.1	50
Thermal conductivity of zirconium oxide					1.20	1.5					1.5	2
Thermal conductivity of zirconium							1.10	1.9			1.9	4
Thermal conductivity of fuel alloy									1.20	15.2	15.2	231
										Total	$\Sigma[\Sigma(3\sigma)]^2$	5453
										Sq Root of Total = 3σ =		73.8 F

(Continued on next page)

TABLE II (Continued) - HOT CHANNEL FACTORS FOR URANIUM HOT SPOT IN HOTTEST FUEL PIN

Uranium hot spot located at fuel alloy length fraction, $X/L = 0.90$

Maximum uranium temperature without hot channel factors = 1061 F (50% confidence)

Maximum uranium temperature with hot channel factors:

$T_U = 1061 + 25 = 1086$ (1σ = 84.1% confidence)

$T_U = 1061 + 49 = 1110$ (2σ = 97.7% confidence)

$T_U = 1061 + 74 = 1135$ (3σ = 99.87% confidence)

A value of three standard deviations (3σ) is associated with each maximum expected ΔT deviation, equal to ΔT (hot channel factor - 1.00), as recorded in the (3σ) columns. If the effects of given uncertainties on the various temperature differences are not linked by causal relationship, e.g., each of the tabulated uncertainties in Table II, the 3σ values are placed on different horizontal lines. If the effects are linked by causal relationship, e.g., maldistribution of power in Table II, the 3σ values are placed on the same horizontal line.

By defining $\Sigma[\Sigma(3\sigma)]^2$ as the 3σ variance, the combined effect of each uncertainty on the central uranium temperature can be calculated by the variance principles, as shown in the last two columns of the tables. The uranium temperature deviation corresponding to three standard deviations is obtained from the square root of the 3σ variance. This value is used to obtain the maximum uranium temperature with the hot channel factor correction. The application of three standard deviations in calculating the uranium maximum temperature implies a confidence limit of 99.87 per cent. Under these circumstances, there is a probability of only 1.3 in 1000 that the hottest fuel pin will exceed the specified maximum temperature. By comparison, with no hot channel factor correction, the probability of exceeding the specified maximum temperature is 500 in 1000.

C. IRRADIATION EFFECTS

Because prolonged neutron irradiation increases the diameter of the fuel pins, the sodium flow area decreases and, in turn, reduces the flow rate. This reduction in flow causes an increase in the sodium temperature and, hence, in the central metal temperature. This latter temperature increase aggravates the swelling. For each subassembly location in the core, the limiting burnup has been conservatively estimated from temperature data and from the irradiation results presently available for U-10 w/o Mo alloy.

The removal burnup values for the fuel pins were selected in the following manner: The spring dimples on a guiding grid do not touch a new pin, but they would just touch a pin with an 8 per cent oversize diameter.

Most of the subassemblies in the core will have maximum temperatures of 800 to 1000 F. At 8 per cent swelling, this is equivalent to a maximum local burnup of 0.8 to 0.9 a/o. When averaged over the core, this results in an average burnup of 0.5 a/o.

III. DESIGN DESCRIPTION AND PROBLEMS - CORE A

A. ARRANGEMENT OF CORE AND BLANKET

The Enrico Fermi reactor is an assembly of 870 removable and, to a certain extent, interchangeable units, all assembled on a square lattice spacing of 2.693 inches. The reactor vessel support plates provide the basic definition of this lattice and support the core, blanket, thermal shield regions, and the control rod guide tubes. The general arrangement of the reactor is shown in Figure 3.

In plan, the core and upper and lower axial blankets occupy a roughly circular region in the center of the lattice. This region, as shown in Figure 4, includes 10 lattice positions used for control rods, an expected 105 lattice positions used for core subassemblies. Each core subassembly, as shown in Figure 5, consists of three basic regions: a lower axial blanket, the fuel-bearing core region, and an upper axial blanket. The 105 core subassemblies in their lattice positions approximate a cylindrical fuel-containing core region with an upper and lower axial blanket region. The core region is about 30.5 inches high with about the same diameter. The axial blanket regions are each 17 inches high.

The 32 lattice positions immediately surrounding the core region comprise the inner radial blanket region. When these positions are filled with inner radial blanket subassemblies, an annular region is formed, the bottom of which is at the same elevation as the bottom of the lower axial blanket, and the top of which is at the same elevation as the top of the upper axial blanket.

The next 499 lattice positions surrounding the inner radial blanket comprise the outer radial blanket region. When the lattice positions are filled with outer radial blanket subassemblies, an annular region is formed the top and bottom of which are at the same elevation as the top and bottom of the inner radial blanket.

Surrounding the outer radial blanket are 198 lattice positions used for steel subassemblies that provide thermal and irradiation shielding of the reactor vessel. Three of these positions contain surveillance specimens to allow additional studies of the effects of fast neutrons on nonfissionable materials.

The 149 central lattice positions that are used for core, inner radial blanket, and control rods are supplied with sodium flowing upwards from the plenum which is fed directly from the discharge of the primary sodium pumps. Because they have a large pressure drop, the central subassemblies require downward mechanical restraint in addition to their own weight to prevent their ejection from the lower support plates. This restraint is supplied by the hold-down plate.

The remaining 721 lattice positions are supplied with sodium coolant from the low-pressure plenum that is fed from the primary sodium pumps

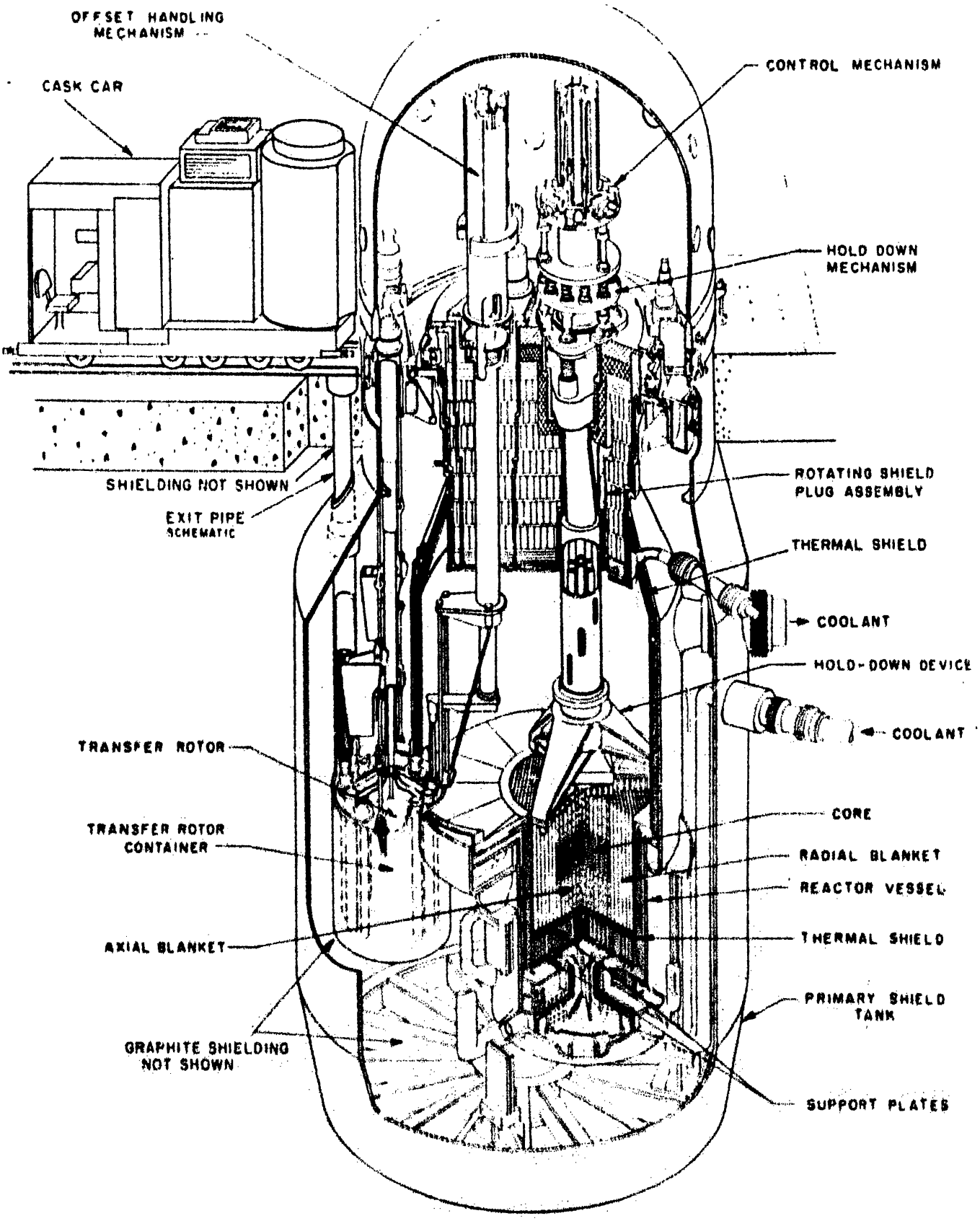

PERSPECTIVE VIEW OF REACTOR
FIGURE 3

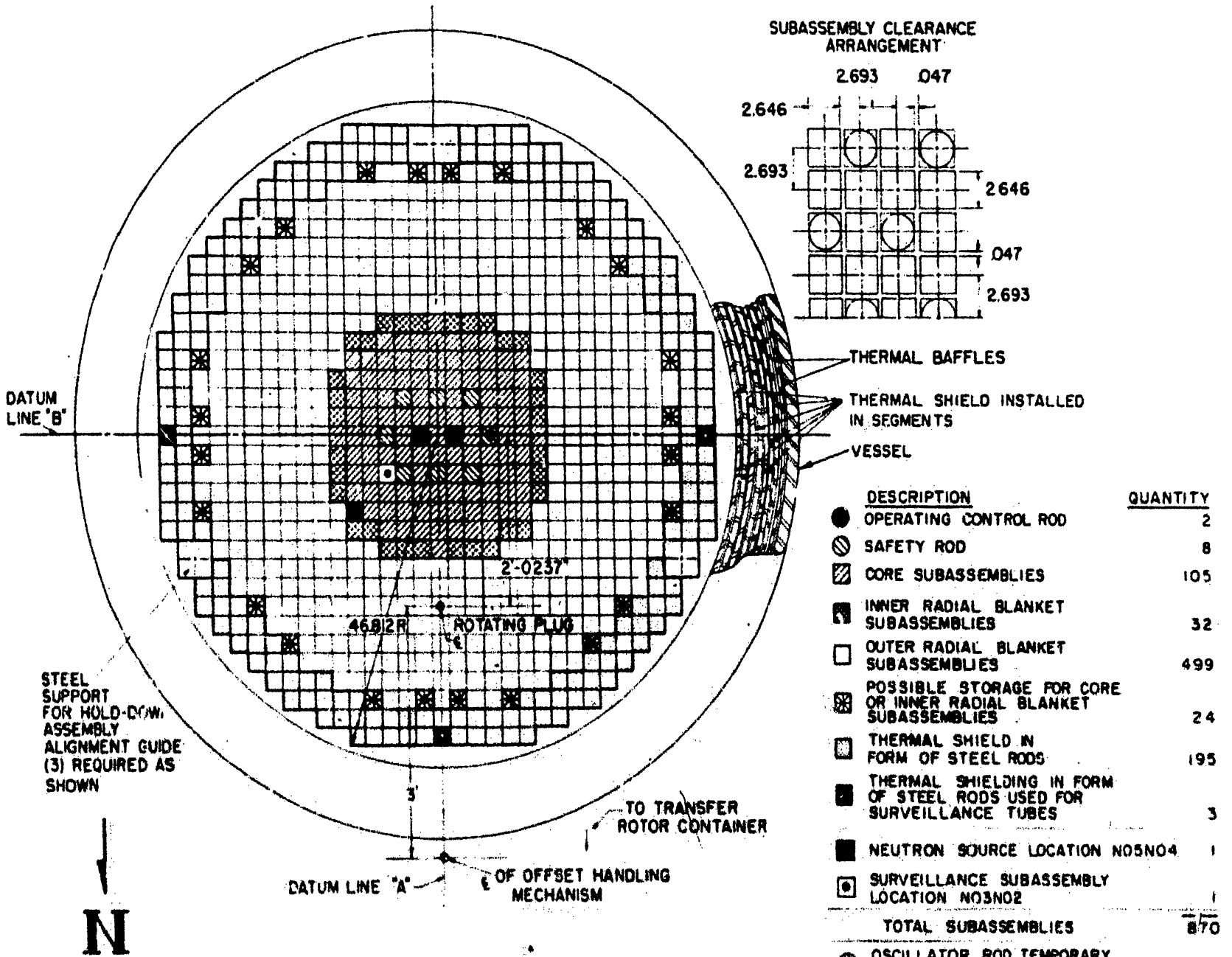

DESCRIPTION	QUANTITY
OPERATING CONTROL ROD	2
SAFETY ROD	8
CORE SUBASSEMBLIES	105
INNER RADIAL BLANKET SUBASSEMBLIES	32
OUTER RADIAL BLANKET SUBASSEMBLIES	499
POSSIBLE STORAGE FOR CORE OR INNER RADIAL BLANKET SUBASSEMBLIES	24
THERMAL SHIELD IN FORM OF STEEL RODS	195
THERMAL SHIELDING IN FORM OF STEEL RODS USED FOR SURVEILLANCE TUBES	3
NEUTRON SOURCE LOCATION N05N04	1
SURVEILLANCE SUBASSEMBLY LOCATION N03N02	1
TOTAL SUBASSEMBLIES	870
OSCILLATOR ROD TEMPORARY LOCATION P03P00	

THE POSITION UNDER THE CENTER OF THE ROTATING PLUG, P00N09, IS VACANT

REACTOR CROSS SECTION
FIGURE 4

through three throttle valves. The pressure-drop force acting on these subassemblies is less than their weight and, therefore, no hold-down is required.

Since high-pressure sodium and a hold-down are available, core subassemblies can be located in the 32 inner radial blanket positions to provide control of reactivity or to increase the reactor power output with new type cover at a late date. The characteristics of the core and blanket are outlined in Table III.

B. DESCRIPTION OF CORE SUBASSEMBLIES

To facilitate handling, the fuel-containing core region and the upper and lower axial blanket regions are mechanically incorporated into a single structure, the core subassembly.

The subassembly consists of the outside wrapper tube, which is a square stainless-steel tube measuring 2.646 inches on a side with a nominal wall thickness of 0.096 inches and a minimum of 0.084 inches. A combination handling head and hold-down contact is attached to the top of the wrapper tube. To the bottom of this wrapper tube is attached a lower support section consisting of two concentric round tubes, the outer of which fits into the lower support plate of the reactor vessel. A preset spring between the outer and inner tubes allows for thermal expansion of the subassembly structure. There is a strainer at the inlet of each core subassembly. The strainer consists of a supporting flange ring. The screen is made of 25-mil-thick stainless steel sheet pierced with 40-mil holes on a 75-mil staggered pitch, as shown in Figure 5.

The fuel region of each core subassembly is made up of 140 round U-10 w/o molybdenum alloy pins containing uranium enriched to 25.6 per cent U-235. The overall length of the pins is 32 25/32 inches, and the outside diameter is 0.158 inch. Each pin is clad with 5 mils of reactor-grade zirconium that is metallurgically bonded to the periphery of the fuel alloy and closed at the top and bottom with zirconium end-caps. The lower end of each pin is fastened to the support structure by anchor bars that are threaded through the slotted bottom end-caps. The upper ends are free to accommodate changes in length resulting from temperature changes and growth caused by irradiation effects.

The support structure for the fuel pins has 10 restraining (Type C) grids and 7 guiding (Type F) grids. Photographs of the complete support structure and of a typical support grid are shown in Figures 6 and 7. Details of the pin support arrangement identifying the C and F grids are shown in Figure 8. The support structure holds 140 fuel pins on a square pitch of 0.199 inch. The four corner positions are steel tie rods. The grids, ten of one type and seven of the other, are made of Type 347 stainless steel strips, 0.0115 inch thick and 1/2 inch wide. The strips are slotted and dimpled. The two types of grids follow the same concept for the dimple height. The dimples of the C grids touch the fuel pins throughout core life, while the dimples of the F grid normally do not touch the fuel pins. Initially, the opposing dimples are fabricated so that the distance between them is 147.5 mils. The insertion of a 158-mil pin through this space results in a final separation between the dimples and set of opposing spring forces acting on the pin. The contact restraint is achieved by giving

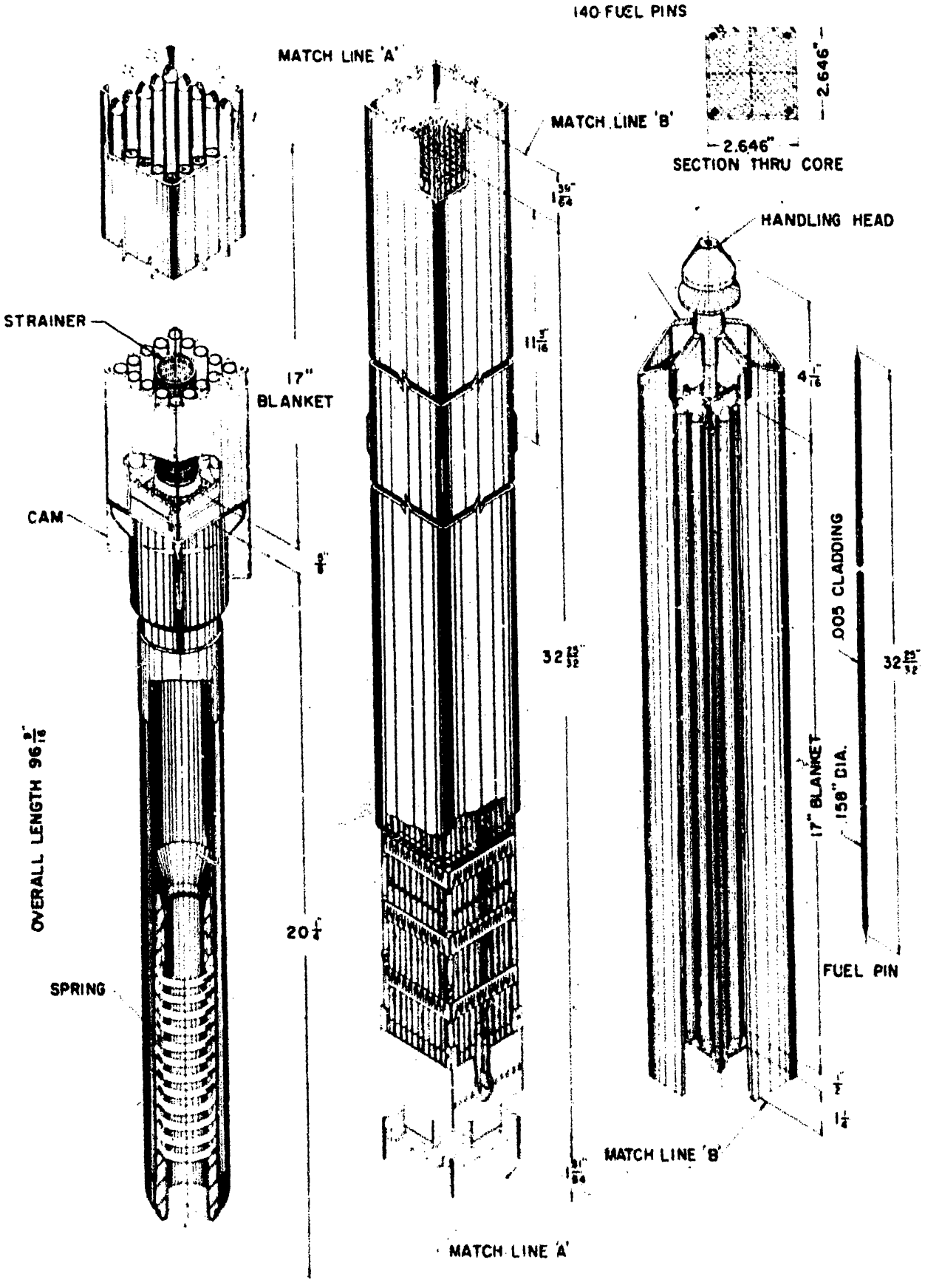

ISOMETRIC VIEW OF CORE SUBASSEMBLY

FIGURE 5

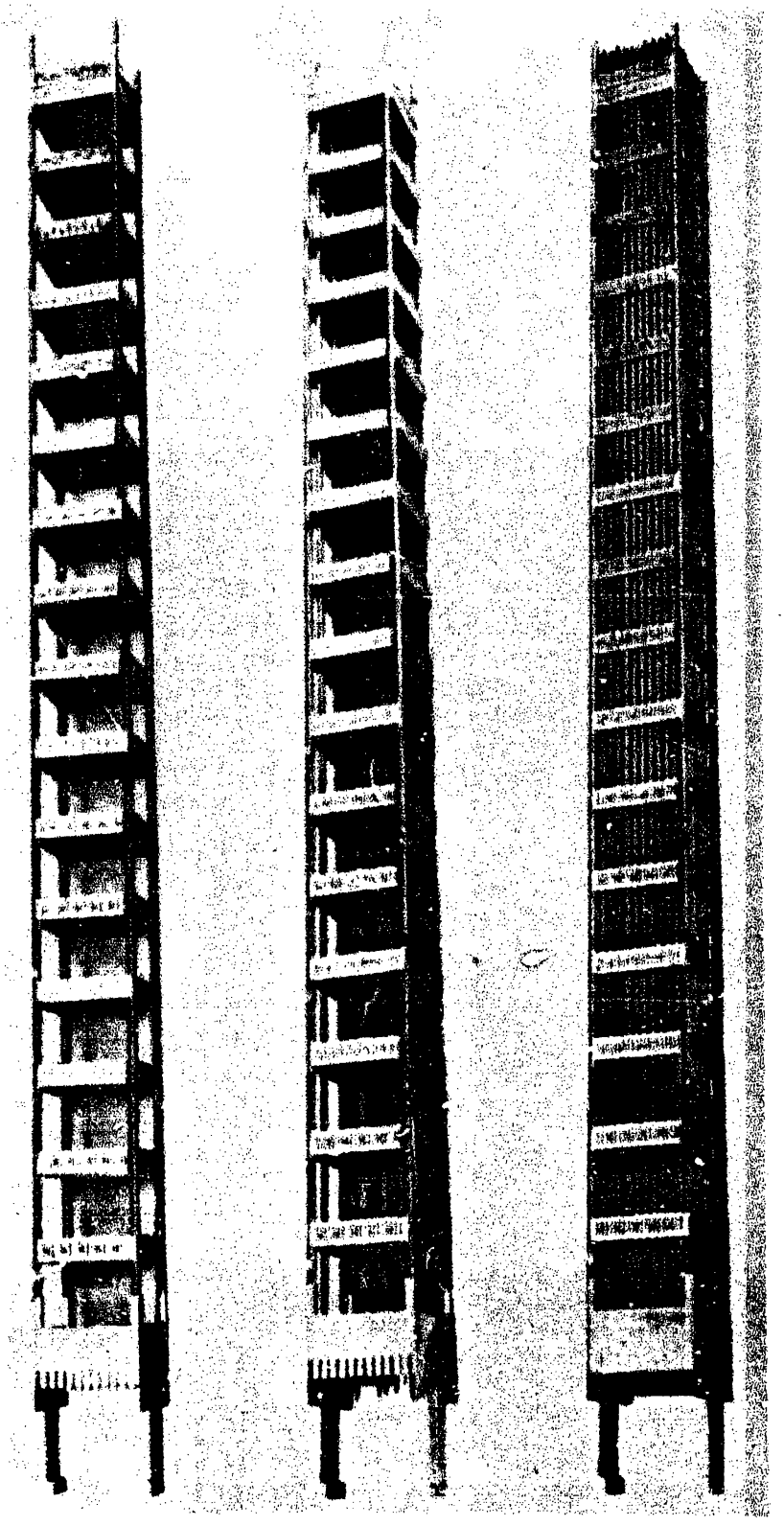

DETAIL OF SUBASSEMBLY FUEL SECTION

FIGURE 6

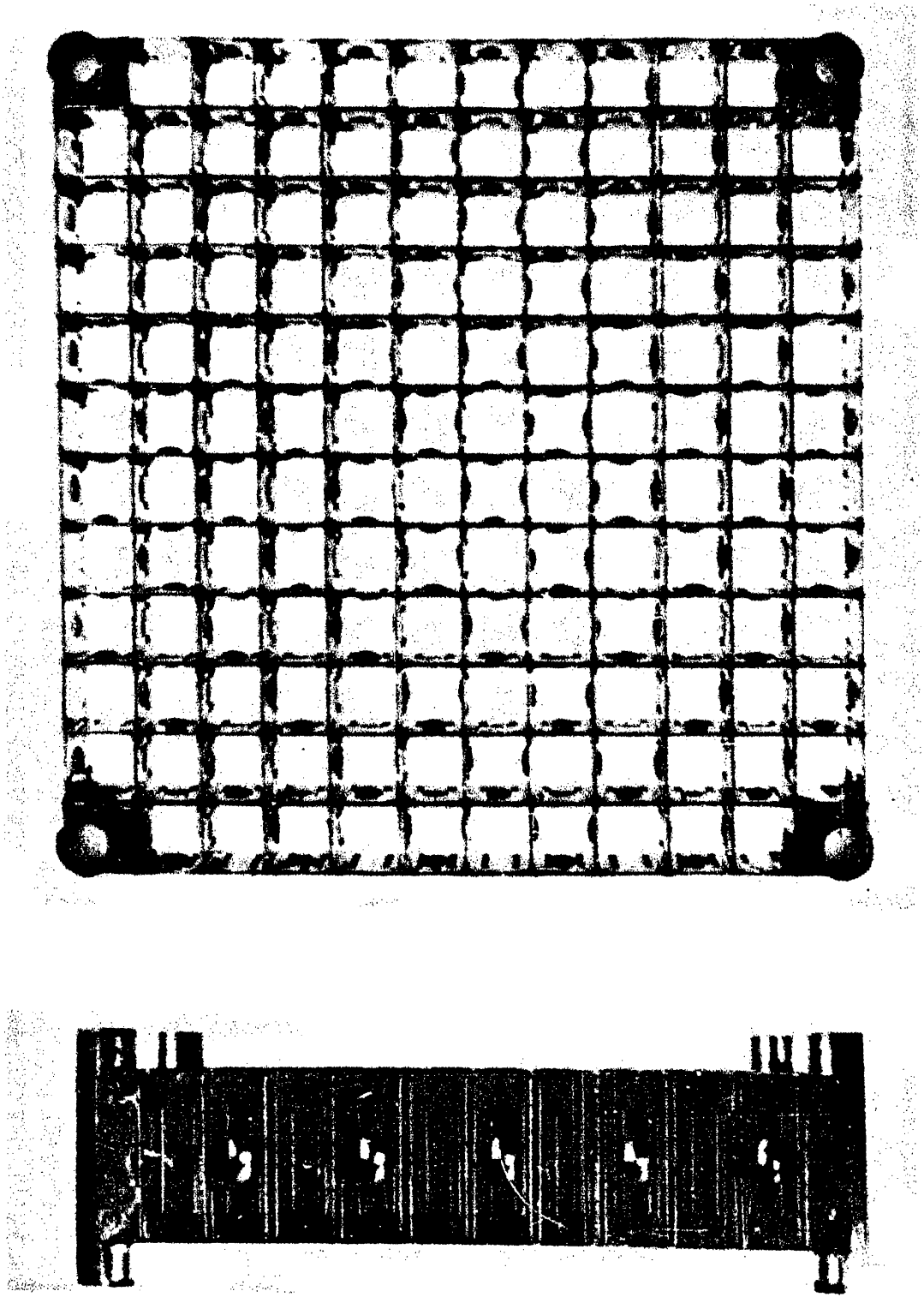

LAYOUT OF GRIDS—HONEYCOMB GRID C
FIGURE 7

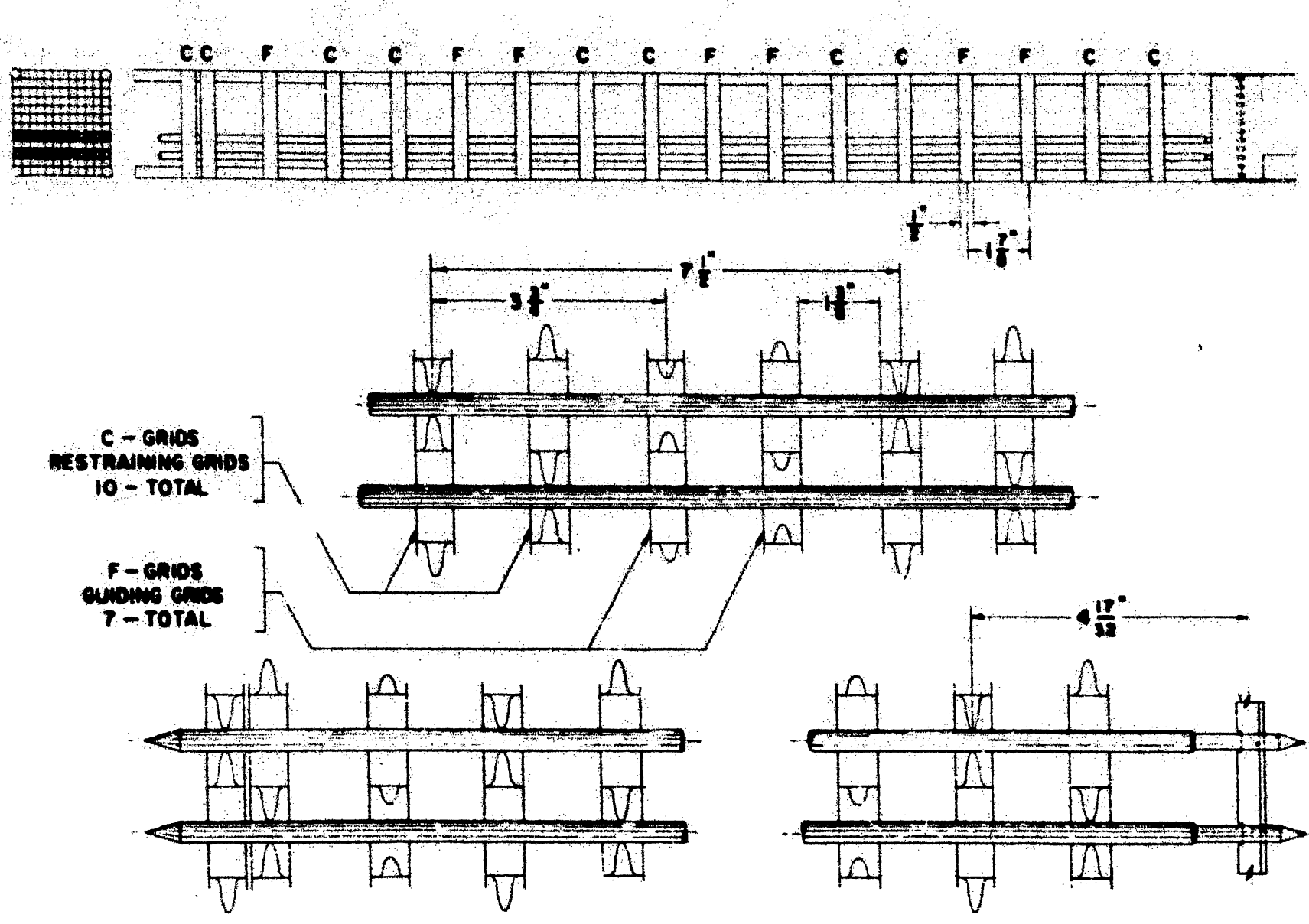

SEQUENCE OF SUPPORTS GRIDS

FIGURE 8

the opposing dimples in the guiding grids an initial separation of 171 mils. The difference between the 158-mil dimension of the cold pin and the 171 mils allows for swelling of the pin due to thermal and radiation effects.

Since the C grids only hold a fuel pin in every other cell, alternate C grids are rotated 90 degrees. This means that any pin is normally held by every other C grid. The F grids are used for guiding fuel pins, and to prevent the fuel pins from moving together. There is a pair of butting C grids at the downstream end of the bundle so that every pin is supported at this position. The anchor bars, which are threaded through each row of fuel pins at the upstream end of the bundle, are notched to assure proper pin positioning and flow distribution.

The support structure is assembled by passing 1/8-inch rods through the corner positions of each grid. The rods are screwed into the lower collar, which positions the anchor bars, and have a nut on the other end. Short lengths of tubing are slid on the rods to space the grids from each other. The typical free clearance between adjacent grids is 1-3/8 inches.

The grid-fuel pin assembly is laterally restrained with the subassembly wrapper tube by a series of screws that bear on one of the four corner posts. The arrangement is shown in Figure 9. By this means, any movement of the spacer support structure within the wrapper tube is prevented in a positive manner. The three other corner posts have stand-off ferrules that provide a flow passage between the birdcage and the wrapper tube. The grid-fuel pin assembly support arrangement couples the fuel pins to the subassembly wrapper tube.

The upper and lower axial blanket regions in each core subassembly contain sixteen 0.395-inch-diameter U-2.75 w/o Mo alloy rods containing uranium depleted to 0.35 per cent in U-235. The pins are enclosed in 10-mil-thick stainless steel tubes having an outside diameter of 0.1443 inch. The radial clearance between the uranium alloy and the tube is filled with sodium to provide a bond with low thermal resistance and allowance for an increase in alloy diameter. Allowance for increase in length of the alloy due to thermal expansion and irradiation effects is provided inside the sealed tube by the sodium annulus and a gas space above the rod. A short stainless steel tube located within the gas space prevents the uranium from rising above the sodium.

The blanket rods are held in the subassembly and spaced around its periphery by lugged grids at the top and bottom of each axial blanket section. The center portions of the upper and lower axial blanket in each subassembly contain no blanket rods. The flow strainer, previously described, projects into the lower portion of this central region of the lower axial blanket.

C. DESCRIPTION OF RADIAL BLANKET SUBASSEMBLIES

There are two types of radial blanket subassemblies, internally identical but differing in details of the support structure (nozzle) and spacer pads. These are shown in Figure 10.

In the inner radial blanket subassemblies, the nozzle contains a thermal expansion accommodation spring like that of the core subassemblies.

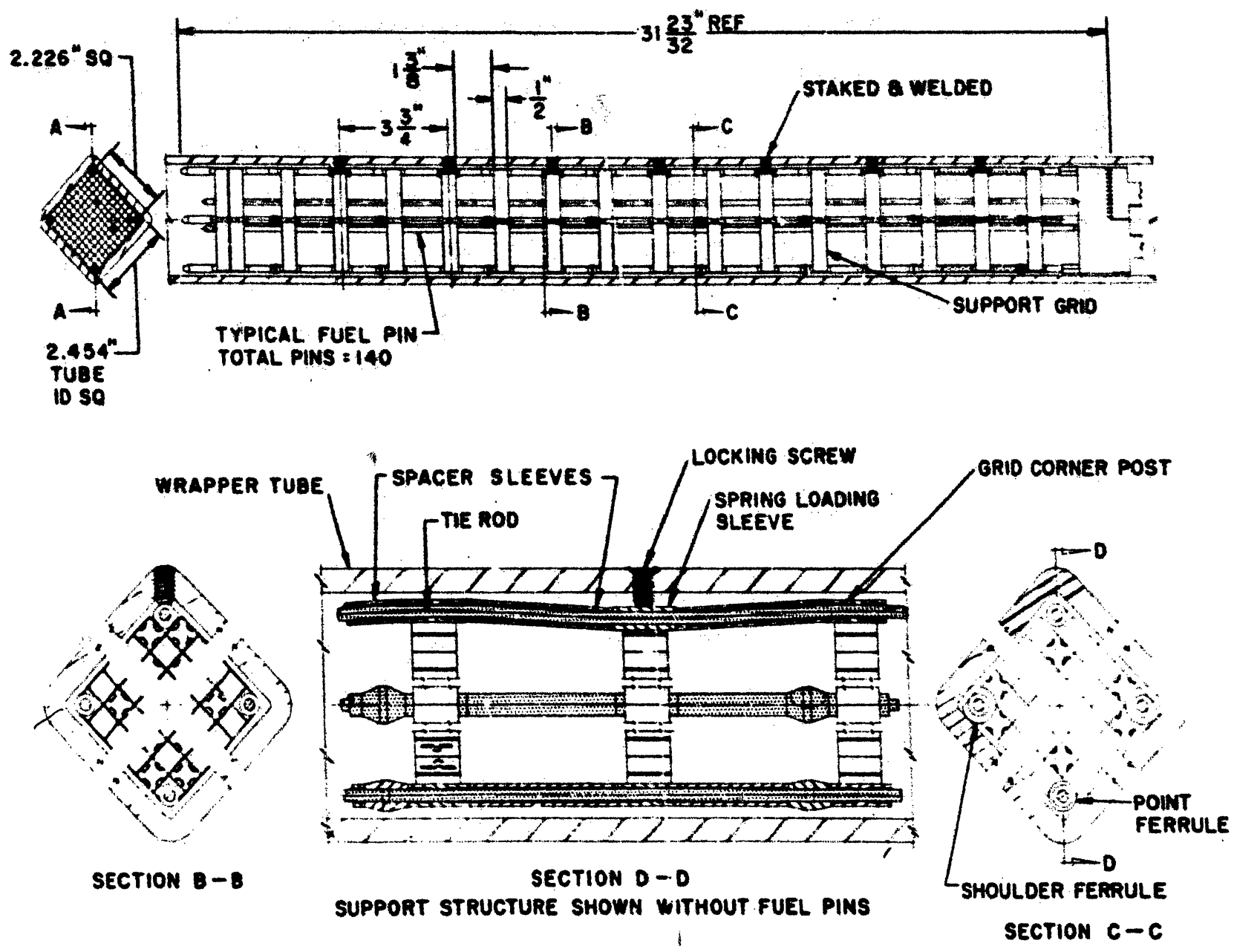

FUEL PIN BUNDLE SUPPORT SYSTEM

FIGURE 9

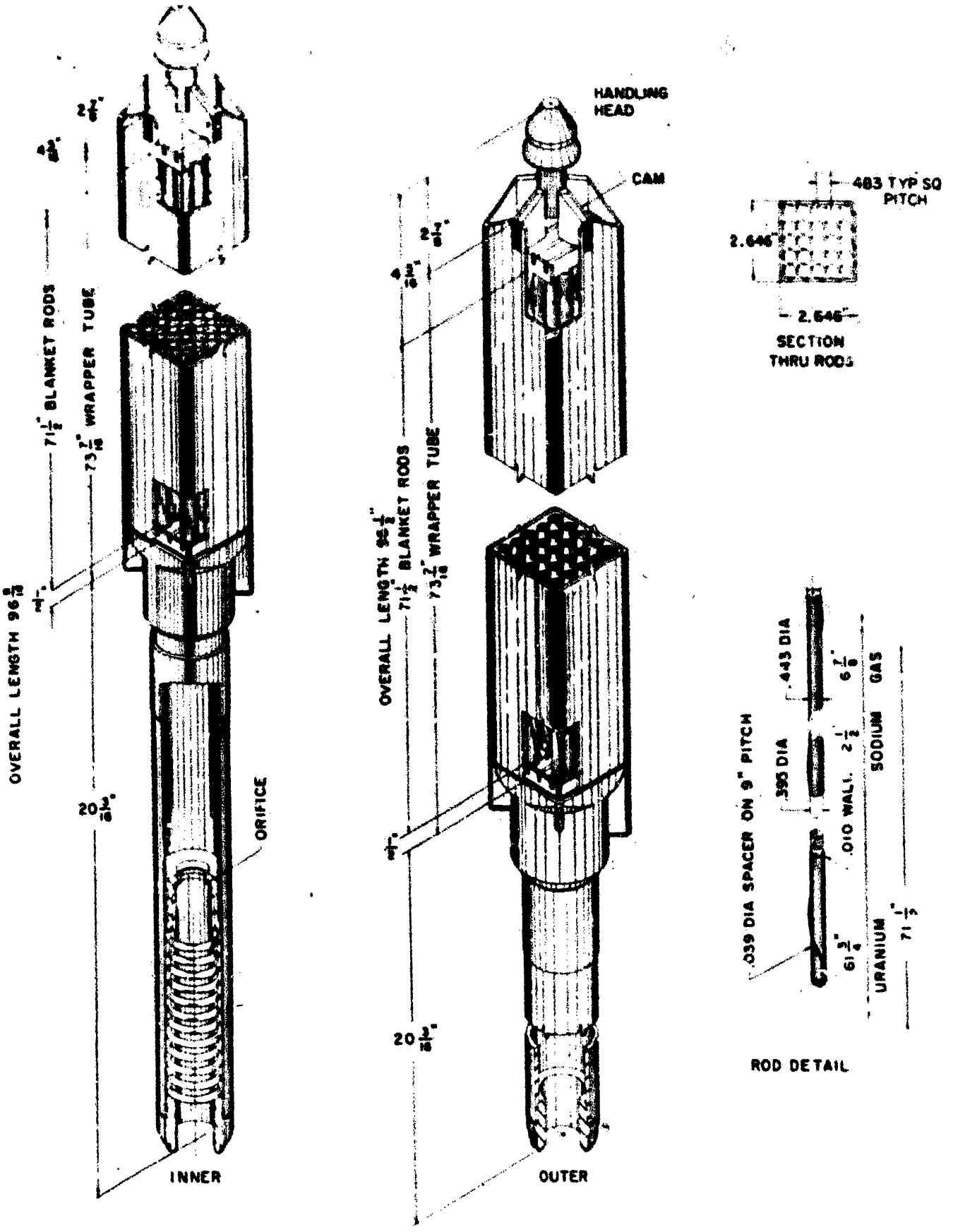

ISOMETRIC VIEW OF RADIAL BLANKET SUBASSEMBLIES

FIGURE 10

The support structure is properly sized to fit the holes in the lower support plates that are intended for core and inner radial blanket subassemblies. The nozzle contains provision for a removable orifice. The spacer pads on the inner radial blanket subassemblies perform the same function as those on the core subassemblies.

The outer radial blanket subassemblies have a simple nozzle structure because, in the absence of a hold-down plate, no special accommodation of thermal expansion is necessary. The nozzle for the outer radial blanket subassemblies is sized for the holes in this region of the lower support plates. These holes are smaller than those provided for core and inner radial blanket subassemblies; therefore, a core subassembly cannot accidentally be placed in an outer radial blanket position.

The radial blanket rods have the same diameter as the axial blanket rods except they are 71.5 inches long instead of 17 inches long and are wrapped with spiral wire. Further, the subassembly contains a complete lattice of 25 blanket rods spaced by lugged grids instead of the hollow lattice used in the axial blankets.

A removable orifice has been inserted into the lower support plate for each outer radial blanket position. An orifice also has been placed in the nozzle of each inner radial blanket subassembly. They have been sized to limit the maximum temperature of the uranium alloy to 950 F.

Table III summarizes core and blanket design characteristics.

D. PARAMOUNT SAFETY CONSIDERATIONS IN DESIGN

The safety consideration primarily involve the core subassembly behavior rather than the behavior of the radial blanket because the core is the major source of reactivity. There are three principal safety considerations in the core design: (1) subassembly movement, which could produce an increase in reactivity; (2) pin movement, which could produce an increase in reactivity; and (3) fuel pin hot spots caused by coolant starvation or pin movement.

1. Protection Against Subassembly (Wrapper Tube) Movement

The most important considerations in the structural adequacy of the core is the maintenance of a negative power coefficient of reactivity. This places restrictions on the types and magnitudes of permissible deformation of the subassemblies.

Because of the physical characteristics of the reactor, the heat generation in the enriched uranium pins of the subassemblies varies in the radial direction. More heat is produced in the fuel pins closer to the center of the core than in those nearer the edge; therefore, in the core subassemblies, coolant passing the fuel pins closer to the core centerline will become hotter than coolant passing the fuel pins closer to the core edge. The temperature of the square subassembly wrapper tube is roughly the same as the temperature of the coolant in its immediate vicinity, since the heat produced in the tube walls is negligible when compared to the heat produced in the uranium pins. The differential thermal expansion between the innermost and outer-

TABLE III - CHARACTERISTICS OF CORE AND BLANKET

Subassembly Dimensions, inches	Core Section	Axial Blanket Section	Inner and Outer Radial Blanket Section
Cross Section	Square	Square	Square
Outside dimension (1)	2.646	2.646	2.646
Wall Thickness (nominal)	0.096	0.096	0.096
Space between subassemblies	0.047	0.047	0.047
Number of subassemblies or sections (2)	105	210 (3)	531
Element Dimensions, inches			
Shape	Round Pin	Round Rod	Round Rod
Clad outside diameter	0.158	0.443	0.443
Clad Thickness	0.005	0.010	0.010
Uranium diameter	0.148	0.395	0.395
Uranium length	30.5	14	61.75
Pitch (square)	0.199	0.483	0.483
Pins or rods per subassembly	140	32 (3)	25
Section composition v/o			
Uranium	27.3	25.6	40.0
Molybdenum	5.5	1.4	2.3
Zirconium	4.6	---	---
Stainless Steel	17.4	16.5	18.6
Sodium	45.2	56.5	39.1
Heat transfer surface, sq ft	1545	455 (3)	7923
Uranium alloy composition	U-10 w/o Mo	U-3 w/o Mo	U-3 w/o Mo
U-235 enrichment, weight per cent	25.6	0.35	0.35

NOTES

(1) Does not include the spacer pads.

(2) There are 105 core, 32 inner radial blanket, and 499 outer radial blanket subassemblies.

(3) Total for both axial blanket sections.

most tube walls of a subassembly results in a distortion depending on the geometrical characteristics of the subassembly, on the magnitude of the radial gradient to which it is subjected, and on its method of support.

If subassemblies were held firmly at the top and at the bottom, and if clearance, i.e., no intermediate spacer, existed between adjacent subassemblies, the radial temperature gradient would cause the core region of the subassembly to bow toward the center of the reactor, until the clearance between subassemblies was eliminated. The resultant compacting of the core fuel would result in a reactivity increase.

To prevent this, closely toleranced spacers are attached at the outside of the subassemblies. These spacers consist of an overlay of Colmonoy metal applied by the oxyacetylene method at the four corners of the subassembly wrapper tube, as shown in Figure 5. The overlay is ground to close dimensions in the final step of subassembly fabrication.

Full contact between adjacent subassembly spacers at all times from zero power upwards is accomplished by a slight inward offset of the hold-down fingers of the hold-down mechanism. The hold-down plate thimbles radially locate the subassemblies by acting as a socket for the handling head on top of each one. The pitch for the spacing between the cups in the hold-down is less than that for the lower support plate and for the subassembly pads. Therefore, when the hold-down plate is lowered, the subassemblies are gathered to form a tight core. When the reactor produces power, the subassemblies are elastically bent towards the center of the core in an S-shape. This produces, on power increase, a small net expansion of the core and a negative power coefficient of reactivity.

The behavior of the wrapper tube under the effect of the thermal gradient may be seen by reference to diagrams I, II, and III in the top portion of Figure 11. Diagram I represents the element with no restraints. Diagram II indicates the shape the element would take if it were restrained at the top and at the support plates. Diagram III represents the shape taken by the element when restrained at the top, at the support plates, and at the spacer pad when subjected to the radial thermal gradient.

The effect of movement of the support points under the action of the support loads and thermal expansion, as well as the initial offset at the top of the tube, also affect the final deflected shape. The composite action of these factors together with that of the thermal gradient is illustrated in diagrams IV, V, and VI of Figure 11. Diagram IV represents the shape of the tube when cold. Diagram V illustrates the shape of the tube under the action of thermal gradient if the restraints at the support plates and spacer pad were perfectly rigid. Diagram VI represents the actual final shape of the tube under the combined effects of thermal gradient and support movement.

Consideration was also given to whether a tube could undergo a permanent deformation of a degree which would make possible loss of core tightness on reduction to a lower power level. Examination of

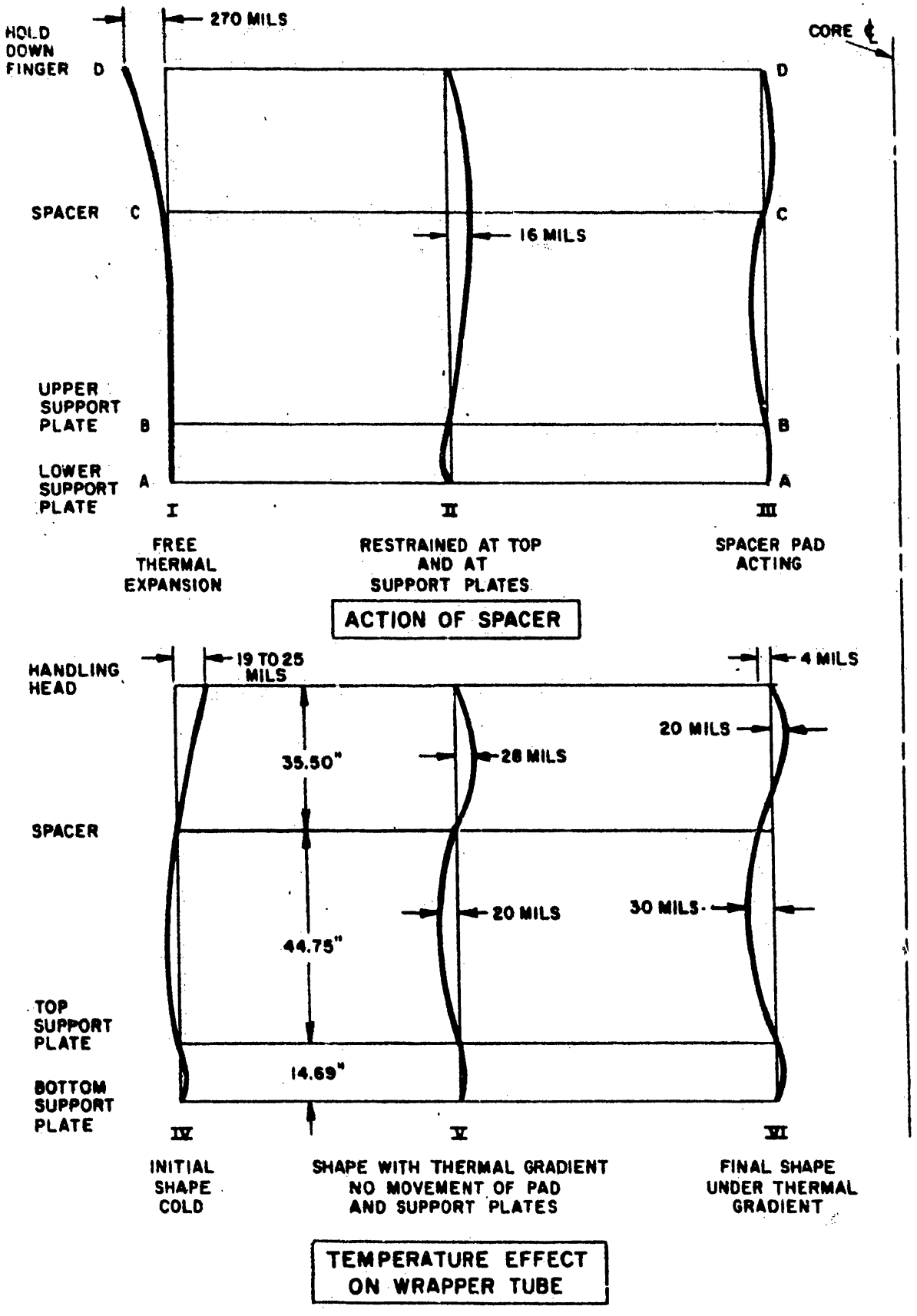

DISTORTION CURVES OF CORE SUBASSEMBLY CAN

FIGURE 11

the geometry of the situation, of the tolerances, and of the magnitude of possible permanent deformations in the portion of the tube at the pad areas where the stress conditions are high and the temperature is relatively high, indicates that there is no possibility of a permanent deformation at a high power level which would be of such magnitude as to cause loss of core tightness at a lower power level.

In addition to the effects induced by the thermal bowing, the wrapper tube is subjected to pressure stresses arising from the coolant flow. Since the coolant flow is upward through the core, these pressure effects are predominant at the bottom of the wrapper tube and are exhibited as a pressure differential between the inside and outside of the tube. As a result of this pressure differential, the tube walls tend to bow outward. In order for such bowing to result in touching of adjacent tube walls, the midpoint of the tube wall would have to be deflected 6 mils with most adverse tolerances, or 23.5 mils for nominal dimensions. However the maximum short-time deflection which will exist is 2 mils. The axial position of the tube where the 2 mils would exist is at the inlet portion or cooler portion of the tube. At the temperatures (600 F) existing at this point and with a stress of 12,700 psi, there is no appreciable creep of the tube material. The pressure differential is lower at the top of the core section of the tube so that the short-time deflection is less than 0.5 mils. The temperature is higher but at the existing stress of 10,000 psi, creep is practically nonexistent. At the spacer section of the tube, the stress is 15,700 psi at 850 F. The elastic deflection of the wrapper tube at this point due to the pressure differential is less than 1 mil. The proportional limit of the material at this temperature is 22,000 psi so that no plastic component exists to increase the elastic deflection. The creep rate at the aforementioned stress and temperature is negligible.

The foregoing figures are for the 0.096-inch ($\pm$0.002 inch) subassembly wrapper. The thickness of the wrapper has been reduced locally (minimum 0.084 inch) to produce a straighter wrapper. The maximum stress for the 0.084-inch wrapper is 17,600 psi which, since it is below the proportional limit, is a satisfactory stress level.

2. Protection Against Pin Movement

The method used to fix the position of the wrapper tube, as discussed in the previous paragraph, provides adequate protection against undesirable movement of the wrapper tube. Since the wrapper tube is stiffer than the fuel pin assembly, the gross fuel pin movement will follow the gross movement of the wrapper tube as long as the fuel pins are firmly coupled to the tube.

As mentioned previously, the fuel pins are maintained in a square pitch in the wrapper tube by a spacer system of honeycomb grids positioned every 1-7/8 inches along the axis of the fuel pin bundle. It is vital that this spacer structure be incapable of excessive lateral movement within the wrapper tube since independent spacer structure movement would produce a movement of the pin bundle within the tube. The possibility of independent grid structure movement is prevented by confining the grid structure to one corner

of the wrapper tube. Three of the corner rods that connect the honeycomb grids are equipped with ferrules which touch the walls of the tube. The grid structure is maintained in its position in one corner of the wrapper tube by screws threaded through the opposite corner of the tube and pushed against the adjacent corner grid tie rod (Figure 9). The strength of the screw threads and the strength of the tie rods proper preclude, in a positive manner, the movement of the grid structure within the wrapper tube.

The slots in the Type C restraining grids provide an elastic spring support of the fuel pins in the grid. With this type of spring support, the elastic deflection of the fuel pins under transverse thermal gradients, and the column action induced by the partial frictional constraint to axial expansion will be sufficient to move the fuel pins only 0.0005 inch laterally, a value too small to adversely affect gross reactivity. The 0.0005-inch movement is based on the nominal grid arrangement. Enough thermal bowing of the fuel pins to cause the pins to touch would require either that the elastic supports were at least 13 inches apart (compared to the nominal 3-3/4 inches), or that the coefficient of friction at the grid dimples be over 32. Thus the failure of a very large number of dimples throughout the core, or welding of the fuel pins to a very large number of dimples throughout the core, would be required for freedom of pin movement within the support grids.

Calculations indicate that lateral thermal and hydraulic gradients across the fuel pins could impose loads as high as 0.5 pounds on the dimples of the support structure. Since these dimples were designed to take loads between 3.5 and 5.0 pounds (these design values were confirmed by test), the dimples are strong enough to restrain the fuel pins.

3. Protection Against Fuel Pin Hot Spots

There are two basic causes of fuel pin hot spots: maldistribution of coolant or warping of fuel pins.

Engineering tests on coolant flow have shown that adequate provision has been made for proper coolant flow distribution throughout the core subassemblies. Tests to be described in another section show the distribution obtained.

Clumping would arise if, under thermal, hydraulic, and irradiation effects, the transverse deformation of neighboring pins were large enough to cause them to touch. A series of tests were run which indicate that clumping is unlikely. These tests included a prolonged study of normal flow forces (endurance test), tests on the effect of phase changes (thermal cycle tests), and tests on longitudinal pin movement (galling tests). These tests are discussed later.

A reference core subassembly with all new depleted-uranium pins has undergone a 1-month isothermal sodium endurance test. The flow was 230 gpm and the temperature was 1100 F. The subassembly was in good condition after the test and showed no evidence of pin warpage.

IV. FUEL FABRICATION

A. ASSEMBLY OF COMPONENTS INTO A CORE SUBASSEMBLY

1. Inspection and Handling

Each core subassembly consists of four main components: (a) the handling head and upper axial blanket unit, (b) the wrapper tube, (c) the fuel pins and supporting structure, and (d) the lower axial blanket combined with the nozzle-strainer assembly. These four components were first assembled individually and then assembled together forming the complete core subassembly.

Handling procedures and requirements were as stringent as during fabrication of the component parts. Clamping and positioning fixtures were used to provide proper alignment during welding operations and, when necessary, during other joining and assembly operations. As component parts were fabricated, they were thoroughly cleaned and bagged or otherwise protected against contamination. Personnel were required to wear lint-free, throw-away-type gloves when handling finished and cleaned parts. Storage of components prior to final assembly was done in areas designated as clean areas where personnel and material access was controlled. Precautions were taken to minimize air-borne contamination in the form of dust and fumes containing oil vapors and particulate matter. Storage racks and containers were used to further protect the components and also to provide for a neat, orderly flow of material during the assembling process.

2. Assembly of Wrapper Tube

Although each section of wrapper tubing was inspected and accepted by PRDC inspectors at the tube mill, they were reinspected upon receipt by the fuel fabricator. The four Colmonoy spacer pads were then applied in their proper location to the tube corners; the tubing was inspected for dimensional requirements and cleaned. Deposition of the Colmonoy was accomplished by fusion welding which necessitated a post heat treatment of the tubing to relieve any residual stresses. The spacer pads were machined approximately to size with slight excess stock remaining sufficient for the light grinding of the pads, the final machining operation, to achieve the desired close tolerances.

Four slots were machined into the top end of the tube to receive and locate the handling head and upper axial blanket unit. This unit consists of a handling-head weldment and a blanket-retaining grid assembly. Sixteen axial blanket elements were positioned within the unit, which was welded to the handling head weldment. The weldment was made up of the handling head or lug, collar, collar retaining ring, blanket element support grid, and four grid support bars. The grid support bars serve also as the upper camming surfaces for the subassembly.

The handling head and upper axial blanket unit fits within, and is

welded to the upper end of the wrapper tube so that the four grid support bars are positioned in proper alignment with the four tube slots. As with all welding employed in constructing the subassembly, a sequential or programed technique was used to maintain dimensional stability of the welded parts.

The upper end of the tube was machined to provide the upper orientation camming surfaces and then machined to its required length. The unit was cleaned, inspected, given a dimensional check, and was then ready for loading of the fuel pins and supporting structure.

Each fuel pin support structure, shown in Figure 6, was assembled by hand using detailed drawings as pictorial guides in positioning and orientating all of the components in their proper location. Any one structure was assembled complete from start to finish by one individual, or assembler, who was required not only to recheck the location of each component as it was assembled, but also to inspect each component in the completed assembly. The units were then completely inspected by a supervisor and again by a representative of the customer. Finally, the units were completely inspected upon receipt at the fuel fabricator's plant. It was required that units duplicate exactly the pictorial representation depicted in the assembly drawings.

Each component of the support structure itself was thoroughly inspected. If a component did not meet specifications, it was destroyed to prevent its inclusion with acceptable components. For example, each cell of each grid was inspected with the aid of an optical comparator at 20X to determine cell dimensions and dimple configuration. If the image on the comparator from any one cell did not fall within the prescribed maximum and minimum tolerance limits, the entire grid was rejected and immediately destroyed. No grid cells and dimples were checked by contact gages, since such gages would tend to deform the dimples and would not indicate true dimensions.

3. Assembly of Fuel Pins and Supporting Structure

As a result the support structure was received by the fuel fabricator as a complete unit ready for loading of the fuel pins. All handling and storage of the units was performed within the clean area designated for the final assembly of all components. This clean area was a totally enclosed group of connecting rooms all supplied with clean air under a slight positive pressure.

A hydraulically operated loading device was used to insert the fuel pins into the support structure. The loading device consisted of two main units: a clamping and vertical indexing unit for the support structure and a support rack and loading ram unit for the fuel pins. Fuel pins, sufficient for a complete horizontal row within the grids were laid on the support rack; an anchor bar was inserted through the slots of the fuel pin end caps; and then the entire row of pins was inserted into the support structure. Before the next row of pins was inserted, each pin, after insertion, was inspected for spacing, proper gripping by the dimples of the birdcage grids, and surface condition.

The inspection required that the pins not show any signs of galling after insertion into the grids and that they be firmly gripped by the grid dimples. The unit was indexed an amount equal to the grid spacing, and another row of fuel pins was inserted and inspected. This process was repeated until the entire support structure was loaded with 140 fuel pins.

The support structure was initially loaded with dummy or steel leader pins which have a diameter slightly less than that of the fuel pins. The leader pins touch the dimples of the birdcage grids but exert only contact pressure. The bottom end of each leader pin is countersunk and shaped to fit the pointed end of the fuel pin. When the fuel pins were loaded into the support structure, their pointed ends mated with the bottom of the leader pins and displaced the leader pins uniformly through each grid cell. This technique provided straight-through alignment of each grid cell and uniform bearing pressure of the grid dimples against the fuel pins during the loading process.

When the support structure was completely loaded with fuel pins, the anchor bars were locked into position by individual keeper bars. The two remaining side plates of the anchor collar were welded in place, preventing any movement of the ends of the fuel pins. The anchor collar itself then had four side tabs which were subsequently welded to the lower axial blanket unit and nozzle strainer unit. Full longitudinal surface support was provided during all handling to prevent distortion of the assembled and loaded support structure.

4. Assembly of Lower Axial Blanket and Nozzle-Strainer Unit

The lower or nozzle end of the subassembly was assembled as a separate component, consisting of a lower cam casting, a strainer, and a nozzle tube formed of two concentric sleeves separated by a helical spring. The lower cam casting permits the attachment of the round nozzle to the square wrapper tube and also contains the lower orientation cam fingers. The strainer provides additional assurance against plugging of the subassembly by discrete particulate matter contained within the sodium coolant. The sodium is otherwise filtered and cold-trapped, and particulate matter is not expected to be present. The nozzle acts as the coolant entrance to the subassembly and serves to position the subassembly within the reactor core lattice.

The contacting or mating surfaces of the two concentric nozzle sleeves is limited to two areas which are provided with wear resistant surfaces. The inner sleeve has spray welded deposits of Colmonoy No. 4, and the outer sleeve is nitrided all over. After the inner nozzle sleeve was inserted within and welded to the lower cam casting, the Colmonoy surfaces were accurately machined to provide the desired concentricity requirements. The inner sleeve was aligned with respect to the machined top surface of the lower cam casting so that over-all straightness is assured when the wrapper tube is welded to the casting.

An Inconel-X spring was next inserted over the inner nozzle sleeve and the outer sleeve inserted over the spring. Both sleeves contain machined shoulders for seating of the spring ends. The bottom

end of the inner sleeve fits through and was rolled against the bottom end of the outer sleeve with the spring compressed to a preload value of 380 pounds.

The strainer, a welded assembly of Type 304 stainless-steel plate containing numerous punched holes and a threaded support collar, was screwed into the lower cam casting opposite to the nozzle and was seated against the upper end of the inner nozzle sleeve. The threads were staked in place through each of four holes drilled into the sides of the cam casting. Sixteen axial blanket rods, four on a side, were positioned between two sets of blanket-retaining grids. (One set is attached to the cam casting, and one set attached to four tie rods.) The bottom end of the tie rods was welded into holes drilled in each corner of the cam casting, thereby securing the lower axial blanket unit to the nozzle and strainer assembly.

There are now three separate components ready for assembling as a fuel subassembly: (a) a wrapper tube with a handling head and upper axial blanket, (b) a support structure loaded with fuel pins, and (c) a lower axial blanket and nozzle-strainer unit.

5. Final Assembly

Two design features assure rigid placement of fuel within the wrapper tube: (a) The support structure is pinned, at its anchor collar, to the wrapper tube. (b) A series of seven locking screws with Colmonoy No. 4 tips are located along one corner of the wrapper tube in line with the long leg of the lower orientation cam and corresponding to the seven fuel pin grids, which have a nitrided sleeve at their corner. The lower axial blanket and nozzle-strainer unit, was inserted within the wrapper tube and a closure weld made where the bottom of the wrapper tube contacts the lower cam casting. Adjustment for over-all subassembly length was made during fit-up of this joint prior to making the final closure weld. The locking screws were inserted in drilled and tapped holes along the wrapper tube corner, tightened against the nitrided grid sleeve with a specified torque, locked in place by both staking and tack-welding and dressed off to blend into the outer corner surface of the wrapper tube. All welding was performed in a manner that prevents distortion of mating parts.

The fuel subassembly was then put into a special checking fixture, which held the subassembly in a vertical position and supported it in a manner identical to that within the reactor. All dimensional requirements were checked and the finish grinding requirements established for the wrapper tube spacer pads. The subassembly was removed from the checking fixture and positioned in a horizontal grinding device for completing the spacer pads. The light grinding of the spacer pads to achieve the close tolerances desired was the only fabrication operation, other than the final closure weld on the clean wrapper tube containing clean fuel and blanket elements.

The completed subassembly was given a final inspection in the special checking fixture; inserted within a polyethylene bag, which is alternately evacuated and purged with dry nitrogen; and then hermetically sealed. The bagged subassembly was placed in a specially

constructed and shockproof container and shipped to the plant site.

6. Assembly of Radial Blanket Subassemblies

The operating temperature and loading conditions imposed upon the radial blanket subassemblies permits a less complex design for their hardware components than that for core subassemblies. This, coupled with fewer components, greatly facilitated their assembly although they were assembled with the same care as the core subassemblies.

A loading fixture was used to position and support the radial blanket elements and the lower component (blanket retaining grid, cam casting and nozzle unit) so that the upper component (handling head and wrapper tube unit) could be placed over the axial blanket elements. This operation was done in the vertical position, as was the final closure weld at the intersection of the wrapper tube and the cam casting. The loading fixture permitted checking of the subassembly for concentricity and length requirements.

Since there are no spacer pads on the outer radial blanket wrapper tubes, no machining operations were performed on the subassembly subsequent to the final closure weld. The inner radial blanket subassemblies have the spacer pads attached and are machined similarly to core subassemblies.

Packing and shipping of the radial blanket subassemblies and acceptance at the plant site was conducted in the same manner as for the core subassemblies, except that three radial blanket subassemblies are shipped in one container, whereas only one core subassembly is shipped in a container.

B. FABRICATION OF CORE AND BLANKET ELEMENTS

1. Reduction of UF_6 to Metal

The enriched (25.6%) uranium and depleted (0.36%) uranium were obtained as UF_6 from ORNL. Chemical and isotopic analyses of the UF_6 were performed by ORNL. The processes for reduction of UF_6 to metal are nearly identical for both enriched and depleted uranium.

The UF_6 was directly converted to UF_4 in a reaction chamber in batches of 300 pounds. After passing through a blender, the green salt (UF_4) was sampled for isotopic content. A homogenous mixture of green salt and calcium was compacted and sealed into MgO_2-lined graphite crucibles. The sealed crucibles were placed into a controlled induction-heated furnace and were heated to the ignition temperature of calcium. Upon completion of the reaction, the crucible was allowed to cool and the derby was removed from the crucible. Each derby was permanently identified, pickled in nitric acid, sampled, inspected for surface condition, and weighed. The depleted UF_4 was reduced to metal derbies of approximately 300 pounds each, whereas the enriched UF_4 was reduced to metal derbies of approximately 10 pounds each.

Approximately 35 grams of drill chips were taken from each enriched metal derby to be used as samples for chemical and isotopic analyses. To insure that the samples were representative of the entire derby, the drill was made to penetrate halfway into the derby at two separate random locations on opposite sides. The chips from the individual derby samples were cut up into a large number of small pieces after which the samples from 6 to 10 derbies were blended into a composite sample. Samples from depleted uranium derbies were obtained as chips from saw cuts, and the chips from two derbies were blended to form a composite sample. The composite samples were divided into three aliquots: one for the use of the metal reducer, one for the use of the fuel fabricator, and one for use as a referee sample. Each composite sample was analyzed by the metal reducer for impurities. The allowable impurity content of the enriched metal was as follows: boron, 10 ppm; carbon, 100 ppm; copper, 75 ppm; iron plus nickel, 250 ppm; nitrogen, 75 ppm; oxygen, 400 ppm; chromium, 300 ppm; calcium, plus silicon, plus aluminum, 250 ppm, and zirconium, 100 ppm.

The major process controls used by the metal reducer to insure product quality were:

a. Controlling use of UF_4 slag in the metal reduction step.

b. Controlling temperature of furnace for the reduction.

c. Pickling the surface of each derby to remove slag.

d. Use of high-purity process chemicals and reagents.

To establish confidence in the process controls used during derby production, experimental runs with depleted uranium were conducted, and the end product was sampled to determine its quality. Fifteen hundred pounds of depleted uranium were processed in exactly the same manner as the enriched uranium. This material was subsequently used by the fuel fabricator in the fuel fabrication qualification run. In addition, fifty of the initial enriched derbies produced were randomly selected, broken, and inspected for slag entrapment. There was no evidence of slag in any of these derbies.

The depleted uranium and enriched uranium were processed and identified in a manner that allowed each derby to be traced back to an individual batch of UF_6. The quality of the derby, impurity content, and accountability history records were recorded under each derby identification number.

2. Alloying of Core Material

The quality of the alloyed casting is dependent upon good practices and experience. To insure a high material yield, each casting had to have minimum impurity content, minimum shrinkage cavity, minimum porosity, and clean surfaces. During the qualification trial run, approximately twenty melts were made to establish the proper casting procedures and to train personnel. Acceptance of an alloyed casting for processing was based upon a surface inspection and results of an

impurity analysis. All pertinent information on material history was recorded including time, temperature, electrical power to the induction heating coils, source and quantity of material used, and operation sequence.

The charge for each melt contained molybdenum pellets, usually 30 per cent recycled alloyed uranium scrap, and about 70 per cent unalloyed uranium derbies. The chemical composition, weights, and source of the various materials charged to the melt were recorded. Each melt weighed approximately 150 pounds and produced a casting about 4 inches in diameter and 19 inches long, which yielded approximately 250 core elements.

The scrap used in melting was obtained from previous processing steps and was in the form of solids or fine particles. The solid scrap was obtained from primary and secondary extrusion end defects and from rejected fuel elements. Rejected core elements were sheared into four 6-inch lengths, and the clad was chemically removed for subsequent uranium melting. The fine scrap particles were obtained from machine turnings and sawing operations. These particles were degreased and compacted by a forging press into solid wafers weighing 4 to 6 pounds. The origin and identity of all scrap was recorded to insure that its addition to a casting did not result in excessive impurities.

Materials used in a given melt were weighed to the nearest 0.1 gram to insure that the molybdenum content was held within specified limits. Furthermore, each melt was mechanically stirred to assure complete melting of the molybdenum pellets and to obtain a uniform dispersion of molybdenum. Prior to melting, the materials charged to the crucible were dispersed within the crucible, except for the molybdenum which was placed at the bottom of the crucible.

The melting and alloying was performed in an induction-heated vacuum furnace, and the melt bottom poured at a temperature of 1350 C. The ingot was allowed to cool in a vacuum for a minimum of three hours. Upon removal, each ingot was stamped with an identification number, dipped into a dilute nitric acid bath, and subsequently wire-brushed to assure cleanliness. The porosity in the ingot hot top was removed at a later step when the extrusion ends were cropped.

The crucible and molds used were made of graphite, which was coated with a zirconia wash and degassed prior to use. The mold position in the furnace and the mold thickness were adjusted to minimize and control the amount of shrinkage at the top of the ingot. At the bottom of each mold, a 1-inch-diameter by 3/4-inch-length well was provided for sampling. The sample was sawed from the ingot face and a 1/4-inch-thick sample used for impurity and isotopic analyses; the remaining portion of the sample was stored.

3. Initial Extrusion of Core Alloy Casting

Since the cast ingot must be reduced to a size suitable for coextrusion, an initial primary extrusion step was required. The ingot and canning surfaces were cleaned with acetone prior to assembly.

Alundum slurry was painted on the ingot surface. The ingot was wrapped in a thin copper foil and placed in a mild carbon steel can the end of which was welded closed. The assembled components were then sized by being drawn through a die; and the other end, with its attached evacuation tube, was welded in place. A vacuum was established through the evacuation tube in the front (as related to extrusion direction) end of the assembly. The surface was heated to 800 F with an acetylene torch to degas the assembled components. Upon completion of degassing, the evacuation tube was sealed and severed, and the seal-weld was helium leak-checked.

The sealed assembly was extruded in a 1000-ton horizonal extrusion press at a billet temperature of 1600 F, and at a die temperature of 900 F. The extruded subassembly was straightened by rotation in a sleeve immediately after extrusion and then allowed to cool in air. The primary extrusion reduced the 4-inch-diameter casting to a cylindrical rod 1.5 inches in diameter and approximately 100 inches long.

The jacketing material was mechanically stripped from the extrusion, an identification number stamped near the front end, and the alloyed rod pickled in nitric acid. Both ends of the rod were cut off one or more times until no defects could be visually observed in the alloy. A sample was then removed and metallographically inspected for microscopic defects and inclusions. If any defects were observed, additional cropping and inspection was continued until all defects were removed. The length of defective portions of a primary extrusion averaged approximately 12 inches. A 30-gram sample was taken from the nose end of the extrusion for molybdenum content analysis. The extruded rod was cut in approximately four-inch-length billets.

4. Coextrusion of Core Alloy Billets

Each billet was machined to a smooth surface and to close tolerances. A special carboloy tool bit was used. The machine-turning chips from each ingot were identified and returned to storage for subsequent remelting. The machine billet was tagged to identify it with the ingot number and its position relative to the front end of the extrusion. The machined surfaces were visually inspected for defects (cracks, pits, spots not machined, etc.); and length, weight, and concentricity measurements were made. Wherever defects were found, the billet surface was repaired by blending it into a smooth surface. After inspection, each billet was thoroughly cleaned with water and detergent.

The machined, alloyed uranium billet was placed inside a tight-fitting reactor-grade zirconium sleeve. Then the sleeve with billet was assembled into a mild carbon steel jacket with copper-nickel nose and tail inserts between the end of the billet and the carbon were thoroughly cleaned with acetone prior to assembly except for the zirconium sleeve which was pickled in acid. The history and impurity analysis of the zirconium tubing were recorded in material history records. After the assembly was sized through a die, the end piece with its evacuation tube was seal-welded in place. The assembly was then evacuated, heated to 800 F with an acetylene torch to degas it, the evacuation tube severed,

and the seal welds helium leak-checked. If a leak was found, the billet was rewelded and rechecked. The billet was then heated in a furnace to 1600 F and held at this temperature no longer than 1-1/2 hours prior to coextrusion by a 300-ton press. In the process of coextrusion, the rod diameter was reduced from 1.5 inches to 0.310 inch. The jacketed rod was hand straightened shortly after extrusion, air-cooled, the steel jacket removed chemically, and the rod rinsed in deionized water. For both the primary extrusion and the coextrusion, data were recorded on ram speed, extrusion temperature, time, and pressure; and these data were made part of the material history.

5. Production of Core Pins

The 10-foot-long extruded rods were subjected to rotary cold swaging to obtain a good surface finish and further reduction in diameter. In eight passes, the rod was swaged from 0.310 inch diameter and 10 feet long to 0.158 inch diameter and 26 feet long. The diameter at various points along the rod length was checked during each swaging reduction with frequent changes made in the swaging dies to insure good surface quality. The swaged rod was cut with an emery cut-off wheel into 30.5-inch lengths. Samples for metallographic, chemical, and isotopic analyses were cut under the supervision of PRDC personnel, the location of each sample recorded, and the samples sealed into individual envelopes and forwarded to the respective laboratories for analyses.

The blanked pin identities were maintained by storing pins in compartmented drawers. Each drawer contained one batch of pins from a coextrusion, and a series of drawers maintained the identity of the pins with the ingot.

6. Final Processing of Core Pins

After cleaning, approximately 150 pins were annealed in a vacuum furnace at 800 C for one hour. Pin identity was maintained by logging each pin into a honeycombed graphite block holder used to vertically support the pins in the furnace. A furnace vacuum of one micron was maintained throughout the heating and cooling cycle. Heating and cooling rates were controlled at a rate of 100 C per hour. The temperature was recorded at the furnace baffles, and at three axial positions within the graphite fixture. All charts and logged data are part of the material history.

After heat treatment, the pins were weighed, and one end of each pin was prepared for swaging to a point. The pin ends were heated in air to a temperature of approximately 800 C by an induction-heating coil timed to control the pin temperature. While the pin end was still hot, it was partially pointed and the pin clad ground back to a smooth contour with the uranium alloy. This procedure was used to allow the cladding and uranium to flow at the same rate during the final pointing reduction so as to give a uniform configuration. Pin ends are completely clad except for an approximately 50-mil diameter tip area which is not covered. Each pin tip was visually examined for defects, the tip contour checked with a functional fit gage, and then the entire pin ultrasonically inspected. The ultrasonic test was completed on

part of the pins prior to swaging.

Zirconium caps, which were drilled to the pin end contour, were slipped over the ends and cold swaged to the pin. The caps are locked to the pin by a dog-bone-shaped interference fit, which is formed in the pin during cold swaging of the specially designed cap. Although only a few pounds of holding force are required to hold the pin, tensile loads of 500 pounds at room temperature were required to separate the cap from the pin. Each end-cap was X-rayed at 90-degree positions to insure a proper locking angle and a gap of not more than 3.0 mils between the cap and pin. An end cap with a known 2.7-mil gap was used for a comparison X-ray standard. All end-capped pins rejected for other causes were examined metallographically to check the condition of the pin ends internally for cracks in the clad alloy and end-cap fit. Each end-cap is permanently marked to identify the element with the material history records. The final inspection of the pins included visual examination of surfaces, a diameter check, and a straightness check. Upon completion of this inspection, pins meeting all specifications were cleaned and stored in containers holding 140 pins to later be assembled into the subassembly structure. All rejected elements at the time of rejection were placed into special containers and sheared into short lengths for remelting.

7. Melting and Alloying of Blanket Material

The melting and alloying of depleted uranium produced ingots of 150- and 1600-pound sizes. Approximately fifty per cent of the blanket subassemblies contain material fabricated from 150-pound ingots. The 150- and 1600-pound ingots were processed in a similar manner except that the 150-pound ingots required only a single extrusion step and no swaging operation, while the 1600-pound ingots require two extrusions and a swaging operation. The melt charges for a 1600-pound ingot were from material which contained approximately 40 per cent recycled scrap in the form of scrapped slugs, hot tops, and extrusion tips. The remaining charge was composed of 300-pound depleted derbies plus powdered molybdenum. A vacuum induction furnace, bottom poured at 2500 F and utilizing a graphite crucible and mold with zirconate and magnesia wash, respectively, was employed. After pouring, the furnace was back-flushed with helium, to facilitate cooling. The resultant ingot was approximately 8.5 inches by 42 inches. The ingot hot top was removed and cut in half. A complete analysis was made of impurities from samples taken from the top and bottom of each casting. The surface of each casting was machined for extrusion.

The 150-pound ingot process was based on melting and alloying of castings the same size as used in the enriched uranium production. The casting surfaces were pickled and not machined. The extrusion billet was similar to the one in the enriched process except that it was jacketed in a copper can and its nose piece was not tapered. The extrusion billet length ranged from 10 to 20 inches.

8. Extrusion of Blanket Ingots

The 150-pound ingots were reduced from an ingot diameter of 4

inches to a rod diameter of 0.430 inch in one extrusion step using a 1000-ton press. The 1600-pound ingots which were cut in half, were stamped and extruded from 8.5 inches to 0.430 inch in two extrusion steps using a 2400-ton press. In the first step, the 8.5-inch by 20-inch primary billet was heated to 1650 F in a salt bath and extruded to a 3.5-inch by 10-foot rod. The rod was cut into 5-1/2 inch lengths which were shot blasted and hand ground to remove all scale. These lengths were heated in a salt bath and extruded at 1500 F to a 0.430 inch diameter, and immediately cooled by being ejected into a water-cooled jacket at the extrusion die exit. Following this indirect quench, the rod was quenched from 400 F to room temperature in a water tank. The 0.430-inch extruded rod was stamped near the nose on the extrusion for identification, cut in two places, bundled, weighed, and stored. The extrusion butts and scrap were used for subsequent remelting.

9. Reduction of Blanket Material to Final Size

The 12- to 16-foot-long extrusions were cut to 57-inch lengths and the ends stamped with the same numbers as used on their parent rods. Wafers 1-1/16 thick were also cut to be used for a check on molybdenum and carbon content. The rods were degreased with acetone and pre-annealed in a vacuum furnace at 850 C ± 15 C for 1/2 hour. The rods were supported in the furnace in an Inconel pipe, the inside of which was molybdenum lined and the outside coated with Al_2O_3. Except when materials were being degassed, a pressure of one micron was maintained throughout the heating cycle. Heating and cooling each required a minimum of 2 hours with a total heat treatment cycle of 5 hours.

The pre-annealed rod surfaces were lubricated and the rods reduced to 0.410-inch diameter in one or more passes through a swager. If surface cracking was observed during the second or third passes, the rod was re-annealed at 850 C for one-half hour.

The swaged rods were degreased in acetone and re-annealed in a vacuum furnace at 850 C for one hour at an absolute pressure of one micron. Approximately seventy 62-inch rods were heat treated in one furnace loading. The cycle required 24 hours. Approximately 4 hours were required to heat to 850 C and 6 hours to cool to 500 C. The rods were not removed from the furnace until room temperature was attained. A furnace profile study showed that the temperature did not vary more than ± 15 C throughout the furnace, as required by specification.

When necessary, the annealed material was passed through a straightener. The rods were then cut into 15.44 ± .05-inch lengths and an identification number recorded on the cut face. These lengths, referred to as slugs, were hand straightened on an arbor press to a bow less than 0.004 inch as determined by the use of parallel plates. The slugs were ground on a centerless grinder to a final size of 0.395-inch diameter and inspected. The slugs were processed in lots of 150 to 180, and 25 slugs from each lot were inspected for diameter, length, and surface. If one slug was rejected, all slugs in that lot were inspected. Then all the slugs were inspected for surface defects, straightness, and proper identification. Each slug was ultrasonically tested, cleaned, weighed to the nearest 0.1 gram, and stored in a dry

box for subsequent bonding.

The 150-pound ingot process did not require swaging prior to grinding since the 0.430-inch size included a copper jacket. The rod was cut to final lengths of 5-3/4 inches and 14 inches, annealed at 850 C for 1 hour, and ground to a final diameter of 0.395 inch. The grinding removed the copper jacket and a small amount of uranium alloy. Other handling was similar to that for the 1600-pound ingots.

10. Sodium Bonding and Assembly of Blanket Rods

Preparation for assembly of blanket elements was begun by degreasing end-caps and stainless-steel tubing. The lower end-cap was then semiautomatically welded by heli-arc. All welds were helium leak-checked. One tube per hundred tubes welded was selected by the PRDC resident inspector for destructive metallographic examination to determine whether proper weld penetration had occurred. The weld was required to penetrate 10 per cent into the base material of both upper and lower caps. Additional samples of the upper and lower caps were tensile tested. They were required to withstand an axially applied load of 315 pounds.

Three of the five slugs that constitute the final blanket element were inserted into an end-capped tube. These assembled units were placed in a retort which was evacuated, filled with argon at one atmosphere, heated to 500 F, and liquid sodium inserted into the tube. The sodium was kept in an inert atmosphere at all times and was filtered prior to insertion into the tubes. The remaining slugs and a sleeve insert which is used to keep the uranium below the sodium level at all times were inserted into the tube. The retort was cooled and the end caps automatically welded. For welding, a 2 per cent thoriated tungsten electrode and argon shield were used. The sealed elements were removed from the dry box and a permanent identification stamped on their upper end-caps so they could be identified with their respective material histories. During the assembly, the identity of each slug and its position in the tube had also been logged. The elements were placed in a furnace and heated to 1000 F for a minimum of 1 hour to insure wetting and removal of voids in the sodium annulus.

The final weld on the upper end-cap was metallographically examined and tensile tested in the manner previously discussed. Each upper end-cap was helium leak-tested in a retort. Following the leak test, the elements were cleaned. Each element was then eddy-current-tested and inspected. The diameter of the end-cap weld was measured, and the surface of each element was inspected for dents and scratches. Fifteen per cent of the elements were inspected with a snap gage for length, slot width of end-cap, and tube diameter at three positions. If any element inspected on a sample basis was rejected, the entire batch of 25 elements was inspected.

The spiral wire was welded to the end cap, wrapped on a 9-inch pitch, and welded to the opposit end cap. The pitch and the tension on the wire wrap are determined by the wrapping fixture. Looseness of the wire was cause for rejection. The end cap welds and the spiral wire welds were die-checked for imperfections and cleaned with alcohol

after inspection. A final inspection of welds, location of the spiral wire, surface defects, and proper spiral pitch was conducted prior to storage or assembly into the structural components.

Axial blanket rod fabrication was similar to that for the radial blanket except that the total length was much shorter and the spiral wire was not required.

/

V. NONDESTRUCTIVE TESTING OF CORE A FUEL AND BLANKET ELEMENTS

A. INTRODUCTION

Stringent specifications were established on Core A fuel and blanket elements and element components. Rigorous quality control measures - especially, sensitive and dependable nondestructive testing (NDT) techniques, were required to ensure that the fabricated elements met the design specifications.

1. NDT Development

When no proven, off-the-shelf nondestructive tests were available for testing the Core A elements and element components to the required specifications, the fabricators generally had little capability for, or interest in, accepting the responsibility for developing testing techniques. Thus APDA and PRDC assumed the responsibility for developing these special tests, engineering and fabricating reliable production test equipment, establishing test standards, correlating instrument and destructive test data, and training the fabricators' quality control personnel in the operation and interpretation of the tests.

Contracts for laboratory feasibility studies for some of the required tests were performed by Argonne National Laboratory (ANL) and Metals and Controls Nuclear (M&C). These organizations were chosen primarily because of ANL's experience in testing the sodium-bonded fuel and blanket for EBR-II (similar to Core A blanket) and M&C's experience in testing a coextruded alloy element (similar to Core A fuel).

In order to select calibration standards and to develop a high degree of confidence in the interpretation of test data from the various testing techniques, a large number of instrument data and destructive test data were correlated and recorded on each test before it was accepted for production application. Correlation was continued throughout the course of production testing to verify and refine interpretation of test data.

2. NDT Application

The resulting comprehensive NDT program was critically applied to the inspection of the Core A elements and element components.

None of the tests were performed on a sampling basis--the applicable tests were performed on all units. All scanning-type tests were run over the full length of each unit. And in the case of radiography of end-caps, for example, not one but two exposures were made (at 0 degrees and 90 degrees) on each end-cap to confirm the integrity of

the interlock.

PRDC employed full-time resident inspectors who were intimately faimiliar with the various testing techniques. These resident inspectors were responsible for performing the correlation of test data, training and checking the fabricators' operators in the operation and interpretation of the tests, as well as verifying the fabricators' other quality control responsibilities.

B. SPECIFICATIONS AND APPLICABLE TESTS

1. Fuel Element

The fuel element is nominally a 0.158-inch-diameter by 30.5-inch-long cylinder consisting of a core of uranium, enriched in U-235 to 25.6%, alloyed with 10 w/o Mo, and clad with 0.005 inch of metallurgically bonded zirconium.

The element is fabricated by hot coextrusion and cold swaging. The zirconium anchor and free end-caps are mechanically locked on either end by swaging.

	Pertinent Fuel Specifications		Method of Checking
*1.	Internal defects (including non-bonds, and defects in clad or core)	1/64 in. max. (in any direction)	Ultrasonics
*2.	Cladding thickness (at any point)	0.003 in. (min.) 0.007 in. (max.)	Ultrasonics plus sample metallography
*3.	Cladding thickness (average through any cross section)	0.0045 (min.) 0.0055 (max.)	Ultrasonics plus sample metallography
*4.	Cladding surface flaws	"None" permitted. (Actually, flaws penetrating approx. 0.0005 in. radially are permitted.)	Ultrasonics plus dye penetrant (penetrant method discontinued because of superior sensitivity of utrasonics)
5.	End-cap interlock (gap between I.D. of cap and O.D. of zirconium clad)	Approx. 0.0025 in. (Arbitrated specification)	Radiography (at 0 and 90 degrees)
6.	Total U-235 content (per unit)	± 5.5% relative	Auto-gamma spectrometer

* These specifications were all verified simultaneously with the one ultrasonic test.

2. Blanket Elements

The axial and radial blanket elements are essentially identical except for the difference in length (axial elements are approximately 17 inches, overall; radial elements are approximately 71 inches, overall.)

The blanket elements are nominally 0.443-inch in diameter by 0.010-inch thick stainless-steel tubes, hermetically weld sealed, and containing 0.395-inch-diameter slugs of uranium, depleted in U-235 to 0.35%, alloyed with 2-3/4 w/o Mo, and thermally bonded to the cladding tube with an annulus of sodium.

Each element contains an expansion space between the top of the alloy slugs and the bottom of the upper end cap. This space contains (1) excess sodium for thermally bonding the slugs when they expand longitudinally, (2) an inert gas space to permit expansion of both slugs and sodium, and (3) a stainless-steel sleeve insert to prevent the slugs from ratcheting above the surface of the sodium.

Pertinent Blanket Specifications		Method of Checking
Components		
1. Tubing		
a. Defects in wall	10% of wall thickness (max.)	Hydrostatic pressure (for penetrations and near penetrations) plus Eddy current (for smaller defects)
b. External surface flaws	10% of wall thickness (max.)	Eddy current (substituted for original dye penetrant specification)
c. Internal surface flaws	10% of wall thickness (max.)	Eddy current
2. Bare U alloy slugs		
a. Internal and surface defects	1/32 inch (max.) (in any direction)	Ultrasonics
3. Assembled Elements		
*a. Nonbonds, foreign matter, and non-wet grease in sodium bond	1/32 in. max. (in any direction)	Eddy current

Pertinent Blanket Specifications		Method of Checking
*b. Overall length of slug loading		
(1) Axial elements	nominal ± 1/8 in.	Eddy current
(2) Radial elements	nominal ± 1/4 in.	
*c. Height of sodium over slugs		
(1) Axial elements	nominal ± 1/4 in.	Eddy current
(2) Radial elements	nominal ± 1/2 in.	
4. End-cap weld integrity	No pinholes No leaks ≥ 10^{-8} cc/sec	Helium leak test plus dye penetrant

* These specifications were all verified simultaneously with the one eddy current test. Variations in slug diameters were also easily detected with this same test.

C. DETAILS OF NDT METHODS

Details of some of the more unique of the various NDT methods employed on Core A elements are outlined below.

1. Fuel Element

a. Ultrasonic Test. The special through-transmission ultrasonic technique used in this test requires a very close positioning of the fuel element; drastic and critical collimation of both the energy incident upon, and emanating from, the fuel element; high-gain transducers; and a dynamic couple of recirculating water.

The fuel element is mechanically translated and rotated through a tight-fitting bushing made of teflon. Teflon serves both as a "slick" bearing material and a sound absorber. This bushing has a precisely positioned, small, rectangular collimating slot (about 0.045 by 0.310 inch) machined completely through the teflon. The centerline of the slot intersects and is perpendicular to the axis of the bushing and also to any fuel element being fed through the bushing (Figure 12).

The main axis of the narrow collimator slot is oriented parallel to the axis of the fuel element (1) to minimize variations in signal caused by intermittant reflection of energy induced by the mechanical vibration of the element and (2) to increase the sensitivity of the test to longitudinally oriented defects (the predominate orientation in this extruded and swaged product). See Figure 13.

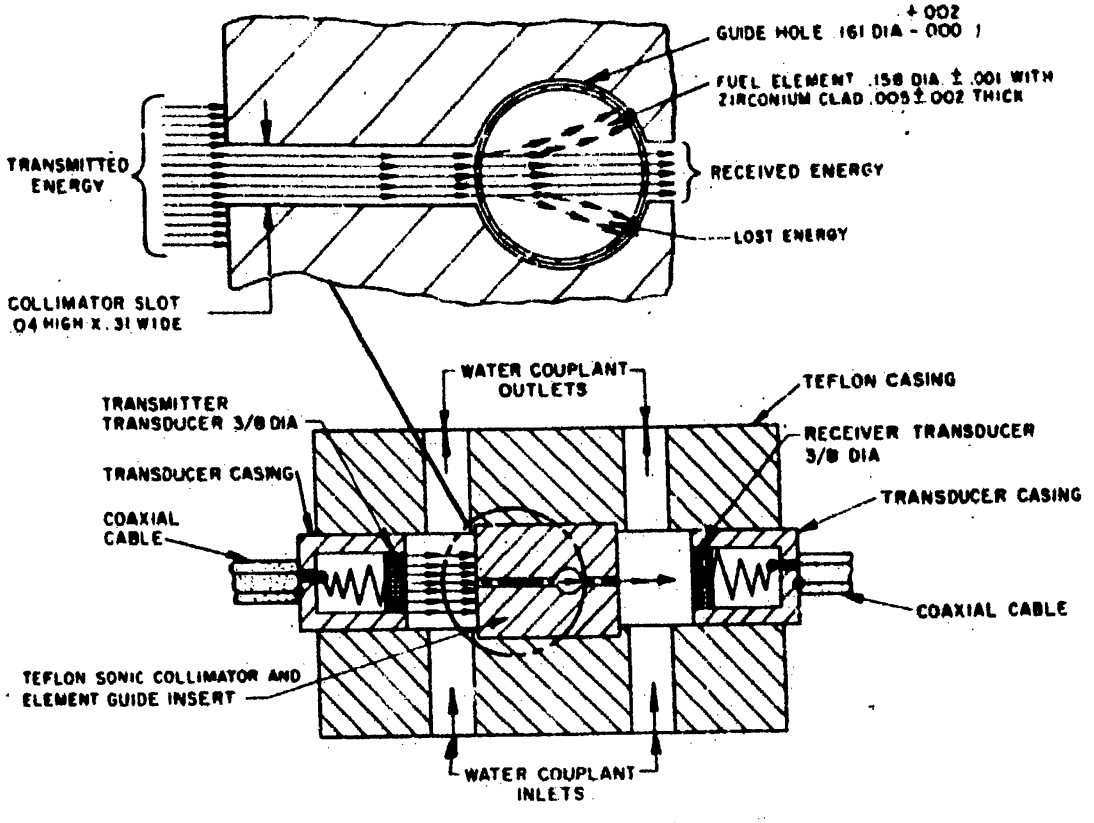

(SECTION THRU SONIC COLLIMATOR AND ELEMENT GUIDE ASSEMBLY)

ULTRASONIC CORE ELEMENT TESTING

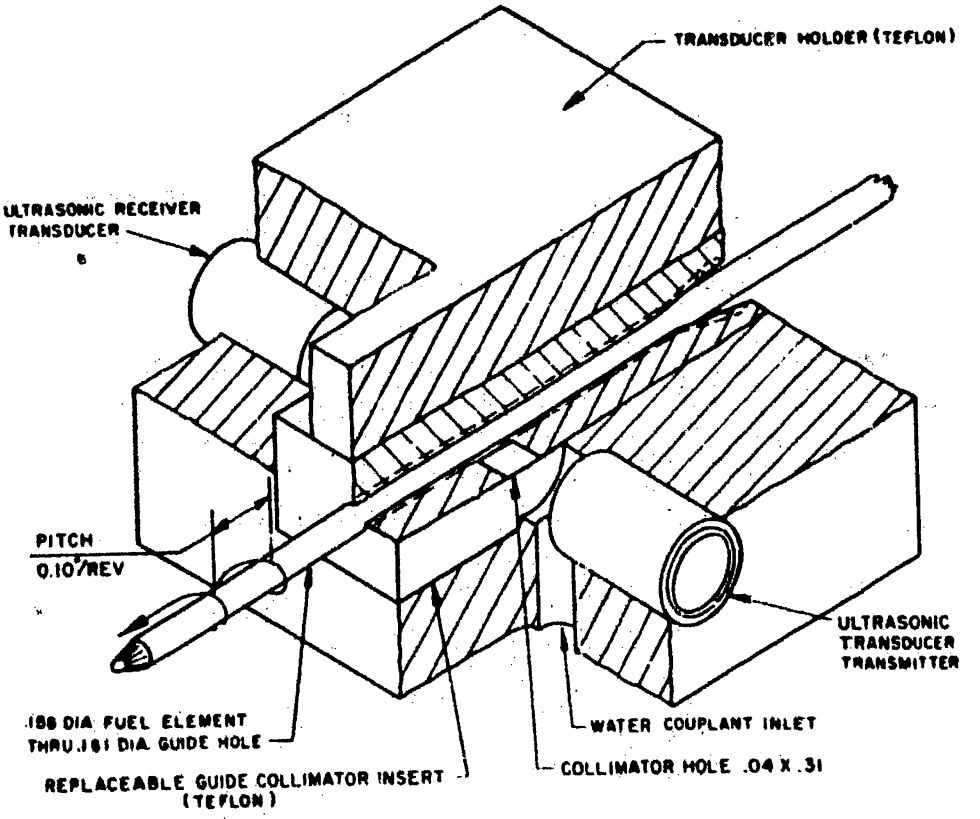

ULTRASONIC COLLIMATOR AND FUEL ELEMENT GUIDE

FIGURE 12

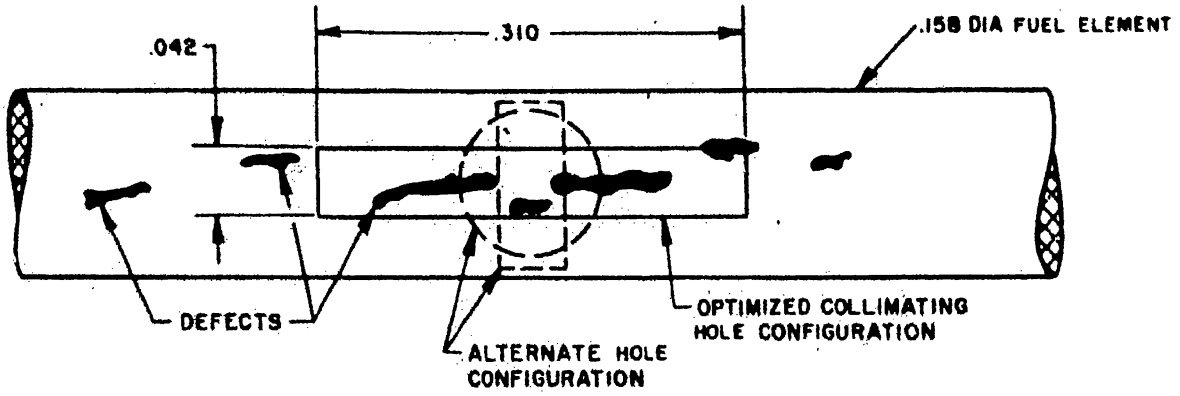

VARIOUS COLLIMATOR HOLE TYPES SHOWN RELATIVE TO TYPICAL ELONGATED DEFECTS IN THE CORE ELEMENTS

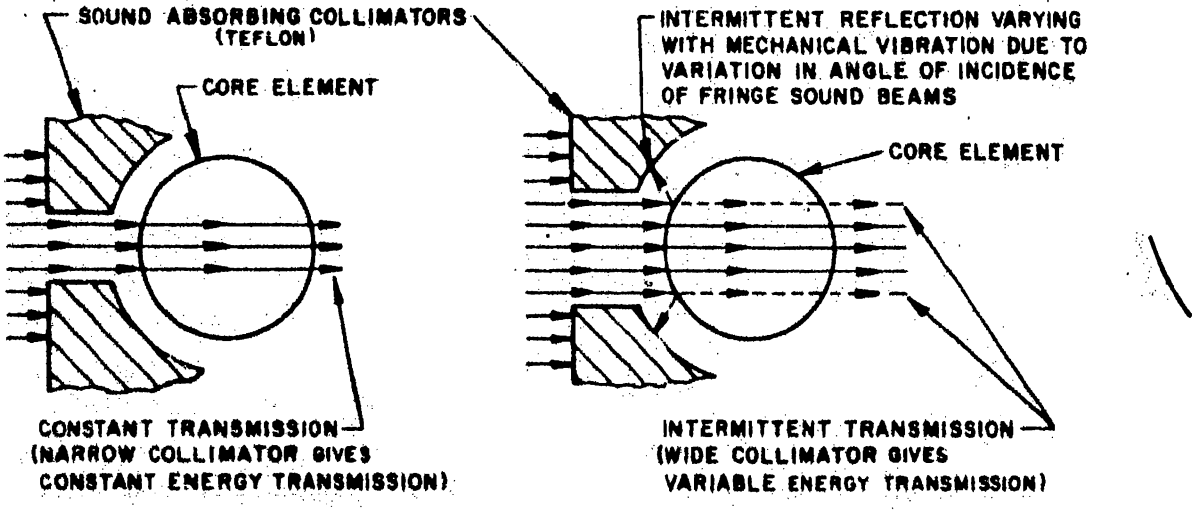

SONIC TRANSMISSION STABILITY
VS
WIDTH OF COLLIMATOR SLOTS

FIGURE 13

A 2.25 or 5 mc, 3/8-inch-diameter, ceramic-type, "Hi-Z" Branson transmitting transducer, driven by a Sperry Reflectoscope, is placed at one end of the collimator slot. An identical, but receiving, transducer is placed at the other end. The transducers are coupled to the fuel element by flowing water, recirculated and deaerated to eliminate air bubbles which cause false indications of defects.

Lower-gain transducers will not function in this test because of the severe masking by the small collimators.

The output signal from the receiving transducer is permanently recorded on a strip chart recorder. Discontinuities, cladding variations, and other anomalies in the fuel elements attenuate and cause variations in this signal. With enough correlation data and interpretation experience, one can identify the type of defects represented by the various signal anomalies. See Figures 14, 15, and 16 for examples of correlation data on some typical defects.

b. Radiography of End Caps. Both the anchor and the free end-caps were radiographed twice, at 0 and 90 degrees, to detect defective interlocks and other irregularities. Careful, but not uncommon, precautions were taken to maximize resolution.

c. Auto-Gamma Spectrometry. A single-channel gamma spectrometer was employed to measure the total U-235 and the U-235 distribution in a fuel element by counting the gammas from the radioactive decay of U-235.

The fuel element was scanned by pushing it at constant speed through the hole in the center of a specially designed, integrally shielded, sodium-iodide, thallium-activated scintillating crystal, positioned inside a five-inch-thick lead shield. The hole in the crystal increases its counting efficiency; the integral lead shields increase the sensitivity of the crystal to localized variations in U-235 concentration; and the large, external shield reduces extraneous background gammas (Figure 17).

The scintillations and amplified pulses are proportional to the energies of the gamma rays incident upon the scintillating crystal. The pulses are fed through a pulse-height analyzer set to pass only those pulses equivalent to gammas of energies greater than 130 Kev, namely, the 184-and 143-kev U-235 gamma rays. The interfering 50-kev U-238 gamma rays and secondary gamma rays from the shielding are not passed. The analyzer output goes to a scaler-printer and a count-rate meter-recorder.

The scaler-printer measures the total U-235 content by integrating and printing out the total gamma rays striking the scintillator during the scan. The count-rate meter-recorder measures the distribution in U-235 by recording the variation in count rate along the length of the element.

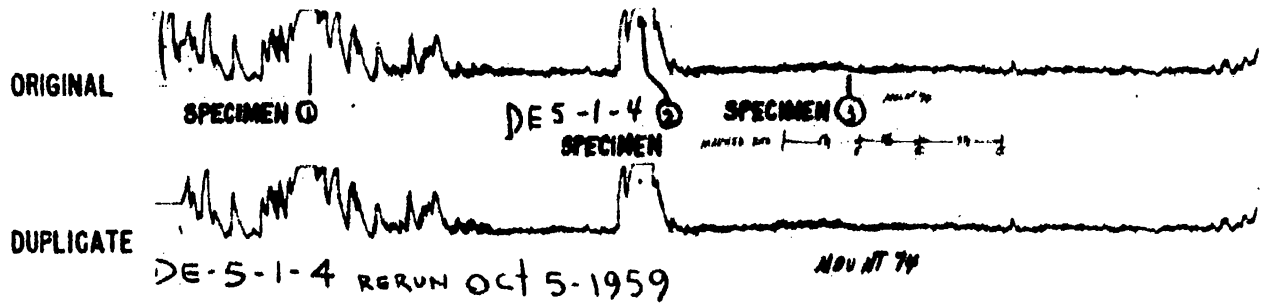

SPECIMEN 1 - FIG. 1
DEFECT - .019 IN. MIN.
PHOTO AREA .019 X .025 IN.

SPECIMEN 2 - FIG. 1
DEFECT - .025 IN. MIN.
PHOTO AREA - .037 X .050 IN.

SPECIMEN 2 - FIG. 2
DEFECT - .025 IN. MIN.
PHOTO AREA - .019 X .025 IN.

COMMENTS:

SPECIMEN 1 - UNIFORM CLADDING. GROSS CLOSED PIPE FOUND IN CENTER OF CORE WITH SOME ASSOCIATED INCLUSIONS.

SPECIMEN 2 - UNIFORM CLADDING. GROSS PIPE AS IN SPEC. 1.

SPECIMEN 3 - UNIFORM CLADDING. NO PIPING OR OTHER DEFECTS IN CORE.

GROSS PIPES OR CRACKS IN CENTER OF CORE

FIGURE 14

ORIGINAL

SPECIMEN 9

SPECIMEN 0

E-10-17-3

DUPLICATE

E-10-17-8

STD #8

STANDARD

SPECIMEN 0 - FIG. 1
.187 IN. REMOVED IN .010 TO .015 IN. INCREMENTS FROM FIRST CUT BEFORE DEFECT FOUND.
DEFECT - .0052 IN. MAX.
PHOTO AREA - .019 X .025 IN.

SPECIMEN 0 - FIG. 2
.006 IN. FROM FIG. 1
DEFECT - .0056 IN. MAX.
PHOTO AREA - .019 X .025 IN.

SPECIMEN 0 - FIG. 3
.016 IN. FROM FIG. 1.
DEFECT - .0032 IN. MAX.
PHOTO AREA - .019 X .025 IN.

COMMENTS:

SPECIMEN 9 - UNIFORM AND SOUND CLADDING NO DEFECTS IN CORE AS DETERMINED BY SUCCESSIVE .010 TO .015 IN. SECTIONS.

SPECIMEN 0 - AFTER FIRST CUT .161 IN. WAS REMOVED IN INCREMENTS. SPECIMEN DISPLAYED SOUND, UNIFORM CLAD AND SOUND CORE. AFTER .187 IN. (FIG. 1) AN INCLUSION APPEARED. AFTER REMOVING .016 IN., INCLUSION STILL REMAINED. UPON REMOVING ANOTHER .012 IN., INCLUSION DISAPPEARED.
DEFECT LENGTH AS ESTABLISHED BY SUCCESSIVE SECTIONING .016 IN. MIN., .044 IN. MAX.

INCLUSION AND/OR PIPE IN CENTER OF CORE

FIGURE 15

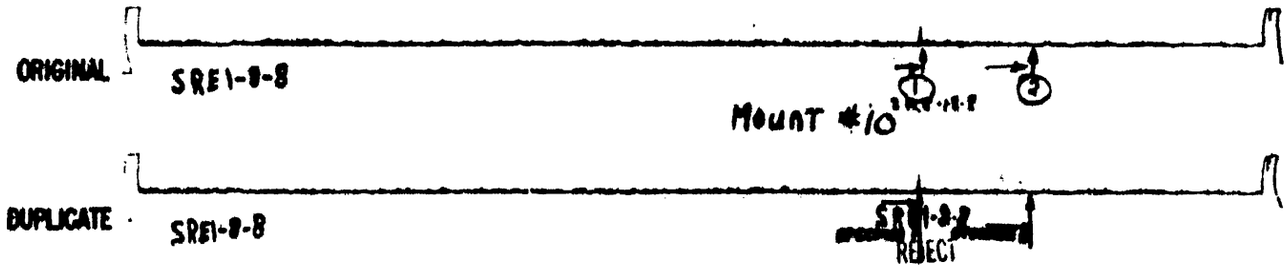

SPECIMEN 1 FIGURE 1
POLISHED AS FIRST CUT
DEFECT - .0032 IN. MAXIMUM
PHOTO AREA .019 X .025 IN.

SPECIMEN 1 FIGURE 2
.024 IN. FROM FIGURE 1
DEFECT - .0044 IN. MAXIMUM
PHOTO AREA .019 X .025 IN.

SPECIMEN 1 FIGURE 3
.056 IN. FROM FIGURE 1
DEFECT - .0064 IN. MAXIMUM
PHOTO AREA .019 X .025 IN.

SPECIMEN 1 FIGURE 4
.085 IN. FROM FIGURE 1
DEFECT - NEARLY DISAPP'RD
PHOTO AREA .019 X .025 IN

COMMENTS

SPECIMEN 1 - CLADDING UNIFORM. INCLUSION IN CORE JUST UNDER CLADDING. MINIMUM DEFECT LENGTH AS ESTABLISHED BY SUCCESSIVE SECTIONING - .085 IN.

SPECIMEN 2 - CLADDING UNIFORM. NO DEFECTS IN CORE.

INCLUSION AND/OR PIPE NEAR PERIPHERY OF CORE

FIGURE 16

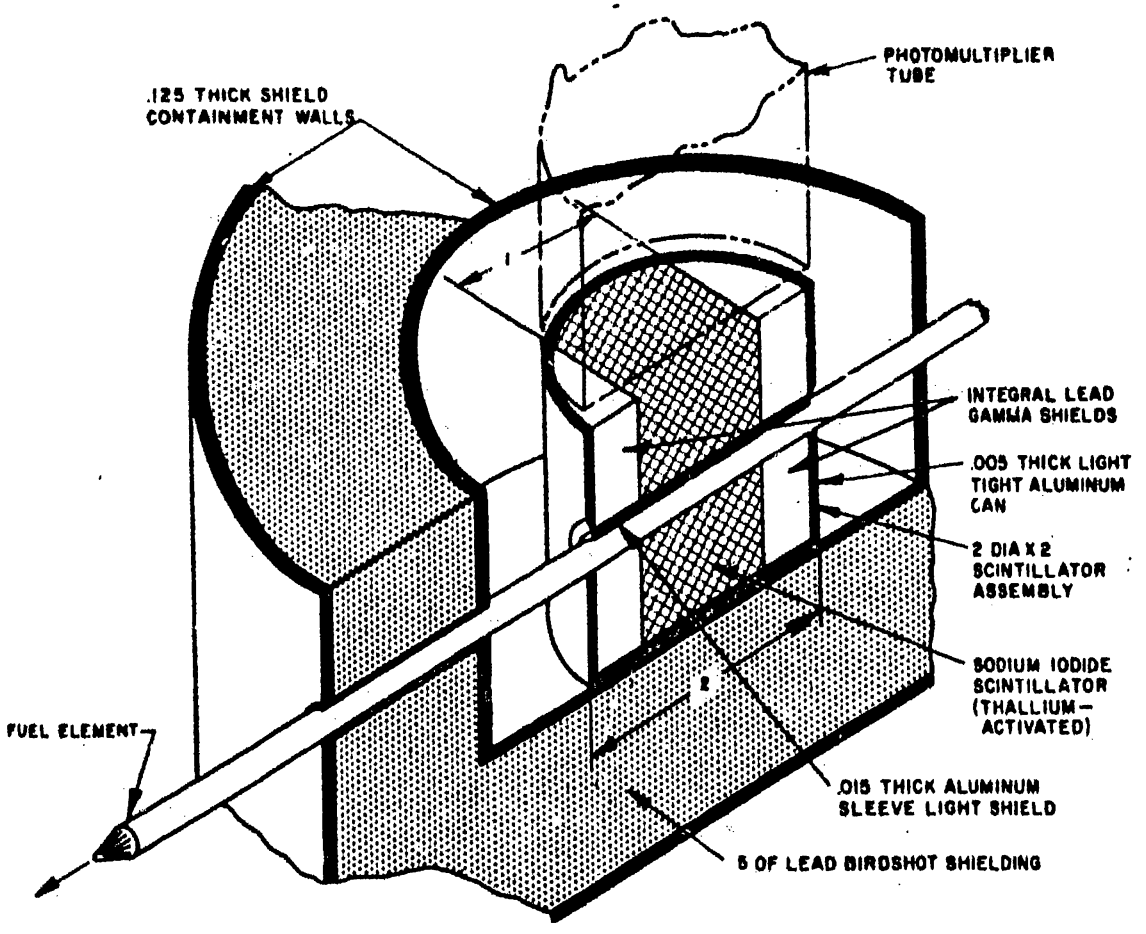

SCHEMATIC OF GAMMA SCINTILLATOR CRYSTAL AND SHIELD ASSEMBLY

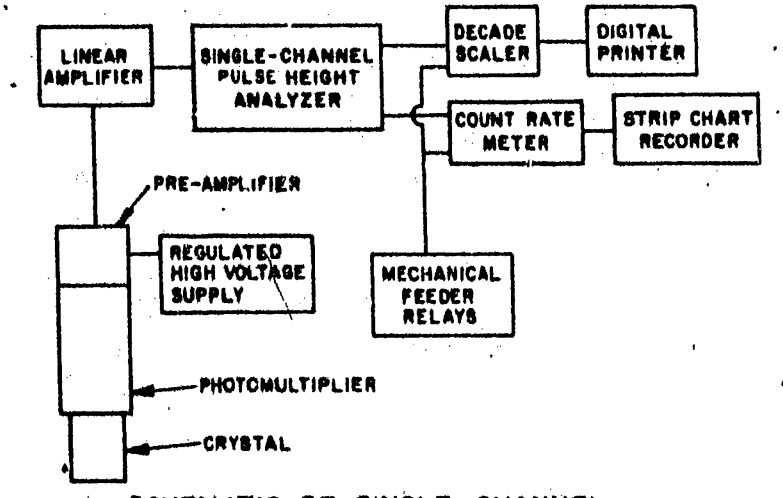

SCHEMATIC OF SINGLE-CHANNEL GAMMA SPECTROMETER

FIGURE 17

2. Blanket Elements

a. Element Components

(1) Cladding Tube

(a) The hydrostatic pressure test was performed according to ASTM A-269-58, Section 10.

(b) The eddy current test was instituted at the request of tubing vendors in lieu of the dye penetrant testing originally specified. Substituting the eddy current inspection for dye penetrant inspection affords the vendors the advantages of speed and low cost. The substitution affords the customer the advantage of receiving data on the internal integrity of the tube wall and the inside diameter of the tube.

The test is performed with a type multi-frequency, Magnetic Analysis Corporation, Model 7-58 eddy current instrument using a test probe consisting of two electrically balanced coils mounted immediately adjacent to each other around a common axis. Test frequencies between 35 and 60 kc supplied satisfactory results on the blanket tubing.

The instrument is calibrated by using a "standard" tube. The "standard" tube, a length of tubing from the lot being tested, is fabricated by milling longitudinally oriented, 0.001-inch-deep by 1/2-inch-long grooves on the inside and outside diameter. The instrument is calibrated to just reject these "standard" defects of known depth.

(2) Bare U Alloy Slugs

The NDT technique used on the slugs is virtually identical to the through-transmission ultrasonic test used in testing the fuel elements. However, because of the relatively larger diameter of the slugs and the increased impedance to sonic transmission, the transmitted signal is relatively weaker. This problem is reduced by increasing the narrow dimension of the collimator and increasing the Reflectroscope output.

As with the fuel element, defects in the slugs are detected by the manner and magnitude in which they attenuate the transmitted sonic energy. See Figure 18 for an example of correlation data on one type of defect.

b. Assembled Blanket Elements

(1) Eddy Current Testing

This test is performed with a J. W. Dice Company, Model C, Cyclograph, employing an encircling-coil-type test probe of special design that oscillates at 160 to 180 kc. The coil is wound on a small-diameter (0.455-inch), narrow (0.030-inch)

spool and is shielded with ferrite disks. This coil design concentrates the flux of the coil within a very short length of the blanket element and increases the sensitivity of the test for detecting small bond defects and determing uranium and sodium positions precisely. See Figure 19 for a schematic of the coil and Figure 20 for an example of correlation data on bond defects.

(2) Weld Integrity Tests

The bottom weld was checked, prior to element assembly, by evacuation helium leak testing.

After element assembly, both the top and bottom welds were checked by pressurization, helium leak-testing, and dye penetrant testing.

ORIGINAL TRACE

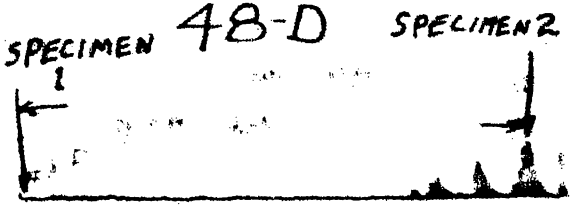

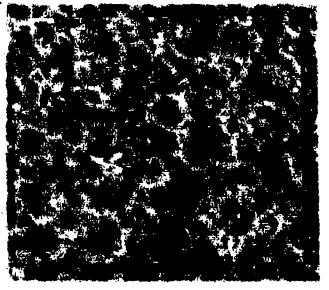

SPECIMEN 1 - FIG. 1
SOUND INTERIOR & SURFACE
PHOTO AREA - .041 X .050 IN.

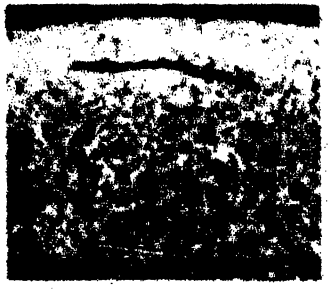

SPECIMEN 2 - FIG. 1
INCLUSION AND/OR PIPE
NEAR PERIPHERY OF SLUG
DEFECT - .029 IN. LONG
.001 IN. WIDE
PHOTO AREA - .041 X .050 IN.

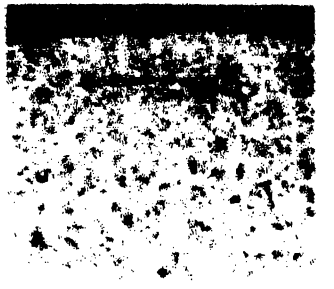

SPECIMEN 2 - FIG. 2
SAME DEFECT AS SHOWN IN
FIG. 1 BUT WITH .020 IN. REMOVED
DEFECT - .028 IN. LONG
.0005 TO .0010 IN. WIDE
PHOTO AREA - .041 X .050 IN.

COMMENTS:

SPECIMEN 1 - SOUND ON INTERIOR AND SURFACE.

SPECIMEN 2 - INCLUSION AND/OR PIPE JUST UNDER SURFACE. INTERIOR SOUND. NOTE INTERMITTENT OSCILLATION ON TRACE AS THIS PERIPHERAL DEFECT ROTATED IN AND OUT OF THE SONIC BEAM.

INCLUSION AND/OR PIPE NEAR PERIPHERY OF SLUG

FIGURE 18

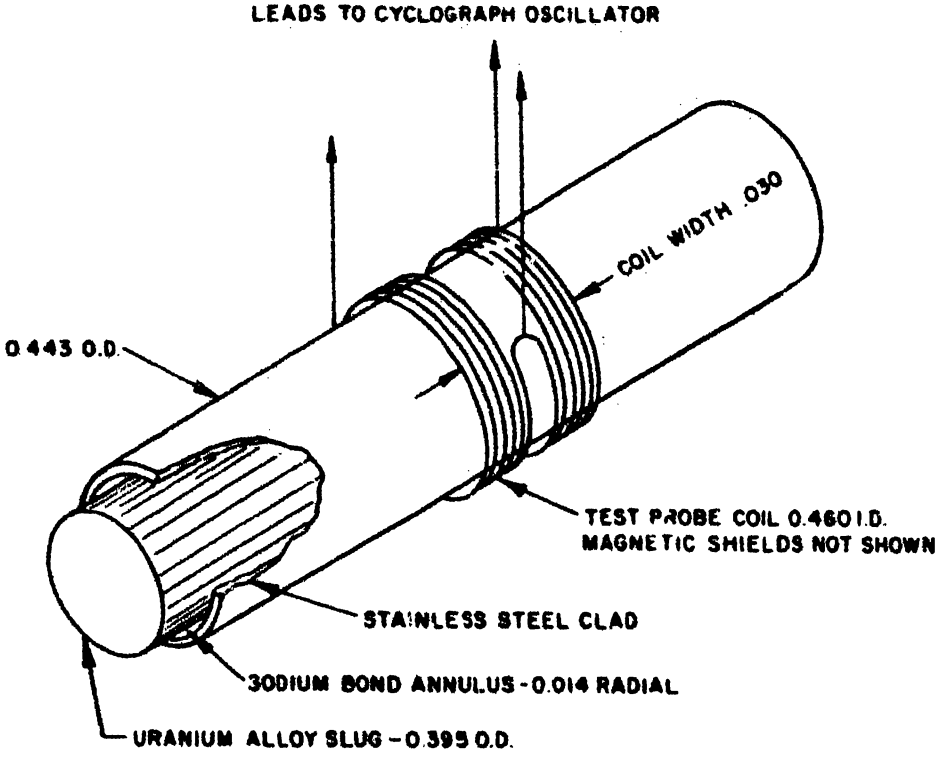

SCHEMATIC OF RELATIVE POSITION OF
TEST PROBE AND SPECIMEN

FIGURE 19

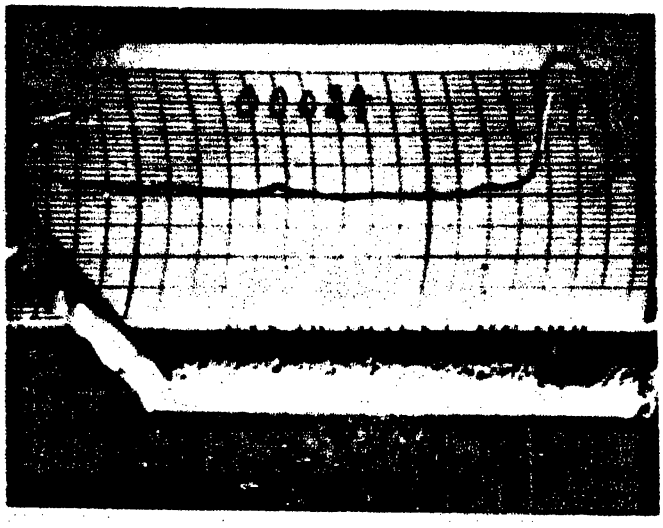

Approximately $\frac{3}{4}$X
Note two small $\sim\frac{1}{16}$ inch defects and one larger $\sim\frac{1}{8}$ inch defect.

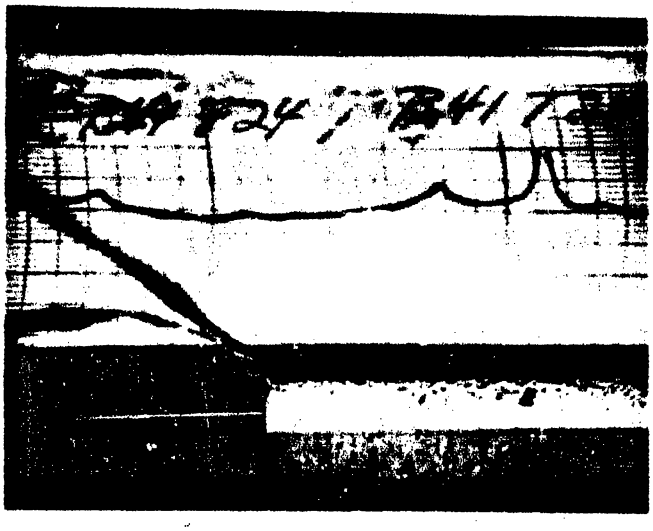

Approximately $\frac{3}{4}$X
Note the small $\sim\frac{1}{16}$ inch defect and one larger $\sim\frac{3}{16}$ inch defect.

TYPICAL VOID DEFECTS IN SODIUM BOND
FIGURE 20

TABLE IV. CORE A NDT COSTS

		COST ($)
PRDC		
FEASIBILITY STUDIES	-	50,000
ANL - $25,000		
M&C - $25,000		
ENGINEERING, ASSEMBLY AND DELIVERY OF EQUIPMENT, CORRELATION WORK, ETC.	-	122,000
OPERATING CONTRACT CHARGES	-	168,000
PRDC RESIDENT INSPECTORS' TIME ON NDT	-	45,000
APDA		
ENGINEERING	-	25,000
APPROX. TOTAL	-	410,000
PROJECTED TOTAL CORE A COST	-	5,000,000
206 FUEL SUBASSEMBLIES		
100 INNER ROW BLANKET SUBASSEMBLIES		
500 OUTER BLANKET SUBASSEMBLIES		
RELATIVE COST OF NDT	$\frac{410}{5000}$	$\sim 8\%$

VI. SUMMARY OF U-10 W/O MO IRRADIATION DATA

A. BASIS OF MATERIAL SELECTION

The selection of the U-10 w/o Mo fuel alloy was based on several fundamental design requirements: (a) sufficient radiation stability to insure that dimensional and physical changes would not block coolant flow at burnups in excess of 1 a/o at temperatures as high as 1300 F, (b) small reductions, if any, in the possible breeding gain that could be caused by alloying elements, (c) ease of fabrication into the desired diameter and length with an integral cladding, (d) the ability to be put into production to meet schedule requirements, and (e) suitable physical and mechanical properties to insure a safe and controllable reactor core, to prevent any sudden change in reactivity, and to result in a prompt negative coefficient of reactivity due to fuel expansion.

Based on the results of a fuel-alloy screening irradiation program, on uranium alloyed with small amount of chromium, zirconium and molybdenum [1], sponsored by APDA through 1955, it was concluded that the uranium-molybdenum and uranium-zirconium alloys offered the most promise of satisfying the design requirements.

B. IRRADIATION TEST PROGRAMS

A second screening program, conducted from 1955 to 1957, produced data on high-alloyed uranium-zirconium and uranium-molybdenum fuels. In December 1955, the data available on these materials, together with information developed in the work of others, [2, 3] led to the tentative selection of U-10 w/o Mo alloy as the reference fuel material. Of all the materials studied, this alloy appeared to possess the best combination of radiation stability, ease of fabrication, and such safety features as reproducible and positive temperature coefficient of expansion and containment of fission products. The second screening program was continued as planned, and U-10 w/o Mo alloy was confirmed as the best choice of those alloys tested.

An extensive testing program, using both the MTR and CP-5 and exclusively devoted to U-10 w/o Mo, was begun in 1956 and is still in progress.

- -

(1) APDA-122, "The APDA Irradiation Test Program on Selected Uranium Fuel Alloys: June 1954 to June 1957.

(2) WAPD-127, "Development and properties of Uranium-Base Alloys corrosion Resistant in High Temperature Water - Part I: Alloys Without Protective Cladding (Declassified September 1957) - Part IV: Radiation Stability of Uranium-Base Alloys", May 1957.

(3) Konobeevsky, S. T., et al, "Effect of Irradiation on Structure and Properties of Fissionable Materials", Proc. Intern. Conf. Peaceful Uses of the Atom, Vol. 7, pp 433-440, 1955.

Its aim has been to provide detailed data on the effect of operating variables which could effect the irradiation stability of the alloy. These operating variables include fission rate, burnup, operating temperature, and the effect of such fabrication variables as fabrication procedures, heat treatment, composition and clad thickness on diametral swelling. Data obtained prior to January 1961 are presented and discussed below.

1. MTR Irradiation Results

The MTR results have been reported in detail by Battelle Memorial Institute (4) and by APDA (5) and are shown graphically in Figure 21 as a plot of per cent diameter increase versus total atom per cent burnup. About 100 specimens of U-10 w/o Mo alloy were irradiated in 40 capsules, of which six were equipped with thermocouples for use as temperature monitors and with auxiliary heaters for purposes of temperature control. Although some of the controlled capsules were successful, in most cases the thermocouples and/or heaters failed before the end of the irradiation period. The other 34 capsules were not temperature controlled, although a few had temperature-indicating devices.

Burnup on each specimen was calculated from flux estimates, analysis of dosimeter wires incorporated in the capsules, and by radiochemical methods. Analysis of the deviation in indicated burnup from these three independent methods suggests that the burnups given in Figure 21 could be in error by $\pm$ 30%. In the capsule which did not contain thermocouples, the temperatures were calculated from the power generation of the specimens. Since power generation is the first derivative of burnup with respect to time, the uncertainty associated with the temperature difference between the fuel specimen centerline and the MTR reactor, as indicated in Figure 21, is necessarily as great as that associated with the burnup. It must be recognized, therefore, that wide data scatter is to be expected, and conclusions must be based on the preponderance of data rather than on specific points.

The solid curve in Figure 21 is considered to be a conservative basis on which to predict swelling as a function of burnup for temperatures less than 1100 F and for material irradiated at a fission rate high enough to maintain the metastable gamma phase. Because only three specimens, which are believed to have operated at temperatures less than 1100 F, do not fall beneath this curve, the extension to the solid curve, indicated by a dashed line, may more accurately illustrate the burnup dependence beyond a burnup of 1.5 a/o. (Burnup is given as percent of total alloy atoms fissioned.) A very conservative extrapolation is shown beyond a burnup of 2.25 a/o because of the lack of data in this region. The good quality of the surface of several specimens after irradiation is illustrated in Figure 22.

- -

(4) BMI-APDA-660, "Irradiation Studies of U-10 w/o Mo Fuel Alloy", January 26, 1961.

(5) MAT-759, "Summary and Evaluation of Irradiation Data on U-10 w/o Mo Fuel Alloy as of April 12, 1960". (memo, P. R. Huebotter, A. A. Shoudy to D. O. Leeser.)

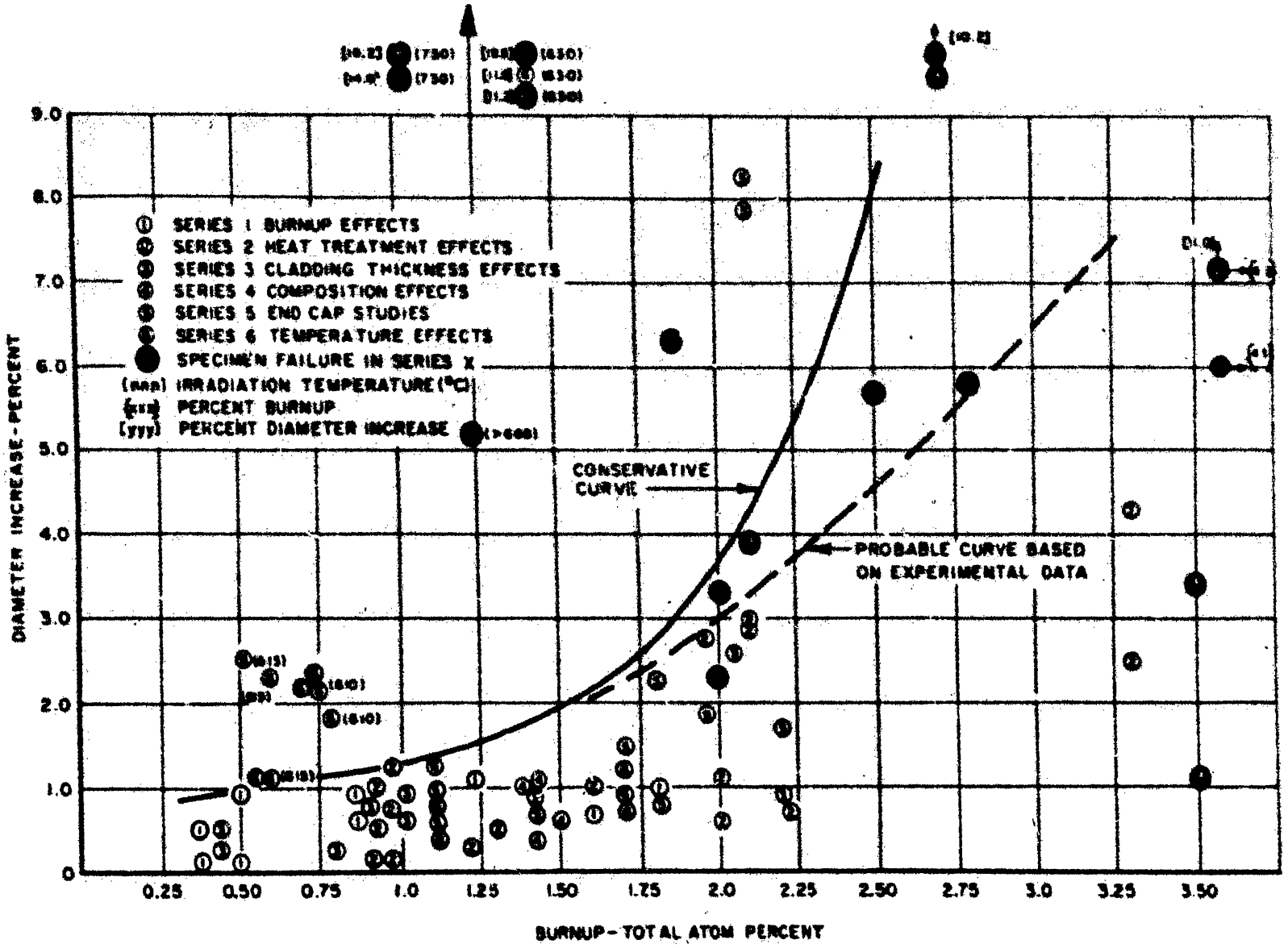

PERCENT DIAMETER INCREASE AS A FUNCTION OF BURN-UP
FOR U-10 w/o Mo FUEL ALLOY (MTR DATA)
FIGURE 21

2. CP-5 Irradiation Results

In the CP-5 irradiation program, full-length, 30-inch fuel pins were irradiated in finned capsules cooled by forced-air convection,[6] which produced a wide range of specimen temperatures over the length of the pin even when the burnup rate range was relatively narrow. Figures 23 and 24 present the pertinent data on representative specimens CP-5-1 and CP-5-3. The fin-root temperature curve was established by taking readings from ten thermocouples spot welded to the body of the capsules at 3-inch intervals. The pin power was determined from air temperature rise and flow rate. By integration over the in-pile time, the burnup values which are believed to be reliable within 10% were determined. An uncertainty analysis of the calculation of centerline temperatures from the fin-root temperature curve revealed that the uncertainty is ± 50 F. Hence, the temperature and burnup data from the CP-5 program are believed to be considerably more reliable than the data from the MTR program. There was no significant swelling on any portion of the CP-5-2 pin.

C. VERIFICATION OF DESIGN REQUIREMENTS

1. Swelling and Length Changes at Low Temperatures

Figure 21 suggests an almost linear effect of burnup on diametral growth up to 2.0 a/o burnup. It also suggests that the data above and below 1110 F should be analyzed separately. The small changes in length that were observed are considered to be of secondary importance in the Fermi design.

Assuming a linear diametral change with burnup, the data below 1110 F were correlated in Figure 25 as a plot of per cent diameter increase per atom per cent burnup versus temperature. Considering only the MTR data, it is apparent that increments of burnup over 2.0 a/o produce disproportionate amounts of swelling. The solid line would seem to be a conservative curve for predicting per cent diameter increase per atom per cent burnup at temperatures below 1100 F and at burnups less than 2.0 a/o. Judging from the slight slope in the curve, there seems to be very little temperature dependence below 1100 F.

The striking feature in Figure 25 is the large disparity between the CP-5-1 results and the remainder of the data in the range of 750 to 1100 F. The CP-5-1 results in the temperature range from 750 to 1100 are described by a dotted curve that peaks widely apart from the continuous curve relating to other data. An explanation of this difference and experiments to verify the effect will be discussed later.

The striking feature of the CP-5-1 test itself was that, in spite of the gross swelling encountered, the general appearance of the pin was good over its entire length with no evidence of cracking or rupturing. A photograph of the region 9 inches from the top of the pin, where the

(6) APDA-130, "Irradiation Testing of Enrico Fermi Prototype Fuels Pins in CP-5", April 1960.

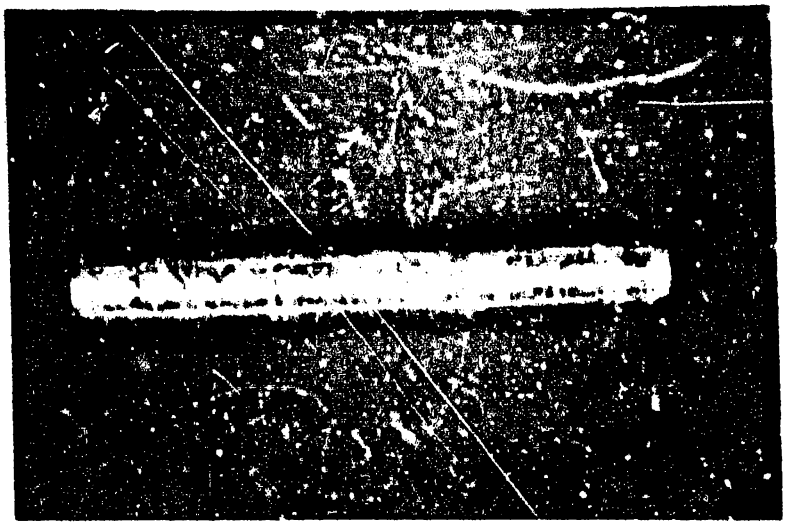

(9-7: HT-7) 4X (HC-777)
Burnup 1.3 Total a/o — Centerline Irradiation 880-920 F

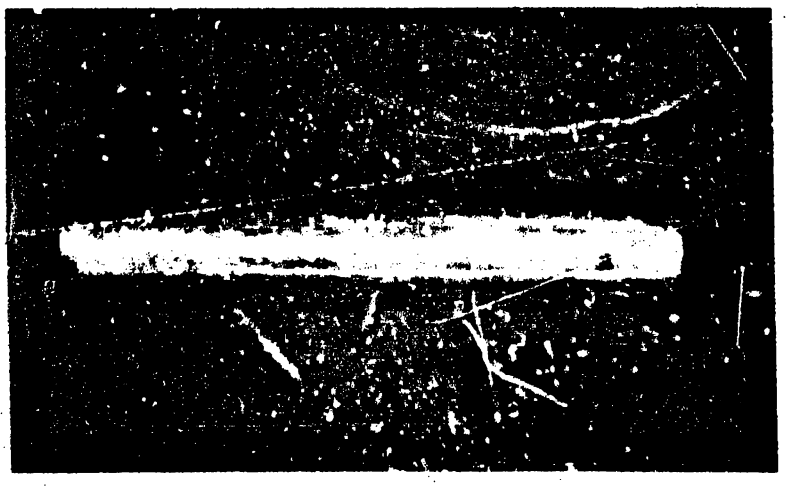

(9-8: HT-8) 4X (HC-786)
Burnup 1.6 Total a/o Centerline Irradiation 880-1000 F

Zirconium cladding applied to alloy billet by coextrusion at 1200 F (die temperature at 900 F), finished size obtained by cold swaging. Heat treated at 1630 F for 24 hours, water quenched and stress relieved at 630 F and air cooled.

SPECIMENS OF U-10 w/o Mo AFTER IRRADIATION ILLUSTRATING EXCELLENT SURFACE APPEARANCE

FIGURE 22

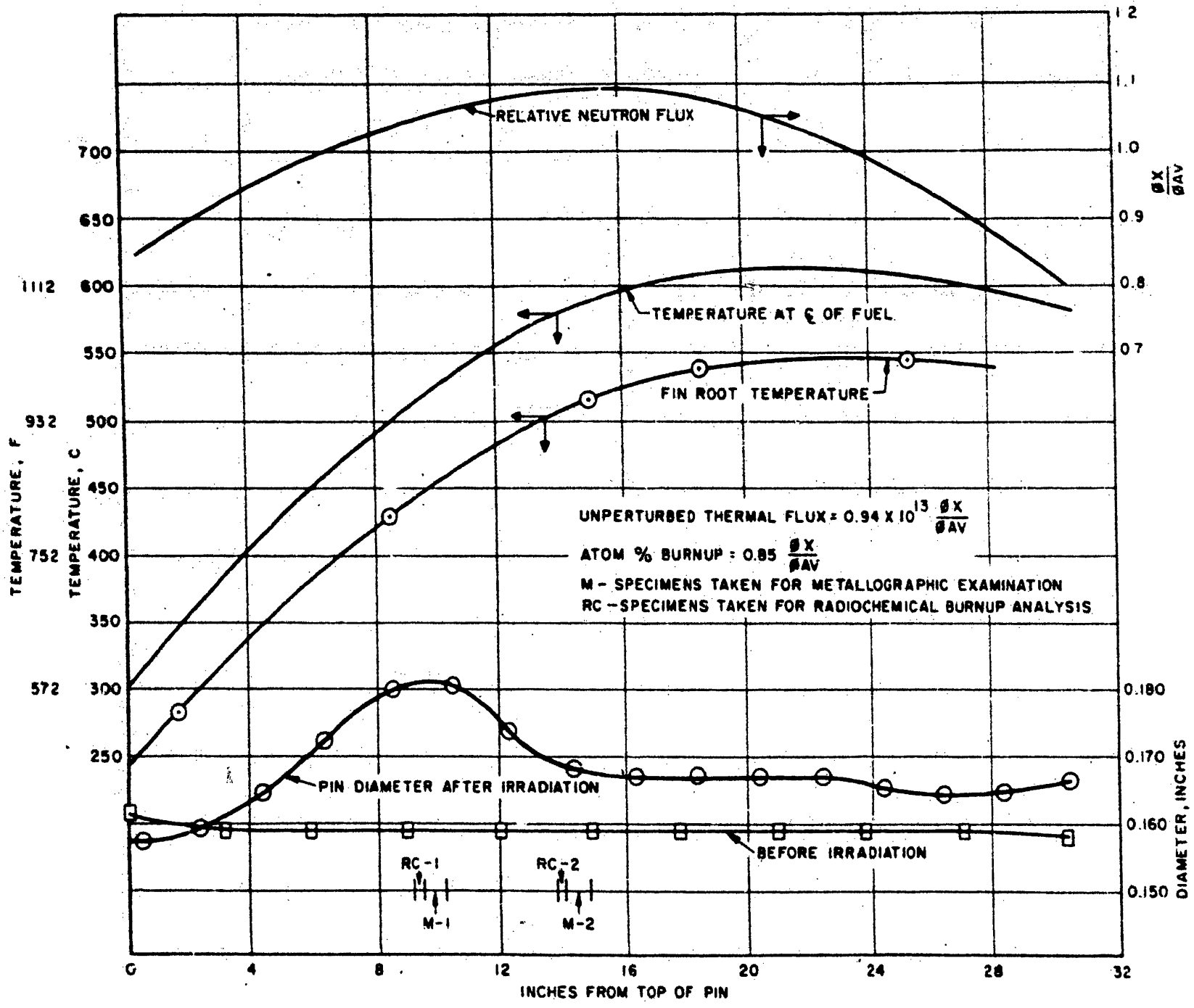

IRRADIATION RESULTS OF CP-5-1 TEST
FIGURE 23

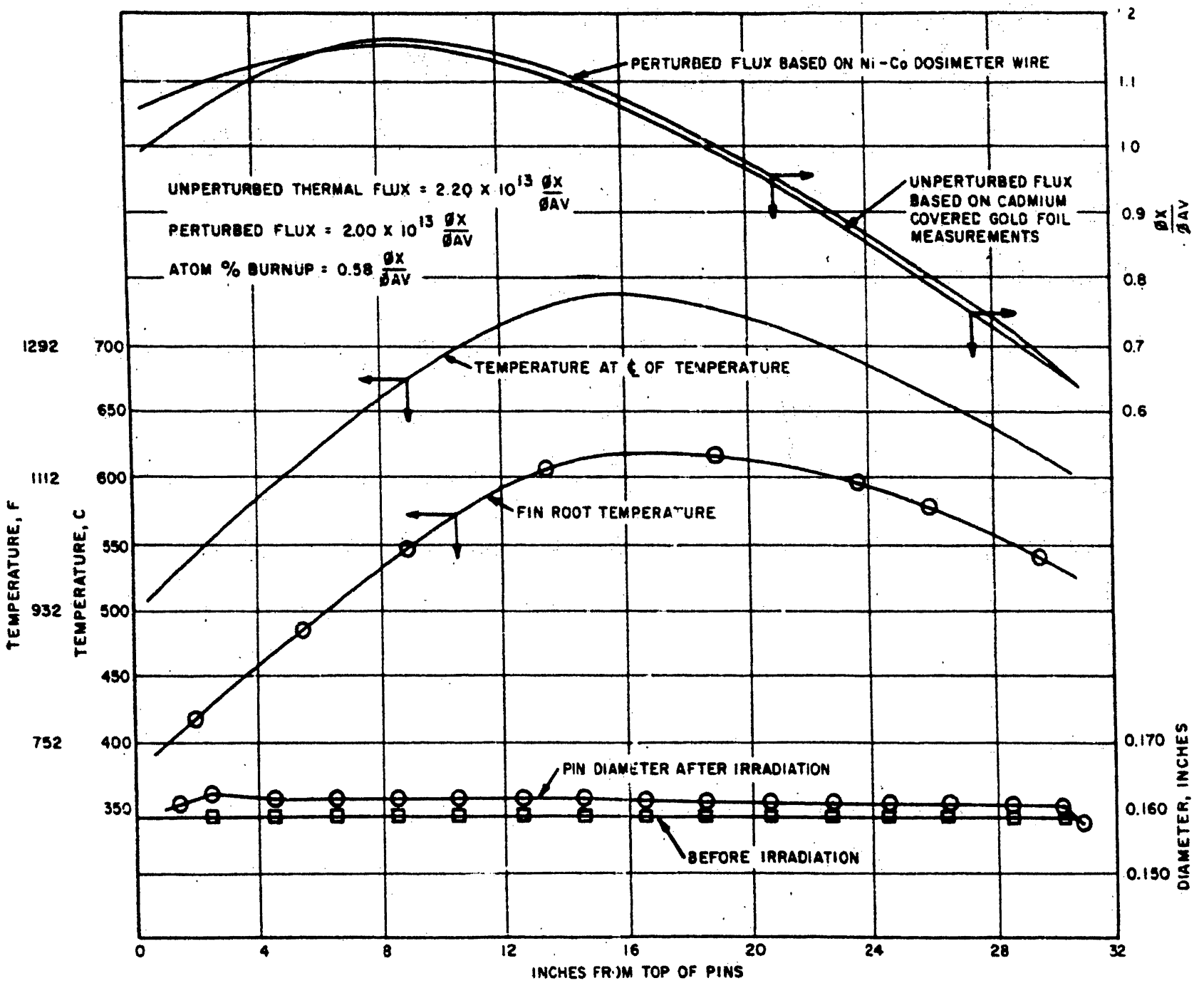

IRRADIATION RESULTS OF CP-5-3 TEST

FIGURE 24

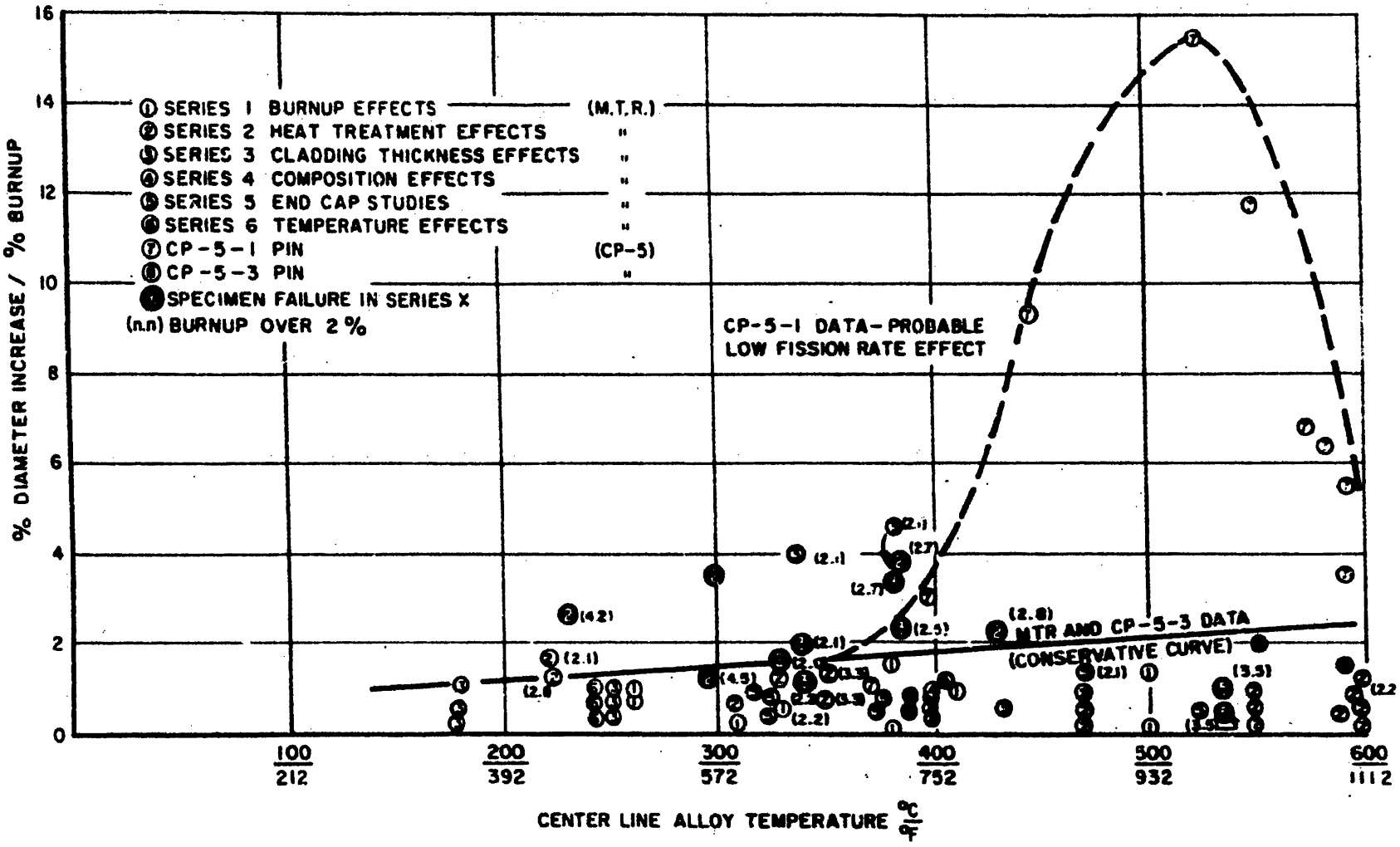

PERCENT DIAMETER INCREASE NORMALIZED TO 1% BURNUP FOR SPECIMENS IRRADIATED AT CENTERLINE TEMPERATURE LESS THAN 600°C

FIGURE 25

greatest swelling occurred and where the burnup was about 0.9 a/o, is shown in Figure 27.

2. Swelling and Length Changes at High Temperatures

The irradiation data of diameter increase versus burnup at temperatures over 1100 F are shown in Figure 26. Swelling at temperatures over 1100 F seems to be a power function of burnup. All available data fall within the bank shown in Figure 26. Extrapolation of the band beyond 1.0 a/o is based on very few and inaccurate data. Generally speaking, the high temperature points fall closer to the upper boundary, and the data points between 1100 and 1165 fall closer to the lower boundary. The upper boundary is based on 1345 F.

The only major exception to this generality is the point at 0.52 a/o burnup, which shows a 2.5 per cent diameter increase at a calculated operating temperature of 1127 F. Since this is one of the MTR specimens on which relatively large burnup and temperature uncertainties exist, it can probably be discounted in establishing the upper boundary of the scatter band. Quite unlike the correlation below 1100 F, Figure 26 indicates good agreement between the MTR and CP-5 data.

3. Analysis of Possible Causes of Swelling

Three hypotheses have been advanced to explain the large discrepancy between the CP-5 and MTR results in the low temperature region.

a. Transformation Effect. The swelling, centered on the 980 F portion of the CP-5-1 pin, may have resulted from transformation of the gamma phase to the alpha-plus-epsilon phase which is less radiation stable. The uranium-molybdenum equilibrium diagram in Figure 28 [7] shows the gamma phase for 10 w/o Mo to be stable above 1060 F, the alpha-plus-gamma phases to be stable between 1045 and 1060 F, and the alpha-plus-delta (epsilon and delta terms used interchangeably) phases to be stable below 1045 F. For isothermal transformation of gamma to alpha-plus-epsilon (or alpha-plus-delta), for prototype U-10 w/o Mo fuel pins, the "nose" of Time-Temperature-Transformation curve (TTT curve) appears at about 900 F as shown in Figure 29. Transformation is initiated in less than 4 hours and completed in 66 hours at 900 F. [8]

Several investigators have shown that under irradiation, the

---

(7) Dwight, A. E., "The U-Mo Equilibrium Diagram Below 900 C," Journ. Nuclear Materials, March 1960.

(8) Bodzin, J. J., and Hoffman, H. E., "Determination of the Transformation Kinetics of U-10 w/o Mo Alloy at Temperatures Between 600 and 1100 F", Detroit Edison Engineering Research Department Report 60H19, January 20, 1961.

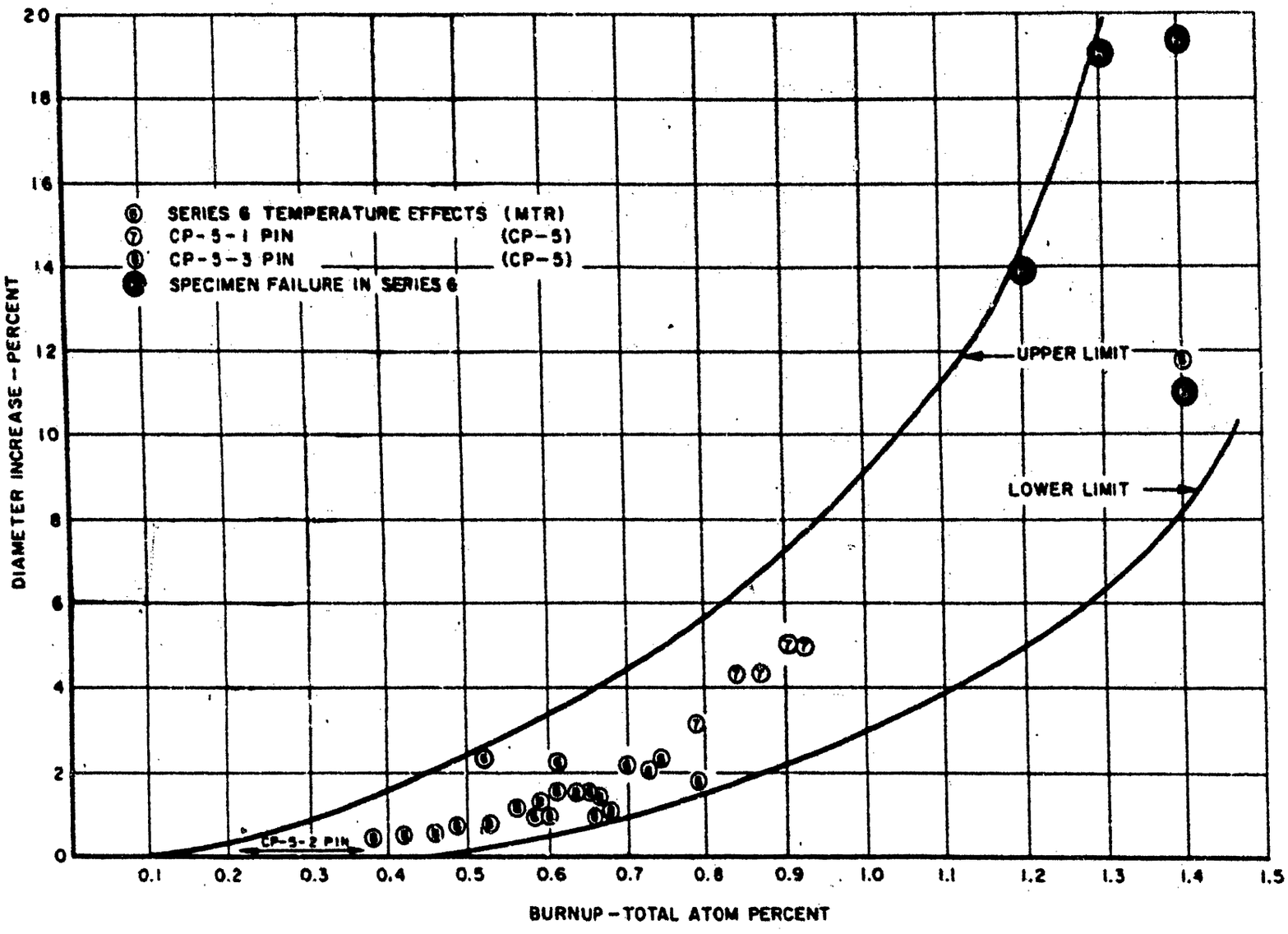

PERCENT DIAMETER INCREASE VS. BURNUP FOR SPECIMENS IRRADIATED AT CENTERLINE TEMPERATURES ABOVE 600°C

FIGURE 26

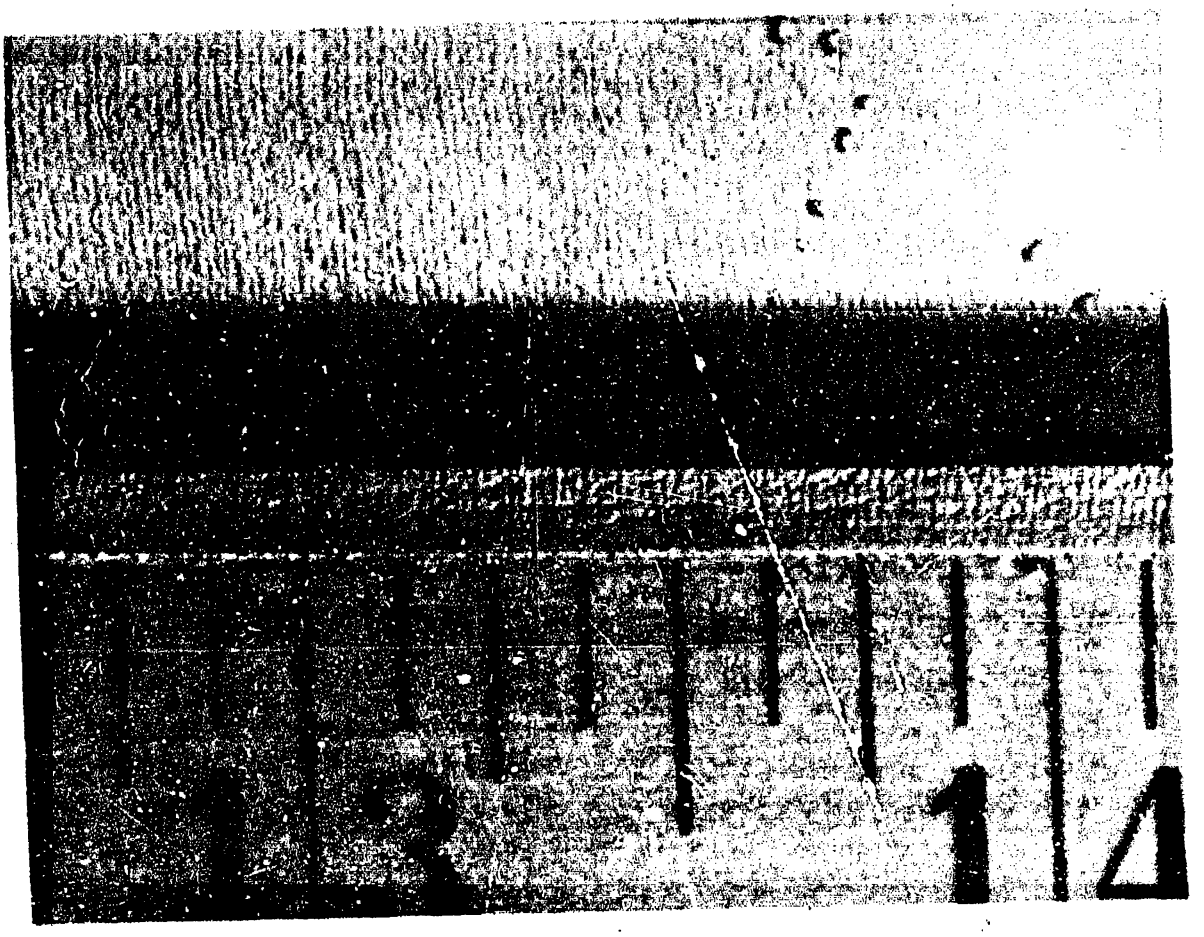

ENLARGED VIEW OF SURFACE OF IRRADIATED CP-5-1 PIN AT AREA OF MAXIMUM SWELLING

FIGURE 27

high-temperature phase becomes thermally stable at low temperatures.[3, 9] It has been proposed that a critical fission rate exists, probably between 10^{13} to 10^{14} fissions/cc/sec for U-10 w/o Mo alloy at irradiation temperature near the nose of the TTT curve, which is able to maintain the high-temperature phase, and if this rate is not achieved, the alloy reverts to the normally stable phase. In other words, two competing processes occur in the alloy under irradiation: (1) thermal spikes from fission events tending to maintain the high temperature phase, while (2) the macroscopic temperature, when it is below 1060 F in this alloy, tending to transform it from gamma to alpha-plus-epsilon. The critical fission rate would logically be highest at the nose of the TTT curve and lower at other temperatures at which there would be less driving force in the direction of thermal transformation.

Electrical resistivity of specimens irradiated in the MTR, near the critical temperature but at a much higher fission rate than CP-5-1, showed no evidence of an alpha-plus-epsilon phase. Metallographic examination of the swollen region of CP-5-1 showed apparent transformation, but the examination was inconclusive because of the severe swelling of the metal. Metallographic examination of specimens taken from the CP-5-2 pin verified that transformation had occurred in the temperature range at which gross swelling took place in the CP-5-1 pin. The fact that the CP-5-2 pin operated at a higher fission rate than CP-5-1 leaves little doubt that transformation to the alpha-plus-epsilon phase also occurred in the CP-5-1 pin. The fact that dimensional changes were not detected in the CP-5-2 pin after an average burnup of 0.27 a/o, suggests that swelling of alpha-plus-epsilon material follows a power function of burnup and, as was the case in CP-5-1, the swelling reaches large proportions at a burnup less than 1 a/o.

b. Thermal Cycling Effects. The CP-5 reactor scrammed 674 times or an average of 70 times per month during the irradiation of the CP-5-1 specimen. This scram frequency was much higher than that normally experienced in the MTR and at least 50% higher in the total number of scrams experienced by the CP-5-2 and CP-5-3 pins. Since out-of-pile thermal cycling tests by APDA on unirradiated U-10 w/o Mo fuel pins resulted in only slight dimensional changes, this explanation was not too plausible. However, the combination of thermal cycling with irradiation may lead to a significiant effect.

c. Internal Defects. Commercial nondestructive testing methods were not available at the time the CP-5-1 specimen was fabricated. Since then, however, an ultrasonic technique has been developed

---

(3) Konobeevskey, S. T., et al, "Effect of Irradiation on Structure and Properties of Fissionable Materials", Proceedings of International Conference on Peaceful Uses of the Atom, Vol. 7, 1955.

(9) Bleiberg, M. L., "A Kinetic Study of Irradiation-Induced Phase Changes in Uranium", Nuclear Science and Engineering, Vol. 5, February 1959.

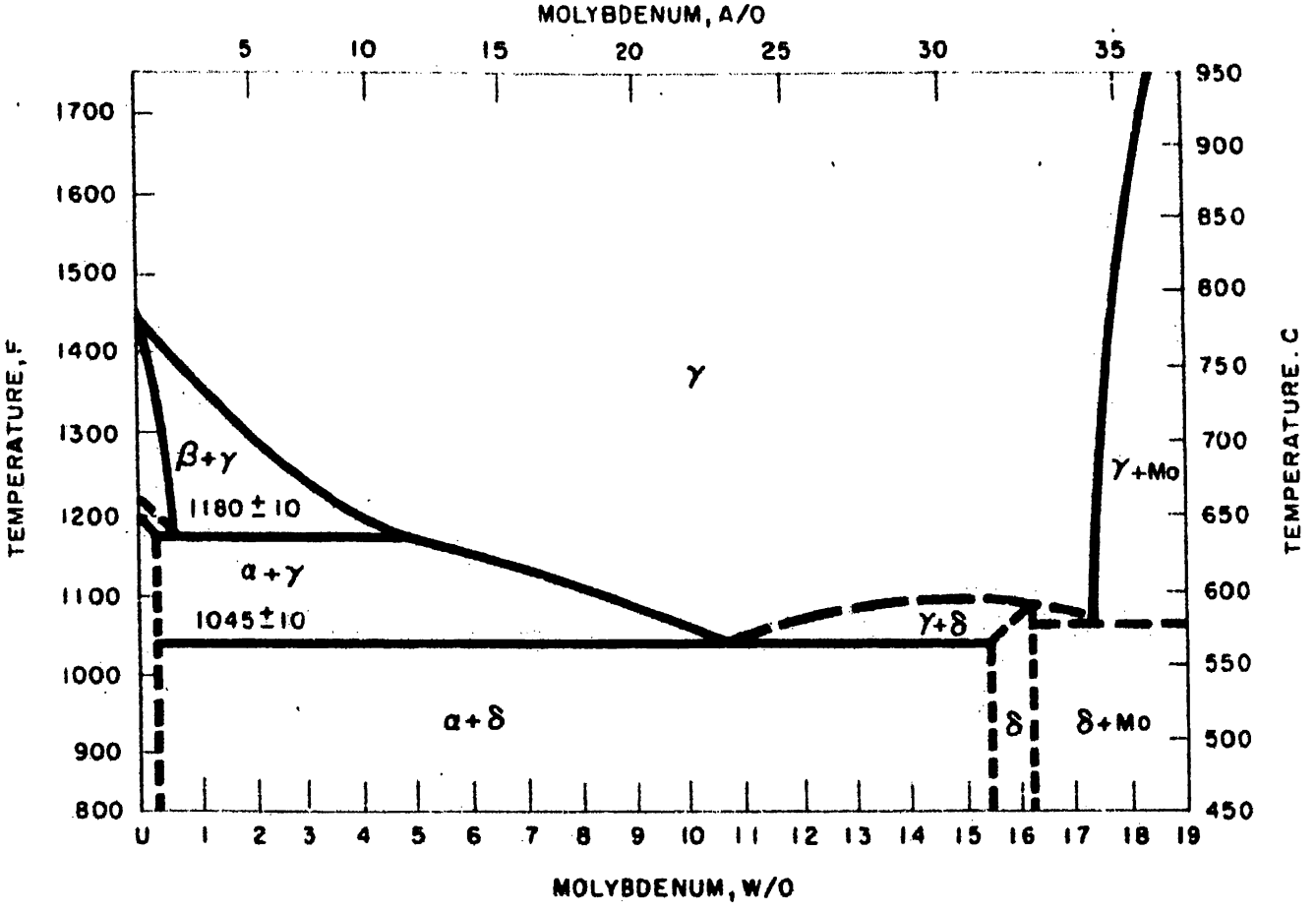

U-Mo EQUILIBRIUM DIAGRAM TO 19 WT % Mo

FIGURE 28

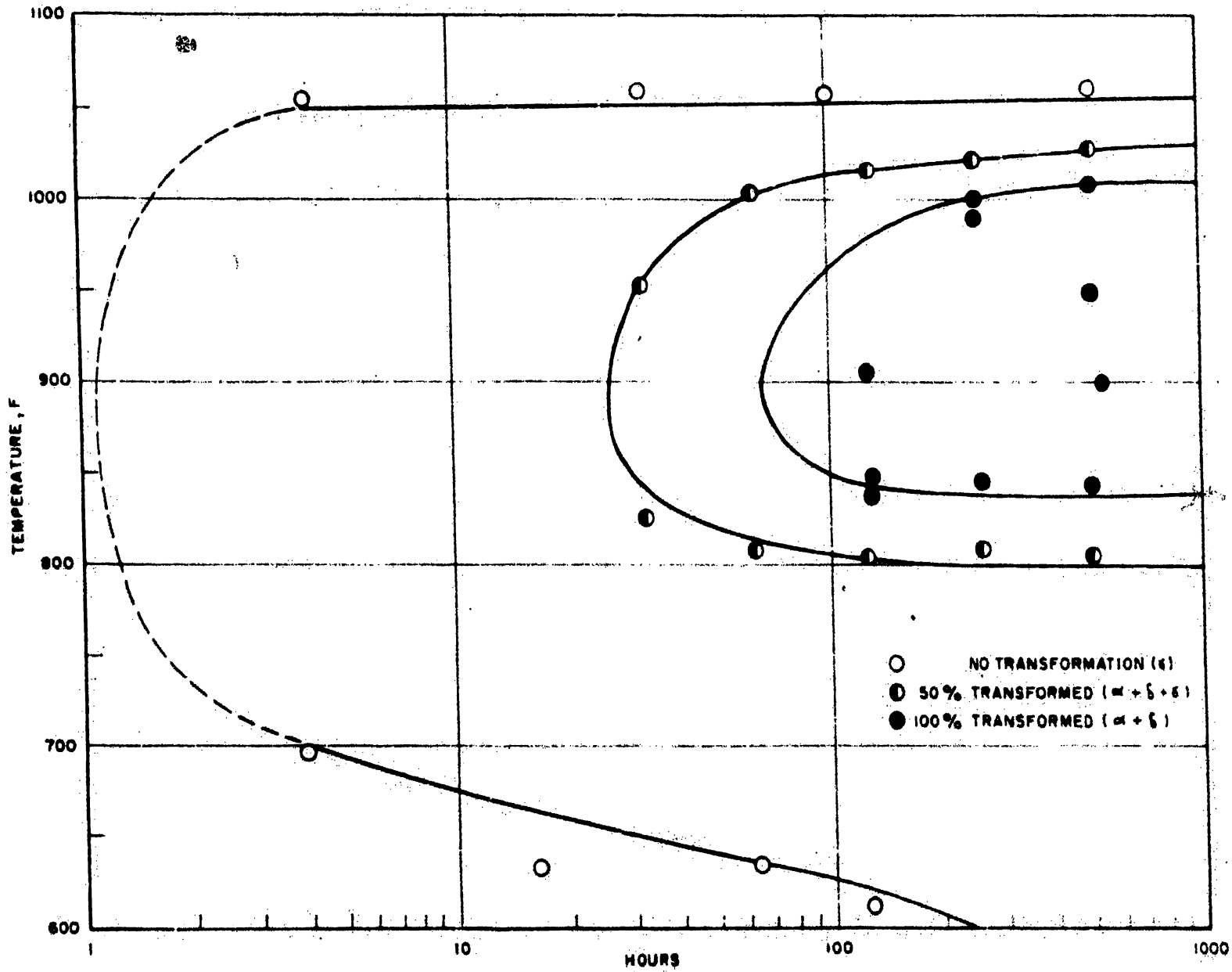

T-T-T CURVE FOR U-10 w/o Mo, FABRICATED INTO FUEL PINS-DETERMINED METALLOGRAPHICALLY

FIGURE 29

for inspection of the Fermi fuel pins. As soon as nondestructive techniques were developed, testing of the fuel pins that were made at the same time and by the same fabricator as the CP-5-1 pin, indicated that virtually all pins made at that time would have been rejected on the basis of Fermi fuel requirements and specifications. However, no gross defects such as cracks or nonbonding of cladding were observed in the postirradiation metallography of the CP-5-1 pin, and the swelling is not believed to be due to internal defects.

At the present time, the fission-rate effect is considered the most plausible theory as evidenced by the MTR irradiation test results and by test results on a similar alloy.* The fission rates for the MTR irradiation program, [4] were generally greater than 10^{14} fissions/cc/sec, and all low burnup specimens probably were maintained in the more stable gamma phase or were transformed to this stable phase.

4. Postirradiation Mechanical Properties

Postirradiation stress-strain properties of the U-10 w/o Mo alloy were determined by means of instrumented bend tests on specimens irradiated to burnups of 2.1 total a/o.[10] The effect of burnup on ultimate strength and strain-at-fracture for a 932 F test temperature is shown in Figure 30. A marked reduction in strength and ductility is seen to exist after irradiation, with the most drastic reduction occurring prior to a burnup of 1 a/o. Clad specimens were observed to exhibit greater ductility than bare specimens; this effect is believed to result primarily from reduction in effective surface defects.

The effects of temperature on the modulus of elasticity of irradiated 10 w/o Mo specimens is also shown in Figure 30. The modulus is seen to decrease with test temperature and with burnup.

The data presented above for postirradiation strength, ductility, and elastic modulus require some qualification. During the course of testing, the specimens were effectively subjected to a postirradiation heat treatment; microstructural examination of tested specimens indicated that partial decomposition of the gamma phase had occurred. Tests of unirradiated material show that transformation of the gamma phase results in an increase in dynamic modulus. Thus, at the 932 F test temperature in particular, a portion of the change in mechanical properties is undoubtedly obscured by this transformation. Consequently, the direct application of properties determined by postirradiation measurements to in-pile behavior is not regarded as valid.

Hardness measurements obtained during the course of postirradiation metallographic examinations showed that only a slight increase was

---

* Personal Communication, R. Fillnow, BAPL.

(10) BMI-APDA-638, "Stress-Strain Properties of Irradiated U-10 w/o Mo", January, 1958

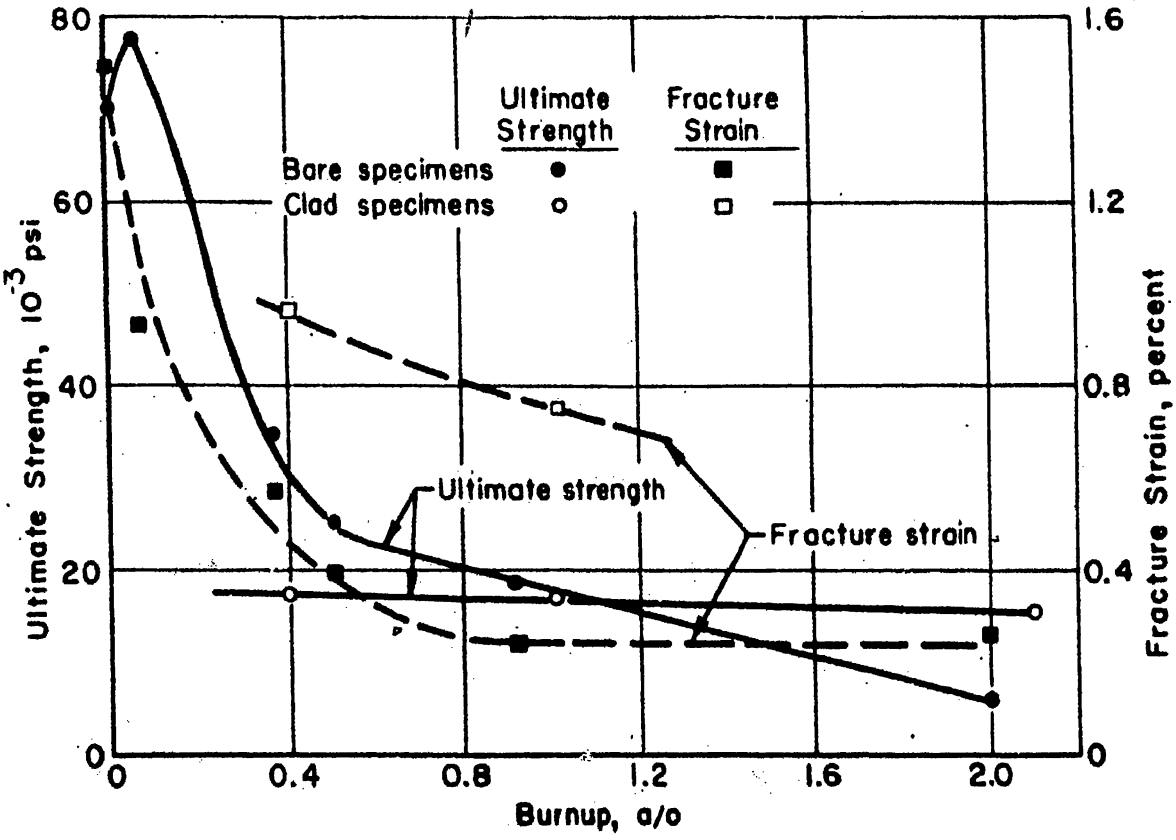

EFFECT OF BURNUP ON POST IRRADIATION ULTIMATE STRENGTH AND FRACTURE STRAIN OF URANIUM-10 w/o MOLYBDENUM AT 932F

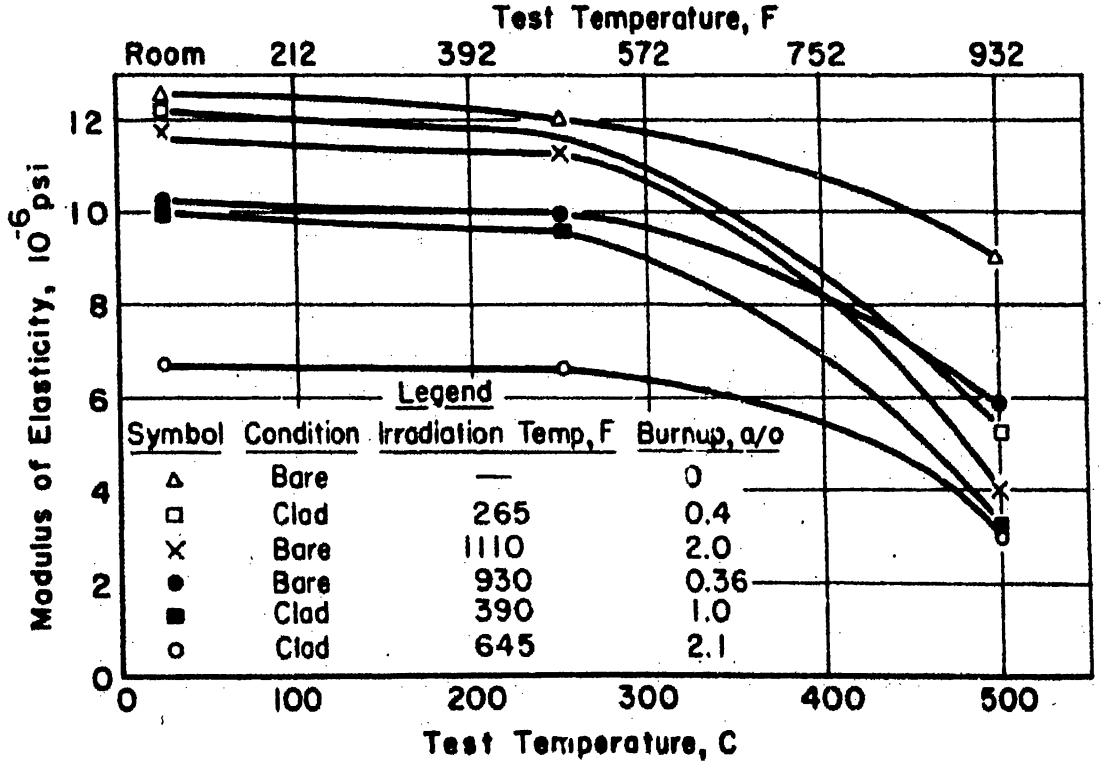

EFFECT OF BURNUP AND TEMPERATURE ON POST IRRADIATION ELASTIC MODULUS OF URANIUM - 10 w/o MOLYBDENUM

FIGURE 30

produced as a result of irradiation. The unirradiated gamma-phase U-10 w/o Mo alloy exhibits a hardness of about 300 DPHN (Diamond Pyramid Hardness Number); an increase in hardness of between 30 and 60 DPHN accompanied irradiations to burnups of 2.2 a/o. The only exceptions noted were in the specimens which had swelled excessively; in these speciments, hardnesses as low as 230 DPHN were obtained. The decreased hardness suggests porosity in the alloy resulting from fission-gas void formation.

5. Postirradiation Physical Properties

Electrical resistivity measurements were obtained during the course of the MTR irradiation program. These were designed primarily to provide information concerning the stability of the gamma-phase during irradiation. The electrical resistivity of the metastable gamma-phase at liquid nitrogen temperature is approximately 75 microhm-cm, while the resistivity of the transformed alpha-plus-epsilon phase in the U-10 w/o Mo alloy is about 35 microhm-cm. Postirradiation electrical resistivity measurements showed that the resistivity of initially transformed specimens increased to values characteristic of the retained gamma phase, while the resistivity of specimens irradiated in the retained-gamma condition was essentially unchanged. The results were taken as an indication of gamma-phase stability in the presence of a neutron flux and of radiation-induced gamma-phase reversion of initially transformed alloy specimens. They parallel those reported by other investigators[2].

The effect of irradiation on the postirradiation linear-thermal expansion of the U-10 w/o Mo alloy is summarized in Figure 31. The curve for the expansion of the unirradiated specimens represents an average for a heating and cooling cycle. As shown in Figure 31, no significant effect of difference in burnups between 0.97 and 2.0 a/o on thermal expansion between room temperature and 932 F was noted. However, irradiation apparently produced a slight increase in the magnitude of expansion for the alloy when compared with the unirradiated control specimen. Probably of greater significance though, is the unrecoverable increase in over-all length resulting from a single cycle to 930 F on these two irradiated specimens. Also, density and electrical resistivity measurements showed that the dilation test had produced both a density decrease and a decrease in resistivity indicative of the initiation of gamma-phase decomposition. The change in linear-thermal-expansion characteristics resulting from irradiation is probably due to swelling during postirradiation testing. When both of these specimens were irradiated previously at a maximum temperature of about 1100 F, density decreases of 3.5 and 3.9 per cent were observed. These changes occurred during an irradiation period of a minimum of 58 days. Density changes of 0.9 and 2.1 per cent accompanied postirradiation heating and cooling over a 6-hour period. The results of heating to temperatures greater than 932 F are discussed in paragraph 8 (Postirradiation Heating), below.

Compared by the transient heat-wave method, irradiation affected the thermal conductivity of U-10 w/o Mo alloy as follows: no changes in thermal conductivity were observed to burnups of 0.35 a/o; but a drop of about 15 per cent was observed on specimens irradiated between 0.5

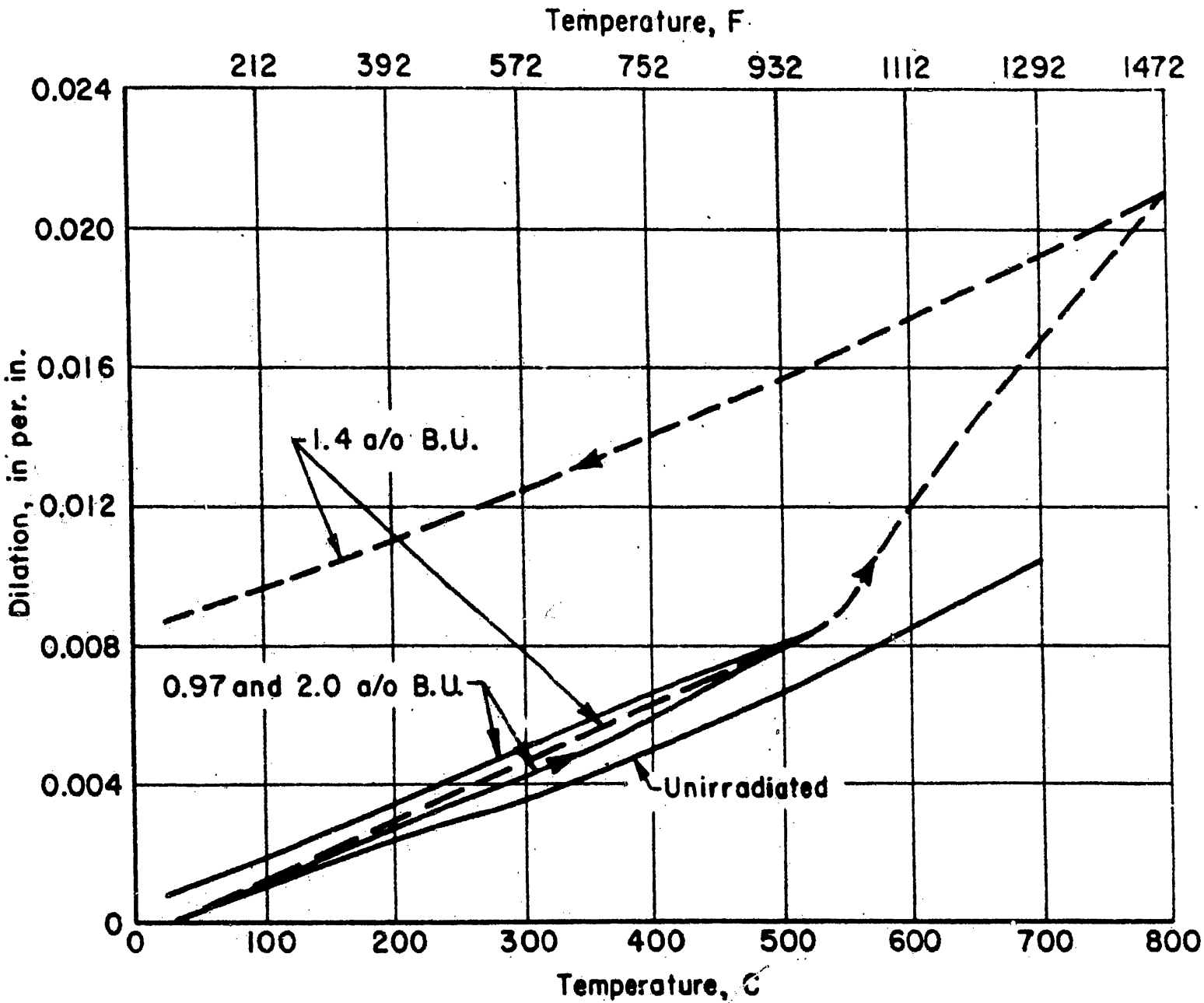

EFFECT OF IRRADIATION ON LINEAR THERMAL EXPANSION OF URANIUM-10 w/o MOLYBDENUM ALLOY

FIGURE 31

and 1.2 a/o. On the basis of these comparisons, a 15% safety factor was applied to the thermal conductivity values used in the design calculations.

6. Effects of Composition, Fabrication and Cladding Thickness

Analysis of the MTR data has led to the conclusion that small variations in composition and cladding thickness have little or no effect on the stability of the alloy. Heat treatment does not appear to be a significant parameter except when the treatment fails to stress relieve the fabricated alloy.

Specimens of U-9 w/o Mo and U-11 w/o Mo were irradiated, and the data were in substantial agreement with those from the more numerous U-10 w/o Mo irradiations. It was therefore concluded, that ±10% variance in the molybdenum content has no significant effect on the radiation stability of the alloy.

To determine the effect of zirconium cladding thickness on radiation swelling, twelve 2-inch long specimens, four each with 4-, 8-, and 11-mil cladding, were irradiated. At very high burnup, 2.0 to 2.7 a/o, large growth and density changes occurred and severity of cracking increased with increasing thickness of the cladding and burnup. However, since cracking was apparently initiated at the ends of the specimens where the burnup was highest, the role of cladding thickness was not certain. The real causes of failure were uncertain because many variables existed during the early days of specimen preparation. Generally, the quality of specimens irradiated in this early program were inferior to production fuel elements for the Fermi reactor.

The effects of inhomogeneity and impurities, particularly, were carefully scrutinized during this program to determine the radiation stability of production pins. The fuel specimens that were not stress relieved after the cold swaging operation were highly stressed. In addition, some of the specimens exhibited a high degree of micro-heterogeneity as a result of coring introduced during casting. Since the effect of the coring was not eliminated during subsequent fabrication processes, as evidence by a swirl pattern in the pins after the extrusion and swaging operations, a study was made to determine the possible benefits of a more homogeneous, stress-free conditions. Specimens were irradiated after various postfabrication heat treatments.[4] Only one heat treatment appeared to produce incongruous results. This treatment was the only one that did not sufficiently stress relieve the fuel alloy. Fermi fuel specification heat treatment insures a stress-relieved alloy with a minimum of micro-heterogenity.

7. Fission Gas Release

The release of fission gases measured from specimens irradiated in eight MTR capsules is detailed in a Battelle report[4]. There was little loss due to diffusion of the fission products through the cladding during the irradiation exposure of any of the clad specimens. In the unclad specimens the release was due to recoil and diffusion. Only where the burnup or in-pile temperature was excessive and specimens

ruptured or their claddings failed severely, as described in the preceding paragraph did the release of fission gas significantly increase above the amount to be expected by recoil from the surface.

Accordingly then, the only time that large amounts of fission gas can be expected to be released into the primary system of the reactor will be in case of a ruptured pin or of a severe cladding failure. The waste gas disposal system has been designed to accommodate all the fission gas recoiled from the surface of both ends of each fuel pin, assuming an exposed surface area at each end equivalent to a 0.100-inch diameter.

8. Postirradiation Heating

Postirradiation dilation measurements tend to confirm the critical swelling temperatures of material maintained in the gamma condition during irradiation as shown in Figures 21 and 26. A dilation curve for a specimen irradiated to about 1.4 a/o burnup at a temperature of 900 F and tested to 1472 F is shown in Figure 31. A marked increase in expansion occurs at about 1020 F indicative of the onset of swelling in the speciment. A density decrease of 3.2% was found to result from this test. The temperature at which swelling occurs during postirradiation heating can be correlated indirectly with the temperature at which swelling is observed during in-pile irradiation for this alloy, and hence, has provided an out-of-pile method of estimating the onset of swelling[4].

Postirradiation heating studies were also conducted for various periods of time at temperatures ranging from 1200 to 1850 F,[11,12] and post-heating diameter changes were measured.

Figure 32 shows the estimated diameter changes to about 1850 F. These curves were derived from the isothermal heating experiments for varying periods of time and for samples having varying burnups. The dashed portions of the curves represent the estimated regions while the maximum diameter change was derived from actual experimentation.

These data have been utilized in designing postirradiation handling equipment and in estimating the effect of in-pile temperature transients on the fuel.

9. Cladding Stability

Correlating the results of sodium corrosion tests with the in-pile postirradiation tests, cold trapping of the sodium to 30 ppm results in a maximum oxide penetration of the cladding of only about 1-1/2 mils even after 5 months at 1000 F. Sodium as such does not attack zirconium corrosively, and oxygen penetration is nominal for the life of

(11) BMI-646, "Postirradiation Heating Studies of U-10 w/o Mo Fuel Alloy."

(12) BMI-APDA-656, "Meltdown Studies of Irradiated U-10 w/o Mo Fuel Pins," April 1960.

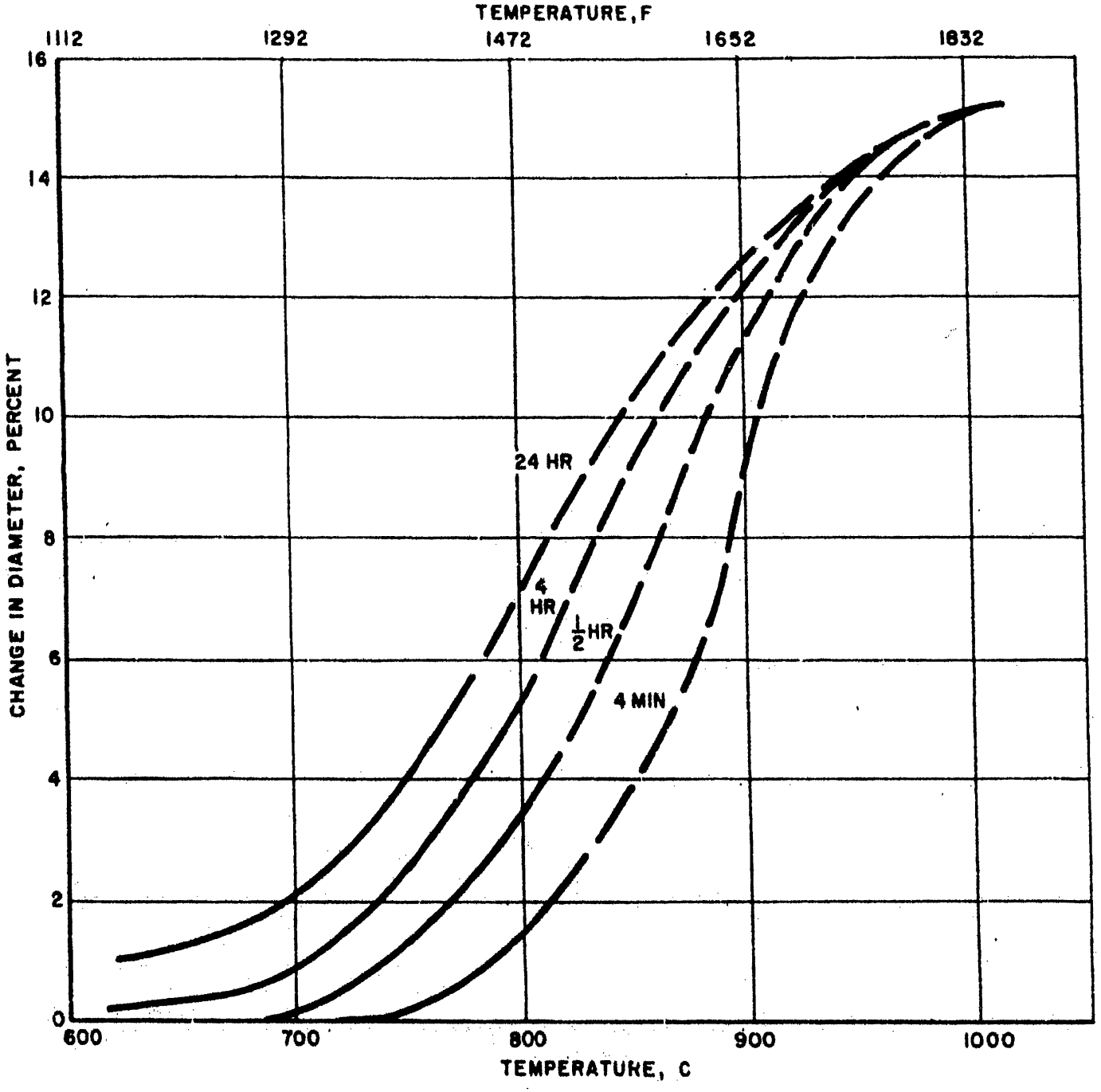

ESTIMATED PERCENT DIAMETER CHANGES WITH TIME AND TEMPERATURE FOR ZIRCONIUM-CLAD URANIUM-10 W/O MOLYBDENUM FUEL PIN IRRADIATED TO 1 % BURNUP

FIGURE 32

individual pins. The excessive swelling of the CP-5-1 pin, which not only had an original oxide layer formed during fabrication and a certain amount of buildup from the contained NaK bond, did not cause any cracking or rupturing of the clad surface. All cladding failures, shown for samples exposed in the MTR in Figure 21, occurred at burnups higher than 2 total atom percent; failures of unclad samples occurred at temperatures above 1110 F and/or at burnups greater than 2 a/o.

D. CONCLUSIONS

Based on irradiation data obtained prior to January 1961, some general conclusions may be made about the dimensional stability of the reference fuel alloy.

a. U-10 w/o Mo alloy, retained in the gamma phase by a high fission rate, will undergo little swelling at burnups less than 2.0 a/o when irradiated at centerline temperatures below 1100 F.

b. Under the conditions where the gamma phase is retained, the diametral growth proceeds linearly with burnup, and the influence of temperature is minor up to 1100 F to 2 a/o.

c. At temperatures above 1100 F, swelling is influenced by temperature and proceeds as a power function of burnup.

d. U-10 w/o Mo alloy in the transformed alpha-plus-epsilon condition is much less stable under irradiation, and swelling appears to be a power function of burnup. However, on the basis of the sparse data now available, a minimum burnup of 0.77 a/o is predicted for transformed material before the diameter increases by 8%, which has been conservatively selected as the design limit.

e. The likelihood of transformation to alpha-plus-epsilon is greatest at 900 F (the nose of the TTT curve), at which temperature the minimum fission rate required to prevent transformation is probably between 10^{13} and 10^{14} fissions/cm^3/sec.

E. CURRENT IRRADIATION PROGRAM

The consequences of the above-mentioned analysis in terms of the operation of the reactor at design conditions are that most of the fuel pins will transform in some regions, and the life of the core will be determined by the swelling of alpha-plus-epsilon material. Because the effect of burnup on the economics of the plant, irradiation experiments are continuing with the primary objectives of:

a. Determining the swelling behavior of the alpha-plus-epsilon phases of U-10 w/o Mo alloy.

b. Determining the minimum fission rate required to prevent transformation at all operating temperatures.

For these reasons, an irradiation program in the MTR was started in May 1960. Six specimens 1-1/2 inches long are being irradiated in capsules

at a target temperature range of 750 to 1100 F and at fission rates from 3 to 5 x 10^{13} fissions/sec/cm^3. The capsules are equipped with thermocouples for temperature monitoring; however, they are not temperature controlled. The burnup range will be 0.5 to 1.1 a/o. Most of the data are expected to be available by September 1961, and the program is expected to be finished in December 1961. Work in CP-5 has been accelerated and the program is to be finished by September. Four U-10 w/o Mo pins were in the reactor in April 1960. These pins will be irradiated to about 1.0 a/o burnup with inspections at twointermediate burnup levels. The temperatures of all four pins will fall within or will bracket the critical range for transformation.

All the pin stock to be used for specimens for the new MTR and CP-5 programs has been nondestructively tested by the ultrasonic method developed for the inspection of Fermi production pins. Some of the specimens contain defects in known areas, and the defects will be useful in the overall evaluation. About 75% of the stock meets the rigorous PRDC specifications for Fermi core material.

1. Preliminary Results

Some results have been obtained on zirconium-clad U-10 w/o Mo pins that were irradiated in the CP-5 and MTR in the current program.

The pertinent irradiation information for the pins that were irradiated in the CP-5 reactor are presented in Table V together with the per cent density and length changes that were observed after irradiation. Originally, the samples in the water-boiler capsules were 15 inches long; those in the air capsules were 23 inches and 31 inches long for the CP-5-5a and CP-5-5b irradiations, respectively.

Figures 33 through 38 present the local burnup, fuel centerline temperature, and per cent diameter change for these irradiations.

Table VI presents information concerning the irradiation results of reference zirconium-clad U-10 w/o Mo samples irradiated in two different temperature-monitored capsules in the MTR. These samples, 1-1/2 inches long x 0.158 inches in diameter, originally in the as-received gamma condition, and three samples transformed at 930 F were included in each capsule. From the values given in Table VI there does not appear to be a significant difference in the swelling characteristics of gamma material as compared to alpha-plus-epsilon material.

Metallographic and electrical resistivity results indicated that samples in the 35-3 capsule were about 65 percent gamma, while electrical resistivity results showed that gamma comprised about 90% of each sample in the 35-1 capsule. In all cases, there was no significant difference between the transformed or untransformed samples within a capsule. The swelling was greater for samples in the 35-3 capsule where the temperature was higher and the percentage of alpha higher.

To compare the results of these irradiation with those estimated

from the CP-5-1, CP-5-2 and CP-5-3 irradiations in which the fission rate was thought to be low enough to have the transformed structure during irradiation, the recent data on the estimated diameter increase versus burnup curve given previously and reproduced with the new points was plotted as shown in Figure 39. On this figure, all points for temperatures between 700 and 1070 F have been included, although the amount of alpha present for all the points is, at this time, unknown. These values will be estimated at a later date with electrical resistivity measurements.

The points as plotted indicate a larger diameter increase than was estimated from the CP-5-1, CP-5-2 and CP-5-3 irradiations. This is particularly true in the low burnup region.

2. Preliminary Conclusions

a. The new data as plotted in Figure 39 show somewhat larger diameter changes than were predicted from the earlier CP-5 work.

b. Although the diameter increase is greater than anticipated, the design value of 8% increase in the diameter of the fuel will not be reached in Fermi when the local burnup is 0.4 total a/o.

TABLE V - SUMMARY OF DATA ON CP-5 IRRADIATIONS

Specimen	CP-5-5a	CP-5-6a	CP-5-7a	CP-5-6e	CP-5-7e	CP-5-9b
Original Microstructure	$\alpha+\epsilon$ [1]	$\alpha+\epsilon$ [1]	γ	$\alpha+\epsilon$ [1]	γ	$\alpha+\epsilon$ [1]
Capsule Type	Air-Cooled	Water-Boiler	Water-Boiler	Water-Boiler	Water-Boiler	Air-Cooled
Location in Reactor	VT-27	VT-16	VT-17	VT-16	VT-17	VT-26
Average Burnup*, Total a/o	0.31	0.33	0.31	0.21	0.21	0.52
Average Fission Rate, $\frac{\text{Fissions}}{\text{Sec-cm}^3} \times 10^{13}$	1.1	1.4	1.4	4 to 7.5**	3. to 7.0**	1.3 raised to 2.6
Average % Change in Length	+1.12	+0.39	-2.45	+0.31	- - - -	+3.2
Average % Change in Density	-1.97	-3.8	-1.6	-3.3	-2.9	-5.5

[1] Transformed at 930° F.

* For local burnup see the detailed figures.

** The values given here are for the fission rate ranges.

TABLE VI - MTR IRRADIATION DATA

Irradiated Design		Unirrad. State	Burnup, a/o	% Δ Density	% Δ Length	% Δ Diameter
BMI-35-1*						
	Sample 2	γ	0.57	-4.0	+1.3	+ 1.8
	3	α+ε	0.59	-4.2	+1.5	+ 1.2
	8	γ	0.61	-2.8	+1.0	+ 0.6
	9	α+ε	0.62	-5.4	+0.3	+ 1.9
	11	γ	0.62	-4.2	+1.6	+ 1.3
	12	α+ε	0.64	-3.8	+1.4	+ 1.2
BMI-35-3**						
	2	γ	0.44	-8.4	+2.8	+ 2.9
	3	α+ε	0.45	-9.7	+3.6	+ 3.4
	5	γ	0.43	-9.7	+3.6	+ 3.5
	6	α+ε	0.44	-9.8	+3.6	+ 3.4
	8	γ	0.47	-7.3	----	+ 3.4
	9	α+ε	0.43	-5.9	+2.0	+ 2.1

*The average fission rate for samples in the 35-1 irradiation capsule was about 3.5×10^{13} $\frac{\text{fissions}}{\text{sec-cm}^3}$ and the temperature approximately 900 F.

**The average fission rate for samples in the 35-2 irradiation capsule was about 4.3×10^{13} $\frac{\text{fissions}}{\text{sec-cm}^3}$ and the temperature approximately 1000 F.

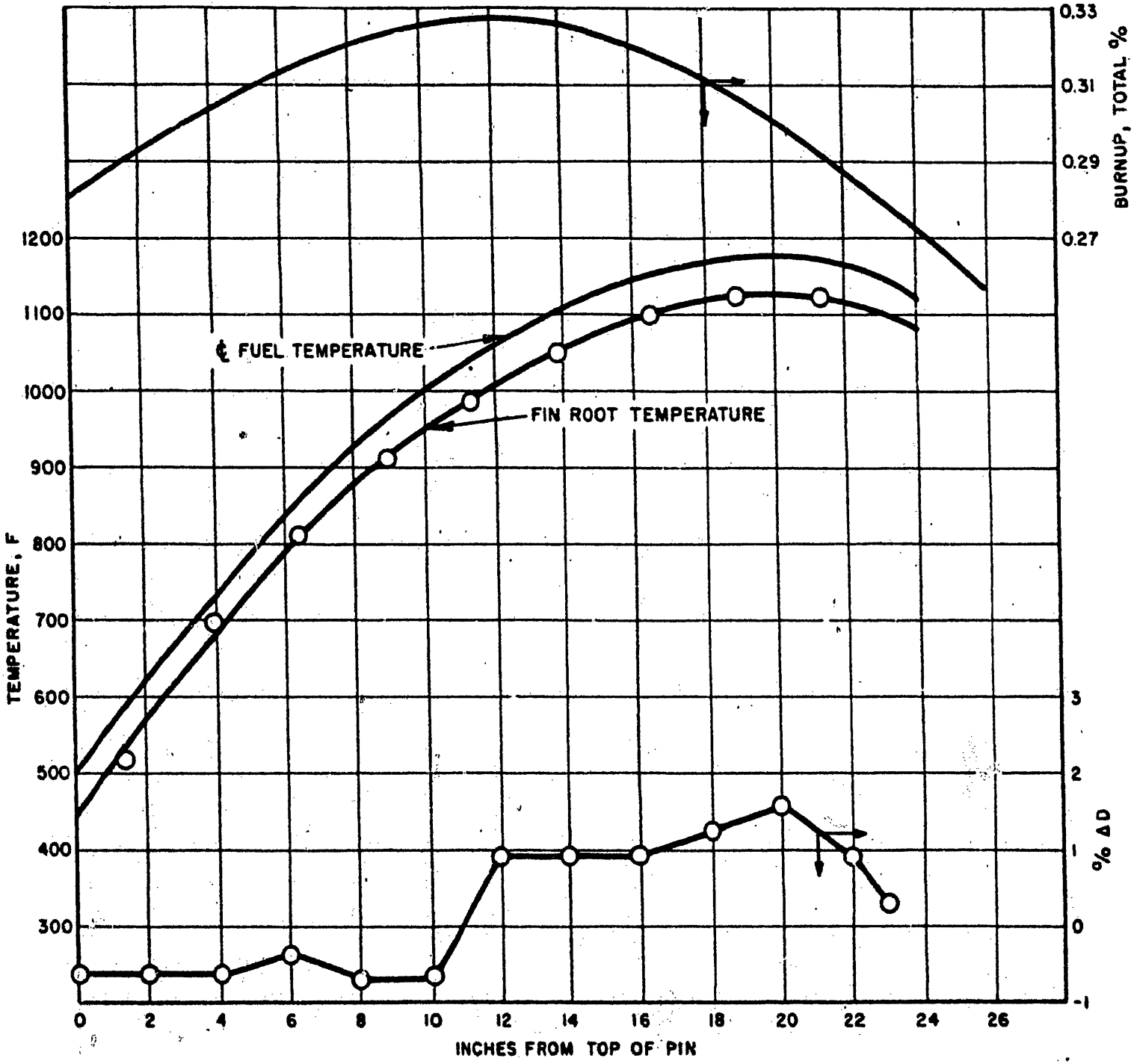

RESULTS OF CP-5-5a IRRADIATION
(FIRST BURNUP INCREMENT)
FIGURE 33

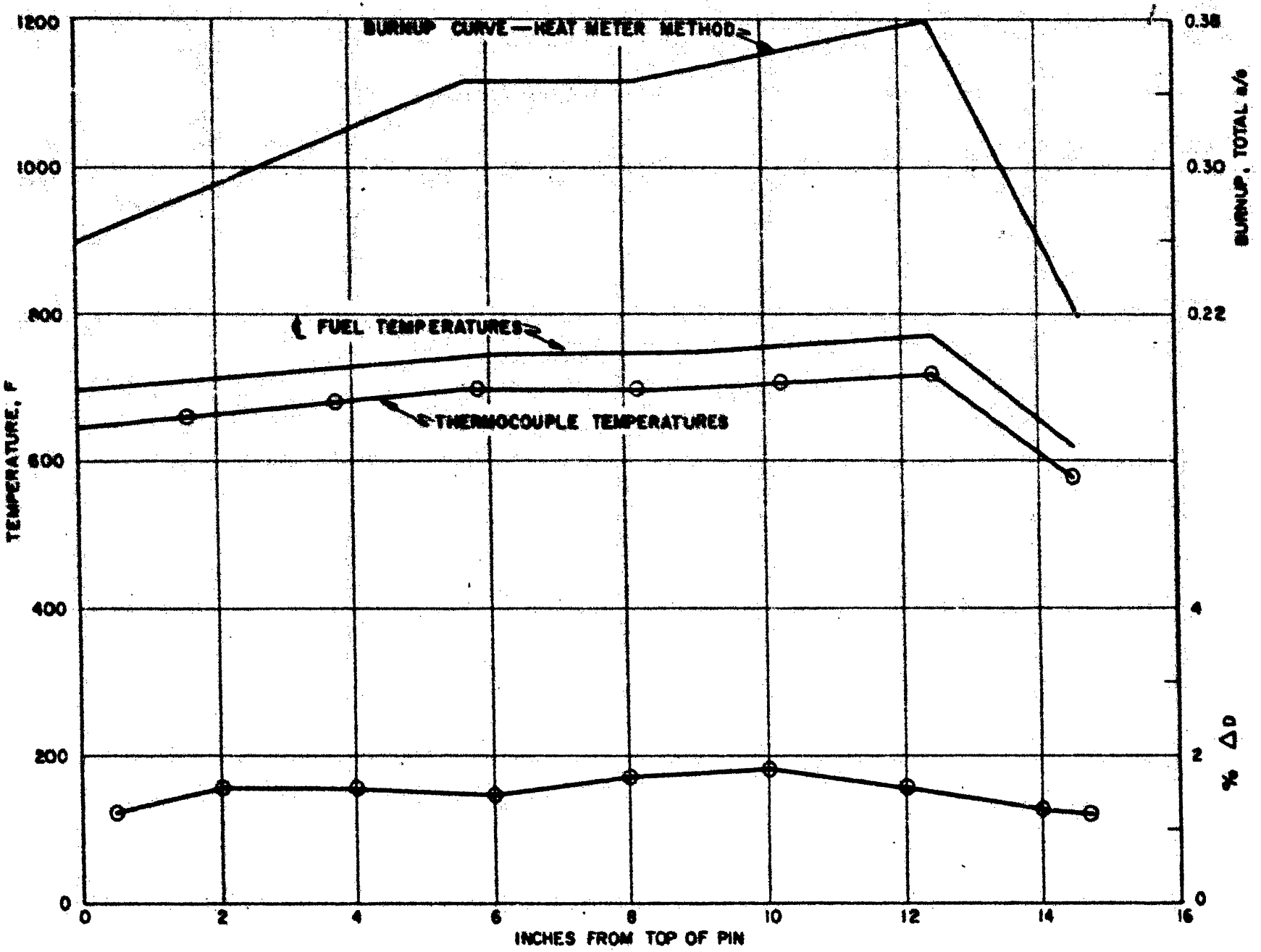

RESULTS OF CP-5-6A IRRADIATION

FIGURE 34

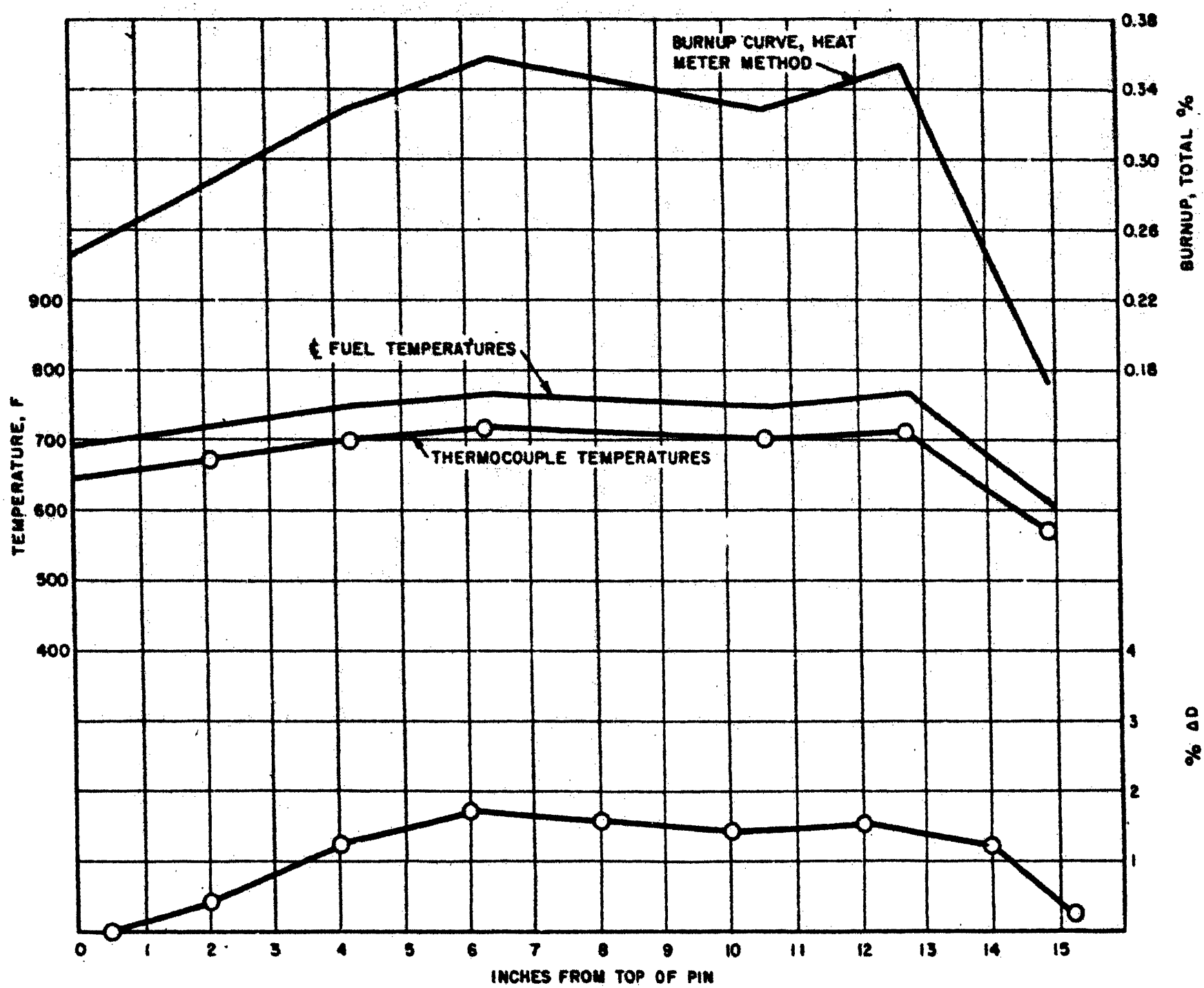

RESULTS OF CP-5-7a IRRADIATION

FIGURE 35

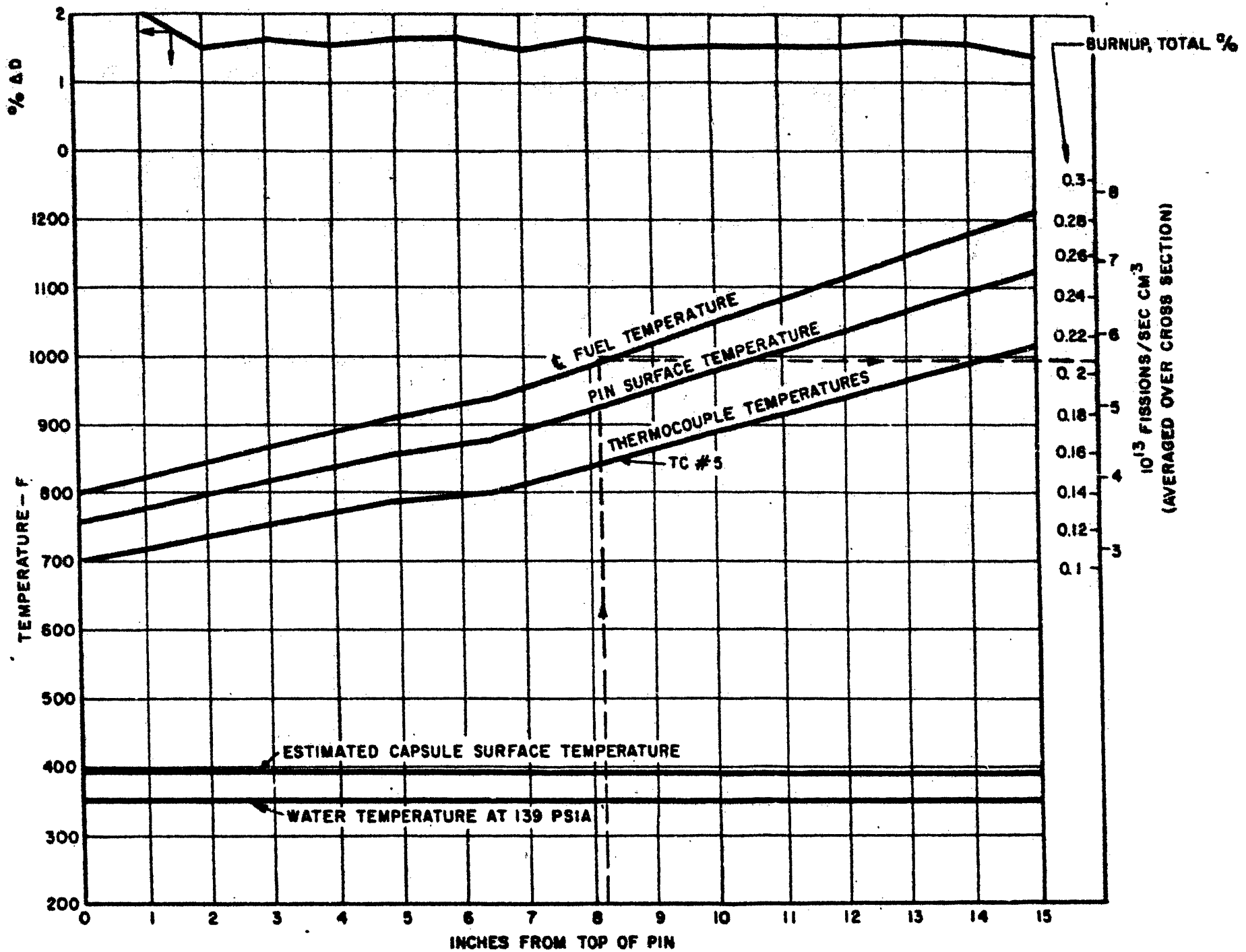

RESULTS OF IRRADIATION OF CP-5-6e
(FIRST BURNUP INCREMENT)

FIGURE 36

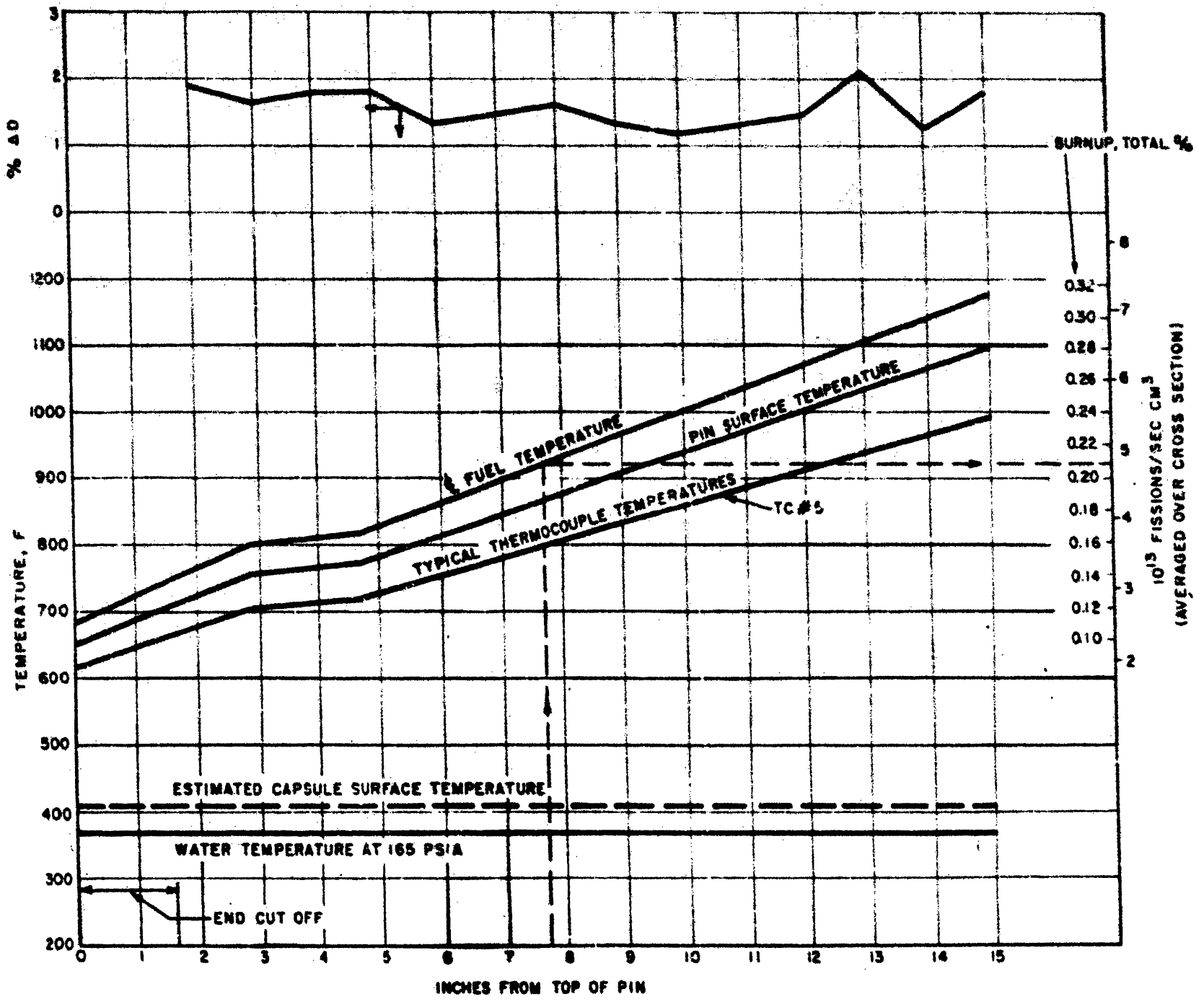

RESULTS OF CP-5-7e IRRADIATION (FIRST BURNUP INCREMENT)

FIGURE 37

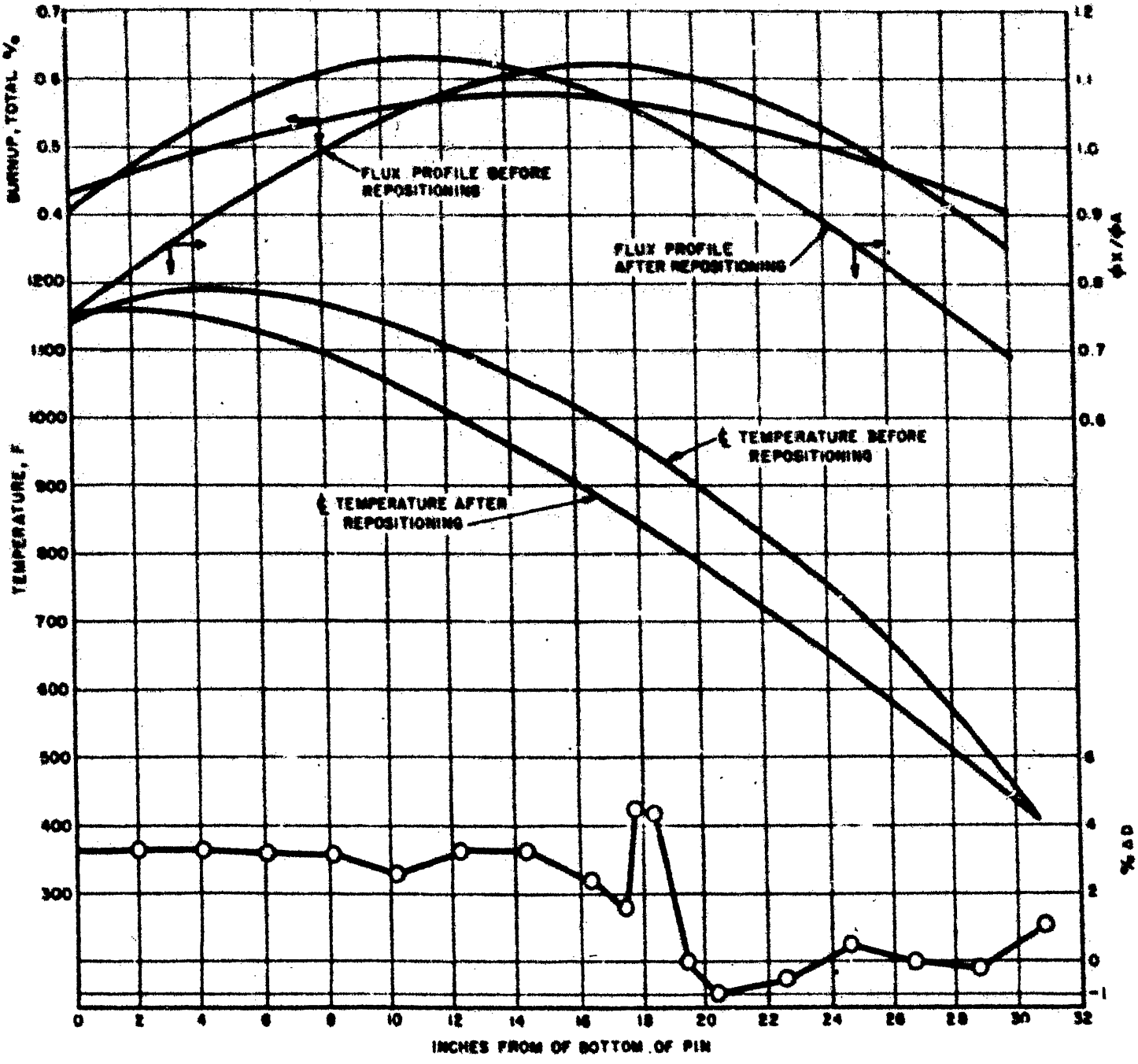

RESULTS OF CP-5-5b IRRADIATION
(FIRST BURNUP INCREMENT)
FIGURE 38

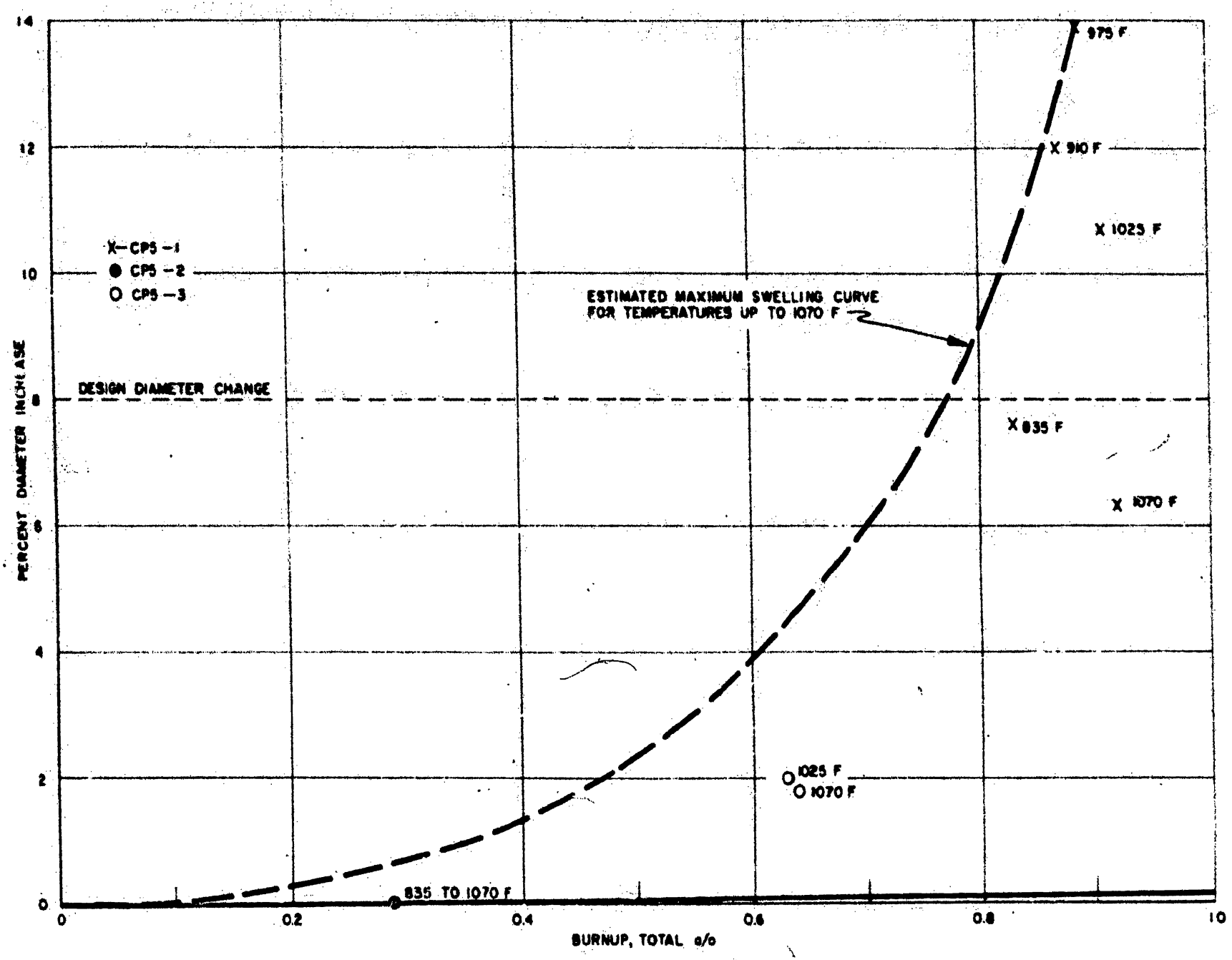

SWELLING ESTIMATES FOR U-10 w/o Mo IN THE $\alpha + \epsilon$ CONDITION UNDER IRRADIATION DERIVED FROM CP5-1, 2, 3, EXPERIMENTS

FIGURE 39

VII. SUMMARY OF U-3 W/O MO IRRADIATION DATA

A. BASIS OF MATERIAL SELECTION

The selection of the blanket alloy was made on the requirement of a maximum allowable local burnup of 0.5 total a/o and a small reduction in the breeding gain caused by alloy constituents in the depleted uranium. Based primarily on irradiation data obtained by ANL in 1956[1], it appeared that unalloyed uranium did not have sufficient radiation stability, whereas U-3 w/o Mo, properly heat-treated, would meet the burnup requirements for the Fermi reactor.

B. DESIGN REQUIREMENTS

1. Design Requirements

The radial blanket consists of rods, 0.395 inch in diameter, that are hermetically sealed within, and sodium bonded to, stainless-steel tubes having a nominal internal diameter of 0.423 inch. The diametral clearance is approximately 7% of the initial diameter of the alloy. It is uncertain whether the stainless-steel cladding will restrain the growth of the U-3 w/o Mo alloy; therefore, a subassembly will be removed from the reactor before the estimated swelling of the uranium alloy is such that the alloy is in full circumferential contact with the cladding in any one of the 25 elements within a subassembly.

C. IRRADIATION TESTING

In addition to the work done by ANL[1] and Atomics International[2], data has been obtained from the irradiation of two blanket material pins, identified as CP-5-4a and CP-5-4c, in the CP-5 reactor. Both pins were unclad, and originally 0.106 inches in diameter and 24-7/16 inches long. These dimensions and an enrichment of 10.54% were chosen so that the irradiation could be completed in a reasonable time while test conditions were maintained comparable with those expected in the Fermi reactor.

In these tests finned, air-cooled capsules, identical in design to those used in the CP-5 irradiation of prototype Fermi fuel elements, were used. A temperature profile similar to that expected in the hottest Fermi radial blanket rods can be established in this type of capsule and maintained (a) by positioning of the pin with respect to the flux profile and (b) by control of the mass flow rate of air that is used to transfer heat from the finned capsule.

---

(1) ANL 5736, Smith, K. F., "Irradiation of Uranium Fissium Alloys and Related Compositions," September 1957.

(2) Private Communication with Atomics International, Preliminary Data.

Figure 40 shows the nominal readings of the thermocouples spot-welded to the body of the CP-5-4a capsule, along with the resultant calculated centerline temperature profile of the pin. Temperatures were held quite constant throughout the five-month test, varying no more than 50 F from the nominal values except when the reactor shut down. The burnup profile is also shown in Figure 40. The average burnup for the pin was 0.42 total a/o. The number of reactor scrams was 245 during the test; the average fission rate of the specimen was 2.04×10^{13} fissions/sec cm^3; and the average heat flux at the specimen surface was 140,000 Btu/hr ft^2.

The temperature history of the CP-5-4c test indicated on accidental coolant maladjustment which was corrected after 24 hours. Figure 41 shows the typical centerline temperature profile, which is very similar to that of the CP-5-4a test, and the profile which existed for the 24 hour period of the coolant maladjustment when the burnup was about 0.33 total a/o. The final burnup values are also plotted on Figure 41. The average burnup was 0.61 total a/o. The reactor scrammed 343 times during this test, and the fission rate and heat flux were virtually the same as in the CP-5-4a test.

D. RADIATION STABILITY AND DESIGN VERIFICATION

Shown in Figures 40 and 41 are diameter changes which were measured for the CP-5-4a and CP-5-4c irradiation samples. These curves also plot the local central-metal temperatures and burnups at which these changes occurred. These data show that large diameter increases in the CP-5-4a pins occurred at temperatures in excess of about 850 F, and it is assumed that the 24-hour temperature excursion which the CP-5-4c pin experienced was too short to affect seriously the swelling of the alloy.

If the difference in burnup between diameter increases reported at temperatures of 920 and 950 F shown in Figure 41 for the CP-5-4c pin were to be disregarded, there appears to be an anomaly because of the higher temperature causing less swelling. This anomaly may be associated with the transformation kinetics of this alloy. This possibility is considered unlikely, however. Another way of interpreting the data in Figure 41 is that there is little temperature effect, and that the differences in burnup were the factors that determined swelling above 850 F. To clarify this last point, Figure 42 was drawn showing the CP-5 burnup vs. diameter-increases data temperatures above 850 F and assuming no significant temperature effect in this range. This is the more conservative approach since, if one assumes a large temperature effect, less swelling is indicated at temperatures greater than 920 F. Also included in Figure 42 are (a) data reported by ANL[1] for U-2-1/2 w/o Mo given a similar heat treatment as the Enrico Fermi blanket rods and (b) preliminary AI[2] data for as-cast U-3 w/o Mo. Although there is some scatter, the AI data compares reasonably well with the CP-5 results, and the ANL results are considerably better.

Based on the interpretation of these data, the design of the blanket element can accommodate the diametral growth associated with a local burnup of 0.57 total a/o when the central metal temperature is in excess of 850 F. At the present time, there are not sufficient data to ascertain what burnup the lower temperature portions of the blanket rods may attain without intimately contacting the stainless steel. It is apparent, however, that removal

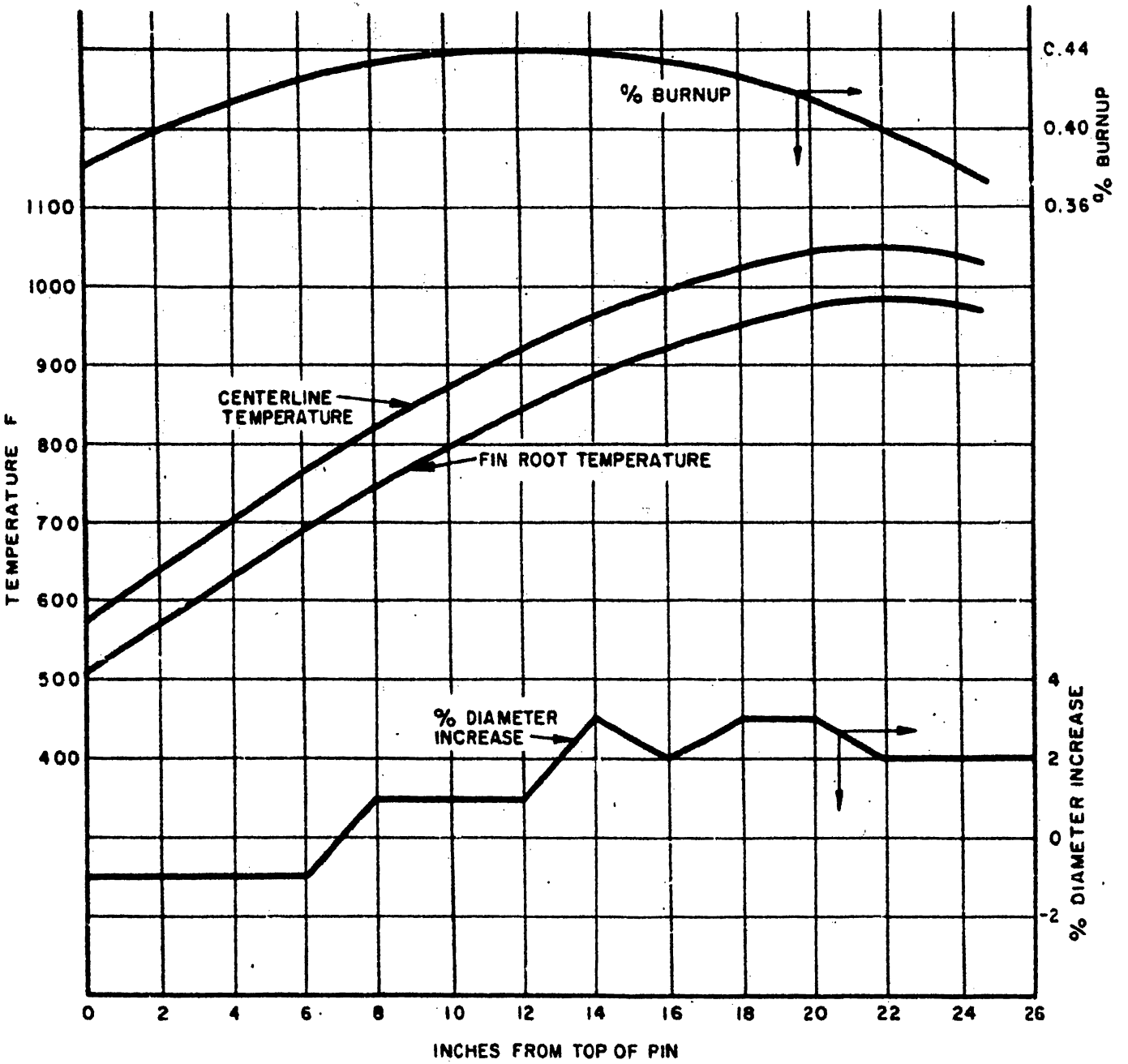

IRRADIATION RESULTS OF CP-5-4a TEST

FIGURE 40

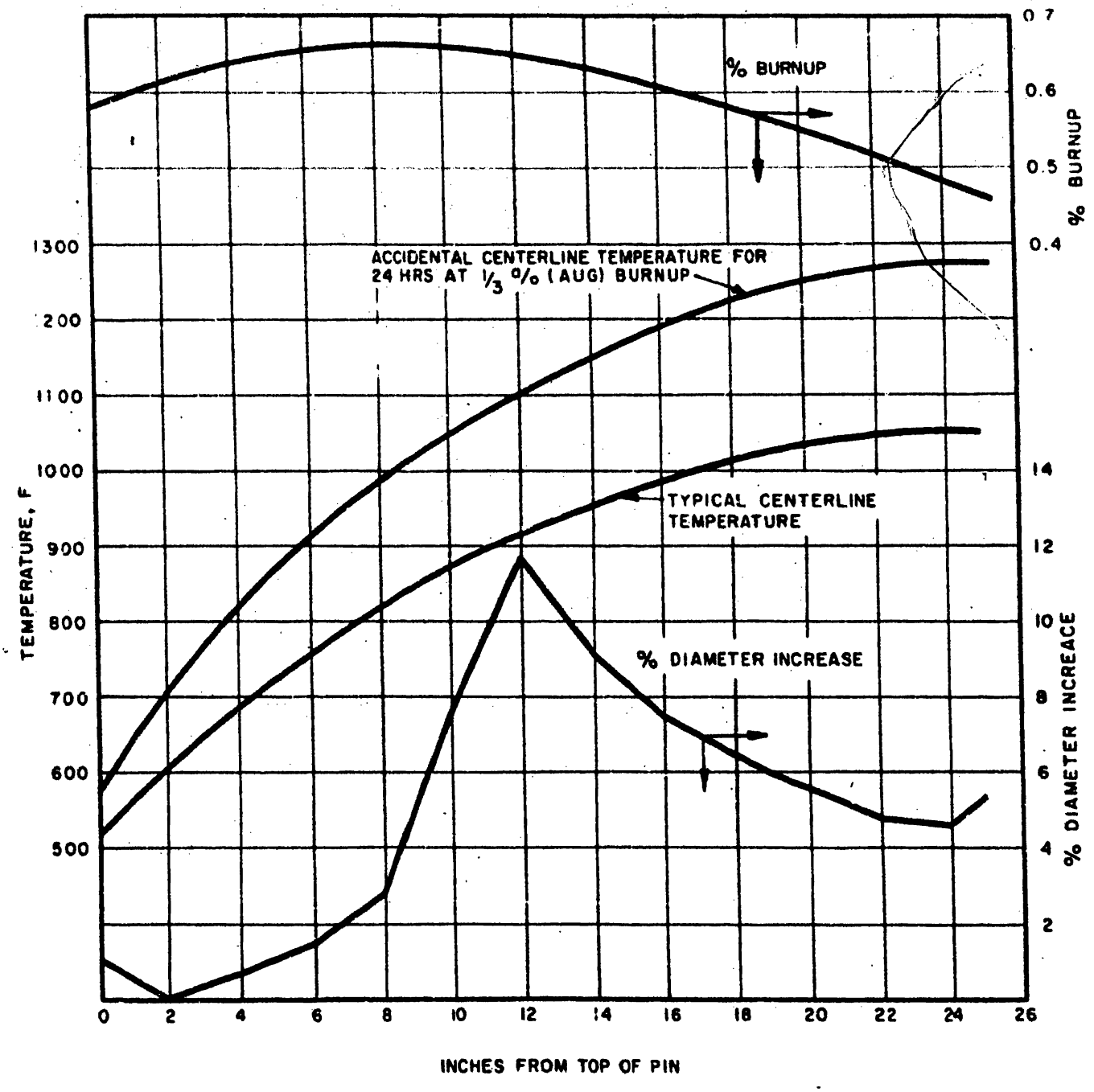

IRRADIATION RESULTS OF CP-5-4c TEST
FIGURE 41

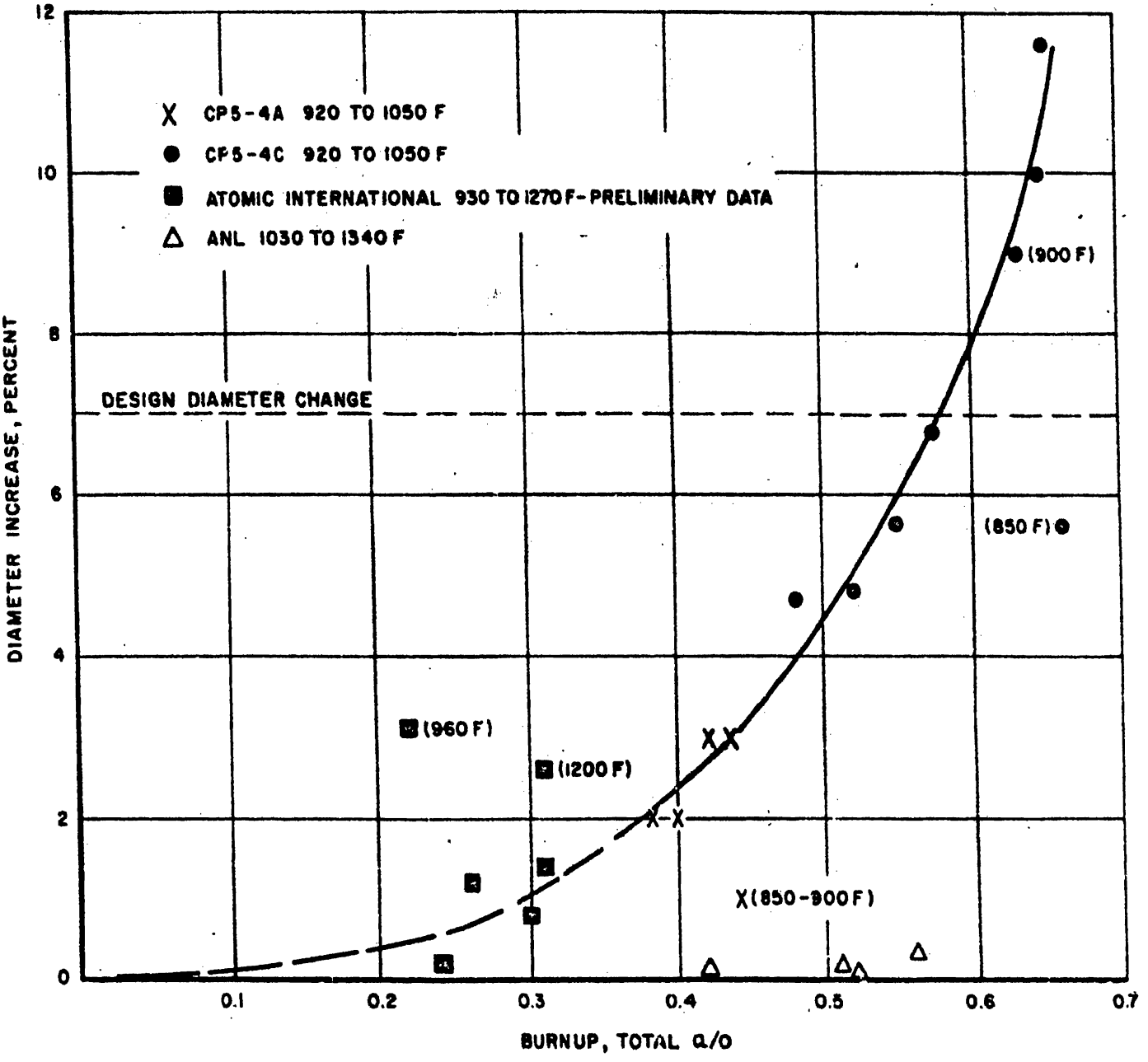

DIAMETER INCREASE OF URANIUM - 3 w/o MOLYBDENUM ALLOY AS A FUNCTION OF BURNUP AT TEMPERATURES GREATER THAN 920 F

FIGURE 42

will be dictated by the swelling of the section of the rods operating at higher temperatures.

The changes in length were also estimated, although both pins were somewhat warped after irradiation because of the lateral restraint caused by a zirconium spacing wire that was attached to each end of the pin and spirally wrapped around it. Calculations, which were made on the pin warped profile, indicated an over-all change in length for the CP-5-4a and CP-5-4c samples of 3.2 and 3.7%, respectively. There does not appear, therefore, to be any problem of the pin growing in length and extending out of the sodium.

Data on volume increases, calculated from pre-irradiation and post-irradiation measurements of density, appear in Table VII. It may be seen by comparison of Table VII with Figure 41 and 42, that the larger volume changes occurred in the specimens in the regions that showed large diameter changes. The over-all volume increases for the CP-5-4a and CP-5-4c pins were 4.66 and 10.67%, respectively. It has already been stated that the design will accommodate a U-5 w/o Mo volume increase of 7.5% (exclusive of fission products by recoil). In the CP-5 tests, the maximum-to-minimum burnup ratios (along the length of the pin) were about 1.2 and 1.4; whereas in the Enrico Fermi reactor, the maximum-to-minimum ratio is much greater than 2, thereby making the total volumetric change smaller for a given maximum swelling. The large swelling occurred at temperatures greater than 850 F, so the irradiation tests were conservative in that a considerably greater fraction of each CP-5 pin was above 850 F than will be the case even in the hottest blanket pin in the Fermi reactor.

E. CONCLUSIONS

The Fermi blanket elements were conservatively designed from the standpoint of a volume and length growth, and it is actually the diametral growth that determines the allowable burnup. Diametral growth will be less than that allowed for, if the subassemblies are removed upon attainment of a local burnup of no more than 0.5 a/o. Unless a postirradiation inspection program is initiated, all blanket subassemblies will be removed at 0.25 a/o local burnup to provide an adequate margin of safety.

The upper and lower axial blanket elements are integral with the core subassemblies and, since their burnup will be very low, swelling will be negligible. The maximum burnup in the axial blanket is approximately 5% of the maximum burnup in a core element. Therefore, when the maximum core burnup is 0.4 a/o, the maximum axial blanket burnup is 0.02 a/o.

TABLE VII - CALCULATED VOLUME CHANGES

Pin Designation	Condition	Location on Pin	Density (gram per cm^3	Increase in volume*%	Average Burnup, a/o	Nominal Centerline Temp. Range, F
CP-5-4a	Unirrad.	Entire Pin	18.47	--	--	--
	Irrad.	Entire Pin	17.65	4.66	0.42	570-1050
		Top 13"	18.15	1.77	0.42	570-935
		Lower 12-1/2"	17.08	8.15	0.42	935-1050
		1-3/8 to 6-1/4" from top	18.18	1.6	0.41	610-760
		7-1/8 to 12" from top	17.96	2.84	0.43	790-915
		12 to 13" from top	17.60	4.95	0.44	915-940
		13 to 18" from top	16.98	8.8	0.43	940-1020
		19 to 24" from top	17.01	8.6	0.40	1030-1050
CP-5-4c	Unirrad.	Entire Pin	18.46	--	--	--
	Irrad.	Entire Pin	16.68	10.67	0.61	515-1050
		Top 9-1/2"	17.97	2.74	0.64	515-860
		Lower 15-5/8"	15.95	15.75	0.59	860-1050
		1 to 4.8" from top	18.49	0	0.62	555-715
		5.8 to 9.5" from top	17.42	5.97	0.66	750-860
		11.5 to 12.5" from top	14.55	26.9	0.65	905-925
		12.5 to 17.3" from top	15.28	20.9	0.62	925-1005
		19.2 to 24.1" from top	16.75	10.2	0.52	1025-1050

*Calculated from density data

VIII. REACTOR ENGINEERING TESTS - CORE A

A. SUMMARY OF TEST RESULTS

This section contains summaries of the most important reactor engineering tests that were performed to substantiate the adequacy of the design for Fermi Core A.

Long-time sodium endurance testing established that the reactor structures would not be affected adversely by hydraulic forces at operating conditions. Endurance tests were run for both core and blanket subassemblies.

Dimensional stability tests established that operation will not be hampered by structural changes of reactor components.

Tests on sliding parts established that adequate protection has been provided against galling.

Flow velocity profile measurements established that all fuel pins will be adequately cooled.

Hydraulic tests established that appreciable flow forces will act to straighten fuel pins if the fuel pins are crooked.

Phase-change tests established that no fuel pins will touch even when phase changes occur that are more severe than those that can be encountered in reactor operation. Creep and thermal cycle tests supplemented the phase-change tests.

The results of these reactor engineering tests show that the design is conservative.

B. SODIUM FLOW ENDURANCE TEST OF CORE SUBASSEMBLY

A flow endurance test established the mechanical reliability of the core subassembly.

A complete reference core subassembly loaded with all new reference depleted uranium pins was tested for 1480 hours in flowing sodium at 1000°F. The subassembly flow rate was 230 gpm (148%) of nominal full flow for 200 Mw thermal operation. In this test, all of the subassembly components were subjected to many millions (effectively an infinite number) of flexing cycles due to vibration. When a test of this type is run for a long enough time, subassembly components will undergo creep and will have an opportunity to react to corrosion and erosion.

The clearance between fuel pins in the bundle between each grid in both directions was measured before and after the test. The spacing-frequency data are shown on Figure 43. The effect of the variation in pin

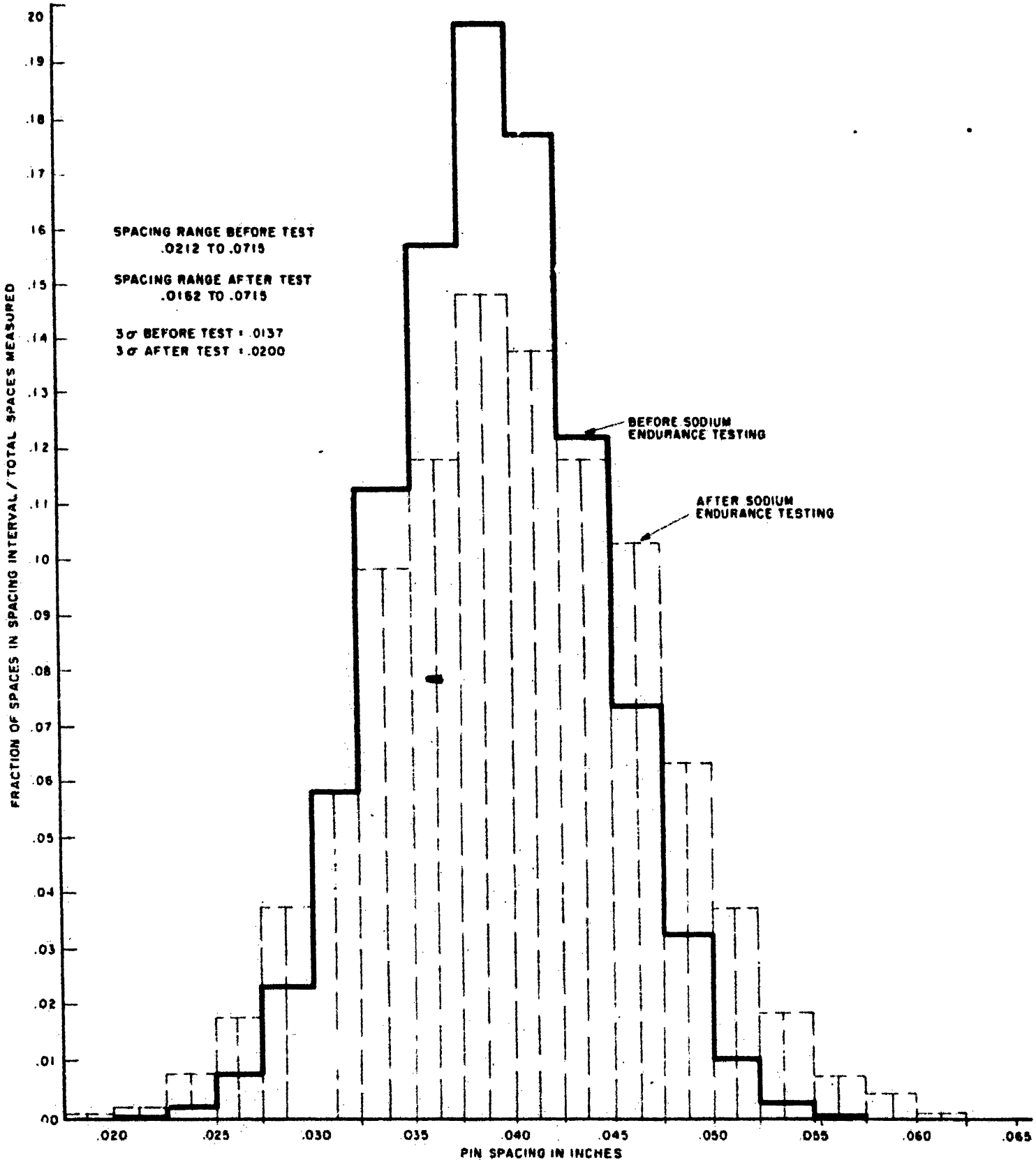

PIN SPACING DISTRIBUTION BEFORE AND AFTER SODIUM ENDURANCE TEST AT 1000 F FOR 720 HOURS

FIGURE 43

spacing on the flow distribution within the bundle, and the resulting hot channel factor on the maximum fuel temperature, were calculated for the spacing distribution obtained before and after the endurance test. The 3σ hot channel factor was 1.05 before the test and 1.14 afterwards. A hot channel factor of 1.15 was used as the design value. The fuel pins showed no tendency to touch. The entire subassembly, including all components, was in excellent condition after the test.

C. SODIUM FLOW ENDURANCE TEST OF BLANKET SUBASSEMBLY

A reference outer radial blanket subassembly was isothermally tested in flowing sodium at 800 F and 105 gpm for 815 hours. All subassembly components, including the spiral wires on the blanket rods, were in good condition after the test. There were no signs of buckling, collapse, or galling.

D. DIMENSIONAL STABILITY TESTS OF CORE SUBASSEMBLY

A subassembly was tested to see whether reactor temperatures would cause a permanent set in the subassembly. A permanent set could cause the core to loosen at low power and could cause difficulty during subassembly removal.

A dummy core subassembly was subjected to various environments and checked for concentricity of the pads about a centerline of rotation between the handling head lug and lower inner sleeve. The subassembly was first held in gas at 1050 F for 1-1/2 hours and then cooled and measured. The unit was next soaked in sodium at 700 F for 3 days. It was then drained, cooled, steam cleaned in a chamber designed for that purpose, and re-measured. In the last test, the unit was again soaked in sodium, but it was cleaned in the open air with a steam hose. Following this test, the unit was re-measured once a day for 8 days. Small variations in concentricity occurred after each test, but these were no larger than the changes that occurred from day-to-day, which apparently were due to small temperature gradients across the subassembly caused by non-isothermal room conditions. From the results of this test, it is concluded that reactor temperatures will not cause any permanent set in the subassemblies.

Four subassemblies were tested to determine the effect of the major operating stresses upon the stability of the square wrapper tube. Again, these wrapper tubes would have to be extremely unstable dimensionally before they could cause a reactivity control problem.

The following stresses were simulated:

a. Bending stress due to thermal bowing of the subassembly and to prebending of the subassembly by the inward offset of the hold-down fingers.

b. Bending stress in the walls due to internal pressure and to the reaction of the fuel bundle with the walls.

c. Lateral compressive stress in the walls due to the reaction at the spacer pads.

d. Internal stresses due to the fabrication process.

In operation the subassembly is also subjected to an axial compressive stress caused by the vertical load exerted by the hold-down, but this compressive stress is only 600 or 700 psi and was not simulated. The test was in a fixture which applied loads to the wrapper tube so that calculated operating stresses were nearly duplicated. In operation, the internal pressure decreases from the inlet to the outlet. The test was conservative since the whole tube was pressurized to the inlet pressure, 80 psi. The tube was heated by electrical resistance-heaters. In operation, the tube temperature varies from about 600 F at the inlet to 900 F at the outlet. In the test, the tube was isothermal with some runs at 600 F and some at 900 F. The fixture was designed so that measurements were taken of bow, outside dimension at the spacer pads, and flatness profile of the wall near the spacer pads.

These tests were run for 1000 hours. The wrapper tube dimensions changed by 0.002 inch due to the test condition. The walls of two adjacent subassembly wrapper tubes, when both subassembly wrapper tubes have the worst acceptable dimensions, must each bulge 0.006 inch before the wrapper tubes even touch (about 0.023 inch would be required for nominal subassemblies). It was concluded that stress relaxation or creep will not produce serious distortions with subassembly wrapper tubes.

E. TESTS ON SLIDING PARTS

Because of thermal and mechanical bending moments, the sliding surfaces between the inner and outer sleeves of the core and inner radial blanket subassemblies are subjected to a maximum side load of approximately 300 pounds. The rubbing surfaces on the inner sleeve are Colmonoy No. 4 applied over Type 304 stainless steel, and the outer sleeve is nitrided Type 304 stainless steel. The outer sleeve is also subject to rubbing against the support plates during insertion and withdrawal of the subassembly. These side loads are not accurately known, but they are small. The support plates are nitrided Type 347 stainless steel.

The materials were chosen as a result of a series of tests run to determine the self-welding and galling resistance of a large number of material combinations. The basic tests were run in an apparatus arranged to press and rotate two circular material specimens against each other. Most tests were run with the specimens submerged in sodium; a few were run in inert gas. The tests were run at bearing pressures of 1000, 2500, 5000, and 10,000 psi. At each pressure, runs were made at temperatures of 500, 600, 700, 800, 900, and 1000 F. At each pressure and temperature condition, one specimen was rotated 90 degrees relative to the other in two 45-degree increments at 30-second intervals. The specimens were then held at pressure and temperature for fifty minutes and again rotated as above. This procedure was repeated for each combination of pressure and temperature. At the conclusion of the tests, the samples were examined for signs of wear and/or galling. Two sets of samples of nitrided stainless steel against itself were run in sodium and showed little or no damage. Although the nitrided, stainless-steel specimens were not tested in gas, other materials tested both in sodium and gas showed that galling is more likely in a gas atmosphere.

Another test was a closer simulation of the conditions encountered during insertion and withdrawal of the subassembly. A nitrided Type 304 stainless-steel bar of the same diameter as the outer sleeve was cycled up and down in a nitrided Type 304 stainless-steel support plate. Side loads of 100, 200, 400, and 800 pounds were applied to the bar against the upper support plate hole. Ten cycles were completed at each side load. The atmosphere was nitrogen at 750 F. A slight polishing of the nitrided surfaces was the only result of this test.

A third test was of an actual, nitrided Type 304 stainless-steel sleeve in a nitrided Type 347 stainless-steel support plate. This unit was cycled in and out of the support plate in sodium at 750 F. No deliberate side load was applied. On inspection after 6000 cycles, the parts had noticable rub marks, but did not appear to have galled.

Colmonoy No. 4 was selected for the inner sleeve surface subsequent to the completion of the aforementioned tests, although the combination of Colmonoy No. 4 against nitrided stainless steel had not been included in the tests. An actual inner sleeve with Colmonoy No. 4 overlay was therefore tested in an actual nitrided Type 304 stainless-steel outer sleeve. The inner sleeve was cycled up and down in the outer sleeve in an air atmosphere at 550 F. The test included four cycles with a side load of 134 pounds on the inner sleeve at the upper support plate and five cycles at a side load of 300 pounds. Both parts were undamaged at the conclusion of the test.

A later test was run to determine the effect of the Colmonoy No. 4 spacer pads rubbing on each other. The equipment used was the same as that previously described, in which two circular specimens were rotated against each other. The test was run in 800 F sodium with a 2000 psi bearing load on the specimens. One specimen was rotated with respect to the other, through an angle of 60 degrees, 22 times. The specimen was rotated every 30 seconds, except for breaks after the sixth and fourteenth cycles in which the upper specimen was raised to allow sodium to circulate between the specimens. The only effect on the surface of the specimens was a change in color from silver to dull gray.

F. FLOW VELOCITY PROFILE MEASUREMENTS

The coolant velocity profile has been taken as an index of the uniformity of cooling. However, the direct use of the velocity profile for indicating heat removal is conservative because of the large amount of mixing that probably occurs within a subassembly. However, because of the low heat capacity of sodium, extremely uneven velocity profiles could result in local coolant starvation. Liquid metal heat transfer coefficients are extremely high but rather insensitive to velocity changes, because the high conductivity of the liquid metal precludes extreme local hot spots. That only extreme velocity profile maldistribution would be a problem is indicated by the observation that the center temperature of a fuel pin is increased by less than 100 F when the fuel pin is insulated around one-fourth of its periphery while normally cooled at the rest of its periphery.

A reference support structure was filled with reference-diameter stainless-steel pins and placed in a deaerated hot water loop to determine the velocity profile; the equivalent diameter, average velocity, kinematic viscosity, and Reynolds number were the same as for reactor operating

conditions at 675 F. The local velocities were measured with a small Pitot-static tube. Typical velocity distributions in and downstream of the core section are shown in Figure 45. It is noteworthy that the typical profiles measured with the Pitot-static probe agree well with local velocities predicted on the basis of local measurements of pin spacing.

Since the velocity profile is rather flat, no large coolant temperatures should exist at any subassembly cross section.

G. STRAIGHTENING FLOW FORCES

Hydraulic tests near operating Reynolds numbers show that, for the fuel pin geometry and support arrangement used in the reactor, hydraulic forces tend to straighten bent fuel pins. The evidence of the nature of these hydraulic forces was established by measuring the hydraulic effects on two different kinds of pre-bent, simulated fuel pins.

Three separate tests were run with lead pins geometrically identical to the zirconium-clad fuel pins. The strength and creep properties of the lead pins were measured so that experimental results on lead pins could be interpreted in terms of fuel pins. Figure 44 presents curves of psi stress versus tensile secondary creep rate of the lead pins used in the flow test and of fuel pins. Accelerated studies on the effects of flow forces on fuel pins thus could be made by using lead pins instead of fel pins, since the creep rate of the lead at test conditions was an order of magnitude greater than the creep rate of fuel pins at operating conditions. Pre-bent lead pins between spring tab supports, spaced 5 inches and 7-1/2 inches apart, were studied. From the observed straightening of the lead pins and from the physical properties of the lead pins, it was established that lateral forces equivalent to about 0.02 pound center load between grids straightened the lead pins at the rate of about 3×10^{-5} inches per hour. The straightening rate fell off as the pins became straight, showing that the pins were being straightened rather than being bent to some new position.

To independently confirm the measurement of the flow forces acting on the fuel pins, a group of 0.158-inch-diameter plastic pins were placed in typical support grids. Small strain gages were imbedded on the surface of the pins. The ends of the pins were pulled apart with very fine wires until the clearance between the pins between two grids was reduced from 41 mils to 10 mils. When water was forced past the pin array, it tended to separate the pins at all velocities tested (0 to 45 feet per second). For a 4.15-inch span and a velocity of 25 feet per second, the restoring force on a pin was about 0.03 pound.

H. PHASE CHANGE TESTS

The fuel alloy when fabricated is in the gamma phase. This phase is metastable and, if the material is held within a given range of temperatures for a sufficiently long period of time, it will transform to the thermally stable alpha-plus-epsilon phase. At about 930 F the transformation from the gamma phase to the alpha-plus-epsilon phase occurs as described previously. This transformation is inhibited by fission and, if the fission rate is high enough, the transformation to alpha-plus-epsilon can be eliminated. However, at about 1100 F there is a thermal reversion from the alpha-plus-epsilon phase to the gamma phase. These metallurgical transformations are

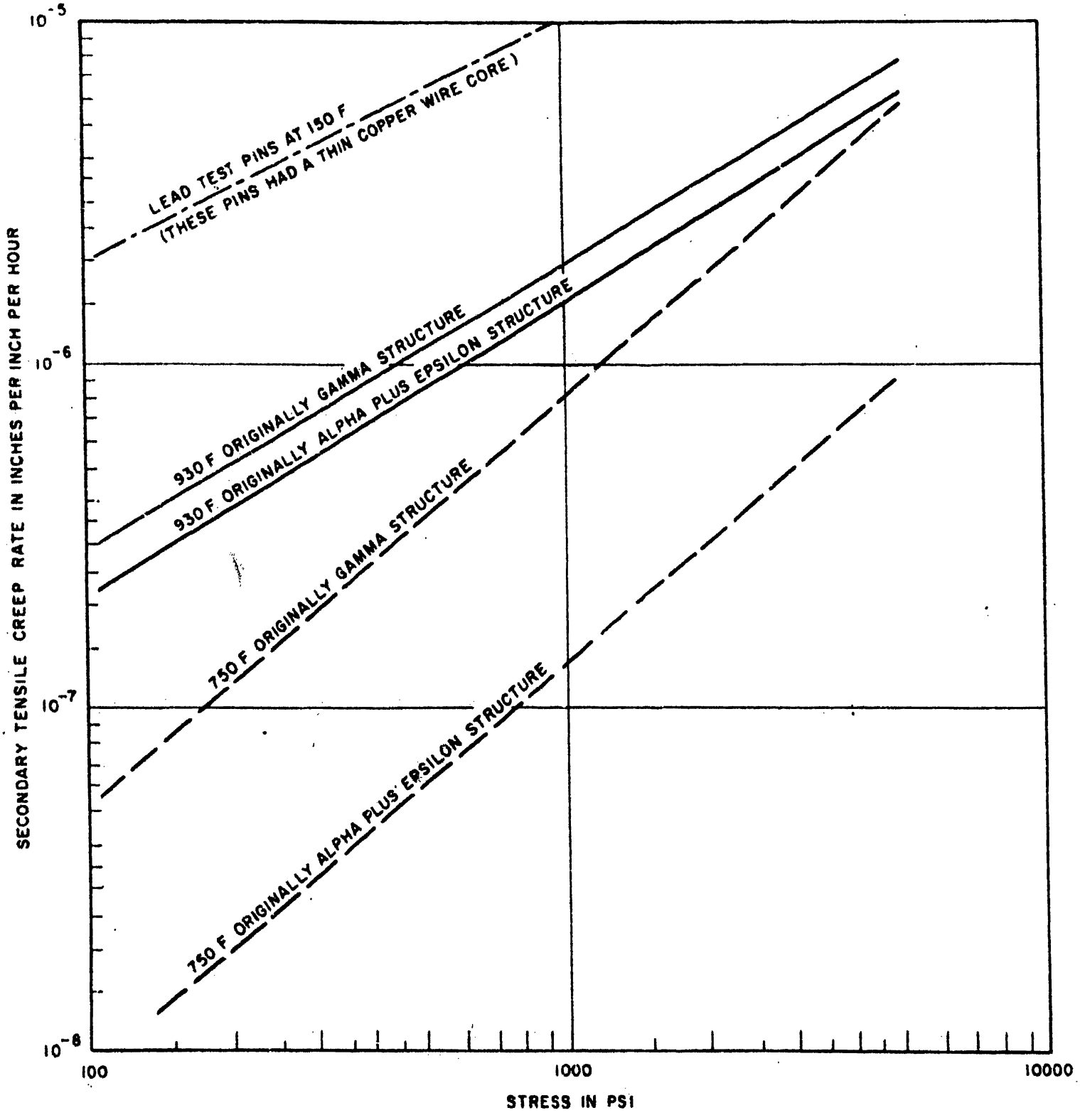

SECONDARY CREEP RATES

FIGURE 44

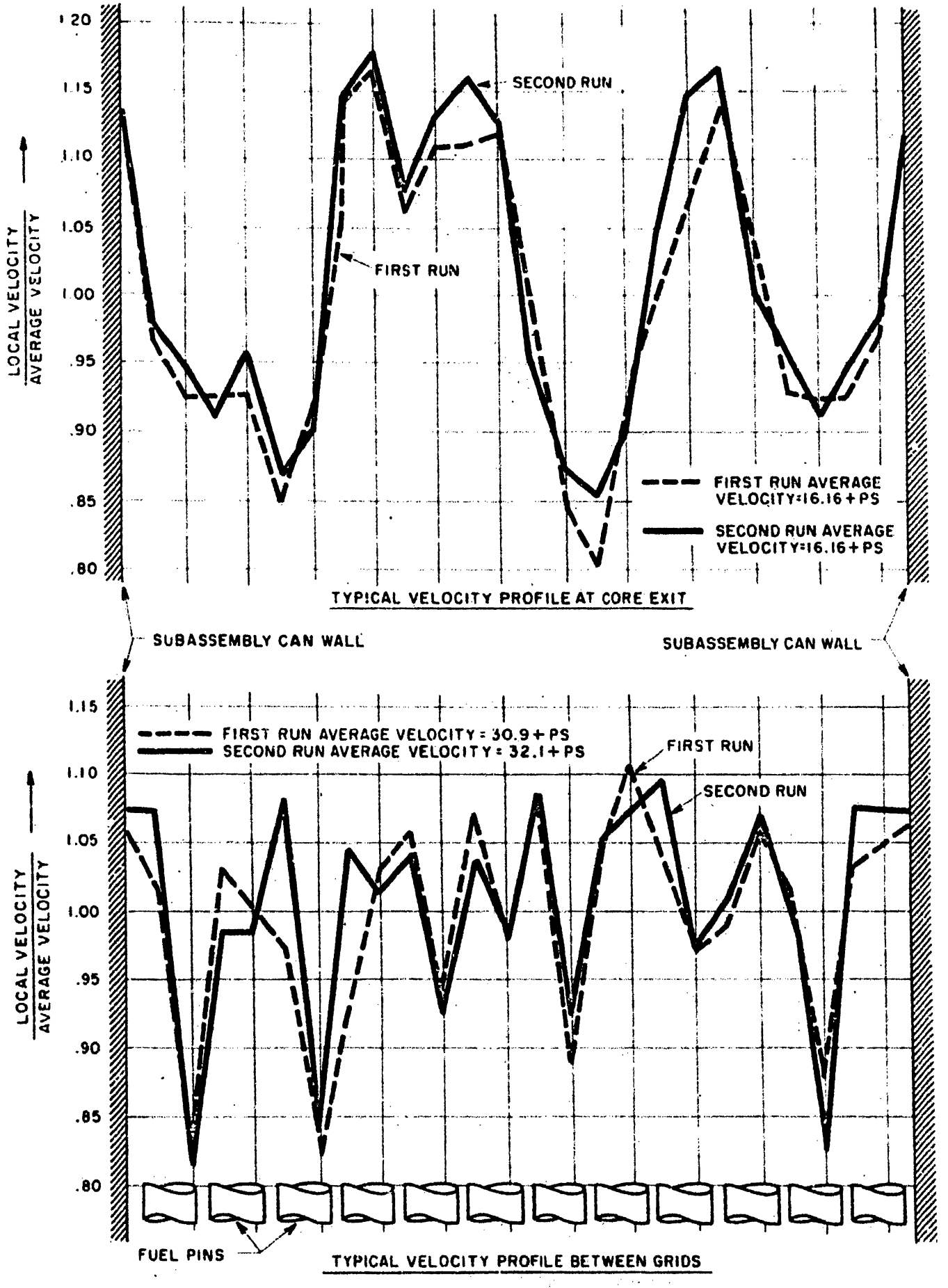

TYPICAL CORE SUBASSEMBLY VELOCITY PROFILES

TESTED IN WATER LOOP AT 194°F AND 264 GPM/SUBASSEMBLY MEASUREMENTS WITH 0.092 INCH DIAMETER PITOT STATIC PROBE TWO RUNS ONE AT EXIT OF CORE AND ONE IN CORE PROPER

BASED ON HB8 TEST

FIGURE 45

associated with volume changes which could warp and distort a fuel pin. The effect of alloy phase-change on the straightness of fuel pins was studied by performing three thermal cycling tests in sodium.

A complete subassembly containing 140 used, reference-design fuel pins, held in a typical support structure, were tested in a sodium loop operating at 325 gpm. After two complete temperature cycles (a complete cycle is from one phase to another, and then back to the original phase by changing the sodium temperature from 930 F to 1150 F, as required), the test piece was cooled, cleaned, and examined. The support structure was in good condition after testing. The pins were removed and tested individually for straightness. The pins were generally somewhat more curved after testing.

The thermal cycle test was repeated with new pins, and using grids with the restraining dimples partially removed so that some fuel pins were completely untouched by dimples. Again, when they were tested outside the support structure, the pins were generally more curved after testing. However, when measured in the support structure after the test (no such measurements were made for the first test), the pins were straighter in the support structure than out of the support structure. No fuel pins were touching in the support structure.

The third thermal cycling test was performed on all new uranium pins in a support structure almost identical to the final design. After the test the structure and pins were in excellent condition. The actual clearances between pins were uniform and no pins touched.

There was some difference in expansion between the pins and the structure during the phase-change thermal tests. Nevertheless, there were no indications of galling from any of the sodium loop tests.

The thermal cycling tests were severe in that they permitted more rapid and more extensive phase changes than those that can be experienced under actual operating conditions. Less rapid phase changes would have permitted hydraulic forces to act to straighten the fuel pins. Less extensive phase changes would, of course, preclude fuel pin warping due to phase changes. However, even with the severe phase-change testing, no fuel pins showed any evidence of touching within the support structure.

I. CREEP OF ZIRCONIUM-CLAD U-10 W/O MO MATERIAL

Depleted fuel pins of U-10 w/o Mo, clad with zirconium, were obtained from the 500 trial pin run, and sections of these pins were used for the creep test. The only departure from Fermi fuel specifications was that the pins were given an ingot homogenization heat treatment of 1880 F before fabrication. This difference is not considered significant.

The temperatures studied in these tests were 750 F and 930 F, and testing was conducted in an argon atmosphere. Samples having a 6-inch span length were supported at the ends and loaded in the center so bending stresses of 100, 400, and 10,000 psi could be obtained. Tests were also conducted at 200 psi, but at 200 psi the weight of the samples themselves was sufficient to provide the stress. Samples of the stable alpha-plus-

epsilon and metastable-gamma phases were tested under these stress conditions. The alpha-plus-epsilon samples were obtained by transforming the gamma-phase, or as-received pins, at 932 F for 60 hours. In all, 32 samples were used at each temperature. Since a given sample was only used or measured for one time interval (5, 50, 250, or 500 hours), and not constantly measured for the maximum time, considerable scatter was noted.

Measurements of original center deflection at room temperature were made to the nearest 0.0001 inch and repeated after testing. Total plastic deflection measured at room temperature was therefore obtained.

Because of the temperature of these tests, the gamma-phase material was transforming to the alpha-plus-epsilon phase faster at 930 F than at 750 F. This transformation was desirable since it may occur in the Fermi reactor if the radiation spiking does not maintain the material in the gamma phase.

Deflection creep data were translated to tensile creep data by methods similar to that given by Papor[1] but corresponding to Fermi loading conditions[2]. Converted secondary creep rates vs. stress are plotted in Figure 44. At 930 F there is good agreement between the curves for the material that was originally in the gamma phase and the alpha-plus-epsilon material; whereas at 750 F the material that was originally in the alpha-plus-epsilon phase appears considerably better.

An observation, predicted and supported by the tests, was the larger amount of primary creep that occurred in the samples that were originally in the gamma phase, as compared with the transformed samples. This difference existed at all stress levels. The probable reason for this occurrence is that, during testing, transformation is occurring and that material is "recrystallizing". The gram boundaries act in a viscous manner causing the sample to show larger amounts of primary creep.

J. THERMAL CYCLING TEST ON U-3 W/O MO AND ZIRCONIUM-CLAD U-10 W/O MO

Several thermal cycling tests were done on U-3 w/o Mo and on zirconium-clad U-10 w/o Mo to determine the effects of reactor thermal cycling and phase reversals on the dimensional stability of these alloys.

The results (Table VIII) of these tests, done in an argon atmosphere, indicate the phases present at the various temperatures of the cycling tests, cycling time, total number of cycles, and the dimensional changes after the completion of the test. In all cases the changes were small and did not indicate any dimensional instability problems associated with thermal cycling.

- -

(1) Papor, E. P., Journal of Applied Physics, "Bending of Beams with Creep," Vol. 20, 1949, 251-256.

(2) Engineering Research Report 60DIM, Detroit Edison Co., "Elevated Temperature Creep Tests on Reactor Fuel Pins Subjected to Binding Stresses."

K. PRESSURE DROP VS. FLOW

The flow pressure drop characteristics of a prototype subassembly measured in hot water is shown in Figure 44.

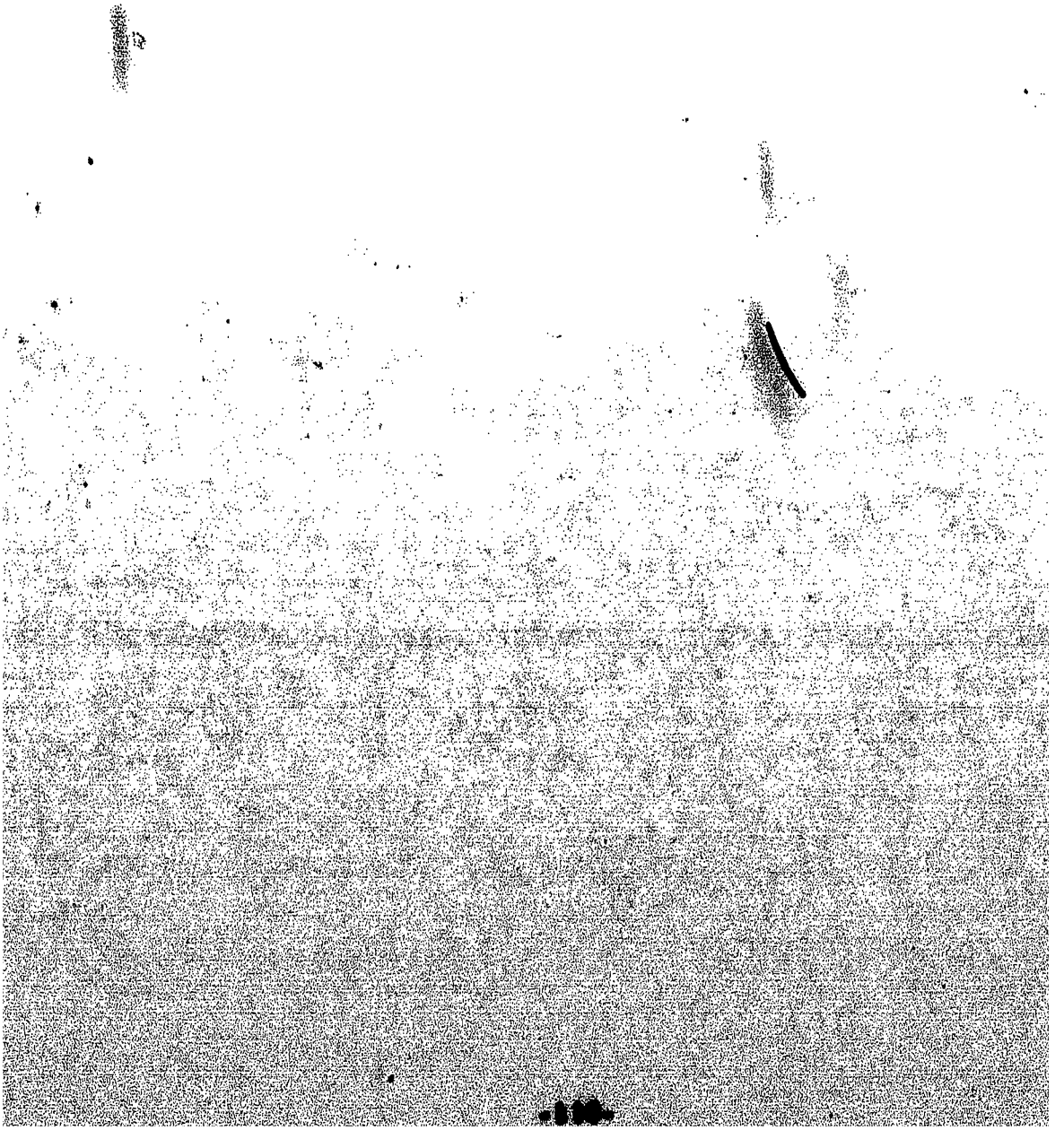

TABLE VIII - THERMAL CYCLING TESTS ON U-3 W/O MO AND ZIRCONIUM-CLAD U-10 W/O MO

Test Desig.	Alloy	Max./Min. Temp. °F	Max./Min. Time, Hr.	Max./Min. Phases Present	Original Dimensions	Total Number of Cycles	% ΔD	% ΔL
	U-3 w/o Mo	980/75	1/0.5	$\alpha + \delta$ *	.415" dia x 4"	700	≤ -0.3	$\leq +0.15$
	U-3 w/o Mo	1100/525	1/1	$\alpha + \delta \rightarrow \alpha + \gamma$	.415" dia x 6-1/2"	150	$\leq +.3$	≤ -0.2
	U-3 w/o Mo	1250/890	2/46	$\alpha + \gamma \rightarrow \alpha + \delta$	.415" dia x 7"	38	≤ -0.6	± 0.2
	U-10 w/o Mo[1]	980/75	1/0.5	$\alpha + \delta$	.158" dia x 6"	504	$\leq +0.3$	≤ -0.1
	U-10 w/o Mo	1250/890	2/46	$\gamma \rightarrow \alpha + \delta + \gamma$	.158" dia. x 6"	70	$\leq +0.02$	≤ -0.5

* The epsilon and delta phases may be considered the same.

They are designated in both ways by various investigators.

(1) These samples were transformed at 930 F prior to testing.

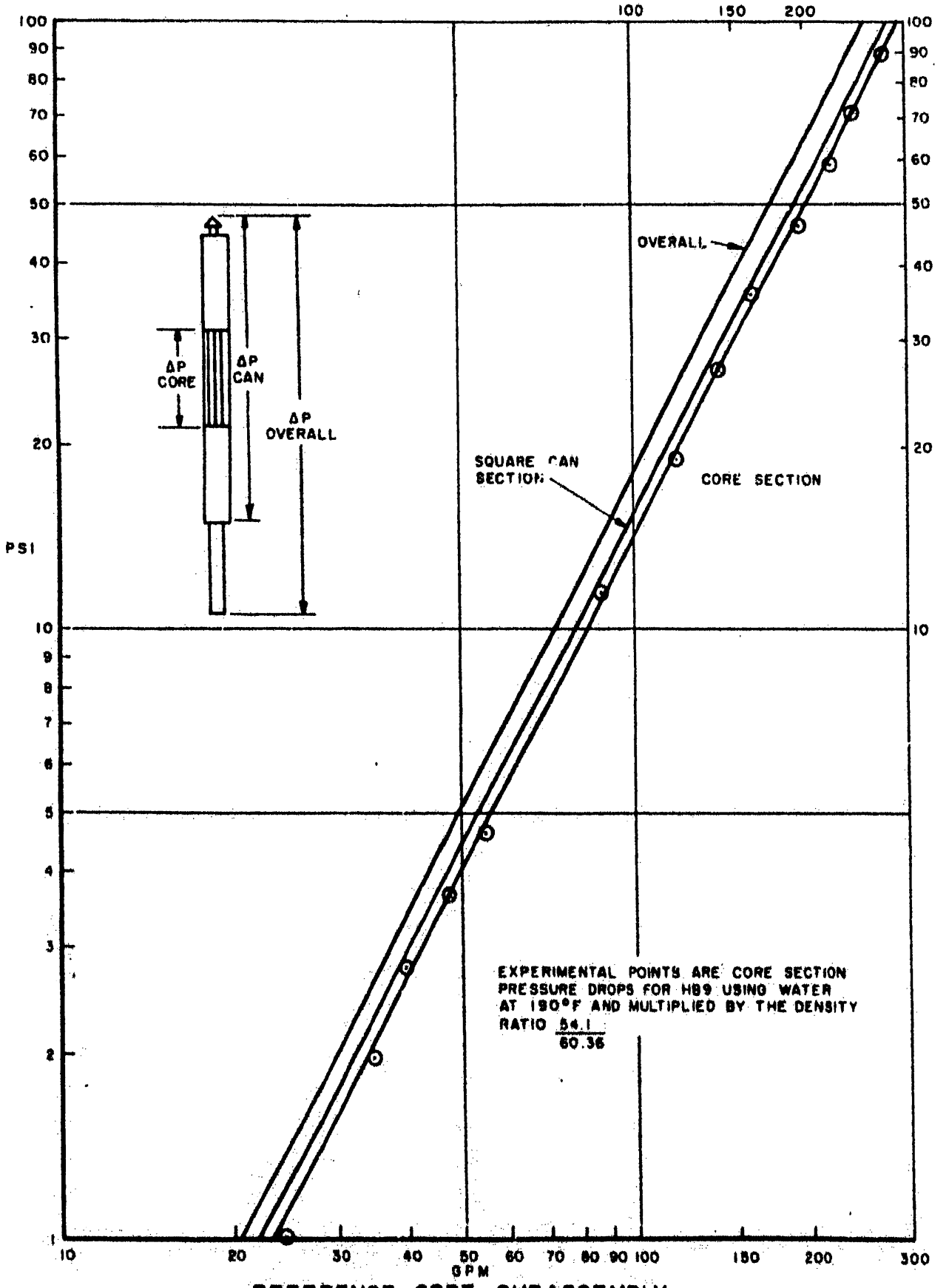

REFERENCE CORE SUBASSEMBLY
PRESSURE DROP VS FLOW FOR SODIUM AT 675°F
FIGURE 46

IX. FUEL SURVEILLANCE

Within the limits to which Core A operation will be confined, there is no necessity for inspection of the fuel after it is removed from the reactor. Operation is based on removal of the fuel when the maximum local burnup reached 0.4 a/o. The fuel pin support structure was designed to accommodate an 8% increase in the pin diameter which, at the operating conditions, would be attained at a maximum local burnup of 0.8 a/o. Thus, a safety factor of 2 has been used in establishing the removal burnup.

It is believed that the removal burnup could be increased safely to 0.8 a/o if the swelling of the irradiated fuel were measured. Space has been provided in one of the pools at the Fermi plant for fuel surveillance facilities; however, no decision has been made to obtain equipment. A comparative cost study has shown that the incremental operating revenue that would result from the increased burnup may not justify the added capital expenditures.

One of the most meaningful measures of the irradiation stability of the fuel pins is the change in the fuel pin dimensions under irradiation. It is also one of the easiest measurements to make, involving only pin length and diameter, both of which could be checked in an underwater facility by the use of simple fixtures, conventional gaging tools, and remote observation equipment such as television, periscope, or even binoculars.

Removal of a fuel pin from the subassembly is a more complex problem. First, the bundle of fuel pins must be separated from the axial blanket sections and removed from the square wrapper tube. To do this, the wrapper tube must be slit along its entire length at opposite sides or at diagonal corners. This cutting operation will be complicated by the tight clearances between the inner walls of the tube and the fuel pins, and by the requirement that the cutting operation shall not cut into the fuel pins or damage them in some other way. A straddle mill could be used for slitting the wrapper tube, and a cut-off machine could be used to separate the handling head and inlet nozzle from the wrapper tube. To obtain individual pins, the pin bundle would have to be disassembled. The structural components to which the fuel pins are attached could be disassembled with the use of a milling or grinding machine.

Shielding and removal of decay heat should not be a problem if the disassembly is performed in the pool. The problem of criticality could be solved by designing the equipment to handle only a single subassembly at one time and by handling fuel pins in containers with a critically safe geometry. Underwater lighting and observation equipment is needed for all operations. Collection and disposal of the chips and scraps from the cutting operations would be necessary.

Other significant measurements of the irradiation stability of the fuel which could be made are phase identification by the electrical resistivity technique, and burnup profile determination by the gamma scanning tech-

nique. The identification of phase in the U-10 w/o Mo alloy through measurement of the electrical resistivity of the irradiated alloy has been used successfully by APDA in its fuel irradiation program. The determination of burnup profile by use of a scintillation counter to establish the gamma activity profile has been demonstrated in hot caves and should be adaptable to underwater use.

A preliminary estimate indicates that the cost of procuring and installing the necessary facilities to perform the above mentioned fuel inspections in the Fermi reactor pool would be in the range of $300,000 to $500,000.

X. FUEL CYCLE CONSIDERATIONS

The topics that have been discussed in preceding sections of this report have been concerned mainly with the design, fabrication, and testing of the fuel. Other parts of the fuel cycle that must be considered in fuel element design are shipping of the fuel from the fabricator's plant to the reactor plant, removal of sodium from the irradiated fuel, shipping of the irradiated fuel to the chemical reprocessing plant, chemical reprocessing of the irradiated fuel, and management of the special nuclear material.

A. SHIPPING OF FUEL FROM FABRICATOR

The allowable movements of the fuel within the subassembly and of the subassembly within the core have been discussed together with the solution of these problems in the design. Once the fuel subassembly has been manufactured and found acceptable according to the rigorous inspection standards, then it must be shipped to the reactor plant without damage. The critical external dimensions of the subassembly such as spacer pad dimensions, subassembly concentricity, and subassembly length are checked before the subassembly is shipped from the manufacturer's plant and checked again immediately upon receipt at the reactor plant; therefore, changes in these dimensions incurred during shipment would be detected by inspection. The critical internal dimensions of the subassembly, such as the spacing of the fuel pins and the preload of the fuel pin bundle against the inside walls of the wrapper tube cannot be checked once the subassembly is assembled. Therefore, damage incurred during shipment could not be detected except by destructive examination. Thus, it is necessary that the subassemblies be transported in containers that are specially designed to protect the subassemblies from being damaged by the vibrations and shocks experienced with truck shipments. The shipping containers being used to transport fuel to the Fermi reactor plant were designed by Applied Design Company of Buffalo, New York, experienced designers of shipping containers for precision components with stringent reliability requirements such as aircraft engines, rocket engines, and rocket guidance systems. Analytical evaluations of the design, made independently by Westinghouse Atomic Power Department and by Dr. R. Daane of Stanford University, were in substantial agreement with Applied Design's analysis. One of the shipping containers containing a prototype core subassembly was subjected to vibration and drop tests that incorporated the worst possible shipping and handling conditions. A check of the external and internal critical dimensions before and after the tests did not reveal any damage.

As an added precaution, an accelerometer will be attached to each container during shipment of the core subassemblies to provide a record of the impact loads to which the shipment was subjected. At the reactor plant the subassemblies are handled in a cart with a specially designed gripper mechanism and hoist to prevent rapid movements or accidental dropping. The subassemblies are stored in a limited-access, air-conditioned vault.

B. SODIUM CLEANING

The process that will be used at the Fermi plant for removing sodium from the irradiated subassemblies consists of a hot argon gas sweep, followed by a super-heated steam reaction period and completed with a cold water rinse and soak. The process concept was developed and proven in tests by APDA. The detail process design was furnished by Vitro Engineering and the plant design was furnished by Americal Machine & Foundry. Design of the fuel subassemblies insures free draining of sodium from the subassemblies and ready access of all surfaces to the argon steam, and water.

APDA also has developed a process for the removal of sodium in which ultrasonic vibrations are used to disperse the sodium into a light oil carrier. Since this process is mechanical in nature, it has an advantage over the steam reaction process in that no heat is generated and no harmful or dangerous reaction products are formed. In addition the subassembly never leaves the liquid coolant phase, which may be advantageous if gas cooling is a problem. However, the ultrasonic process requires an additional process for removal of the oil carrier. The ultrasonic dispersing technique has been tested only on small specimens, and further development work is needed to demonstrate the process on large components.

APDA has been successful in removing sodium from fuel subassemblies by heating them in a vacuum chamber and maintaining an absolute pressure that is less than the sodium vapor pressure. This process is superior to both the steam reaction and the ultrasonic dispersion in cleanliness, inertness, and process control. However, the vacuum operation presents a serious obstacle to removal of decay heat from irradiated subassemblies;, and, therefore, no effort has been made to extend the application of this process to irradiated fuel.

C. SHIPPING OF IRRADIATED FUEL

Arrangements for shipping the irradiated fuel to the reprocessing plant have not been completed yet. PRDC intends to contract for a complete shipping service in which the contractor would provide the necessary casks, transportation facilities, administration, licenses and approvals of the various regulatory agencies, insurances, etc., for a fixed annual rental fee plus operating costs. Several companies already have submitted proposals to PRDC to provide such a service but no definite action has been taken. A delay was necessitated by the redesign of Core A last year. Uncertainties about the designs of future cores, i.e., Core B and Core C, together with the delays in plant start up made it prudent to delay a final decision on the shipping cask design criteria. Present uncertainties about the start-up schedule and plant load factor, the consequences of the 60-day shipping period specified in the AEC draft reprocessing agreement, and the lack of firm design requirements from the regulatory agencies all contribute to the difficulty of making a sound engineering decision on the number and kind of casks required, when they will be needed, and for how long they will be needed. APDA has been working closely with the AEC, the reprocessing plants, the regulatory agencies, the cask manufacturers, and with other reactor plant operators on this important problem.

D. FUEL REPROCESSING

Detailed discussions have been held with the AEC and its contractors to work out an agreement between the AEC and PRDC for the reprocessing of the Fermi plant fuel. The AEC draft agreement and the AEC's earlier letter agreement to PRDC have been used as a basis for discussion. Numerous problems have been identified in the discussions, some of which have not yet been resolved. Principal among these are a mutually satisfactory means of establishing liability if returned fuel does not meet specifications and a mutually satisfactory method for establishing the fissile content of the returned fuel. Problems of lesser import include a realistic formula for establishing limits on the size of a processing batch, a realistic schedule for shipment of a reprocessing batch, and return of the recovered fuel material to the lessee. APDA has worked closely with the Commission and its contractors on these problems. Because of the redesign of the Core A fuel subassembly, the over-all delay in the Fermi plant schedule, and the possibility that a private reprocessing plant might be available (Industrial Reprocessing Group), very little action has been taken on a reprocessing contract during the past 18 months.

E. FUEL MANAGEMENT

The uranium leased from the AEC by PRDC for the fabrication of 200 Core A subassemblies is valued at approximately $22,000,000, of which about $15,000,000 worth will be in the finished subassemblies and $7,000,000 worth will be in the form of virgin metal, recoverable scrap, and losses. Under the terms of the lease agreement, PRDC must pay for all the U-235 destroyed or lost and also must pay for degradation of the enrichment. The contracts which PRDC has with Davison Chemical Company and with D. E. Makepeace Company hold the contractors financially responsible for U-235 losses and enrichment degradation which occurs while the material is in their plants. Davison checked Oak Ridge weights on the UF_6 but did not check the isotopic and chemical analyses. Therefore, for accountability purposes, Davison accepted Oak Ridge figures. On reprocessed cold scrap returned to Oak Ridge, Davison performed analyses; and differences in measurements were resolved by referee measurements. On the derby metal that Davison transferred to the fuel fabricators, all weighings were checked by the fabricators. The impurity content and isotopic content of the derby metal were determined by Davison on all the metal and also were checked by the fabricator on about 20 per cent of the metal. For accountability purposes, the computations of the isotopic enrichment of the derby metal were based on the Oak Ridge isotopic measurements on the UF_6, because, in every instance, this computed value was within the 2σ limits of the isotopic analyses obtained on the derby metal.

A precise determination of the U-235 content in the fuel elements had to be made to establish the losses incurred by the fabricator. The problem is complicated by the fabrication process because the virgin derby metal is alloyed, because it becomes further contaminated with additional impurities introduced throughout the process, and because the material is physically subdivided by a factor of about 35 in going from derbies to fuel pins. Yet, for each 0.1 per cent uncertainty in the U-235 content of the finished product there is a financial risk of about $15,000 to both PRDC and the fabricator. APDA working together with National Lead Company of Ohio,

with the fabricator, and with the New Brunswick Laboratory of the AEC established procedures of random product sampling, product weighing, chemical and isotopic analyses; analytical bias checks, and statistical interpretation of the data to establish the U-235 and uranium content of the finished fuel. As a result of these procedures, the U-235 content of the first 100 core subassemblies is known with a certainty of ± 0.1 per cent at the 95 per cent confidence level. For accountability purposes the fuel will be transferred to PRDC using the weights, chemical, and isotopic data obtained on the finished product.

On the basis of the stringent and precise accountability methods that are being employed on the fabrication of the new fuel, APDA has recommended to the AEC that fabrication records and burnup calculations be used to settle accountability on the irradiated fuel returned to the Commission. APDA has made a preliminary study of the uncertainties attendant with burnup calculations and the indications are that it will be from ±10 to ±20 per cent at the 95 per cent confidence level. With the very low burnup expected in Core A, it is certain that the U-235 content of the irradiated Core A fuel can be established by this procedure much more precisely than the ± 2 per cent to ±5 per cent claimed for dissolver solution measurements.

XI. ENRICO FERMI FUEL CYCLE COSTS

A. SUMMARY

The fuel cycle cost that will break even in the Enrico Fermi reactor is set at about 2 mills/kwhr. At this cost, steam revenue just pays operating and net fuel cycle costs.

Core A fuel cycle costs have increased to the extent that the original 200 subassembly order will not be increased. If this core were operated at steady-state in Fermi, the fuel cycle cost would be in the range of 12 to 24 mills/kwhr.

Core B has been proposed to reduce the Fermi fuel cycle costs. The proposed UO_2-SS cermet core is capable of reducing costs primarily because of the potential for high average removal burnup (20.7 per cent of uranium) and operation at 300-Mwt power level.

Core B is intended only as an interim core because this reactor system does not have a breeding gain so a primary goal of the Fermi reactor is not attained and a lower cost core can be developed. Core B qualifies as the interim core because it can be made available in time to replace Core A when the 200 subassemblies are consumed and thereby dramatically reduce fuel cycle costs to near 4 mills/kwhr during the interim period until a break-even core is developed.

B. CORE A FUEL CYCLE COSTS

Table IX is a breakdown of Core A fuel cycle costs at two plutonium prices. These costs for Core A are given for conditions of assumed steady-state operation at 200-Mwt power level and 75 per cent plant factor. The breeding ratio assumed for this study is 1.2 and the average removal burnup is 0.5 a/o.

1. Burnup and Breeding

Core A is enriched to 25.6 per cent in U-235. At this enrichment, U-235 is worth $16.30 per gram. About one gram of U-235 is destroyed for every MWD of reactor output, and about 1.2 grams of plutonium are formed in the blanket and core per MWD.

An interesting analysis on the current value of breeding plutonium in Fermi is a comparison of the blanket costs and the value of plutonium. Assuming expected alloy blanket performance of 0.5 a/o local maximum burnup, the blanket costs are not equalled by plutonium revenue until the value of plutonium (as nitrate) equals about $15/gram. Of course, the blanket serves other functions (e.g., shielding), and all the costs cannot rightfully be charged against plutonium production. Table VIII shows that the blanket is just breaking even at $12/gram plutonium, even if blanket fabrication charges are assumed chargeable

TABLE IX - CORE A FUEL CYCLE COSTS (MILLS/KWHR)

200 Mwt, 60 mwe — 75% Plant Factor

435 Subassemblies/year — 1/2 a/o Avg. Removal Burnup (6000 MWd/Tonne)

105 Subassembly Cores — R.R. = 1.2

Plutonium Value	$12/gm		$30/gm	
	Core	Blanket	Core	Blanket
U-235 Destroyed	2.4	0	2.4	0
Plutonium Revenue	-0.4	-1.3	-1.2	-3.5
Fabrication	16.5	0.6	16.5	0.6
Reprocessing	2.7	1.0	2.7	1.0
Conversion	0.6	0	0.6	0
Losses	1.1	0	1.1	0
Shipping	0.8	0.2	0.8	0.2
Net	23.7	0.5	22.9	-1.7
Net Overall[2]		24.2		21.2

Note: (1) The total fissionable material in the cycle is as follows:

Kg of U-235	4700
Kg of Pu-239	270

(2) Net Over-all costs at 1 2/o burnup equal 12 mills/kwhr

to the shielding function. The plutonium in a fast breeder reactor is extremely free of Pu-240. Therefore, the price probably should not be based on its value as a fuel for a thermal reactor. For this reason, the plutonium revenues have been set arbitrarily using both $12/gram and $30/gram to illustrate capitalization of this advantage.

2. Fabrication

Core A fabrication costs contribute two-thirds of the net fuel cycle costs. A breakdown of the unit costs for the initial order of 200 core subassemblies and 600 blanket subassemblies is given in Table X. The values given include $1,500 on each assembly, which has resulted from redesign of the core and the accumulation of additional items and changes during fabrication.

3. Reprocessing, Conversion, and Losses

The latest AEC ground rules have been used for computing charges for processing, conversion, and losses. Reprocessing has been assumed to occur during two core campaigns and two blanket campaigns per year. Under the assumed conditions, over 8,000 kg of enriched uranium and 12,000 kg of depleted uranium require reprocessing annually.

Charges for conversion of plutonium to metal and for plutonium losses have been deducted from the plutonium revenue.

A resume of the rules is as follows:

Processing rate	158 kg/day (25.6% E)
Daily processing charge	$16,400
Conversion rate and cost (UNH to UF_6)	150 kg U/day @$32/kg
Losses	1.3% U, 2% Pu
Reduction	$1.50/gram Pu

4. Shipping

The cost of shipping irradiated fuel from the Fermi plant is based on preliminary bids received from vendors for providing this service. The charges have been divided into service and freight charges expressed as dollars per subassembly and an annual cask rental charge. Service and freight charges are $500, $115, and $58 per subassembly for core, radial blanket, and axial blanket, respectively. Annual rental charges are $15,000 and $20,000 for each core and blanket cask, respectively. Four core casks (capacity for four subassemblies) and one blanket cask (capacity 16) would be required for continuous use during operation with Core A at steady state assuming 14-day round trips.

The current revision of the AEC draft reprocessing contract specifies shipment of each processing batch within a 60-day period and a maximum batch size not in excess of one year's reactor discharge. Application of the 60-day rule to Fermi using Core A at steady state, requires either that fourteen core casks be used to process two batches per year, or that fourteen b tches be processed if two core casks are used. The cost to PRDC of either 12 additional casks or the additional

TABLE X - CORE A AND BLANKET FABRICATION COSTS

($/SUBASSEMBLY)

Initial order: 200 Core A Subassemblies
600 Blanket Subassemblies

Item	Core A	Blanket
Material		
Fuel Conversion	$ 3,500	$ 710
Hardware	2,500	730
Scrap and Losses	2,000	
Fabrication	5,300	1,400
Assembly	200	
Axial Blanket	700	100
Non-Destructive Testing	700	100
Inspection and Accountability	100	60
TOTAL	$15;000	$3,000

These costs amount to $815/kg U or $3185/kg U-235.

turnaround time associated with each batch is not included in this study, because a more flexible policy will be sought.

Core A fuel cycle costs have undergone considerable change over the past six years. Figure 47 illustrates the change in outlook that has occured due to reduced burnup, increased fuel fabrication cost and reduced plutonium price. The figure shows how the fuel cycle could be expected to produce revenue when the burnup was 2 per cent and the price of plutonium was high. As the expected fuel burnup has decreased, fabrication costs have increased and the price of plutonium has been reduced until current estimates, which are given later in detail, are based on burnup and plutonium prices of 1/2 a/o and $12 and $30 per gram, respectively. The figure is based on today's fuel fabrication costs of $15,000 per core subassembly and $3,000 per blanket subassembly. A point is shown at 2 per cent burnup and $45 per gram plutonium to illustrate the effect of early fabrication cost estimates of $2,000 per core subassembly and $1,000 per blanket subassembly.

C. CORE B FUEL CYCLE COST

Table XI is a summary of expected Core B fuel cycle costs. The reference Core B case (93 per cent enriched UO_2-SS) is steady-state operation at 300-Mwt power level and 75 per cent plant factor. Average removal burnup, as limited by criticality is 20.7 per cent of the uranium atoms present. The conversion ratio calculated in this case is 0.8.

Referring to the $30 per gram plutonium example, note that the net over all value (without use charge) is within a few mills per kwhr of the so-called break-even point of one mill/kwhr at 300-Mwt power level, i.e., the net fuel cycle cost plus operating expenses, taxes, etc. is within about 3 mills/kwhr of the contract revenue from steam.

1. Burnup and Breeding

Burnup charges contribute a large portion of Core B fuel cycle costs. Core B fission will occur in uranium enriched to 93 per cent in U-235. At this enrichment, U-235 is worth $17.10 per gram, and about 1.17 grams are destroyed for every MWD of reactor exposure while 0.94 grams of plutonium are formed in the blanket. The total fuel cycle costs are now influenced strongly by the AEC prices set for enriched uranium because of the low throughput in the core. Uranium prices can be expected to decrease with time, rather than increase when the free market is allowed to influence the price.

Breeding does not occur in the Fermi reactor while Core B is used because fertile material is not present in the core. The conversion ratio in the blanket is about 0.8. Note that the blanket costs are again just about paid for by a revenue of $12 per gram of plutonium.

2. Fabrication

Core B fabrication costs are estimates because of uncertainties in plate fabrication costs and material costs. Estimated spherical UO_2 costs vary from $260 per kg to $700 per kg; and estimated plate fabrica-

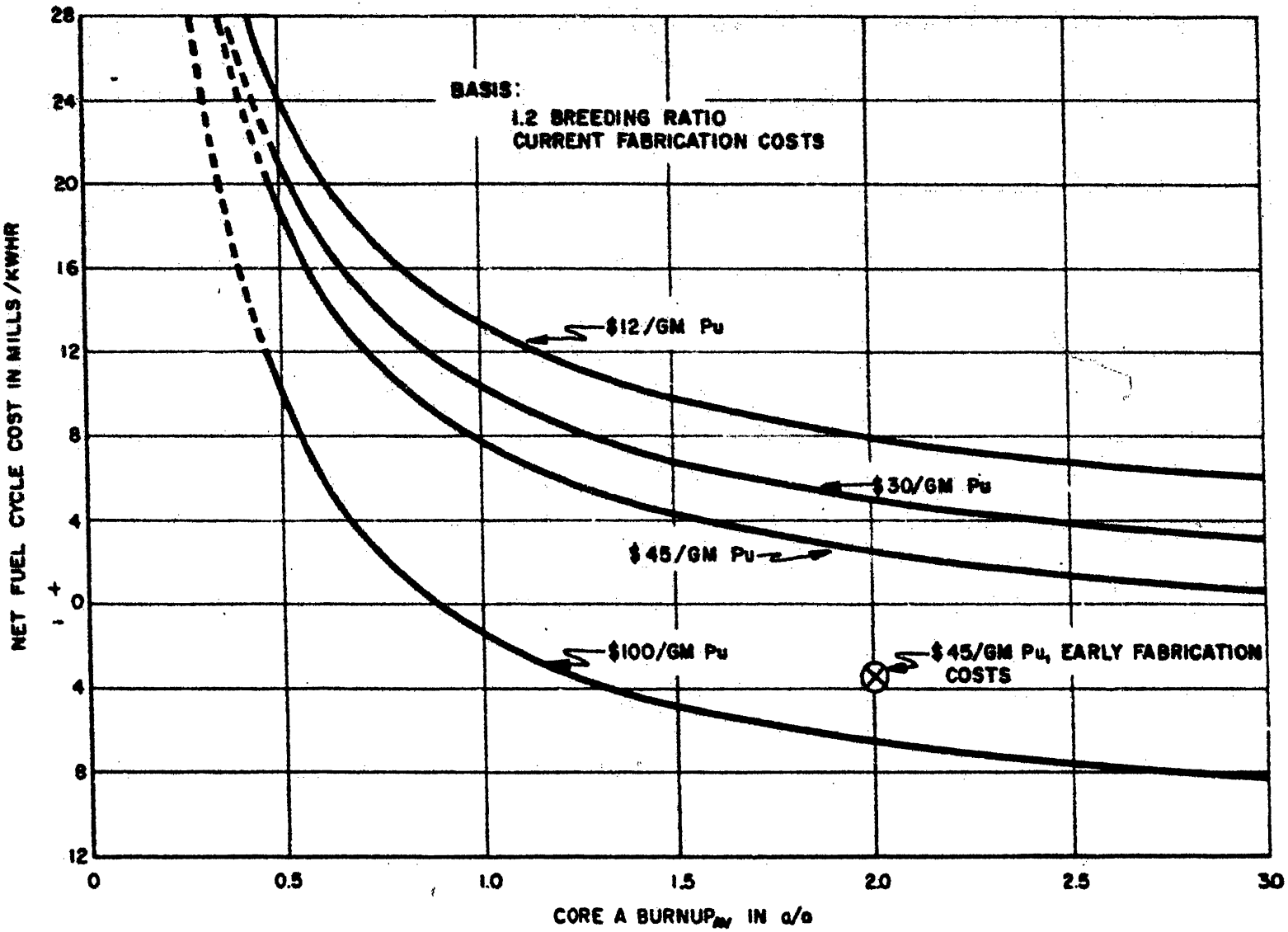

THE EFFECT OF BURNUP AND PLUTONIUM PRICE ON CORE A NET FUEL CYCLE COSTS

FIGURE 47

TABLE XI - CORE B FUEL CYCLE COSTS (MILLS/KWHR)

300 Mwt, 104 Mwe — 75% Plant Factor

81 Subassemblies/year — 20.7% Ave. Removal Burnup

130 Subassembly Cores — B.R. = 0.8

Plutonium Value	$12/gm		$30/gm	
	Core	Blanket	Core	Blanket
U-235 Destroyed	2.4	0	2.4	0
Plutonium Revenue	0	-1.2	0	-3.2
Fabrication	1.2	0.5	1.2	0.5
Reprocessing	0.3	0.4	0.3	0.4
Conversion				
Losses	0.1		0.1	
Shipping	0.1	0.1	0.1	0.1
Net	4.1	-0.2	4.1	-1.2
Net Core plus Blanket		3.9		2.9
Use Charge @ 4% after 1967		1.0		1.0
Net Overall		4.9		3.9

Note: The total fissionable material in the cycle is as follows:

Kg of U-235	1200
Kg of Pu-239	250

tion costs, including non-destructive testing, vary from $75 to $150 per plate. Table XII lists the expected Core B costs, assuming $400 per gram UO_2 and $100 per plate fabrication and NDT costs. This cost could vary between $13,500 and $7,000 if the extremes of the material and fabrication estimates are considered. The maximum effect of this variation of fuel cycle costs is an increase of 0.6 mills/kwhr.

3. Reprocessing, Conversion, and Losses

Reprocessing of the highly enriched core material has been assumed possible under the appropriate assumptions from the AEC's hypothetical plant and pricing schedule.

4. Shipping

One blanket cask and one core cask are adequate for continuous shipping of irradiated Core B and blanket subassemblies.

5. Use Charge

The 4 per cent use charges on U-235, which do not become effective until five years after reactor licensing, have been added to illustrate the effect of this charge on over all Core B costs. In all likelihood, use charges will not be levied during Core B operation.

D. CONCLUSIONS

Core A presents a steady-state fuel cycle cost which ranges from 12 to 24 mills/kwhr. For this reason, a replacement for the U-Mo alloy core has been sought, and the original order of 200 subassemblies will not be increased.

Core B reduces the annual net fuel cycle costs to about 4 mills/kwhr. Therefore, it is obvious why the UO_2-SS cermet core is being developed to fill the gap between the initial order of Core A and Core C.

Cores beyond Core B must demonstrate the potential for revenue in excess of the fuel cycle and operating costs. The use of plutonium in this system may be advantageous when there is an appreciable price differential between uranium and plutonium.

TABLE XII - CORE B FABRICATION COSTS ($/SUBASSEMBLY)

Basis: $400/kg UO_2
90% Yield

Item	Cost
Material	
Fuel Conversion	$2,100
Hardware	1,600
Scrap and Losses	400
Fabrication	2,400
Assembly	1,500
Axial Blanket	600
Non-Destructive Testing	400
Inspection and Accountability	200
TOTAL	$9,200

XII. EVOLUTION AND PRESENT STATUS OF CORE B DESIGN

During mid-1958, APDA began consideration of a Core B for the Enrico Fermi reactor. The initial ground rules for the selection of the Core B fuel material were (1) it must have demonstrated high radiation stability in the temperature range of 700 to 1200 F, (2) there must be considerable experience in fabrication of the selected material, and (3) the external dimensions of the subassembly must conform to those of Core A subassemblies. On the basis of these ground rules, APDA selected the UO_2-SS cermet fuel in the form of flat plates. Preliminary considerations indicated that average burnup over the core would be about 25% of the uranium and that at least three commercial fabricators had experience in producing UO_2-SS fuel plates.

The AEC was requested under the AEC-PRDC assistance contract to initiate a Core B fuel development program at one of the National Laboratories. The AEC agreed and selected ORNL, because of their APPR experience, to be the participating laboratory. In the fall of 1958, ORNL accepted the program and agreed to be responsible for fuel and subassembly development work, not including the axial blanket and accessory hardware; to carry out an irradiation program consisting of three temperature-controlled capsules; and to assist APDA in writing a fuel subassembly specification. APDA's responsibilities included subassembly design and analysis, non-nuclear prototype testing, and writing of the fuel specification. Actual work on the program was initiated in early 1959.

Early design considerations included the use of either a rigid assembly such as that used in the APPR or a mechanical design in which the individual fuel plates are free to move such as was used in the OMRE. It was decided that one could probably design around the thermal stresses that are encountered in the rigid design. In this way the vibration problems that might be encountered in the mechanical design could be avoided. Further, it appeared extremely difficult to establish a mechanical design that would be free of a positive contribution to the temperature coefficient of reactivity.

The initial design considered, essentially that of the APPR, utilized inert end and side plates which would then become an integral part of the subassembly wrapper can. The design incorporated fifteen plates, 0.107-inch thick, and 0.053-inch coolant channels. The end and side plates were 0.096-inch thick. The core height was 36 inches rather than 30 inches as in Core A. A modification of this design, utilizing a central spacer separating the fuel plates, was also considered. A cross-sectional view of the design is shown in Figure 48.

A stress analysis of the mid-plane cross-section of a subassembly at the reactor centerline was made. For this analysis, it was assumed that

1. The mean temperature of all fuel plates was constant.

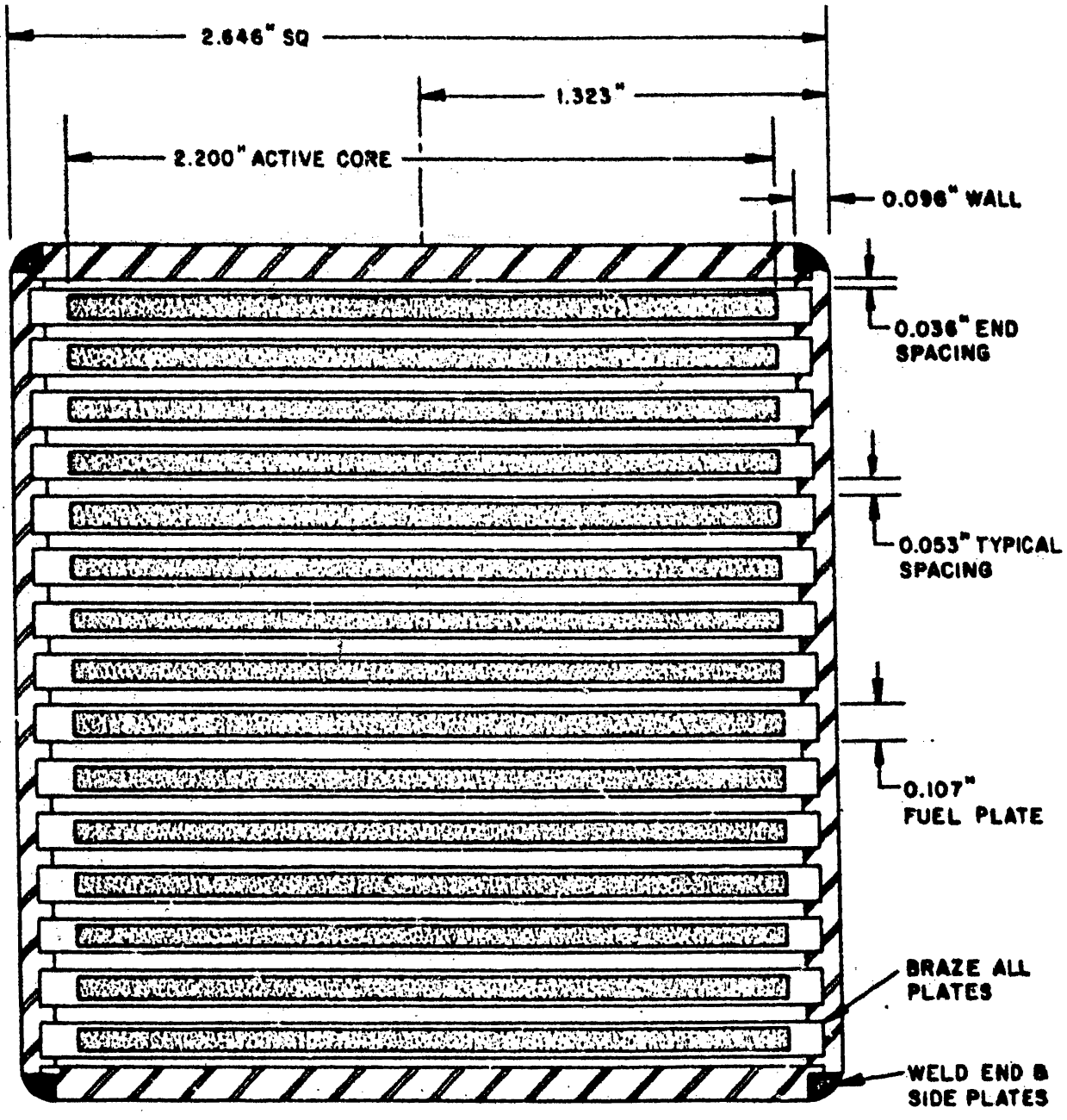

RIGID CORE B DESIGN WITH
INERT SIDE AND END PLATES
FIGURE 48

2. The temperature of the fuel plates was 1030 F and that of the end and side plates was 730 F.

The analysis showed that

1. Stresses at the four corners of the can and on the first and last fuel plates exceeded the yield strength of the material.

2. The addition of a center spacer reduced the maximum deflection of the outer fuel plates from 13% of the original coolant channel spacing to 3%. At the same time, the compressive stress in the fuel plate increased from 26,500 psi to 42,300 psi. This maximum stress occurred at the extreme fiber close to the end plate.

Following this analysis, several design modifications were considered, such as varying the thickness of the end and side plates, and providing loose outer fuel plates. It was considered, however, that these concepts were unsound and therefore, all were discontinued.

The second concept considered was that of a separate fuel bundle which would be inserted into a wrapper tube similar to that used in Core A. This design, shown in Figure 49, incorporated fourteen fuel plates 0.116-inch thick and a cermet core 36-inches long. The plates were rigidly held together by the use of combs spaced every 2 inches along the length of the plates and with through-pins at the alternate two inches. Under the simple assumptions used in the analysis of the first design, this concept appeared promising. However, subsequent analyses based on more realistic assumptions, showed up several weaknesses. They were

1. That when one considered a differential of 100 F in temperature between adjacent plates, a high shearing force was set up between the plates and the combs and the through-pins. It was proposed that the problem at the combs could be avoided by merely welding the combs to the two outer plates and allowsing the inner plates to move. However, this did not avoid the problem at the center pins and, further, introduced problems of vibration and possibly of positive temperature coefficient of reactivity.

2. Because of thermal bowing, it was difficult to insure uniform cooling conditions of the outer fuel plates. Under these conditions, large nonuniform temperature gradients across these plates could exist which would lead to undesirable distortion.

3. Nonuniform cooling of the wrapper tube caused by thermal bowing and by the effect of the intermittent combs on the coolant flow resulted in nonuniform bowing of the tube and, quite possibly, the bowing would be incompatible with that of the fuel bundle.

4. It was difficult to provide sufficient room within the wrapper tube to accommodate thermal bowing of the fuel bundle without increasing the UO_2 loading in the cermet well beyond acceptable limits.

With these thoughts in mind, several basic modifications of the fuel bundle concept were made. To overcome the problem of high shear forces

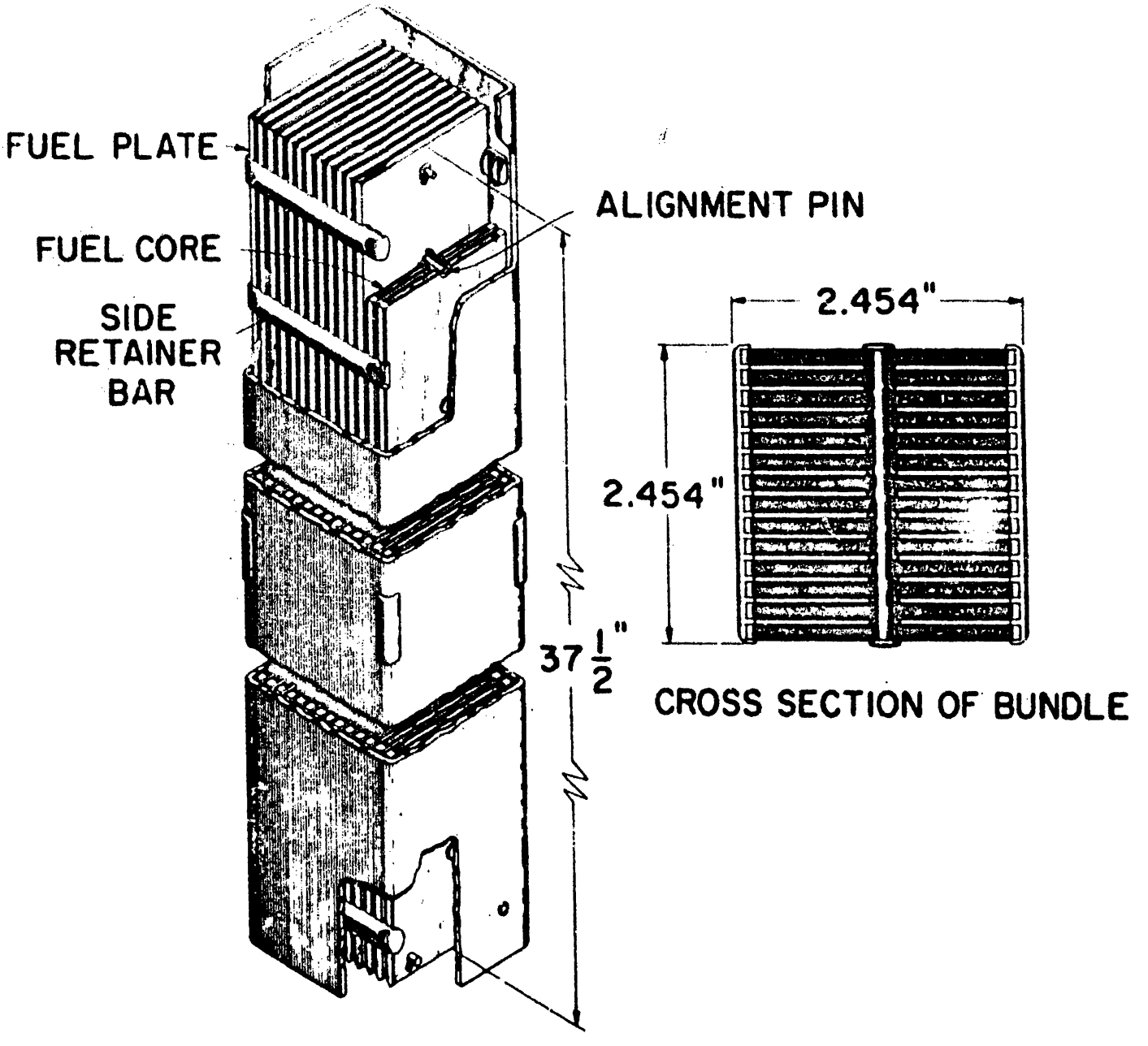

FLAT PLATE CORE BUNDLE

FIGURE 49

on the combs and through-pin, they were replaced with continuous ribs down both sides and down the middle, as shown in Figure 50. This also reduced the pressure drop through the subassembly.

To insure uniform cooling of the outer fuel plates, outer coolant channels were created by the use of thin shrouds. In this way the coolant passage for the outer fuel plate would not vary due to bowing of the fuel bundle.

To reduce the problem associated with thermal bowing of the full-length fuel plates, the plates were made essentially half length, so that a fuel subassembly would contain two in-line fuel bundles. In this way the space provided for thermal bowing could be appreciably reduced. To improve coolant conditions of the wrapper tube and to smooth out the thermal gradients over the tube, it was decided to spiral the coolant flow between the tube and the fuel bundle.

During the first half of 1960, an extensive effort was devoted to a thorough analysis of this design. This effort included heat transfer calculations, thermal stress analyses of the temperature gradients across the plates and at the plate-rib joint, and general hydraulic flow considerations.

These analyses showed that

1. A brazed joint between the spacer ribs and the fuel plates was preferred over a welded joint. This result evolved principally from the ability to achieve a greater joint width by brazing than by welding.

2. The spiral sodium flow between the fuel bundle and the wrapper tube was extremely effective in smoothing out the temperatures over any cross-section of the wrapper tube. The effect was considerably better than anticipated and indicated that essentially there would be no thermal bowing of the can.

3. The analysis of the heat transfer between the sodium in the outermost coolant channel and that in the annulus, indicated that the outer coolant channel, created by the thin shroud, was not as effective as desired with respect to proving uniform cooling of the outer plates. The analysis did show, however, that by proper control of the coolant flow rate in the annulus, an acceptable variation in cooling of the outer plates could be achieved.

4. In Figure 50 it can be seen that the center spacer ribs are applied directly over the fuel bearing portion of the fuel plates. A heat transfer analysis of this case indicated an increase in fuel temperature of about 40 F, which was considered satisfactory.

On the basis of this effort, it was decided to eliminate the thin shroud and to adjust the coolant flow in the annulus to provide the desired cooling of the outer fuel plates. This modified design is shown in Figure 51. It is pointed out that in this design, the seal strips, which provide the desired flow direction in the annulus between the fuel bundle and the wrapper tube, are applied, by brazing, directly to the outer fuel plates. It is estimated that this will locally increase the fuel by 10 or 15 F, an increase of little concern.

UNCLASSIFIED
ORNL-LR-DWG 53039

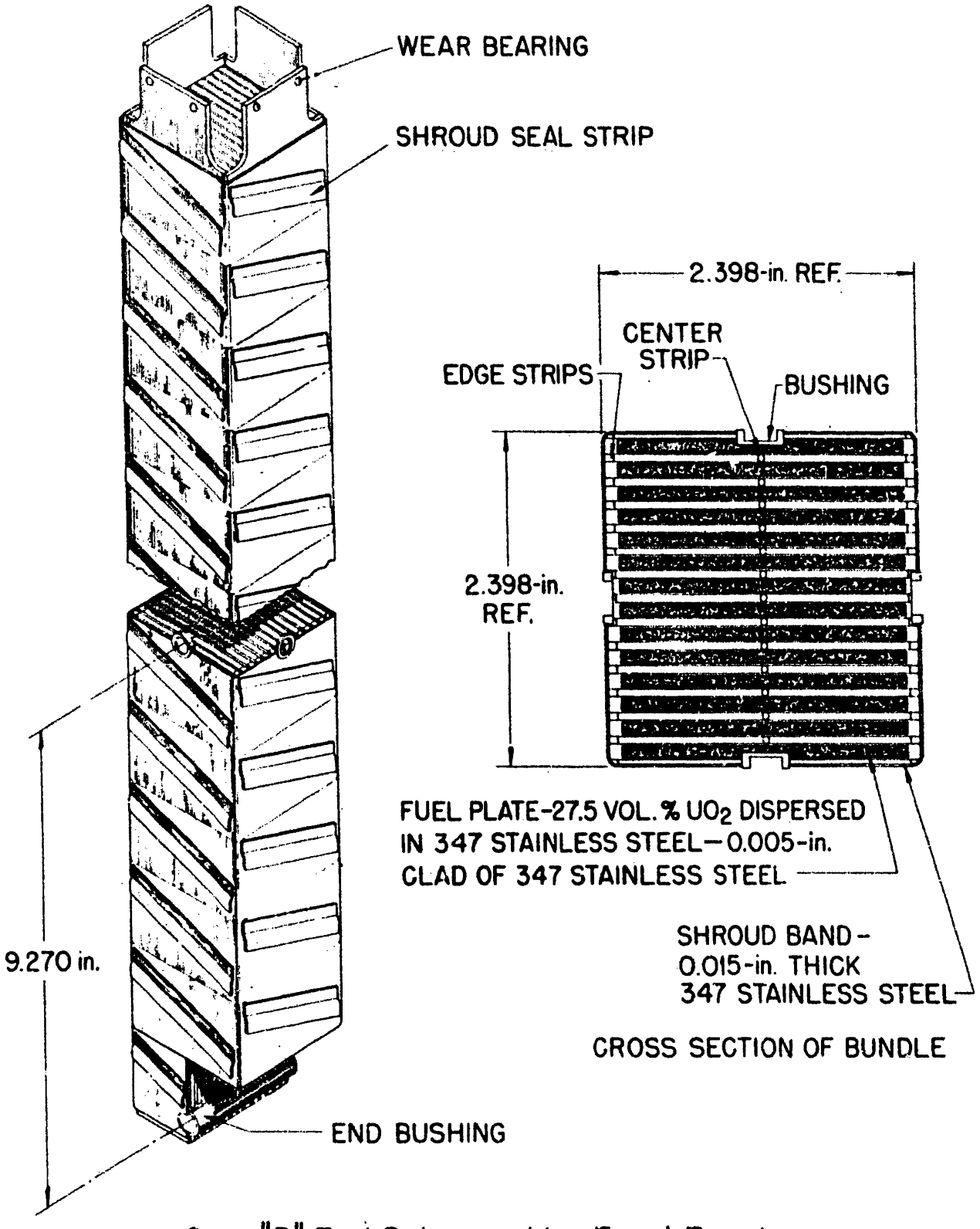

Core "B" Fuel Subassembly—Fermi Reactor

FIGURE 50

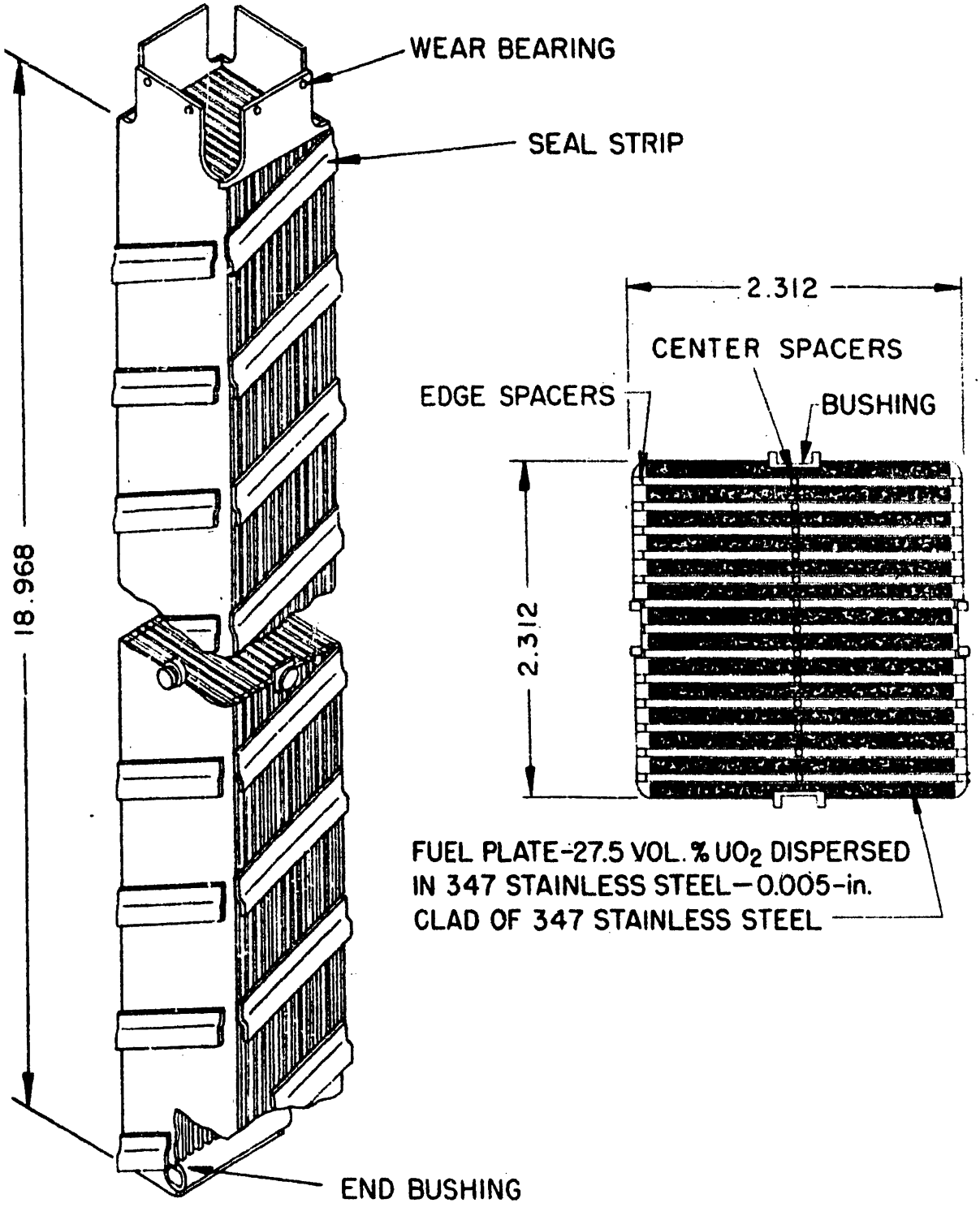

CORE "B" FUEL SUBASSEMBLY - FERMI REACTOR

FIGURE 51

At the present time, detail analysis work is still in progress and a testing program is being formulated.

XIII. CORE B DESIGN DATA AND DESCRIPTION

A. INTRODUCTION AND SUMMARY

Core B uses UO_2-SS cermet fuel to obtain longer fuel life, higher reactor power level, and consequently more economical power production than was possible with Core A. Core B is designed for a core loading of 130 fuel subassemblies (>500 kg U-235) and a reactor power level of 300 Mw, of which 270 Mw is generated in the fuel itself. The reactor coolant inlet temperature is 550 F and the mixed exit temperature is 812 F. Coolant pressure drop across the subassemblies is approximately 90 psi. Burnup is reactivity limited and will average approximately 21 per cent of the U-235 throughput. Additional design and performance data are summarized in Table XIV. Development and performance testing of the Core B design is still underway and therefore approximate, rounded-out data values will generally be used in the discussion here.

B. GENERAL DESIGN FEATURES - COMPARISON TO CORE A

The Core B subassembly, in its external configuration and dimensions, is interchangeable with Core A, as is shown in Figure 52. The fuel occupies approximately the same space in the subassembly and is in the form of two in-line brazed bundles of UO_2-SS cermet plates with stainless steel cladding, as shown in Figures 53 and 54. The bundles are located and supported in the wrapper tube by pins which penetrate the wrapper tube wall to register with bushings in the bundles, and by spring tabs at the outboard ends of the bundles which influence their alignment within the tube (Figure 55). The use of two in-line bundles and the arrangement of the support pins and spring tabs is designed to control the mode and direction of thermal bowing of the bundles to yield a negative power coefficient of reactivity. This is in contrast to the method of support used for the Core A fuel pin bundle, in which elastic preloading is used to override and suppress thermal bowing of the fuel pins within the wrapper tube. The Core B fuel plates are, of course, too stiff relative to the wrapper tube to be subject to this type of bowing control.

Shielding is the primary function of the axial blanket rods in Core B. The rods are similar in configuration to those in Core A but consist of depleted UO_2 pellets jacketed in stainless steel, rather than U-Mo alloy rods sodium-bonded in stainless-steel jackets. Radiation growth and swelling limit the burnup of the Core A alloy rods to much less than that required for Core B (i.e., approximately 4 a/o of U-235 at the core end).

A cylindrical coolant flow strainer unit is located in the lower axial blanket region in much the same manner as in Core A. It is pierced with 40 mil diameter holes smaller than any downstream flow passages and insures that any occasional particulate matter picked up by the sodium (for instance, weld flash) will not reach the fuel coolant passages unless it is small enough to pass through the strainer.

TABLE XIII - CORE B DESIGN AND PERFORMANCE DATA

Core Characteristics and Performance

Core power	270 mw
Coolant inlet temperature	550 F
Average outlet temperature	812 F
Flow rate	26,400 gpm
Pressure drop	75 psi
Number of subassemblies	130 (design)
Equilibrium critical mass	500 kg U-235
Throughput burnup	20.7% of U-235
Maximum* power	1857 w/cc
Maximum* coolant temperature	902 F
Maximum* meat temperature	1043 F

Gross Dimensions

Subassembly length	96-9/16 inch
Wrapper tube O.D.	2.646 inch
Wrapper tube I.D.	2.432 inch
Wrapper tube wall thickness	.107 inch
Overall length of core section (not including spring fingers)	37.958 inch
Overall length of each axial blanket section	14 inch, upper 13 inch, lower

Core Region

Number of plate bundles	2 (in-line)
Bundle Cross section	2.312 inch square
Overall plate length	18-31/32 inch
Meat length	18 inch
Space between in-line bundles	.20 inch
Annulus thickness	.060 inch

* No hot channel factors

Core Region
(Cont'd.)

Number of plates/bundle	14
Plate width	2.312 inch
Meat width	2.177 inch
Plate thickness	.115 inch
Meat thickness	.105 inch
Clad thickness	.005 inch
Channel thickness	.054 inch
Meat composition	35 w/o UO_2 (93% enriched minimum cermet density, 92% of theoretical
U-235/plate	158 grams
Cladding, frame, and rib material	347 stainless steel (low cobalt in cladding)

Axial Blanket Region

Number of rods/lower axial blanket	16, surrounding strainer
Number of rods/upper axial blanket	25, full array
Tube O.D.	0.395 inch
Tube wall thickness	0.015 inch
Tube-pellet annulus	0.002 inch
Pellet O.D.	0.352 inch
Fuel Material	Depleted UO_2, 90% T.D.

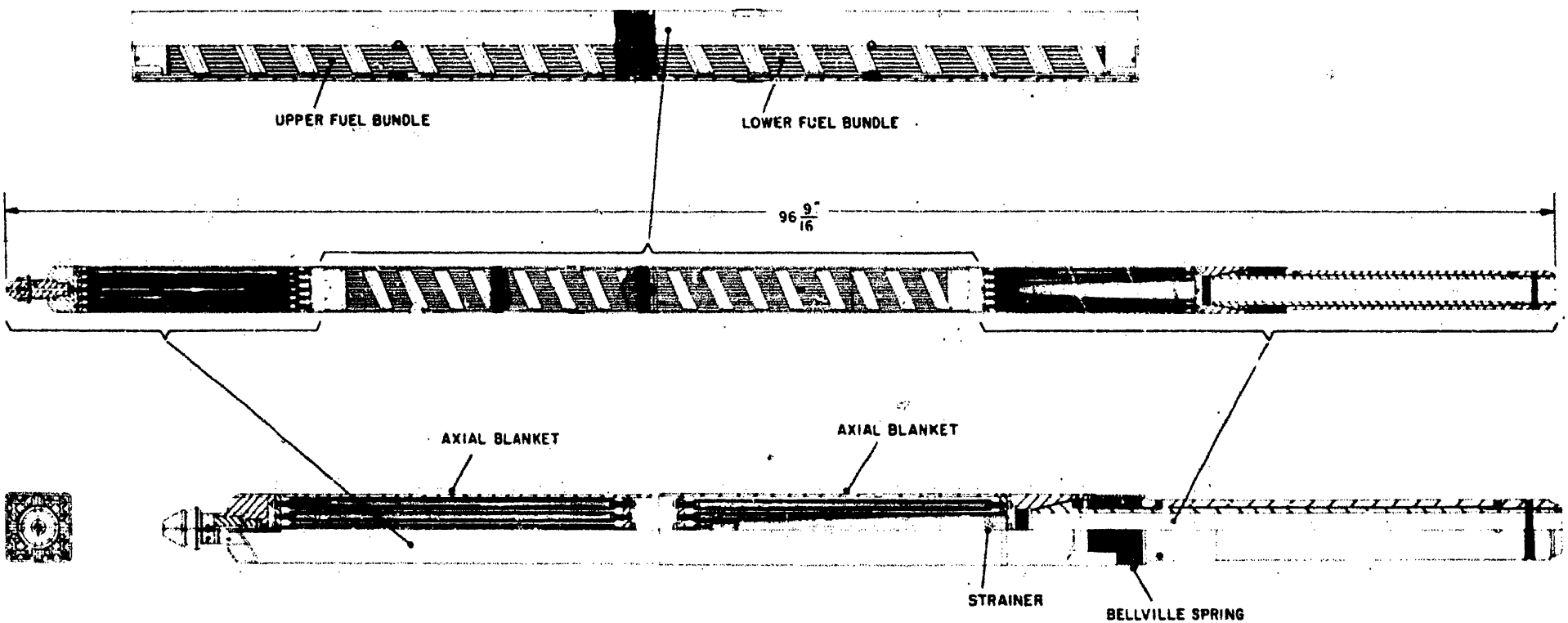

CORE B FUEL SUBASSEMBLY
FIGURE 52

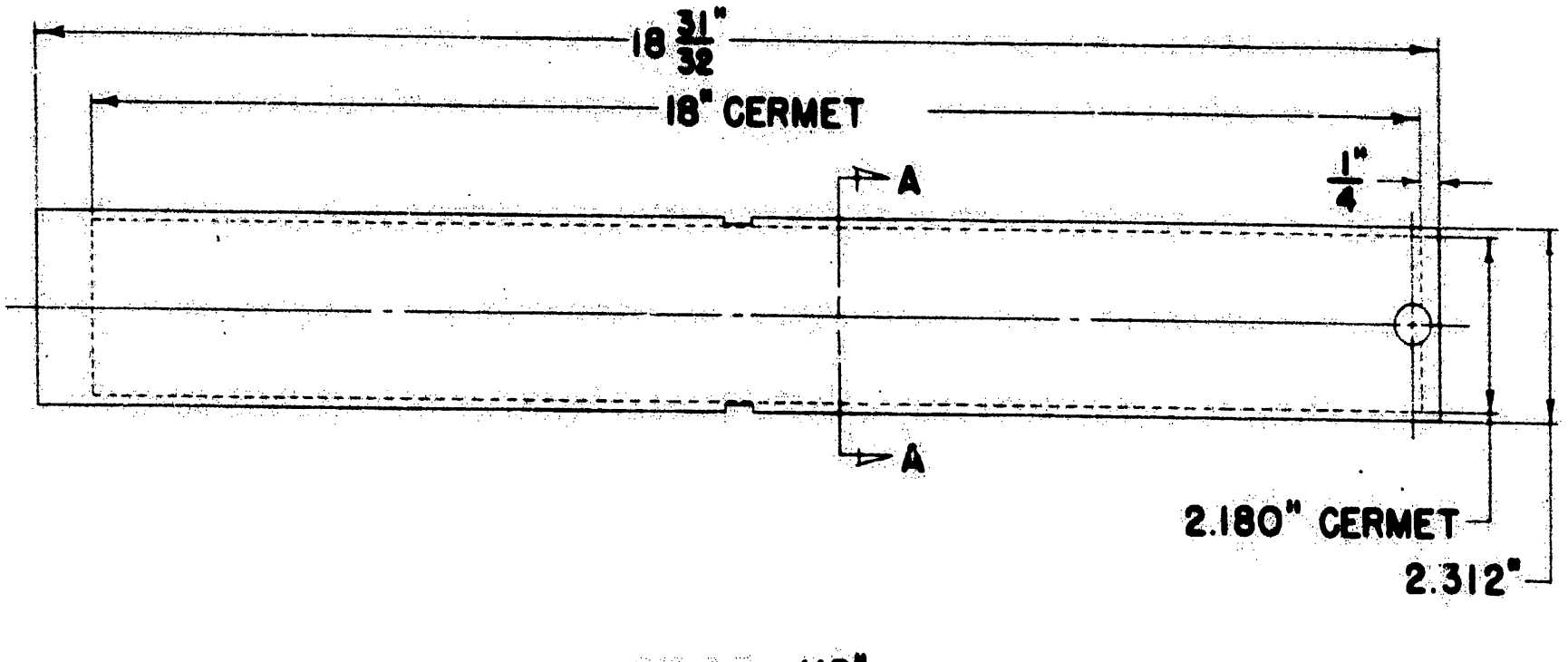

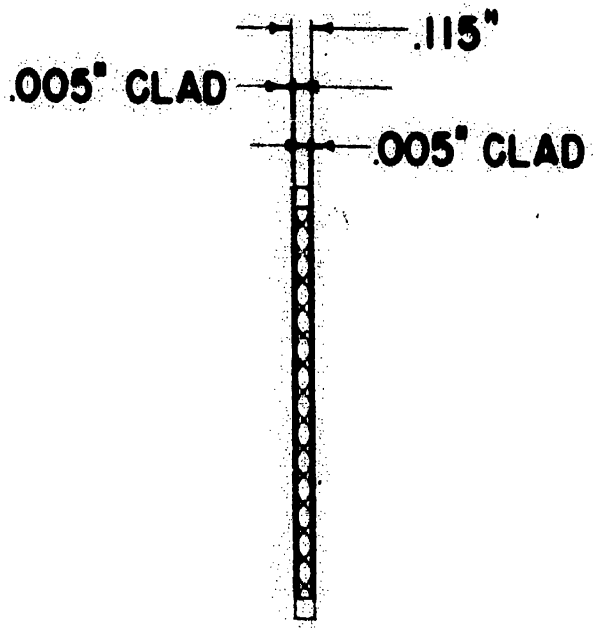

SECTION A-A

FUEL PLATE

FIGURE 53

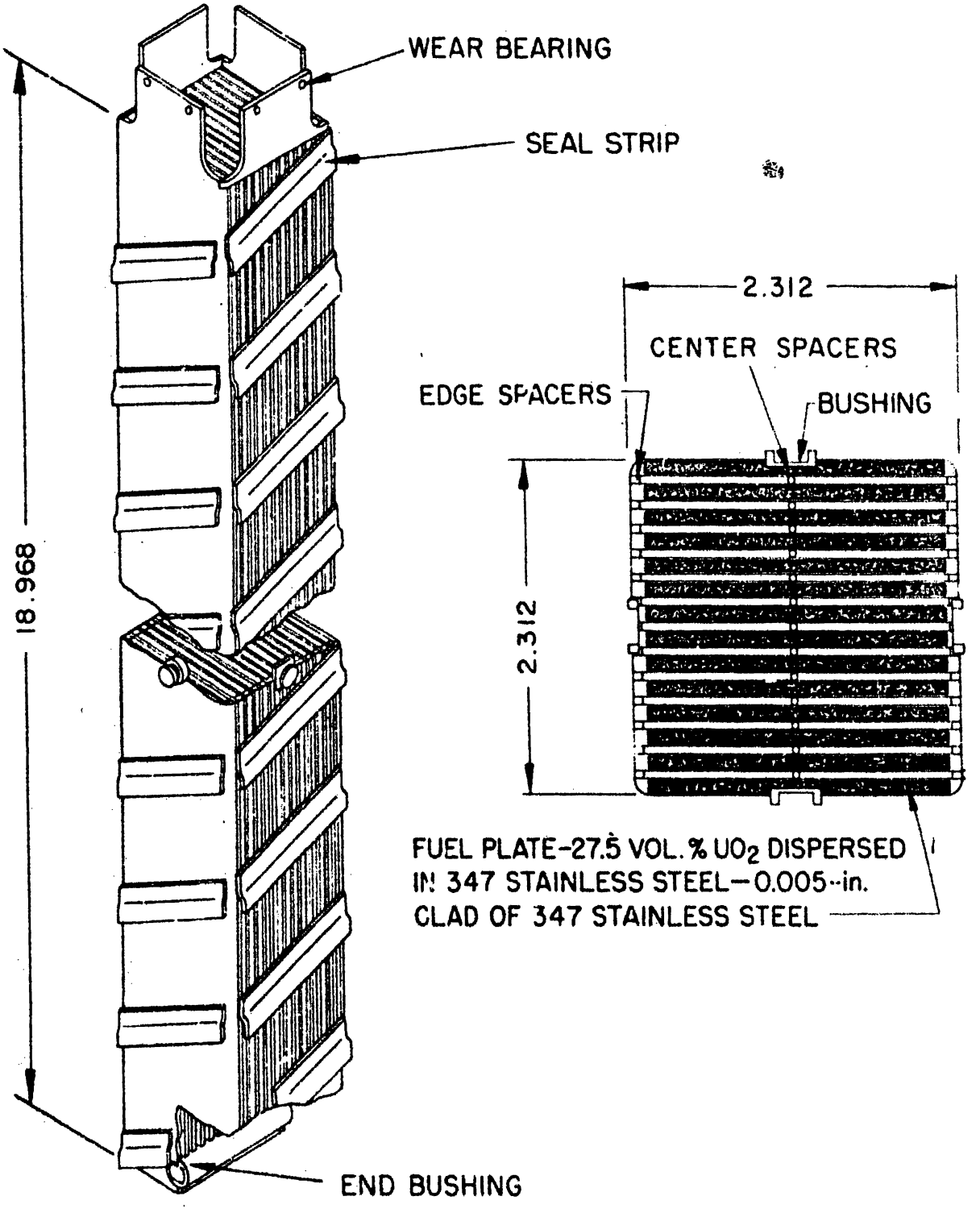

CORE "B" FUEL SUBASSEMBLY - FERMI REACTOR

FIGURE 54

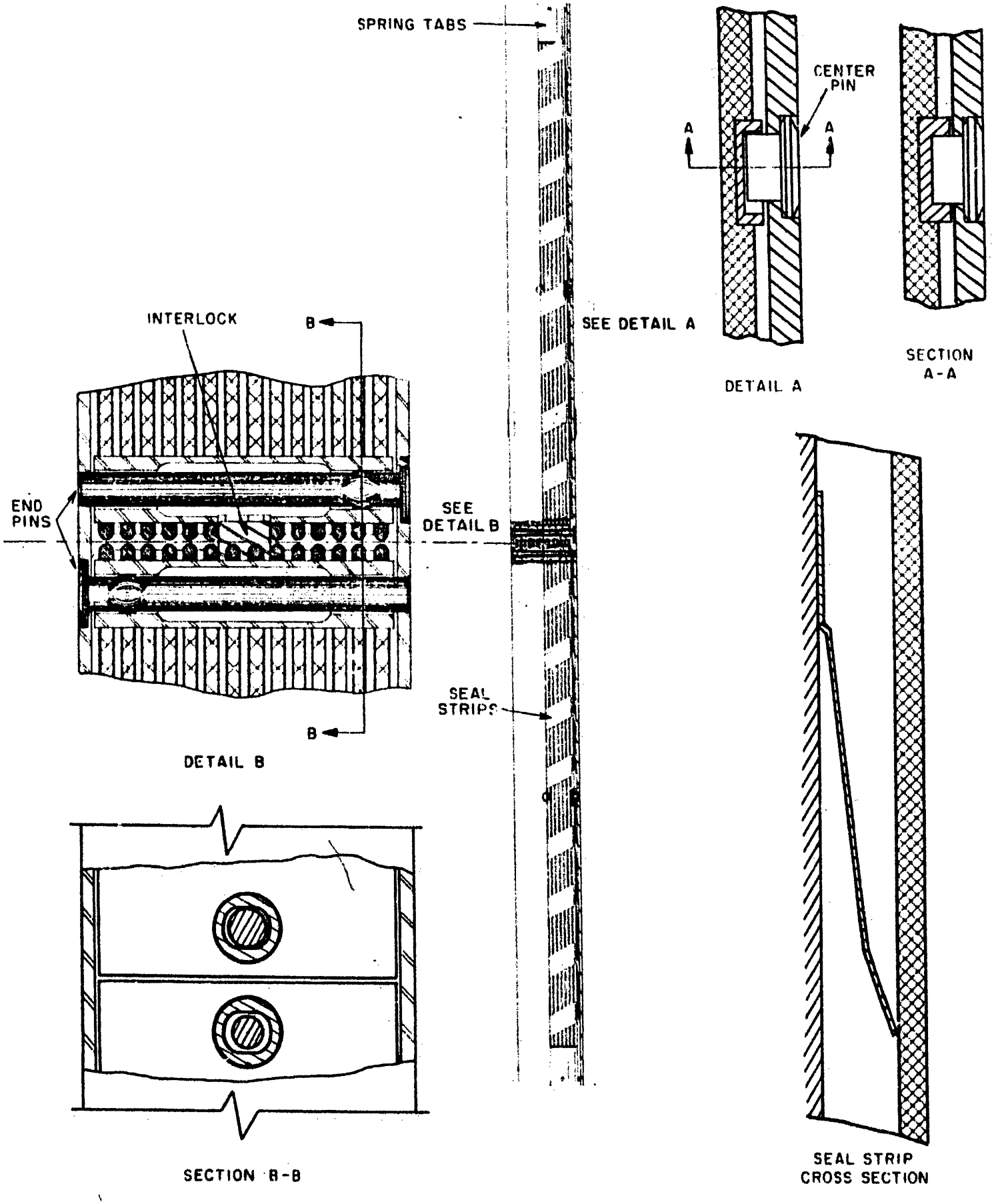

FUEL BUNDLE SUPPORT DETAILS

FIGURE 55

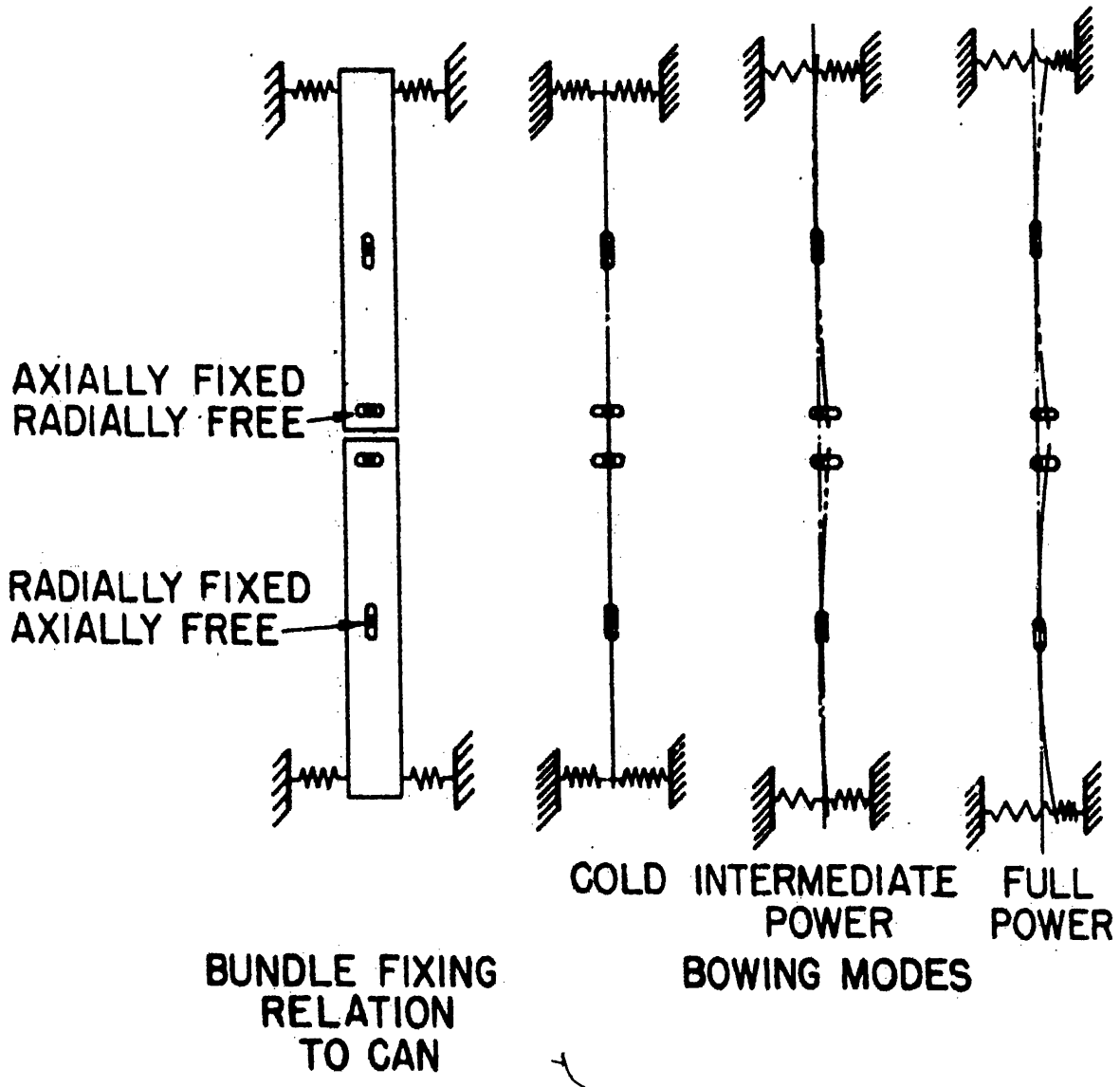

SCHEMATIC DIAGRAMS OF SEGMENTED CORE B BUNDLE

FIGURE 56

The experience and problems encountered in fabrication of Core A are strongly reflected in the design of Core B hardware components, all of which are changed in some detail. These changes are generally in the direction of avoiding distortion and alignment problems and improving the replaceability and reworkability of component parts.

C. SUBASSEMBLY COOLING AND SOURCES OF THERMAL BOWING

The sodium coolant enters the lower end of the subassembly from the vessel plenum below the support grid and flows up through the nozzle, strainer, and lower blanket region with little drop in pressure (~10 psi) and then enters the lower fuel plate bundle. The sodium outside (i.e., between) the subassemblies is at exit pressure and, therefore, this lower region of the wrapper tube is subjected to the maximum internal pressure of 85 to 90 psi. This internal pressure is the controlling load factor which dictates a wrapper tube wall thickness of 107 mils. The bulk of the pressure drop and temperature increase, approximately 75 psi and approximately 250 F, occurs across the fuel plate bundles, and the upper portion of the wrapper tube is subjected to decreasing internal pressure approaching approximately 5 psi with temperature increasing to approximately 800 F.

Power generation rates and temperatures are not uniform across a subassembly when it is located away from the center of the core. An outermost subassembly will generate about half the power of an average subassembly and local power generation rates within such a subassembly will vary across it in a core radius direction by a factor of a little over two. Coolant flow streamlines discharging from an upper fuel plate bundle may therefore differ in temperature by as much as 85 F if it is assumed that no mixing occurs during flow through the bundles.

Sodium coolant also flows through the annular clearance space (60 mils, nominal) which is maintained between the fuel plate bundles and the wrapper tube wall by the pin support arrangement. The outside surfaces of the plate bundles are fitted with a "helical" pattern of flexible seal strips which bear against the wrapper tube wall and force the sodium here to flow up through the annulus in a spiral path, as shown in Figures 54 and 55. This flow cools the outer surfaces of the outer fuel plates of the bundles and also minimizes peripheral variation of wrapper tube wall temperature. The spiral flow arrangement was designed specifically to protect the high-pressure-stressed region of the wrapper tube from additional temperature stresses and, therefore, this portion of the tube will not experience thermal bowing. When this flow discharges from the annulus into the region above the fuel bundles, it will mix somewhat with adjacent streams from the fuel bundle channels and will, furthermore, undergo a small amount of additional, but nonuniform, heating by the upper axial blanket rods. The upper portion of the wrapper tube in this region will develop, therefore, a peripheral temperature gradient in response to the temperature gradient across the sodium coolant stream and will develop a small amount of thermal bowing.

The fuel plate bundles will develop transverse temperature gradients due to the transverse gradients of heat source strength within the material and especially due to the coolant temperature gradient which develops progressively as the sodium flows up through the bundles. Therefore, both

fuel bundles will undergo thermal bowing, the upper one more than the lower one. This bowing, which has a maximum value of 13 mils across bundle flats or 16 mils across the diagonal, will cause variation in the nominal 60-mil-thick annular flow space between the bundles and wrapper tube wall. Stops on the bundles limit constriction of the annulus to 30 mils.

The in-line bundles are separated by a longitudinal gap of 20 mils. Since the upper bundle will thermally bow more than the lower bundle, it is necessary to provide an interlocking nose piece between the bundles to prevent excessive misalignment of the flow channels, which could restrict coolant flow.

D. FUEL PLATE AND FUEL BUNDLE DESIGN

A typical fuel plate, shown in Figure 53, has an enriched UO_2-SS cermet body which is 18 inches long; by 2.180 inches wide, by 1.105 inch thick and which is roll-clad with 5-mil-thick stainless steel by the picture frame technique. The minimum width of the stainless-steel edge frame is 50 mils. End frame widths are 1/4 inch and 3/4 inch (outboard end). Each fuel plate contains 158 grams of U-235 (i.e., 193 grams of UO_2). The cermet contains 35 w/o UO_2 and had a minimum of 92 per cent of theoretical density in the finish-rolled condition. Non-bond areas under the clad will be controlled in sizes over 1/8 inch by the ultrasonic-through-transmission technique. A limited amount of cladding pitting may be accepted as a function of the maximum amount of fission product leakage into the coolant stream which can be tolerated. The problem of detecting and securing quality control of pitting on a production basis is still under study, with emphasis on use of alpha counting techniques which will be sensitive to the degree of exposure of UO_2 particles by pits. Some consideration has also been given to use of an acid bath treatment to leach out exposed UO_2 particles.

Fourteen fuel plates are assembled to form a bundle with 54-mil-thick coolant-flow passages between plates. The plate spacing is fixed by 70-mil-wide stainless-steel strips along each edge and wire spacers 54 mils in diameter that run down the middle of each flow passage. This stack-up is fitted with stellite bushing pieces and flexible seal strips on the outer plate faces. Extra lengths of end frame on the outer plates serve as two of the bundle spring fingers, and these are each fitted with two stellite wear balls. When the stack-up is for an upper bundle it is also fitted with a stellite nose piece which will interlock the upper and lower bundles in the subassembly. The plate stack-up with its fitted pieces is clamped to required stack-up height in a brazing fixture and brazed with GE 81 type or equivalent brazing alloy applied to all joints and seams. The bundle side faces are then finish machined and the remaining flexible seal strips and two spring fingers applied to the side faces by welding.

The principle quality control problem in production brazing of these bundles will be to achieve full penetration of all seams by braze alloy without leaving excessive braze fillets. Excessive braze residue must be avoided because it can impede both coolant flow and heat transfer. It also appears to favor formation of surface cracks in the fillet which may act as stress raisers and affect joint strength.

E. BUNDLE PIN SUPPORT AND THERMAL BOWING CONTROL

The four blind bushings in the middle region of the bundle are engaged in the subassembly by four stub pins which act as a caging spider to keep the mid-portion of the bundle centered in the wrapper tube; i.e., thermal bowing of the bundle relative to the wrapper tube must occur around this centering point. The bundle is positioned longitudinally in the wrapper tube by engagement of the long pin and through-hole bushing at the end of the bundle as can be seen in Figure 55. The holes in the blind bushings, therefore, are elongated longitudinally to allow longitudinal thermal expansion of the bundle. The two bundles in a subassembly are pin-positioned so that this thermal growth is away from the mid-plane of the core. The hole in the through-hole bushing at the end of the bundle is elongated in the transverse direction to allow control of thermal bowing in the manner illustrated in Figure 56. The end pin is machined to engage the bushing with a spherical section so that the same mode of thermal bowing control operates in the other coordinate direction by sliding of the bushing along the pin axis as the bundle bows. Therefore, all thermal growth actions are controlled by the bundle support arrangement to yield a negative power coefficient of reactivity.

XIV. VERIFICATION TESTS OF CORE B DESIGN

The over-all Core B test program has been formulated to provide the experimental data needed to complete the Core B reference design, to check analyses made on the reference design, and to provide proof of adequacy of the reference design. The test program in its present form covers the problems that are recognized because of APDA's past experience. The results from the tests now formulated may indicate requirements for subsequent testing. The tests are discussed under the general headings of (1) Hydraulics, (2) Endurance, and (3) Structure.

A. HYDRAULICS

All of the Core B heat transfer information will be based on hydraulic data. The knowledge of forced convection sodium heat transfer at present is sufficiently complete to permit conservative analyses of forced convective reactor heat transfer when complete data on sodium coolant flow are available.

The gross coolant required to cool the core fuel plates proper can be provided if the pumping power of the plant is sufficient, and if the structure which must withstand the core pressure drop is adequate. Thus, the first experimental question which will be asked is the flow pressure drop relation of the nominal core B design. Since there are two parallel flow paths through the core section proper of the Core B subassemblies--one flow path through the fuel plates, and a second flow path spiraling around the core plates in the annulus between the fuel plates and the core subassembly can--both flow paths must be studied. Since the Core B subassembly contains two core bundles, all questions of the flow pressure drop perturbations due to the tolerances on the nominal design must also be examined.

A question closely associated with core pressure drop is coolant distribution through the core. It is this coolant flow distribution, for the nominal conditions and for the extreme conditions allowed by fabrication tolerances, that establishes the limiting values on core hot spots.

1. Total Pressure Drop in Reference Subassembly

An examination of the existing literature on the pressure drop through plate bundles reveals two general shortcomings of the data with respect to its application to the Core B design.

While the roughness of the tested plates has been described, and the pressure drop through those plates has been explored near operating Reynolds Numbers, the nature of the plate roughness has not been fully described. Early hydraulic studies established that, while irregularly rough surfaces show a leveling off of the friction factor as a function of Reynolds Number at high Reynolds Number, surfaces whose roughness is in the form of orderly waves show a continually sharply decreasing

friction factor with increasing Reynolds Number at high Reynolds Numbers. The pressure drop of the Core B plates will be measured over a sufficiently extended Reynolds Number range to reveal both the operating fluid flow pressure drop data for the core and the nature of the plate roughness.

While the pressure drop between plate bundles previously has been described in the literature, all of that test work related to cases where the coolant thickness was about equal to the fuel plate thickness. Since the Core B coolant channel is only about half as thick as the Core B fuel plates, direct extrapolation of the existing pressure drop data for interrupted fuel bundles to the Core B case might be unreliable.

A Core B subassembly which is non-reference with respect to some of its dimensions, but is near-reference with respect to its surface finish, will be available at an early date. The first flow pressure drop study will be made on that subassembly because of its early availability.

That first subassembly will then be returned to ORNL for reworking to provide a more complete mockup of the reference subassembly. The pressure drop through the reworked subassembly will be established at 100, 200, 250, 275, 300, 325, and 350 gpm, with deaerated water at 190 F. (Water at 190 F has very similar fluid flow properties to sodium at reactor conditions.) After the as-received unit has been flow tested, the core bundles will be offset and the flow test repeated.

The foregoing tests will provide gross flow pressure drop data for the nominal and extreme tolerance core bundles.

2. Annulus Flow Rate

The flow pressure drop relations of the annulus between the core fuel bundles and the subassembly wrapper tube will be tested in a model without fuel plates. The core bundles will be completely blanked off, and the annulus channel thickness will be the main parameter of the test. Annulus thicknesses of 0.055, 0.060, and 0.065 inch will be studied if there is any indication that the 0.060-inch nominal annulus will not be adequate. These annuli will be studied both in the nominal position and with the bundle in positions that simulate the maximum thermal bowing and structural tolerances.

The nominal seal strip angle of 65° will be tested first.

These annulus tests will explore flow pressure drop relations for the annulus. If a continuous seal strip arrangement were used without by-pass flow, there might be undesirable heating of the coolant filaments adjacent to the seal strips as the coolant progressed up the length of the subassembly. If an offset seal strip arrangement were used, there might be too much coolant by-pass flow. Therefore, the by-pass flow associated with several specific seal strip arrangements will be studied to insure that an arrangement is used which will be free of excess heating of the flow filaments adjacent to the seal strips, and which will provide the coolant needed to cool the outside surfaces of the outer fuel plates, and to provide a sufficiently uniform temperature

within the subassembly can. This will be done by dye injection and visual inspection.

3. Flow Distribution Between Plates

The purpose of this test is to determine the flow distribution between the several parallel channels in the Core B fuel element as functions of flow rate and relative positions of the two core bundles.

The two core bundles that will be used for this test will have channel taps in each flow channel. (Note that the space between two fuel plates is made into two channels by the rib spacer between fuel plates.) Each flow channel tap set will be individually calibrated at the start of the test by allowing flow only in the channel being calibrated. Hopefully, the calibration will both provide data for the rest of the test, and provide bases for developing flow pressure drop correlations with channel geometry, since the geometry of each coolant channel will be established by mechanical probing prior to the test.

After the individual channel taps have been calibrated, the bundles will be flow tested in their nominal position without seal strips. They will be flow tested again in extreme positions which mock up thermal bowing and fabrication tolerances. These tests will provide the bases for establishing flow distribution within the fuel bundles, and for establishing the effects of the geometry of the interruption between fuel bundles.

This test might be extended to study means of changing the flow distribution within the fuel bundles and to study the interaction between the fuel bundles and the seal strips. The test will be extended to study the effects of the axial blankets on the flow distribution within the fuel bundles.

4. Annulus Flow Test

Having first studied the gross flow pressure drop relations of a core subassembly, and then separately studied those relations for the seal strips proper, and for the fuel bundles proper, a combined test of the seal strips, fuel bundles, and axial blankets will be run. The details of this test will await the results of the earlier tests.

B. ENDURANCE

The purpose of the Core B endurance test is to determine the effects a Core B subassembly of long-term exposure to high-temperature sodium. The proposed test conditions are 6 weeks of continuous operation at an isothermal sodium temperature of 1000 F, and a flow rate as high as possible, but not to exceed 300 gpm, which is 150% of nominal flow. Pressure drop calculations indicate that the maximum obtainable flow rate will be approximately 245 gpm, at which the total subassembly pressure drop is about 125 psi. Geometric stability, the integrity of welded and brazed joints, and the extent of wear or deformation of the subassembly bundle positioning pins will be determined. It is recognized that the radiation environment,

transient conditions, and thermal gradients characteristic of plant service will not be duplicated. However, general experience indicates that over-nominal flow endurance tests at temperature are good indices of the mechanical integrity of the subassembly.

The first endurance test will be made at the earliest possible date to substantiate the mechanical adequacy of the design. The endurance test will, of course, be repeated if there are major design changes in the core subassembly.

Fabricators are required to provide prototype subassemblies as evidence of ability to execute the design. A subassembly from the selected vendor will also be endurance tested.

C. STRUCTURE

Extensive tests are underway at ORNL to establish the physical properties of the as-fabricated core components. These tests specifically cover the material properties of the material and the mechanical strength of the plate and rib joints.

1. Plate Rib Joint Thermal Cycling

The purpose of this test is to reproduce by electrical heating the shear conditions created in the bundle by a cyclic temperature difference between adjacent plates. The test conditions will be slightly more severe than those expected during operation.

There will be four test pieces to provide some statistical information regarding joint failure. Each test piece will consist of three Core B fuel plates brazed to the side structure, ten thermocouples located throughout the assembly, and two terminal lugs for making electrical connections. The electrical power system will be capable of delivering to the lugs about 2000 amps at 2 volts to the lugs.

The first test piece shall be heated at approximately 1.5 kw. The center inner temperature shall be about 1000 F. A 100 F temperature difference is anticipated between the center and the outer plates. The estimated heating cycle will be 8 minutes on and 25 minutes off. The joints will be visually examined for cracks at the end of 30, 60, 90, and 120 cycles, and the test terminated when cracks appear. If no cracks appear after 120 cycles, the upper temperature will be increased and the cycling will be continued. The maximum upper temperature studied will be 1200 F. The test program for subsequent test pieces will be established after the results of the first test have been avaluated.

Analyses of the strength of the plate rib joint have necessarily been conservative because of uncertainties about the brittle phase in the braze structure. Actually the test is expected to demonstrate considerable reserve strength in the joint. Analyses about the propagation of joint failures is always very involved. The test is expected to provide a realistic basis for joint failure propagation analyses.

2. Core Subassembly Bowing

The purpose of the core subassembly bowing test is to check the proper functioning of the bundle positioning pins. The core bundles will be located in a subassembly wrapper tube by positioning pins, as called for in the reference design. These pins will be in a sodium environment the temperature and oxygen content of which duplicate the worst conditions anticipated in reactor service. The relative movement between the subassembly wrapper tube and the fuel bundle will be mocked up by mechanically causing the subassembly can to bow. The bundle will have an axial load of about 180 pounds to simulate flow forces encountered in service. A lateral movement of about 0.026 inch will be imposed cyclically with a frequency of about one cpm, for a total of about 500 cycles. Examinations will be made periodically for surface wear and positioning pin distortion.

D. GENERAL

The test specifications and procedures have been written for the bulk of the tests which are now anticipated. This presentation has largely been an abstracting of the test specifications and procedures already written. The test program has not yet resulted in any significant test data. The feedback from initial test results is not yet evident. The general plan calls for getting test results early so that changes in the reference design can be made before a vendor gets the design into production.

XV. SUMMARY OF ADVANCED FUEL STUDIES

The first core loading for Fermi was developed from the viewpoint of engineering feasibility. Subsequent core development efforts have been aimed at improving fast reactor economics.

A. BMI--CORE II STUDIES

In 1956, BMI (under APDA contract) began a comprehensive program directed at developing an improved uranium core loading for Fermi or Fermi-type reactors. This effort included mechanical design and thermal, hydraulic, nuclear, and economic analyses. Fuel and cladding materials were carefully evaluated, and fabrication processes were studied in detail.

The fuel systems analyzed were

1 alloy - U-10 w/o Mo

2 ceramics - UO_2 and UC

4 cermets - UO_2 in SS, UO_2 in U-10 w/o Mo, UC in U-20 w/o Mo, UC in Inconel-X.

All of the systems were evaluated for plate geometry and, in addition, the UO_2 and UC ceramics were evaluated in pin geometries.

Figure 57 shows the pressure-bonding method of fabrication selected for metallurgically bonding the alloy and cermet plates. Figure 58 shows a "radiator" design using helium or sodium bonding which is suitable for all fuel types. The ceramic pins designs included both pellets and powders, and both helium and sodium bonding.

In mid-1958 Battelle concluded that

1. The most promising fuels for the near term were UO_2 pellet pins and UC-Inconel-X cermet plates.

2. The fuel cycle cost in a 300-Mwe plant might be 1 m/kwhr with $30/gm Pu buy-back price, or 3-1/2 m/kwhr at $12/gm Pu buy-back.

About this same time, BMI did the initial fabrication development of a cermet of UO_2 dispersed in U-10 w/o Mo and conducted some irradiation tests on this material. The results of these tests were encouraging. Burn-ups of 1 a/o and 2 a/o of the contained uranium were obtained at temperatures of 800 F without swelling.

B. 300-MWe - PFFBR

In the winter of 1958-59 APDA, in co-operation with five member companies, performed a design study on a second-generation fast reactor--

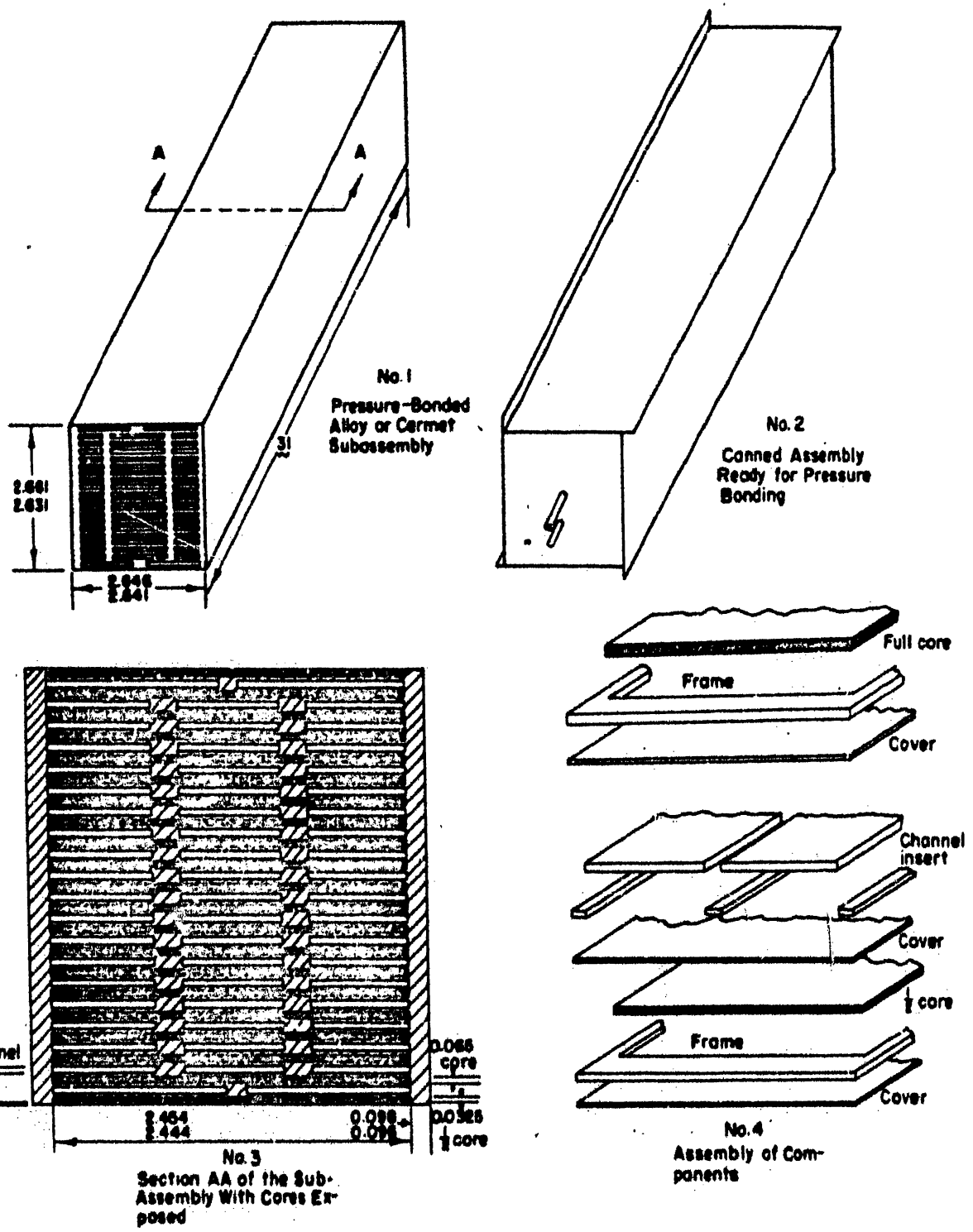

FABRICATION OF FLAT PLATE SUBASSEMBLY DESIGN
BY PRESSURE BONDING TECHNIQUE AS PROPOSED BY BATTELLE
FIGURE 57

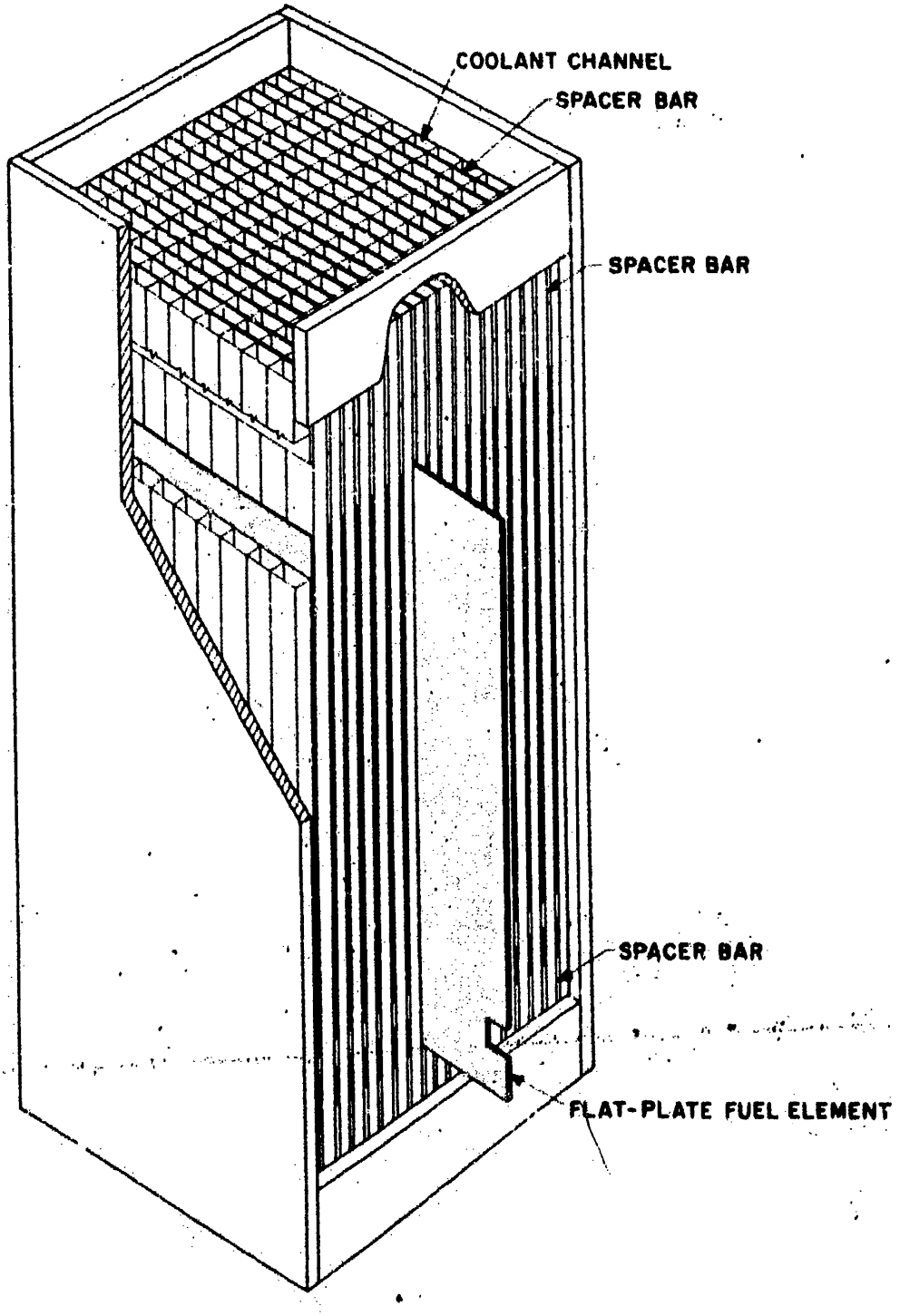

PERSPECTIVE OF FUEL SECTION
CONTAINING FLAT-PLATE ELEMENTS
FIGURE 58

a 300 Mwe Plutonium-Fueled Fast Breeder Reactor.

The reference fuel system was PuO_2-UO_2 powder swaged to 89 per cent of theoretical density in a stainless-steel tube. The fuel element was a 72-inch-long, 3-region composite: a 36-inch core region, a 14-inch depleted UO_2 upper axial blanket region, and a 22-inch gas reservoir. The element is shown in Figure 59. The tube wall thickness was specified to permit 13 per cent burnup of U+Pu with less than 1 per cent strain with either 80 per cent fission gas release at normal full power or 100 per cent fission gas release during a 50 per cent over-power transient. The thermal design was based on the conservative restriction of 1/2 kw/inch maximum power. The core pressure drop was 50 psi. The coolant inlet temperature was 650 F; the average outlet temperature 1000 F.

The fuel cycle cost was estimated at 2-1/2 mills, the total power cost at 9 mills. These costs and all others that follow are based on typical private utility accounting practices: 12 to 14 per cent charge on plant investment, 10-1/3 to 12 per cent charge on working capital and fuel inventory, a market price of $10.50/gm of Pu nitrate, and 70 per cent plant factor.

Two alternate fuel systems were briefly evaluated:

PuO_2 in U-15 w/o Mo cermet plates, Zr-clad by pressure bonding.

Fissium alloy pins, sodium-bonded in SS tubes--the EBR-II concept.

The cermet system has generally superior nuclear performance compared to the reference core and becomes economically competitive at a burnup of about 3 per cent of total atoms.

C. AEC FAST REACTOR PARAMETER STUDY

During the summer of 1959, APDA performed a Fast Reactor Core Design Parameter Study for the AEC. Figure 60 summarizes the costs for each of several fuel systems evaluated for two specific reactor plants: Fermi and the 300 MWe PFFBR.

The major result of the study was conclusive proof that optimization of discretionary design parameters can dramatically reduce costs. In Fermi, the fuel cycle costs of U-10 w/o Mo alloy pins can be cut in half by simply increasing the pin diameter and length, the number of core subassemblies, and the pump speed.

Design optimization requires, and is based on, comprehensive correlations of all pertinent input parameters and calculation techniques. Of these correlations, the most important are materials properties. Plots of physical and mechanical properties of structural materials, as functions of temperature, are basic to rational plant and equipment design. The key to fast reactor core design optimization is the continuous plot of allowable fuel burnup vs. fuel temperature, as exemplified by Figures 61, 62, and 63. Other important correlations are:

Nuclear characteristics, (critical mass and breeding ratio vs. core volume and volume fraction fuel).

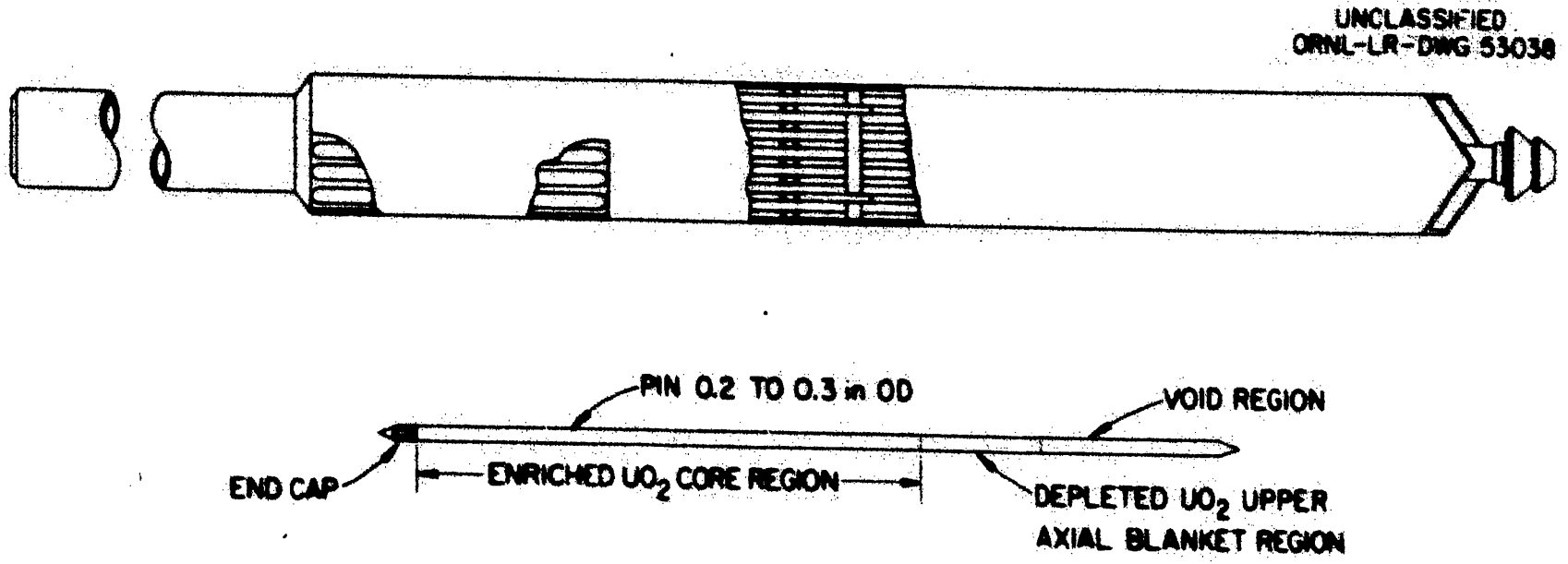

Typical Core "C" Element
Fermi Reactor
FIGURE 59

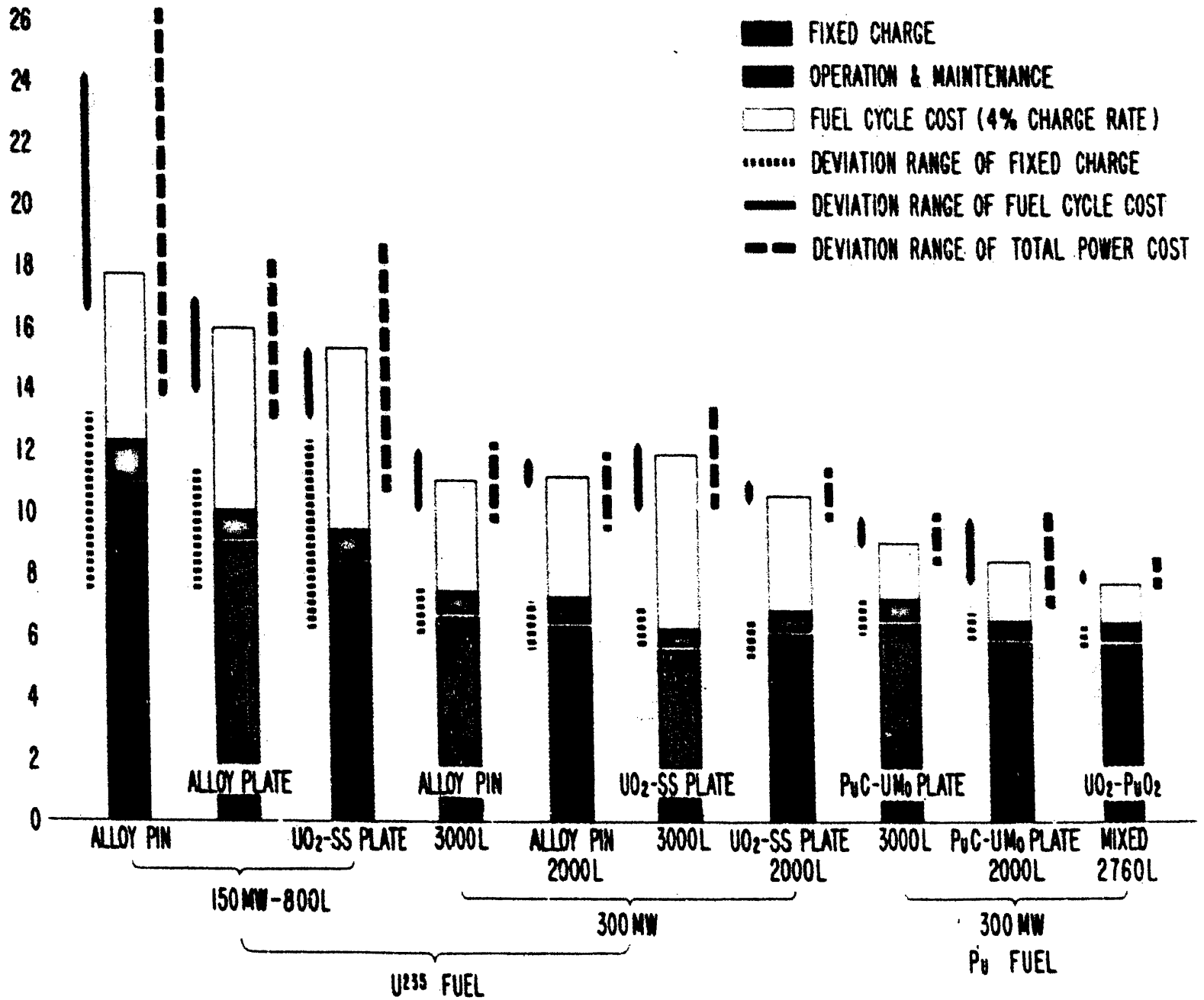

CORE PARAMETRIC STUDY RESULTS

FIGURE 60

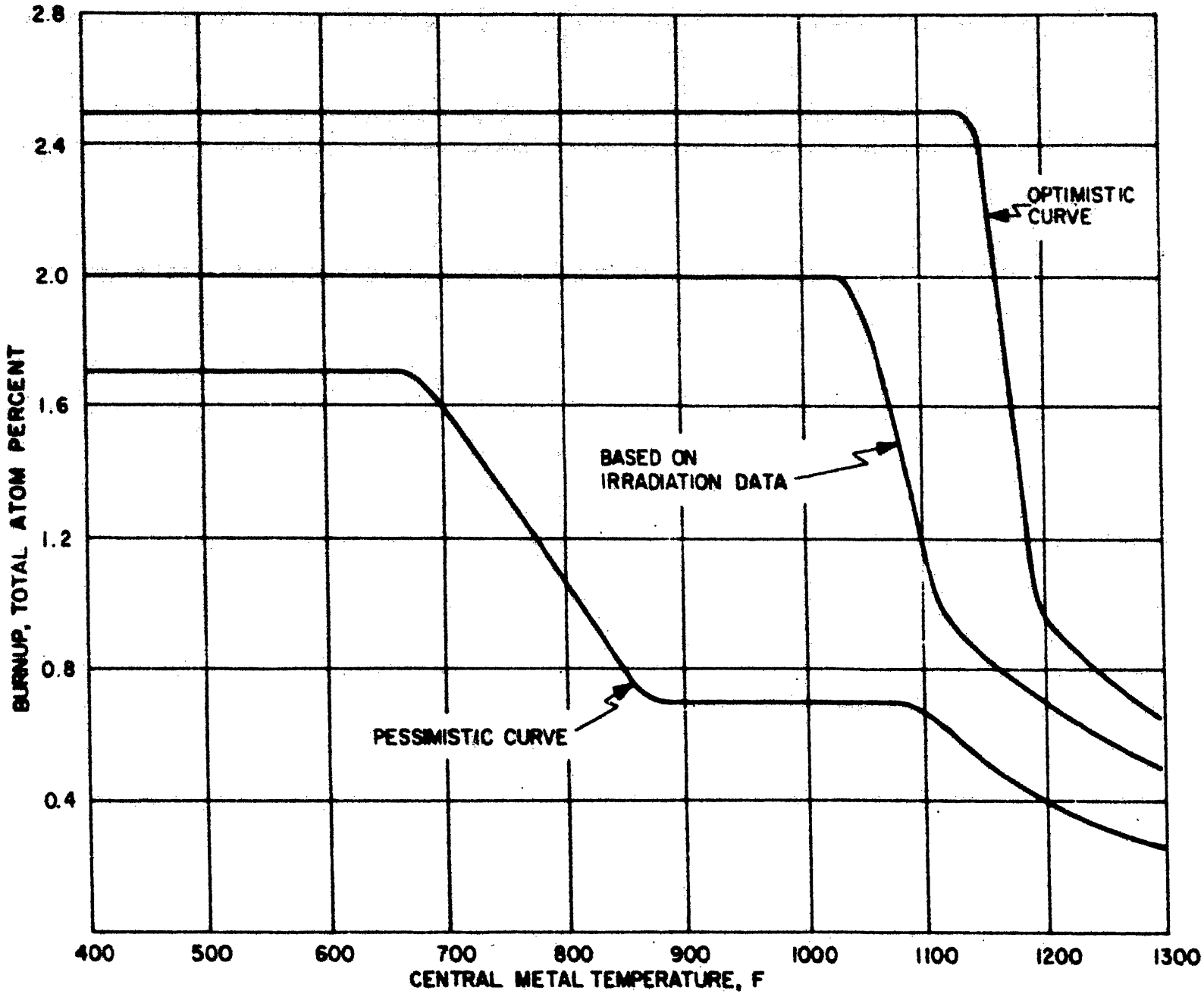

BURNUP LIMITATIONS OF U-10 $^{W}/_{O}$ Mo AS A FUNCTION OF TEMPERATURE

FIGURE 61

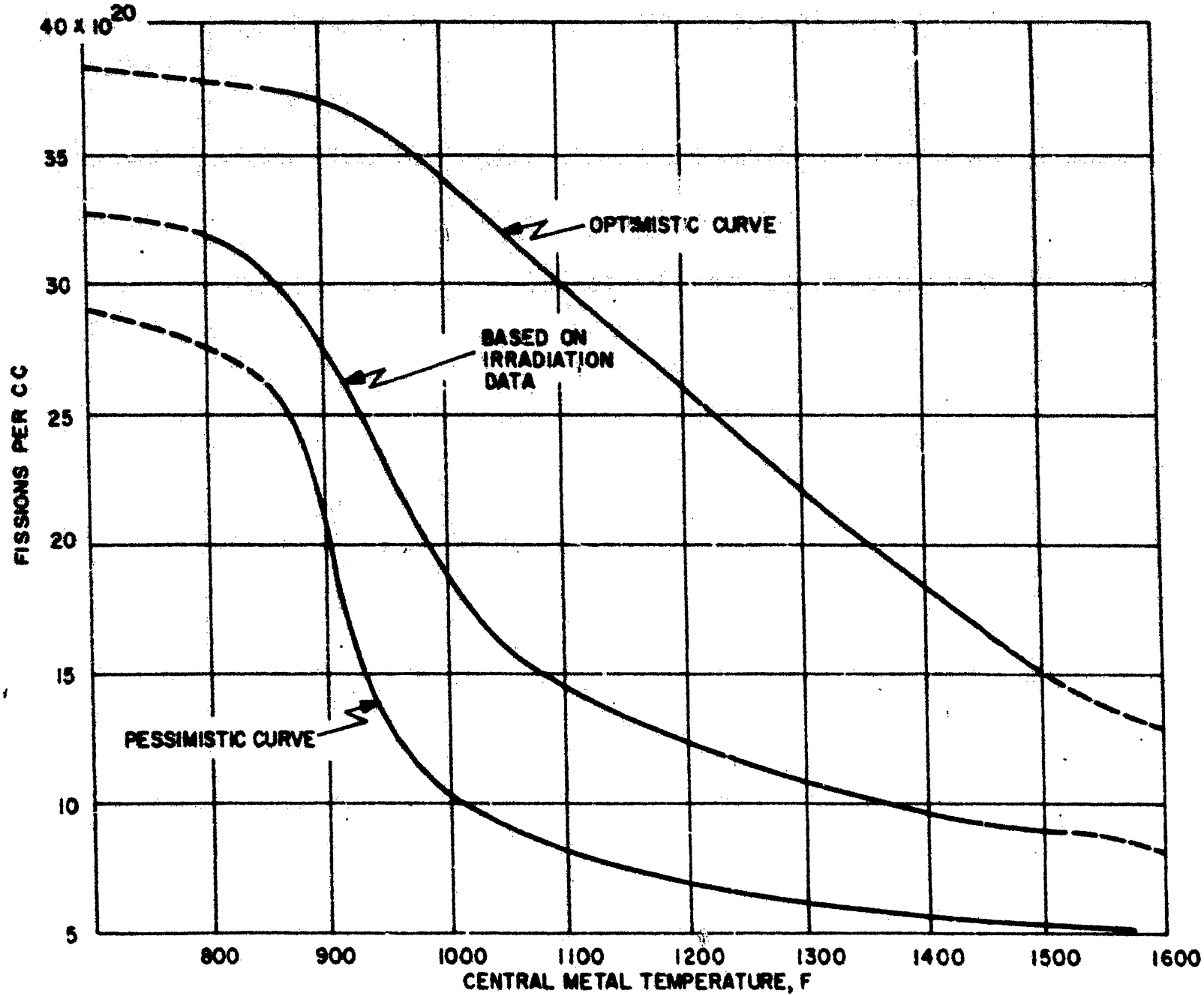

BURNUP LIMITATIONS OF UO_2 IN STAINLESS STEEL FOR LOADING UP TO 30 $^{W}/_{O}$ UO_2

FIGURE 62

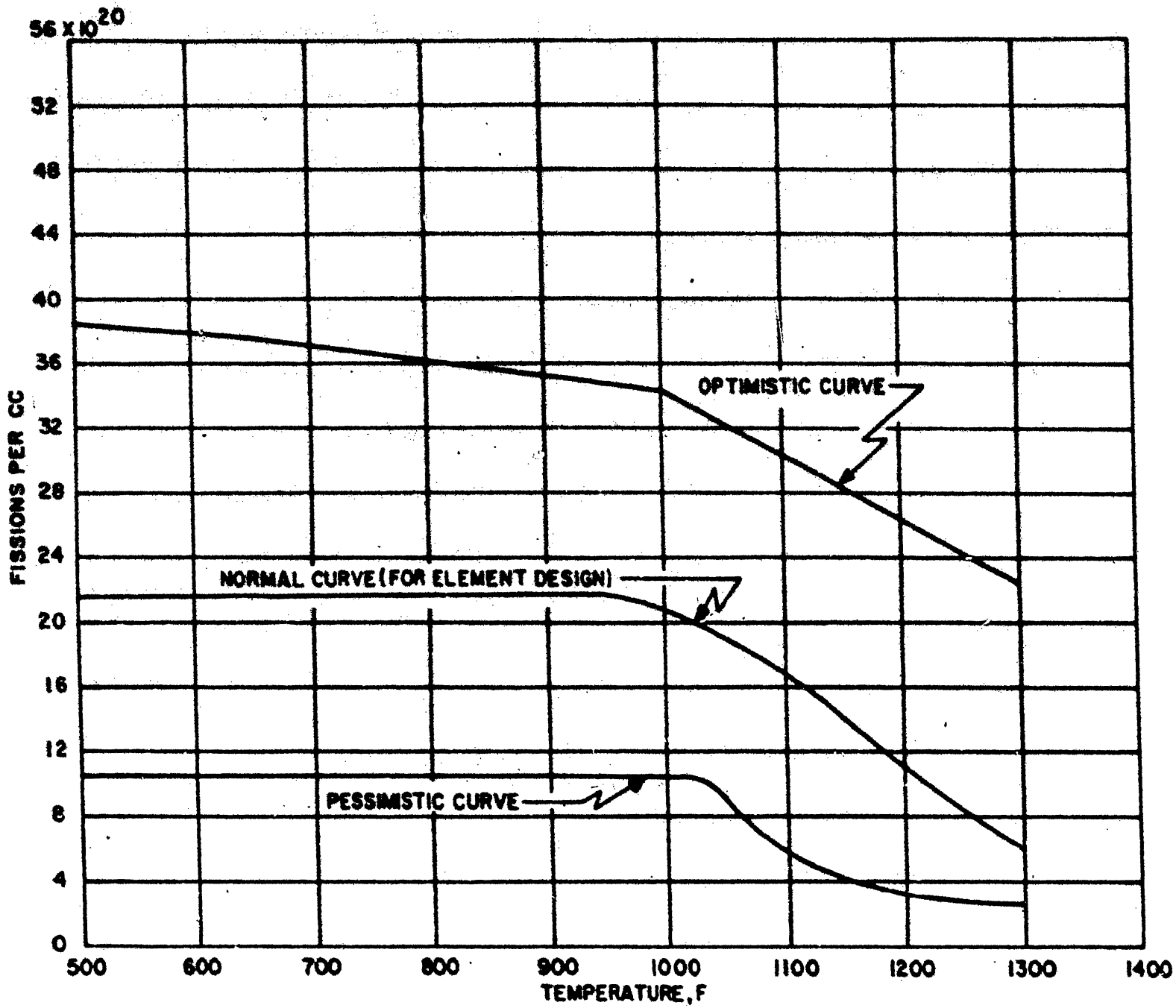

BURNUP LIMITATIONS FOR UC-U15 W/O MO AND PU C-U15 W/O MO

FIGURE 63

Hydraulic characteristics (pressure drop as a function of length, flow rate, and geometry).

Thermal characteristics (fuel temperature as a function of geometry, location, power, etc.).

Throughput characteristics (fuel throughput fabrication as functions of throughput, enrichment, geometry, and materials).

The optimization method used was a cut-and-try process; many of the computations were performed on computers, but the evaluation and the perturbation of parameters was a human task. A closed-cycle, self-optimizing machine program would have had obvious utility, but did not and does not now seem feasible. However, recent studies by APDA and Franklin Institute have shown that both digital and analog machines can be programmed to provide highly useful assistance to the design engineer.

D. 150 MWe PFFBR

One year ago, APDA and five member companies made another design study on a second-generation PFFBR -- this time a 150-Mwe plant. The fuel system, again, was 89 per cent dense $PuO-UO_2$ in a stainless-steel tube. The fabrication process, however, was vibratory compaction instead of swaging. The pin had only a single region, the fission gas being contained by a heavier clad wall thickness.

Both the thermal and hydraulic design bases were double the values of the previous 300-MWe study: 1 kw/inch and 100 psi core pressure drop. The throughput burnup, however, was cut from 13 per cent to 5 per cent of metal atoms.

The fuel cycle cost for this 150 MWe PFFBR was estimated at slightly over 2 mills/kwhr -- nearly 1/4 less than the cost of the higher burnup 300-MWe PFFBR core. This interesting result was directly and almost exclusively caused by more optimum selection of discretionary parameters.

The reactor inlet and outlet temperatures were reduced 100 F, achieving a significant increase in clad strength. The pressure drop was doubled, reducing the required coolant volume. The core length was increased 1/3 and the core diameter reduced 1/5. The over-all result of these changes was a 70 per cent increase in actual weight of fuel in the core which is sufficient to just offset the 60 per cent reduction in burnup.

The small net improvement in fuel cycle costs resulted from a change in the radial blanket fuel system. The U-3 w/o Mo alloy rods of the 300-MWe plant were replaced by UO_2 rods in the 150-Mwe plant. The principal result was an increase in throughput burnup from 0.2 per cent with the alloy to 2/3 per cent with the oxide.

XVI. REQUIREMENTS OF ADVANCED FAST REACTOR FUELS

Before considering the potential of individual fuel systems, it seems worthwhile to set down the general requirements for fast reactor fuels as used by APDA. It is pointed out that with regard to these requirements, and the subsequent discussion, the fuel cycle is based on aqueous reprocessing for the spent fuel and, therefore, the associated long turn-around time. If one considers integral pyrometallurgical reprocessing, such as that associated with EBR-II, it is quite likely that a different set of requirements would be reached.

The APDA general requirements for a plutonium fuel are as follows:

1. Burnup

From an economic standpoint the burnup goal is about 2×10^{21} fissions/cc. Converted to other terms, this is roughly equivalent to 4% burnup in the U-10 w/o Mo fuel, 35% of the uranium atoms in a 30 w/o dispersion of UO_2 in stainless steel or 75,000 Mwd/T in UO_2.

2. Power Density

A maximum power density greater than 1 kw/cc is required to maintain the inventory charges within acceptable limits. For pin-type fuel elements this corresponds to a maximum power density in excess of 1 kw/in. for a fuel pin of approximately 0.200 inches in diameter.

3. Fabrication Costs

The cost of fabricating pin-type elements should not exceed $50/pin, or $1,500/kg of fissionable material.

4. Plutonium-Uranium Atom Density

To achieve a reasonable doubling time, a breeding ratio for high burnup elements must be greater than 1.35. This requires a density greater than 7 g/cc of the fissile and fertile atoms within the fuel element. This corresponds to a core density greater than 4 g/cc of the heavy atoms. The advantages of higher density are great, and any element that can combine high burnup with a higher fuel density will show an advantage.

5. Safety and Control

The principal requirement in regard to safety and control is that the prompt reactivity coefficients due to fuel temperature be negative under all possible operating conditions including very fast power transients. These coefficients arise from fuel expansion as well as from the Doppler effect. It is also highly desirable to have these coefficients, even if they are negative, to be reproducible under all conditions of operation. The principal concern is that the fuel material in achieving

high burnups at high power densities will undergo physical change to such an extent that it will no longer expand in a predictable manner and as a result the effect on reactivity will be uncertain. To increase the internal breeding ratio, it is desirable to have a reasonably large ratio of fertile to fissionable atoms in the fuel. This also results in a larger negative Doppler temperature coefficient which would override any tendency for erratic behavior of the material if it should not expand thermally. However, when the ratio of U-238 to Pu-239 is greater than about eight, the sodium temperature coefficient of reactivity can be positive, which is undesirable. This, therefore, sets a limit on the dilution of the fissionable material with fertile material that can be considered.

6. Coolant Compatibility

The fuel material must be compatible with sodium. In case of a cladding rupture, the fuel must have sufficient integrity or corrosion resistance that a large fraction does not enter the coolant system.

It should be remembered that the above points are generalizations, particularly items 1 through 4. Also, the first four items are interdependent in that higher burnup permits slightly higher fabrication costs and lower fuel and power densities.

In considering advanced fuels for the fast reactor, the goal is to eventually incorporate plutonium as the fissile material. With this in mind, it appears that one can initiate a fuel development program utilizing U-235 as a substitute for plutonium. However, before such a program is started it should be verified with a fair degree of confidence that this substitution will not grossly affect the general performance of the fuel.

There are three general catagories of fuels to be considered: metallic, ceramic, and cermets. The advantages, the disadvantages, and the general problems associated with each of these general catagories and with some specific fuels within each group are discussed below.

1. Metallic Fuels

The one big advantage of metallic fuel systems is the ability to achieve a high uranium density. For example in a uranium-base alloy, with 80 w/o U-20 w/o alloy addition, the uranium density would be about 14 g/cc, or twice the minimum requirement. A second advantage of a metal, an advantage associated with safety is a fairly large thermal expansion coefficient resulting in a negative temperature coefficient. In addition, the high uranium content allows for a high U-238 to U-235 ratio, giving rise to a large negative Doppler effect.

The prime disadvantage of metallic fuel is directly related to burnup potential. One could propose at this time that the use of a U-13 w/o to 15 w/o Mo alloy might raise the allowable burnup of a Fermi-type pin (coextruded-zirconium-clad) to about 2 a/o (1×10^{21} fissions/cc) for maximum fuel temperatures of about 1250 F. This is approximately one-half the required burnup. One can further propose several approaches

to achieve the required burnup by either going to a sodium-bonded pin or considering cladding restraint, both approaches having the effect of decreasing uranium density and power density.

Probably the major disadvantages associated with the metallic fuels are the unknown factors associated with the substitution of plutonium for U-235. The evidence to date indicates a reduction in allowable burnup and in power density due to lower melting points. The determination of the effects of the substitution appears to present the major problem associated with the further development of metallic uranium fuels along with the development of fabrication procedures resulting in lower fabrication costs.

2. Ceramic Fuels

With regard to the ceramic fuels, by far their greatest advantage lies in a high potential burnup. Under low-temperature radiation conditions, UO_2 has been irradiated to about 60,000 Mwd/T, 1.8×10^{21} fissions/cc; under similar conditions, UC has achieved about 25,000 Mwd/T, 0.8×10^{21} fissions/cc. Considering only burnup and power density requirements, both of these fuels appear most promising. One might further propose that UN could also meet these requirements, however, there are no data available to support this proposition.

With respect to fuel and fertile atom density, PuO_2-UO_2 is just borderline for the basic requirement of about 7g/cc of fuel element, considering an oxide density of about 90% TD. PuC-UC offers 30% increase in density over UO_2, while PuN-UN would offer a 40% increase.

From the fabrication cost standpoint, UO_2 certainly meets the basic requirements and, depending on the fabrication procedure used, could be considerably lower. Fabrication costs of UC are still a matter of conjecture, but those involved in UC fabrication feel they could reach the allowable cost. The fabrication costs of UN are completely unknown. If pressed and sintered plutonium-uranium compounds are used, of if vibration techniques are used, it appears that the fabrication cost of plutonium ceramic elements would be acceptable.

The major disadvantage associated with the ceramics is in the area of safety. Although all the ceramics have a positive thermal expansion, it is uncertain at this time if this expansion could be depended on for a negative temperature coefficient of reactivity. On the basis of presently known technology, this statement can be supported for UO_2. It has been shown that UO_2 is grossly cracked both radially and circumferentially following irradiation under high power density. It remains to be demonstrated that the thermal expansion of the UO_2 into the voids created by the cracks, would not increase reactivity in the event of a power transient on startup.

While it has not been demonstrated that a similar situation exists for UC, at least to the same extent, one could assume that such would be the case, under high temperature gradients and on the basis of reported mechanical properties of UC. One would also suspect that such

is true of UN as well.

The major concern about UC lies in its tendency to decarburize in sodium. The general feeling is that a stainless steel can for UC, as in a sodium-bonded element, would not be satisfactory and, further if a suitable cladding is found, the possibility of carburizing other portions of the reactor is ever present in the event of a defective can. It is reported that this problem might be overcome by alloying the UC with Nb. Additional work is required to demonstrate that this approach to the problem is feasible.

With regard to the substiution of plutonium for uranium in the ceramic fuels, it is generally felt that no significant effects would be observed. This feeling is prompted by the fact that the compounds of these metals have the same crystal structure and are in general mutually soluable. Variations in physical properties, such as vapor pressure, may give some problems but it is not anticipated that these will be great.

In summary, it is considered that the major problem associated with the ceramics is connected with safety and, as such, will require considerable experimental evaluation. With regard to UC, additional problems appear to be (1) to increase the stability of the compound and (2) decrease fabrication costs.

3. Cermet Fuels

In considering cermet fuels, one should classify them according to inert and fertile matrix cermets.

An inert matrix cermet is typified by the Fermi Core B fuel in which fully enriched UO_2 is dispersed in Type 347 stainless steel. The advantage of this fuel lies in a high burnup potential coupled with reasonable fabrication cost. Of course, the limitation of the type of fuel lies in the inability to achieve a satisfactory fuel and fertile atom density and, therefore, cannot be considered as an advanced fast reactor fuel.

However, an outgrowth of this fuel system is one in which the matrix is a depleted-uranium-based alloy and the dispersent is a uranium compound, preferably one of higher uranium content than UO_2. Again, by analogy, the prime advantage of this system lies in a potentially high allowable burnup. A second advantage lies in a reasonably high heavy atom density, approaching 14 to 15 g/cc. The disadvantages of this fuel are mainly associated with potentially high fabrication costs and large fabrication development costs.

The fuel system seems particularly adaptable to plutonium since it would simply be used to replace the enriched dispersent.

XVII. PASTE FUEL CONCEPT

A. EVOLUTION OF THE CONCEPT

The paste-fueled reactor concept evolved from fuel cycle cost studies made by APDA. These studies indicated that a liquid-metal-cooled, fast neutron breeder reactor, employing a high burnup fuel, with low inventory and minimum fuel and blanket fabrication, would give truly low-cost nuclear power. It was concluded that such a reactor should use mobile fuel and blanket systems which would move continuously into and out of the reactor during full-power operation, and which would be reprocessed and fabricated on the site in an integrated facility. It was further concluded that the core should be internally cooled by a separate cooling system since transporting of the mobile fuel material through an external heat exchanger to remove all of the reactor heat would involve prohibitive fuel inventories. Consideration of these various requirements led to the concept of using pastes for the fuel and blanket material. Aside from the core itself, the major components of the paste-fueled reactor power plant are almost identical to the corresponding components of existing solid-fueled fast reactor designs, and they are arranged in a similar manner. Hence, the major developmental problems are associated with the core and the fuel and blanket material.

Recognizing the advantages inherent in a mobile-fueled reactor, APDA initiated the development of the paste-fueled reactor concept in 1955. The fuel and blanket consist of small spherical particles containing fissionable or fertile material settled in a liquid metal. These settled, two-phase fuel systems are called "pastes" to distinguish them from "slurries", i.e., two-phase fuel systems in which the particles are dispersed in the liquid by fluid-dynamic forces. The concentration of solids in the pastes is maintained at the settled density of approximately 60 per cent by volume of solids, irrespective of paste movement. A conceptual drawing of a paste-fueled core subassembly is shown in Figure 64. A dilute slurry of fuel particles in liquid metal is fed to a cyclone separator at the top of the core. Concentrated paste from the separator is introduced into the top of each fuel subassembly and flows slowly down through the small passages formed by the spacing between the coolant tubes (paste in the tubes and coolant in the surrounding space is an alternative arrangement). The bottom portion of each subassembly is conical. Paste flows through orifices in this portion into an eductor. Carrier liquid (sodium), which is introduced into a central pipe in each subassembly connected to the eductor, dilutes the paste and fluidizes the particles, which are then carried out to the processing cell adjacent to the reactor vessel. A portion of the fuel particles is reprocessed. Oversized particles, which might result from the sintering of several particles or swelling under irradiation, are screened out. The remaining fuel particles together with fresh particles are returned in a slurry to the reactor vessel and to the cyclone separator, completing the circuit.

The paste-fueled reactor can be controlled by any of the methods applicable to solid fueled reactors. The total out-of-core fuel inventory in the fuel circulating system can be limited so that its total reactivity worth is less than the worth of the safety controls; therefore, no more fuel can con-

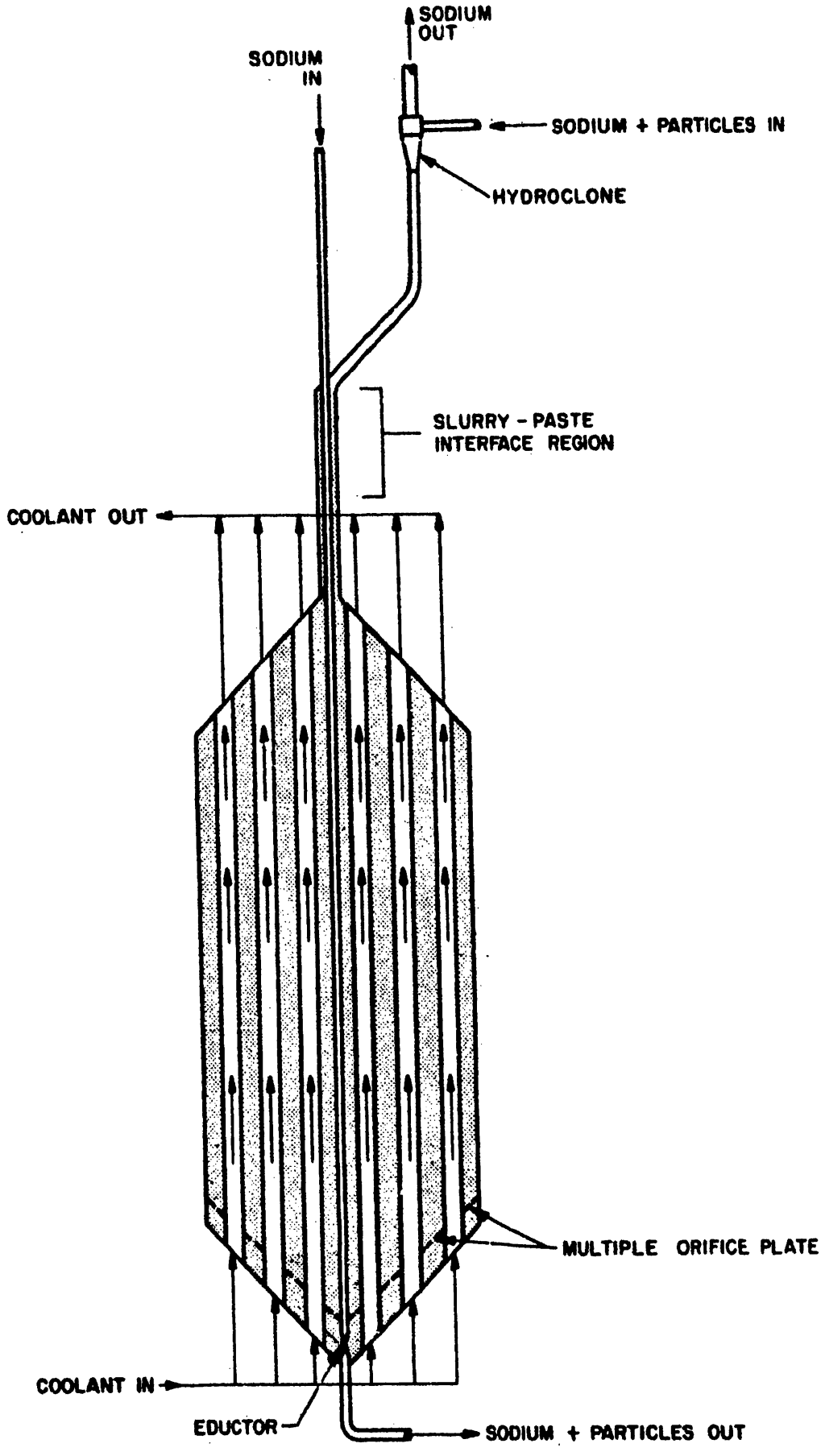

SCHEMATIC DRAWING OF PASTE FUELED REACTOR SUBASSEMBLY

FIGURE 64

ceivably be added to the core than the controls can accommodate.

The paste-fuel system conceived by APDA is distinguished by several features which appear to have overcome the principal technological obstacles that have impeded the successful development of other mobile-fueled reactor concepts. Most notable among these features are the following:

1. Fuel is not used to transport heat from the reactor. Thus, small volumes of fuel can be moved external to the reactor at very low velocities.

2. The use of a noncorrosive liquied metal, such as sodium, to transport the fuel and blanket particles largely eliminates problems of container corrosion and mass transport.

3. The low velocities required in the fuel system minimize the erosion of containers by the particles and breakdown of particles by attrition.

4. Loss of pumping power does not affect fuel concentration in the dynamically stable paste-fuel system, in which fuel particles are at settled density in the reactor core.

In comparison with static bed systems, wherein no throughput of fuel is involved, the paste-fuel system has several advantages. This system allows homogenized burnup and breeding by the continuous intermixing of the particles. It also provides continuous reprocessing of the fuel and continuous removal of fission gases. These features should allow higher mean burnups and breeding ratios than other systems. Further, clogging of the bed by fission gases should cause less difficulty in the paste-fuel system since only the gases released in a single pass through the core are of concern.

In addition, the paste-fuel concept retains all the advantages expected of mobile-fueled reactors over convention solid-fuel systems. These advantages include increased resistance of fuel to irradiation damage and dimensional change; ease of fuel and blanket fabrication; simplification of reactor loading and unloading, which can be a continuous process without interruption of operation; continuous on-site reprecessing; and simplification and improved performance of certain nonfuel portions of the reactor complex.

B. MAJOR TECHNOLOGICAL PROBLEM AREAS

Many problems must be solved so that the technical feasibility of a paste-fueled reactor plant may be demonstrated. The major problems are discussed in the following paragraphs.

1. Core Structure Development

The design of a core structure would be based primarily on a quantitative knowledge of paste flow characteristics, fuel and structural temperature limitations, and heat transport capabilities of a sodium coolant system. Also, the design would require an analysis of the thermal gradients and the mechanical and hydrodynamic forces to which the structure would be subjected, both under normal and abnormal operations. Analytical studies are required also so that criteria may be established

for structural integrity; permissible changes in the core and blanket structures must be determined with reference to the control and safety characteristics of the reactor. The problems here are similar to those of other fast reactor concepts.

The major fabrication problems are (1) fabricating of the coolant tubes, (2) fabricating of the tube sheets, (3) welding or brazing of the coolant tubes to the tube sheets, (4) welding or brazing of the subassembly shell to the tube sheets, (5) inter-locking of the individual subassemblies into a complete structure, and (6) supporting the composite structure in the reactor vessel. To evaluate the various fabrication techniques, it will be necessary to establish the structural requirements by design, analysis, and testing. Both nondestructive and destructive inspection techniques must be developed. These are typical of problems encountered in nuclear reactor designs; however, in a mobile-fueled reactor, they are more acute because the structure must have a much longer life than in a reactor in which fuel is handled as a subassembly or cluster. To date very little work has been done in this area.

2. Fuel Circulating System

APDA has sponsored research at the University of Michigan, Southern Research Institute, and in its own laboratory for the purpose of investigating paste flow fundamentals. Up to the time of our investigations, there was very little published information on the flow of solid-liquid systems. The APDA-sponsored studies have demonstrated the feasibility of the concept of a bed of solids moving slowly downward through narrow channels at settled density. Some of the experimental apparatus used in APDA's paste flow laboratory is shown in Figures 65 and 66. Figure 67 shows three types of paste flow through a single orifice, and Figure 68 shows a time exposure of a flowing paste system in a four-inch-diameter tube containing 37 coolant tubes and 24 orifices.

These studies have established that pastes flow without significant change in the concentration of solids under transient and equilibrium flow conditions. They also have demonstrated that paste flow rates can be controlled. Flow data have been obtained which correlate very well with published generalized correlations of moving beds of solid particles and vapors. From these correlations, it is possible to predict the relative liquid velocity in a moving bed of paste from a knowledge of the available pressures. The flow studies have resulted in correlations between the flow rate of the solids and the relative liquid velocity. These correlations permit a prediction of the absolute flow rates of the solids and the liquid in terms of the available pressures and the physical and geometrical properties of the flow system. The most important factors affecting the flow rate of the solids are the design of the orifices and the relative liquid velocity.

APDA has sponsored an analytical and research program at the University of Michigan to investigate the effects of gas bubbles on paste flow inside narrow fuel passages. It was demonstrated that small bubbles would be carried along with the flowing paste. If large bubbles are formed, however, they can obstruct the flow either in the fuel ligaments or at the orifices. The forming of large gas bubbles depends primarily

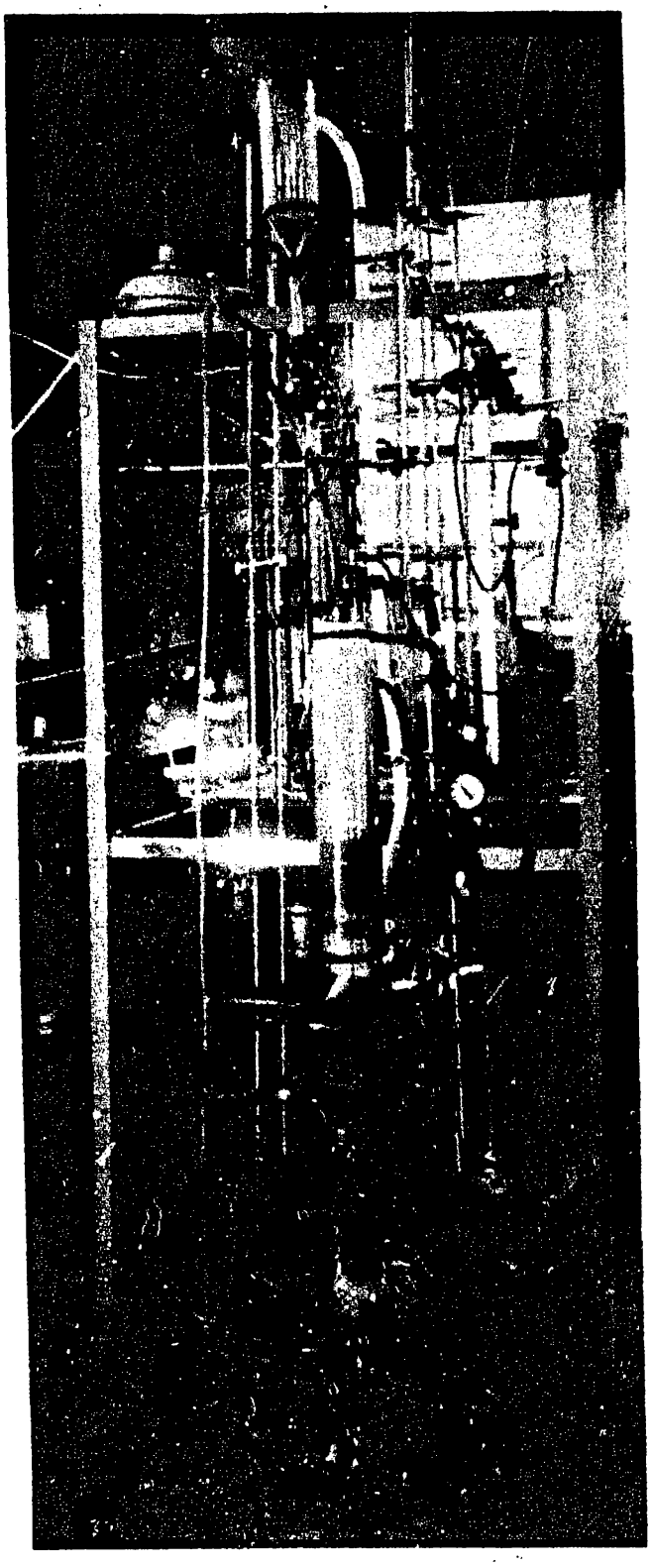

PASTE FLOW EXPERIMENTAL APPARATUS

FIGURE 65

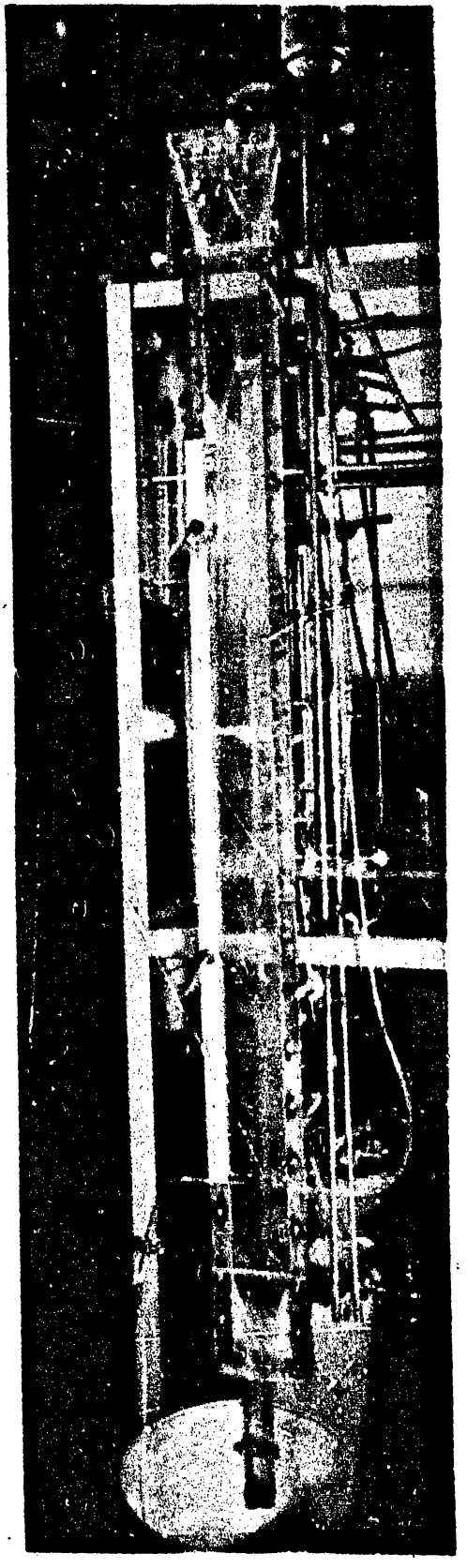

PASTE FLOW PROFILE APPARATUS

FIGURE 66

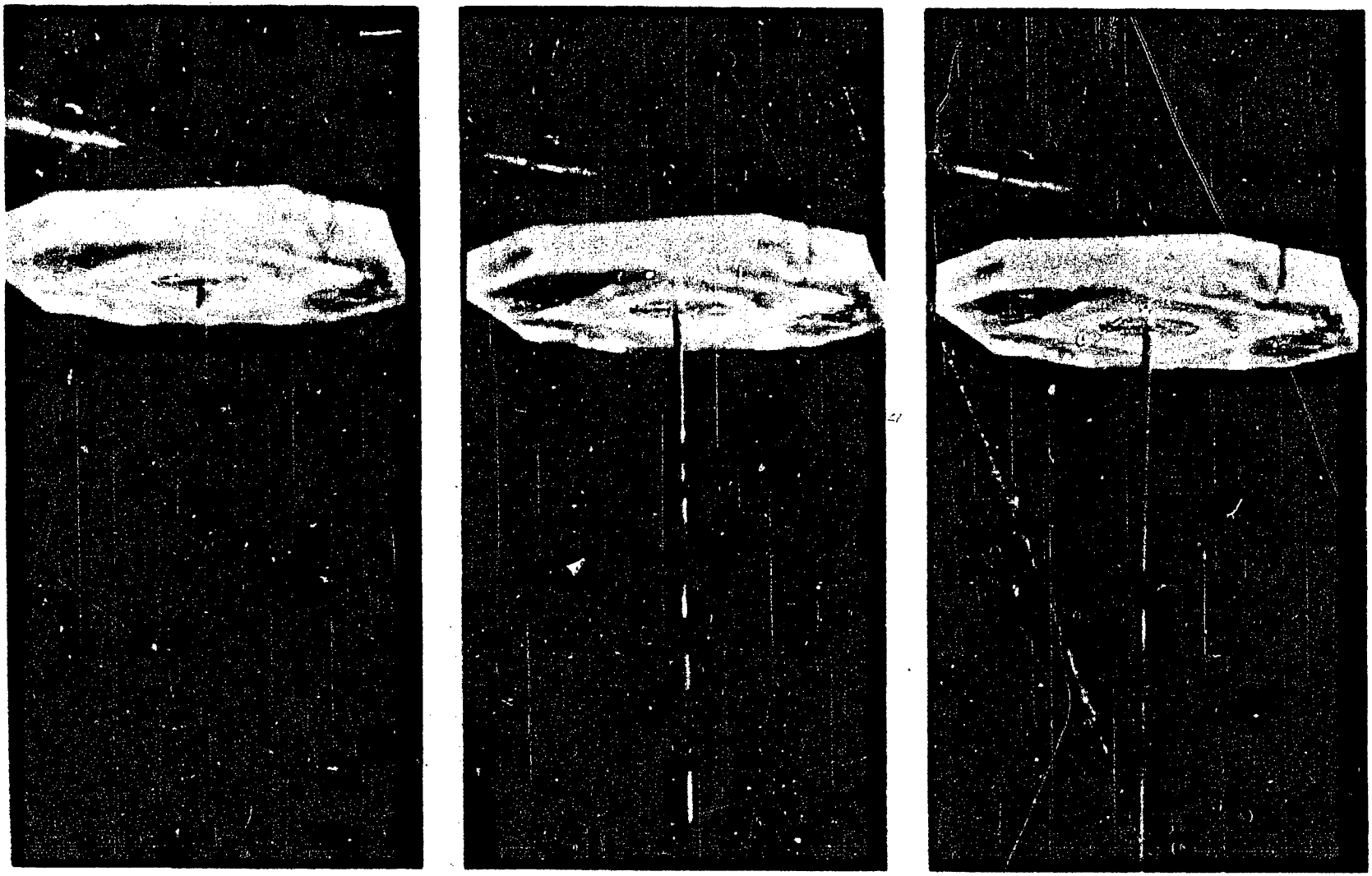

LOW FLOW RATE

INTERMEDIATE FLOW RATE

HIGH FLOW RATE

PASTE FLOW THROUGH A SINGLE ORIFICE

FIGURE 67

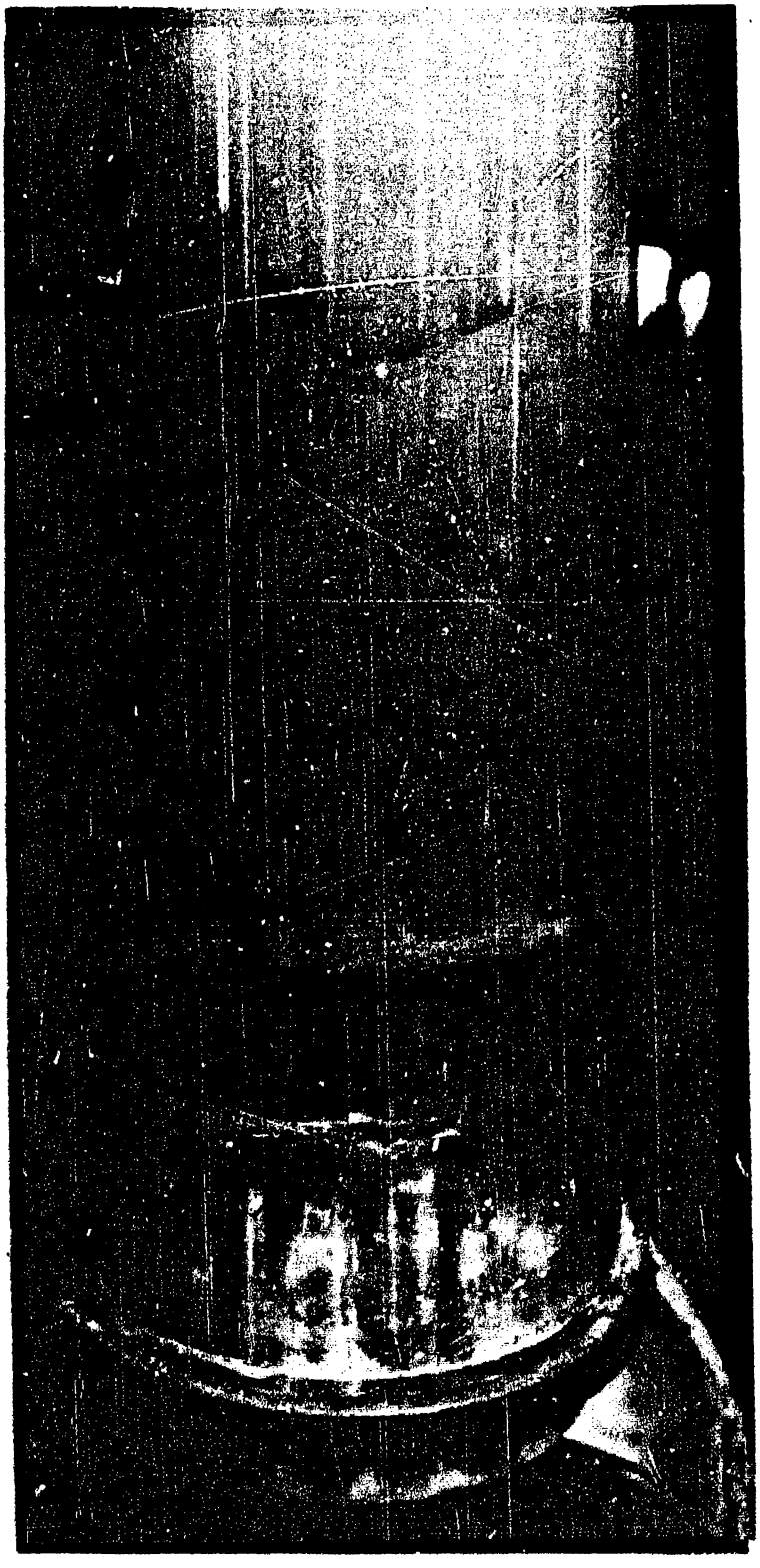

TIME EXPOSURE SHOWING PASTE FLOW IN A LARGE-DIAMETER, MULTIPLE-ORIFICE TUBE

FIGURE 68

on the mode of bubble nucleation and the mechanism of bubble growth. These factors are certain to be influenced by fission density, paste flow rate, thermal gradients in the paste ligaments, and the presence of an intense ionizing radiation. An accurate evaluation of the effects of gas bubbles on paste flow would require a high-fission-density flow experiment.

APDA has constructed and tested simple plastic models of proposed core structures to make observations on the paste velocity profiles, on regions of stagnant paste, on the density of the flowing and static bed, etc. More work with such simple models is required before a full-sized model can be designed and built.

The feasibility of circulating a dilute slurry of uranium particles in sodium has been demonstrated in the flow loop (Figure 69) operated for APDA by Southern Research Institute. Although the literature reports many data on the flow of slurries, most of the data are applicable only to specific systems. No general correlation is available by which these data can be applied to slurry systems containing large-diameter, high-density particles such as are of interest in the conceptual paste-fueled reactor. APDA has conducted experiments to determine the velocities required to transport particles of various density, diameter, and shape in vertically and horizontally oriented plumbing systems. The results of these experiments indicate that velocities in the order of five feet per second would be adequate in the slurry system. More extensive and definitive studies are required, however, before a preliminary design of the plumbing system for the slurry would be possible.

The paste flow studies at Southern Research Institute revealed a general reduction in particle size, probably caused by interparticle abrasion. Although there are as yet no experimental data on the effects of thermal cycling and high burnup on the dimensional stability of the fuel particles, it is expected that some particle break-down and particle growth (swelling, stitching, etc.) will occur. Based on aqueous experiments with less dense particles, the removal of fines appears to be feasible with a hydroclone. However, additional laboratory tests will be required for verification.

The straining out of oversized particles from a slurry stream also appears feasible. Continuous straining or screening devices of simple, rugged construction, which appear suitable for the conceptual design, are already in common use in the ore-dressing industry. However, a research and development program will be needed to scale down the commercially available equipment and to apply it to high-temperature sodium service. After preliminary development, both the hydroclones and screening devices should be included in a full-sized mock-up of the paste flow system.

3. Thermal and Mechanical Stability of the Paste Fuel

To determine whether temperature limitations would preclude the use of alloy fuel particles in the paste-fueled reactor concept, some sintering and compatibility experiments have been conducted for APDA at Southern Research Institute. Static sintering experiments (i.e., paste

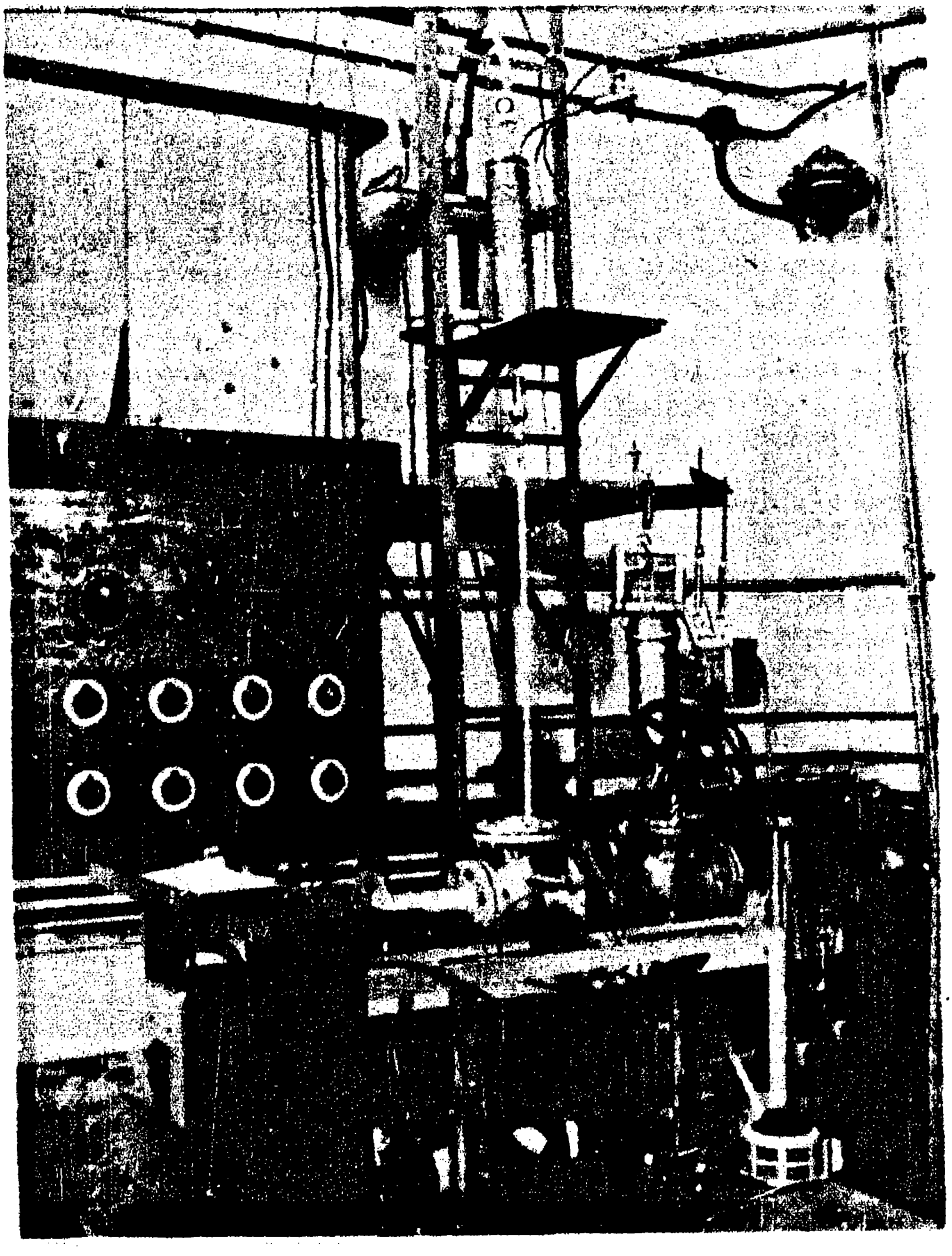

SODIUM-URANIUM FLOW LOOP

FIGURE 69

not in motion) carried out in tantalum capsules, indicated that unalloyed uranium particles begin to sinter around 850 C. Several experiments were conducted to determine the temperature at which unalloyed uranium particles begin to react with stainless steel. These experiments indicated that even under static conditions there was no appreciable reaction between the uranium and the stainless steel at temperatures up to the uranium-iron eutectic temperature (725 C).

APDA has sponsored a few tests on the sintering behavior and attrition characteristics of uranium dioxide particles that were obtained from several different suppliers. Static experiments run in tantalum capsules at 750 C and 850 C for 24 hours showed no signs of particle sintering. The mechanical stability of uranium dioxide particles was studied by observation of the reduction of particle size in shaker-capsule experiments and in the paste flow loop. In general, the oxide particles were not nearly so stable as the unalloyed uranium particles.

4. Irradiation Stability of the Paste Fuel

The possibility that alloy particles in a paste fuel might be quickly welded together into a single mass by irradiation (a phenomena called "stitching," which is caused by microscopic local melting from fission products recoil (was investigated by APDA in a paste irradiation program at Battelle Memorial Institute. The fuel material studied was a 10 per cent enriched alloy of U-10 w/o Mo in the form of spherical particles. The paste samples contained NaK instead of sodium for ease of capsule preparation. During the irradiation tests, the capsules were removed periodically from the reactor, and a radiation detector used to determine whether the paste sample still flowed. Thus far, two test capsules have been tested. The first was irradiated to 0.007 per cent of the uranium atoms. Examination of the particles in this capsule did not reveal any signs of metallurgical bonding (stitching) of the particles. The second capsule was irradiated to 0.08 per cent of the uranium atoms before the paste flow became exceedingly sluggish. Examination indicated no stitching, and it is suspected that oxide plugging was involved in the decreased paste mobility in the second test experiment. Figure 70 is a photograph of the irradiated particles from the second capsule.

The APDA irradiation experiments were conducted with the paste in a static condition rather than in a flowing condition as it would normally be in a reactor. Hence, with respect to the stitching problem, the experiments were conservative, since any motion of the particles relative to one another would tend to reduce or even prevent stitching by breaking the weak bonds which might be created in the short time in which the moving particles would be in contact. Furthermore, fluidization of the particles after each pass through the reactor would tend to break up groups of particles that might be bonded together. Also, provision would be made to strain the oversized particles each time before the fuel is returned to the reactor. Therefore, only the amount of stitching that would occur in a single pass of the fuel through the core is of concern.

Ceramic particles theoretically are more resistant to stitching than alloy particles. Data obtained at ANL on irradiated, dry uranium oxide powder indicates that stitching would not be a problem. APDA believes

IRRADIATED PARTICLES FROM CAPSULE

FIGURE 70

that the irradiation stability of paste fuels has been adequately demonstrated for reactor experiments. However, there are no irradiation data at high burnup and high power density. Simulation of the conditions of paste flow and thermal cycling at high power density requires an in-pile loop test.

5. Particle Fabrication

The fabrication of uranium particles has been demonstrated by the National Lead Company by means of the spinning disk technique. Kilogram quantities of nonenriched uranium have been fabricated in this way into particles in a matter of one or two minutes. The recovery of remeltable material has been over 95 per cent. This method of fabricating spherical particles was successfully adopted by Battelle Memorial Institute in fabricating gram quantities of particles of a 10 per cent enriched uranium 10 w/o Mo alloy for paste irradiation experiments sponsored by APDA.

To support the research effort on development of alternate fuel materials, it may be necessary to develop new particle-fabrication techniques for some of the ceramic fuels, particularly the carbides and nitrides. Uranium oxide particles are already available commercially, and APDA has purchased kilogram quantities of these particles for use in its experiment program. The carbides and nitrides of uranium are produced commercially but only as powders. Since these materials are of interest as dispersion-type fuels, it is likely that particle-fabrication processes will be developed either under the AEC fuel development programs or by commercial suppliers. It is expected that these basic processes will be adaptable to the production of both plutonium and enriched uranium particles in sufficient quantities for the screening tests included in the proposed research and development program.

6. Reprocessing of Paste Fuels

The pyrometallurgical methods developed by ANL for reprocessing EBR-II fuels would be adaptable for the reprocessing of alloy-particle pastes. Except for modifications in sodium-removal and fuel-handling facilities, pastes would be handled like fuel elements. Removal of sodium from pastes and melting of pastes should be investigated.

Methods of reprocessing uranium oxide are well established, and methods for reprocessing mixed oxides of uranium and plutonium are being developed. APDA believes there is adequate effort on these problems under existing programs, and it is expected that carbide and nitride fuels will be included in extensions of these programs.